Microwave spectroscopy of sulfur-bearing molecular species of astrophysical interest

by

Wenhao Sun

A thesis submitted to the Faculty of Graduate Studies of the University of Manitoba in

partial fulfillment of the requirements of the degree of

Doctor of Philosophy

Department of Chemistry

University of Manitoba

Winnipeg, Canada

Abstract

Microwave spectroscopy, which measures rotational transitions in the centimeter-wave region, is a robust technique to study the fundamental chemical and physical properties of gaseous molecules, such as the geometry and the electronic structure. This thesis presents a selection of studies on several compounds of great astrophysical interest including phenyl isocyanate (PhNCO), phenyl isothiocyanate (PhNCS), ethynyl isothiocyanate (HCCNCS) and its longer chain form HCCCCNCS, cyanogen isothiocyanate (NCNCS) and its longer chain form NCCCNCS. The experiments were carried out with two Fourier transform microwave (FTMW) spectrometers: the broadband chirped pulse type, which has the capability of simultaneously probing many molecules together with a bandwidth up to 6 GHz; the narrowband cavity-based type, which focuses on a frequency window of 1 MHz each time with high resolution and sensitivity.

Unlike PhNCO and PhNCS which are commercially available, the other four chemical species are not likely to be synthesized on a laboratory benchtop and were thus prepared by employing a dc electrical discharge. The transient products in the discharge source were probed by the spectrometers and were unambiguously identified by their rotational transitions out of a number of discharge dependent species including both closed-shell compounds and open-shell radicals. Furthermore, in order to better understand the chemical reactivities and kinetics in complex discharge plasmas, a thiazole discharge was investigated on the basis of the identified products in the rich spectrum. Possible decomposition pathways of the products from unimolecular dissociation and isomerization reactions were proposed and modeled using quantum-chemistry calculations. Collectively, these studies not only provided

fundamental insights for a series of potential interstellar species but also allowed

better understanding of the chemistry of the electrical discharge technique.

Acknowledgement

My parents, Baixing Sun and Mingxiang Wang, for your unconditional understanding and support in the progress of my growing up.

Table of Contents

Chapter 1. Introduction

Chapter 2. Fourier transform microwave spectroscopy

List of Figures

List of Tables

List of Abbreviations

ae-CCSD(T)	All electron coupled-cluster single double (triple) excitations
AWG	Arbitrary waveform generator
ALMA	Atacama Large Millimetre Array
BSSE	Basis set superposition error
B3LYP	Becke, 3-parameter, Lee–Yang–Parr
bp	Boiling point
cp	chirped pulse
CASSCF	Complete active space self-consistent field
CBS	Complete basis set
IRC +10216	CW Leonis
dc	Direct current
D3(BJ)	Dispersion correction with Becke-Johnson Damping
FTMW	Fourier transform microwave
FID	Free induction decay
fc-CCSD(T)	Frozen core coupled-cluster single double (triple) excitations
FWHM	Full width at half max
GSRB	Generalized semi-rigid bender
ISO	Infrared Space Observatory
IM	Intermediate
ISM	Interstellar medium
IRC	Intrinsic reaction coordinate
mp	Melting point
MM	Molecular mechanics
NBO	Natural bond orbital
PAH	Polycyclic aromatic hydrocarbon
PES	Potential energy surface
rms	Root-mean-square
Sgr B2	Sagittarius B2
MP2	Second order Møller-Plesset perturbation theory
SNR	Signal-to-noise ratio
SPDT	Single pole double throw
TMC-1	Taurus Molecular Cloud
TS	Transition state
YSO	Young stellar object
ZPE	Zero-point energy

Chapter 1.   Introduction

1.1 Overview of astrochemistry

Astrochemistry is a fast-growing field of science that combines astronomy, astrophysics, and chemistry.[1] It explores the formation, destruction, and other chemical processes of molecular species in astronomical environments[2-3] and uses their chemical evolution as probes to investigate the physical conditions of astronomical objects such as stars, the associated circumstellar and interstellar media[4] and monitor their evolution phases.[5] As stars are formed from giant molecular clouds distributed in the interstellar medium (ISM), the chemistry in star-forming regions is of particular interest. Molecular clouds are composed of gas and dust at very low average density, even the densest regions that are known as molecular cores only roughly contain $\sim 10^{5-6}$ particles per cubic centimeter,[6] which is much sparser than the particle density under standard temperature and pressure ($\sim 2.7 \times 10^{19}\,cm^{-3}$). In such an environment, the chemistry is quite distinct from that on the Earth and many of the species are exotic, including closed-shell molecules, open-shell radicals, and positively or negatively charged ions.

Prior to the formation of molecules, elements must be created. In our Universe, hydrogen, helium, and lithium were first created from the Big Bang;[7] beryllium and boron are thought to be formed through the nucleosynthesis of cosmic-ray particles and lighter gas atoms,[8] and other heavier elements such as carbon, nitrogen and oxygen are produced from neutron star mergers or synthesized from helium fusion reactions in stellar interiors.[9] In certain evolution phases, they are ejected into the ISM and form diffuse clouds,[10] where diatomic molecules and simple

polyatomic species are synthesized. Gradually over millions of years, as these low-mass diffuse interstellar clouds evolve to denser molecular clouds, their temperatures and pressures increase and the chemistry there becomes more diverse which produces a variety of complex species.[5]

Since the first interstellar species CH was discovered in 1937,[11] over 200 molecules have been identified in various interstellar and circumstellar sources as listed in Table 1.1. These molecules range from diatomics to large buckyballs (C_{60} and C_{70})[12] in size, and are comprised of 16 elements that are mainly from the first three rows of the periodic table. Approximately, three quarters contain the element carbon and are classified as organic compounds. As all detected species with six or more atoms are organic, they are conventionally labelled as complex organic compounds and are mainly found in denser interstellar sources.[5] The observation of these species provides unique information about the associated molecular clouds and helps astronomers to better understand these mysterious cosmic environments.

Table 1.1. Molecules detected in the interstellar and circumstellar medium.

#	Known interstellar species						
2	CH	CN	CH^+	OH	CO	H_2	SiO
	CS	SO	SiS	NS	C_2	NO	HCl
	NaCl	AlCl	KCl	AlF	PN	SiC	CP
	NH	SiN	SO^+	CO^+	HF	LiH	FeO
	N_2	CF^+	PO	AlO	CN^-	OH^+	SH^+
	O_2	HCl^+	SH	TiO	ArH^+	NO^+	CrO
	NS^+						
3	H_2O	HCO^+	HCN	OCS	HNC	H_2S	N_2H^+
	C_2H	SO_2	HCO	HNO	OCN^-	HCS^+	HOC^+
	c-SiC_2	MgNC	C_2S	C_3	CO_2	CH_2	C_2O
	NH_2	NaCN	N_2O	MgCN	H_3^+	SiCN	AlNC
	SiNC	HCP	CCP	AlOH	H_2O^+	H_2Cl+	KCN
	FeCN	HO_2	TiO_2	CCN	SiCSi	S_2H	HCS

	HSC	NCO					
4	NH_3	H_2CO	HNCO	H_2CS	C_2H_2	C_3N	HNCS
	$HOCO^+$	C_3O	C_3H	$HCNH^+$	H_3O^+	C3S	c-C_3H
	HC_2N	H_2CN	SiC_3	CH_3	C_3N^-	PH_3	HCNO
	HOCN	HSCN	HOOH	l-C_3H^+	HMgNC	MgCCH	NCCP
	HCCO	CNCN					
5	HC_3N	HCOOH	CH_2NH	NH_2CN	H_2CCO	C_4H	SiH_4
	c-C_3H_2	CH_2CN	C_5	SiC_4	H_2CCC	CH_4	HCCNC
	HNCCC	H_2COH+	C_4H^-	CNCHO	HNCNH	CH_3O	NH_3D^+
	H_2NCO^+	$NCCNH+$	CH_3Cl				
6	CH_3OH	CH_3CN	NH_2CHO	CH_3SH	C_2H_4	C_5H	CH_3NC
	HC_2CHO	H_2CCCC	HC_3NH^+	C_5N	C_4H_2	HC_4N	c-H_2C_3O
	CH_2CNH	C_5N^-	E-HNCHCN	C_5S	SiH_3CN	Z-HNCHCN	
7	CH_3CHO	CH_3CCH	CH_3NH_2	CH_2CHCN	HC_5N	C_6H	c-C_2H_4O
	CH_2CHOH	C_6H^-	CH_3NCO	HC_5O	$HOCH_2CN$		
8	$HCOOCH_3$	CH_3C_3N	C_7H	CH_3COOH	H_2C_6	CH_2OHCHO	C_6H_2
	C_2H_5N	CH_2CHCHO	CH_2CCHCN	NH_2CH_2CN	CH_3CHNH	$(NH_2)_2CO$	CH_3SiH_3
9	CH_3OCH_3	CH_3CH_2OH	CH_3CH_2CN	HC_7N	CH_3C_4H	C_8H	CH_3CONH_2
	C_8H^-	CH_2CHCH_3	CH_3CH_2SH	CH_3NHCHO	HC_7O		
10	$(CH_3)_2CO$	$HOCH_2CH_2OH$	CH_3CH_2CHO	CH_3C_5N	CH_3CHCH_2O	CH_3OCH_2OH	
11	HC_9N	CH_3C_6H	C_2H_5OCHO	CH_3COOCH_3			
12	C_6H_6	$CO(CH_2OH)_2$	C_3H_7CN	iso-C_3H_7CN	t-$C_2H_5OCH_3$		
13	C_6H_5OH	C_6H_5CN					
24	$C_{14}H_{10}$	$C_{14}H_{10}^+$					
60	C_{60}	C_{60}^+					
70	C_{70}						

* The table was constructed from http://www.astrochymist.org/astrochymist_ism.html (as of 03/2019).

Molecular clouds are not statically or evenly distributed in the ISM and are moving and rotating constantly. The density varies from region to region. For one location, the density also changes slowly over the course of time. Consequently, the physical conditions such as temperature, pressure and cosmic radiation keep changing as molecular clouds evolve which causes distinct chemical reactions in different regions and at different times, and produces different type of molecules. Generally, in cold, dense regions, the detected species are quite unsaturated and not common in the

terrestrial environment. As the cold core becomes a hotter more-massive young stellar object (YSO), the abundance of gaseous hydrogen dramatically increases, and the molecules tend to be more saturated and similar to those in terrestrial environments.[5] Therefore, interstellar species are great probes to explore molecular clouds with respect to their physical conditions and evolution phases. Moreover, reactions occurring in these regions also influence the astrophysical environments themselves and further affect the formation process of the stars and planets.[1] Through detecting the molecular species and exploring the associated chemical evolutions, valuable information is obtained to refine current stellar evolution models.

Besides acting as excellent probes of stellar evolution, these species themselves, especially the complex organics, are of great fundamental interest from chemical and biological perspectives. The origin of life in the Universe is one of the most central subjects in this field. Although no direct observation of biogenic molecules has been achieved yet in the ISM, the identification of various prebiotic species shows very promising potential in this respect. For instance, multiple detected species (e.g. formamide $(HCONH_2)$,[13] acetamide (CH_3CONH_2),[14] urea $((NH_2)_2CO)$[15]) contain a peptide bond (- C(=O)-NH-) which is the signature link in peptides and proteins. OCN-containing species, as potential precursors of amides or amino acids, are found to be abundant in a variety of molecular clouds.[16-23] Moreover, the identified aminoacetonitrile (NH_2CH_2CN)[24] is a penultimate product leading to the synthesis of the simplest amino acid glycine (NH_2CH_2COOH) and is well known in the famous Miller-Urey atmospheric discharge experiment.[25] Interstellar glycolaldehyde $(HOCH_2CHO)$[26] is a building block of monosaccharide sugars. Their formation implies that crucial ingredients leading to life such as amino acids may be

created under such harsh conditions as well. If so, this would be a big step to unravel the mystery of the origin of life in the Universe.

In 2016, the existence of glycine was confirmed in the coma of comet 67P/Churyumov-Gerasimenko,[27] which is considered a reservoir of primitive materials generated in the formation process of our Solar system. As our Solar system is a part of the Universe, this finding along with previous detections of amino acids in many primitive meteorites[28] makes this exploration more promising. Therefore, it is of significant importance to develop astrochemistry models to understand interstellar environments, expand the molecule database of laboratory and astronomical detections, connect them through reaction models, and explore their chemical evolutions. The more astrochemists explore, the closer we are to the truth of the evolution of molecules, life and the Universe.

As a fundamental step, identifying as many molecular species as possible is particularly urgent and is achieved by spectroscopy in the radio, infrared, visible and ultraviolet frequency ranges. Radio astronomy mainly collects the pure rotational transitions of molecules from the centimeter to far-infrared wavelength region (lower than 2 THz in frequency) using large radio antennas distributed on the Earth's surface. Pure rotational spectroscopy is a robust technique that is also employed in this thesis and the main details will be demonstrated in Chapter 2. In brief, it can be used to unambiguously distinguish polar interstellar species using their unique spectral patterns that arise from different geometries and isotopologues. As the energy required for these types of transitions is quite low, they are ubiquitously observed in the ISM and account for ~80% of the molecular detections in space.[29] However, for species with no permanent electric dipole moment, such as benzene C_6H_6,[30] there is no allowed rotational transition through absorption or emission in its vibrational

ground state and thus, it is impossible to make the detection in this way. Instead, spectroscopy in the infrared, visible and ultraviolet frequency ranges are employed. Since these signals are easily absorbed or scattered by the constitutents of the atmosphere of the Earth, they are better detected by space telescopes such as Hubble and Spitzer.

The collected observational data are interpreted by comparing with the available laboratory spectral fingerprints of the candidate species in databases. With more and more species identified, astrochemists are able to build and improve reaction models to simulate various environments. However, unlike terrestrial reactions in the laboratory that are normally in solution or the liquid phase, the molecular species that are detected in interstellar space are in the gas phase or trapped in or on dust or ice grains. This implies that the ongoing chemical processes there are dominated by gas-gas collisions or on the surface of ice and grains,[4] which makes they quite different from common laboratory chemistry. As mentioned before, the density of interstellar molecular clouds is very low, for example, the average density of the giant molecular clouds where the Milky Way resides is ~150 particles/cm^3.[4] As molecules are far apart from each other, collisions are quite infrequent and even two-body collisions may take days to occur.[31] The sparse environment with low collision probabilities allows highly reactive species such as radicals and ions to exist for a long period (on the time scale of years). Given the low temperatures, barrierless reactions involving these radicals and ions are found to be more effective and favourable than neutral-neutral collisions.[32] On our Earth, some of these species might be found under certain conditions but more commonly appear as transient intermediates to form other stable compounds. In addition, lots of stable molecules

detected in space are quite rare such as cyano octatetra-yne

HC≡CC≡CC≡CC≡CC≡N,[33] and cannot be synthesized on the benchtop.

Therefore, well-designed laboratory experiments become very crucial to attempt to make these non-terrestrial species and simulate chemical reactions and physical conditions in other environments. Many techniques such as thermal pyrolysis,[34] dc electrical discharge,[35] and photolysis,[36] have been developed to produce molecule candidates and coupled with spectrometers to make spectroscopic characterizations. This is the major driving force of this thesis and dc electric discharge is the method that is used to create such molecules. On the basis of a large amount of laboratory research, astrochemists are able to recognize potential species from the astronomical observations and build reactions models to rationalize their formation in a particular region of space.

As more and more species are identified in certain interstellar sources, the reaction models keep growing in size by including new species and a reaction network can be constructed by piecing together correlated models.[37] A better understanding of the associated reaction dynamics such as reaction mechanisms and rates becomes the next urgent subject awaiting astrochemists.[32] As the stars or planets evolve, the physical conditions of the interstellar environments keep changing and the corresponding reactions become different as well. Species that are not found in current data may be created later. With reliable and accurate experimental data, the key reactions in interstellar molecular clouds can be studied by monitoring the abundance changes of known species and then used to predict upcoming reactions and environmental changes in molecular clouds. Current theoretical models are far from being complete and need to be improved by including more species and associated reaction dynamics. With well-improved models and accurate simulations in the future,

our knowledges of mysterious interstellar environments and the evolution of astrophysical objects would reach a new level.

1.2 Astrochemistry of sulfur

Of the ~200 identified interstellar molecular species, there are over 150 C-bearing and H-bearing species, 80 N-bearing and O-bearing species. On the basis of adequate astrophysical detections, their reaction networks and mechanisms are fairly well-explored with established molecular abundances in various sources.[4,37] In contrast, only 23 S-containing species have been identified since the first detection of CS in 1971,[38] and only five out of them contain three or more heavy (non-hydrogen) atoms which are C_3S,[35,39] HNCS,[40] HSCN,[41] C_5S,[42] CH_3CH_2SH.[43-44] As sulfur is one of the most abundant elements in the universe, S-bearing molecules are playing an important role in astrophysical models and are attracting more and more attention from astrochemists over the past decades. The abundance of S-bearing molecules is found to be very sensitive to the environments in which they reside.[45] Therefore, they are readily used to probe the physical conditions in various interstellar environments of star-forming regions, for instance dense dark clouds[46-48] and their hot cores,[45,49-50] and are proposed as a potential chemical clocks for hot cores to trace the stage of star formations.[50-51]

At the same time, sulfur chemistry is one of the most challenging subjects within astrophysics and the understanding of it is still very insufficient. The biggest puzzle is the elemental abundance of sulfur in molecular clouds and star-forming regions. In the primitive diffuse medium, sulfur mainly exists in the form of ionized S^+ in gas phase.[52] However, in dense dark clouds which are the following evolutionary stage of diffuse clouds, the abundance of sulfur is detected with a drastic drop and only accounts for 0.1% of its cosmic abundance.[53-54] The missing sulfur has

bothered astrochemists since this discovery and many models have been proposed. The most popular one is that sulfur depletes from the gas-phase S^+ into the molecular form of H_2S,[55] OCS[46] and SO_2,[56] and is locked on (or in) interstellar grains and ices. However, this model only explains in part the missing sulfur based on available observational data. Given the very limited number of detected S-bearing species, another possibility is that part of the missing sulfur transforms to gas-phase molecules which have not been identified.[57-58] To assist with interstellar detection, spectroscopic characterization of sulfur-bearing candidates in the laboratory is getting more attention.

Within the 21 identified S-bearing species, four common functional groups are found, which are SH, C=S, S=O and N=C=S. Their derivatives are the top candidates for future laboratory studies. A good example is the interstellar identification of HSCN.[41] Its global-minimum isomer HNCS (27.6 kJ/mol more stable in energy calculated at the fc-CCSD(T)/cc-pwCVQZ)[59] level of theory was detected in Sagittarius B2 (Sgr B2) molecular cloud in 1979,[40] on the basis of the prior well-characterized pure rotational spectrum.[60-61] Under regular terrestrial conditions, the abundance of HSCN is very low (~0.001 % of HNCS) as it is a higher energy isomer. However, previous interstellar detection of the related HNC/HCN isomer pair with comparable relative abundance,[62] despite the energy difference of 8.4 kJ/mol, indicates that HSCN might exist along with HNCS in space despite the unfavourable thermodynamics. Thirty years later, its pure rotational spectrum was successfully measured via microwave spectroscopy in the laboratory,[63] and subsequently identified in Sgr B2 with a HNCS/HSCN abundance ratio of 2-7 as well as in TMC-1 molecular cloud with the ratio close to 1.[64] Thereafter, their relative abundances are effectively

used to probe the kinetic temperatures and dynamic environments in these two interstellar sources.[64]

Other than isomers, the search for carbon-chain derivatives is another direction of current laboratory and interstellar surveys as carbon is ubiquitous in the diffuse medium and molecular clouds and highly unsaturated carbon-chain species, in particular, are abundant in cold, dense regions. The two longest carbon-chains ever identified in such regions are $C{\equiv}CC{\equiv}CC{\equiv}CC{\equiv}CH$[65] and $HC{\equiv}CC{\equiv}CC{\equiv}CC{\equiv}CC{\equiv}N$.[33] Owing that H_mCS (m = 0, 1, 2),[38,57,66] CCS,[67] C_3S,[39] C_5S[42] were previously detected in various sources, a series of sulfur-carbon chains: C_nS (n = 4 – 9),[68] HC_nS (n = 3 – 8),[69-70] H_2C_nS (n = 2 – 7)[70-72] have been systematically investigated in the laboratory. Ethyne- $HC{\equiv}CC(-H){=}S$[73] and Butadiyne- $HC{\equiv}CC{\equiv}CC(-H){=}S$[74] substituted thials (which are isomers of $H_2C{=}C{=}C{=}S$ and $H_2C{=}C{=}C{=}C{=}C{=}S$, respectively) were characterized as well. However, the carbon-chain derivatives of the other S-bearing functional groups, especially SH and NCS, have not been widely studied. Very recently, $HC{\equiv}CSH$,[75] $HC{\equiv}CNCS$,[76] $HC{\equiv}CC{\equiv}CNCS$[77] were successfully created in a molecular beam and their pure rotational spectra were measured using microwave spectroscopy. The laboratory detections of the latter two, $HC{\equiv}CNCS$ and $HC{\equiv}CC{\equiv}CNCS$, are included in Chapters 5 and 6 in the current thesis.

1.3 Polycyclic aromatic hydrocarbons (PAHs)

Another insufficiently studied category from the interstellar species inventory which is attracting astrochemists' attention is aromatic species, especially polycyclic aromatic hydrocarbons (PAHs). In the carbon-rich diffuse interstellar medium, over 10% of the elemental carbon is predicted to reside in PAHs.[78] The large-sized and highly stabilized conjugated features make them crucial components of the ISM from

the perspective of chemical evolution. They could easily balance the charge in molecular clouds as good electron-acceptors and assist in producing other species as good catalysts.[79] Therefore, astrophysical confirmation of their existences is necessary and will not only unveil the diversity of interstellar carbonaceous molecules but also help to improve current reaction models and networks.

However, due to their featured structural configurations, their permanent dipole moments are quite small, if not zero, making detections through rotational spectroscopy unfeasible. Naturally, astronomical observation using infrared or electronic spectroscopy is an alternative means to prove their existence and the former, has been applied successfully to observe the nonpolar methane (CH_4)[80] and C_n species[81-82], for example. Unlike unambiguous identification through radio astronomy, the collected infrared hydrocarbon bands such as vibrational bands corresponding to aromatic C-C or C-H bonds, are not molecule-specific enough and in such studies, could only be attributed to a mixture of PAHs or fullerenes.[78,83] So far, only the single aromatic ring, benzene (C_6H_6) has been identified[30] along with two fullerenes $(C_{60}$ and $C_{70})$,[12] with no dispute.

Although direct confirmation of their prevalence in the ISM is very challenging, detection of their derivatives or related heterocycles by the rotational transitions is possible and could provide support as well. The interstellar detection of phenol $(c\text{-}C_6H_5OH)$[84] and benzonitrile $(c\text{-}C_6H_5CN)$[85] is a good example, which are the first two benzene derivatives observed in space. In the case of $c\text{-}C_6H_5CN$, both theoretical calculations and experimental results suggested that the bottleneck of its generation is the formation of the benzene ring.[31,86] This implies that it was probably produced from the reaction of the CN radical with an existing phenyl radical (C_6H_5) or neutral benzene. If so, more benzene derivatives such as benzothialdehyde

($C_6H_5C(H){=}S$) are likely to be found in the future based on other known functional groups in these regions of space.

In the present thesis, the work was aimed to assist with the interstellar detection of S-bearing species by investigating some top candidates using microwave spectroscopy in the laboratory. A description of rotational spectroscopy and the instruments used, which are known as chirped pulse Fourier transform microwave (cp-FTMW) spectrometer and Balle-Flygare FTMW spectrometer, are provided in the following Chapter 2. Next, Chapter 3 presents the spectroscopic characterization of two O/S-bearing benzene derivatives phenyl isocyanate and isothiocyanate that are commercially available as a demonstration of the spectroscopic technique and its capabilities. In this work, with the measurements of the minor isotopologues (^{13}C, ^{15}N, $^{18}O/^{34}S$), their experimental structures were precisely derived in great agreement with quantum chemistry calculations. Moreover, natural bond orbital (NBO) analysis was carried out to better understand their interesting electronic properties.

Thereafter, a dc electrical discharge technique was employed to create highly unsaturated S-bearing carbon-chains using high voltage, which are difficult to synthesize, if not impossible, on the benchtop. In Chapter 4, the laboratory detection of $HC{\equiv}CC{\equiv}CC(H){=}S$ was achieved by using a precursor mixture of 1,2-ethanedithiol ($HSCH_2CH_2SH$) and acetylene ($HC{\equiv}CH$). In Chapters 5 and 6, the pure rotational spectra of three carbon-chain isothiocyanates which are $HC{\equiv}CNCS$, $HC{\equiv}CC{\equiv}CNCS$, $N{\equiv}CC{\equiv}CNCS$, were investigated from a methyl isothiocyanate (CH_3NCS) discharge. Although this dc electrical discharge technique was proven to be very robust for the formation of these exotic species as well as S-bearing cumulenes, their formation mechanisms have not been systematically established. Therefore, in each project, besides the investigation of the rotational spectrum of the title molecules, an attempt

is made to explain their formation by putting them in empirical reaction networks together with other identified known species from the discharge spectra.

In Chapter 7, an attempt to model the reactions initiated by the dc electrical discharge of thiazole, a simple S-containing precursor, using several quantum-chemical tools is described. This work provides more insight into the chemical processes occurring in the discharge plasma. With a better understanding, the laboratory generation of new species via this method would be more efficient. At the end, Chapter 8 briefly sums up the work in this thesis and describes some future work that expands the current study.

References

(1)   Shematovich, V. I. Formation of Complex Chemical Species in Astrochemistry (a Review). *Sol. Syst. Res.* **2012,** *46* (6), 391-407.

(2)   van Dishoeck, E. F. Astrochemistry: Overview and Challenges. *Proceedings IAU* **2018,** *13* (S332), 3-22.

(3)   Yamada, K. M. T.; Winnewisser, G. E. *Interstellar Molecules: Their Laboratory and Interstellar Habitat*. Springer, 2011; Vol. 241.

(4)   Tielens, A. G. G. M. The Molecular Universe. *Rev. Mod. Physc.* **2013,** *85* (3), 1021-1081.

(5)   Herbst, E.; van Dishoeck, E. F. Complex Organic Interstellar Molecules. *Annu. Rev. Astron. Astrophys.* **2009,** *47* (1), 427-480.

(6)   Di Francesco, J.; Evans II, N. J.; Caselli, P.; Myers, P. C.; Shirley, Y.; Aikawa, Y.; Tafalla, M. *An Observational Perspective of Low-Mass Dense Cores I: Internal Physical and Chemical Properties*. Univerisity of Arizona Press: 2006; p 17.

(7)   Cowan, J. Elements of Surprise. *Nature* **2003,** *423*, 29.

(8)   Fields, B. D.; Olive, K. A. The Revival of Galactic Cosmic-Ray Nucleosynthesis? *Astrophys. J.* **1999,** *516* (2), 797-810.

(9)   Sneden, C.; Cowan, J. J. Genesis of the Heaviest Elements in the Milky Way Galaxy. *Science* **2003,** *299* (5603), 70-75.

(10)   Ehrenberg, R. Molecules of the Interstellar Medium must Break The Rules to Make the Stuff of Space. *Science News* **2010,** *177* (3), 26-29.

(11)   Swings, P.; Rosenfeld, L. Considerations Regarding Interstellar Molecules. *Astrophys. J.* **1937,** *86*, 483-486.

(12)   Cami, J.; Bernard-Salas, J.; Peeters, E.; Malek, S. E. Detection of C_{60} and C_{70} in a Young Planetary Nebula. *Science* **2010,** *329* (5996), 1180-1182.

(13)   Rubin, R. H.; Swenson, G. W., Jr.; Benson, R. C.; Tigelaar, H. L.; Flygare, W. H. Microwave Detection of Interstellar Formamide. *Astrophys. J.* **1971,** *169*, L39-L44.

(14)   Hollis, J. M.; Lovas, F. J.; Remijan, A. J.; Jewell, P. R.; Ilyushin, V. V.; Kleiner, I. Detection of Acetamide (CH_3CONH_2): The Largest Interstellar Molecule with a Peptide Bond. *Astrophys. J.* **2006,** *643* (1), L25-L28.

(15)   Remijan, A. J.; Snyder, L. E.; McGuire, B. A.; Kuo, H.-L.; Looney, L. W.; Friedel, D. N.; Golubiatnikov, G. Y.; Lovas, F. J.; Ilyushin, V. V.; Alekseev, E. A.; Dyubko, S. F.; McCall, B. J.; Hollis, J. M. Observational Results of a Multi-Telescope Campaign in Search of Interstellar Urea [$(NH_2)_2CO$]. *Astrophys. J.* **2014,** *783* (2), 77.

(16)   Snyder, L. E.; Buhl, D. Interstellar Isocyanic Acid. *Astrophys. J.* **1972,** *177*, 619-623.

(17)   Soifer, B. T.; Puetter, R. C.; Russell, R. W.; Willner, S. P.; Harvey, P. M.; Gillett, F. C. The 4-8 Micron Spectrum of the Infrared Source W33 A. *Astrophys. J.* **1979,** *232*.

(18)   Brünken, S.; Gottlieb, C. A.; McCarthy, M. C.; Thaddeus, P. Laboratory Detection of HOCN and Tentative Identification in Sgr B2. *Astrophys. J.* **2009,** *697* (1), 880-885.

(19)   Brünken, S.; Belloche, A.; Martín, S.; Verheyen, L.; Menten, K. M. Interstellar HOCN in the Galactic Center Region. *Astron. Astrophys.* **2010,** *516*, A109.

(20)   Gupta, H.; Gottlieb, C. A.; Lattanzi, V.; Pearson, J. C.; McCarthy, M. C. Laboratory Measurements and Tentative Astronomical Identification of H_2NCO^+. *Astrophys. J.* **2013,** *778* (1), L1.

(21)   Halfen, D. T.; Ilyushin, V. V.; Ziurys, L. M. Interstellar Detection of Methyl Isocyanate CH_3NCO in Sgr B2(N): A Link from Molecular Clouds to Comets. *Astrophys. J.* **2015,** *812* (1), L5.

(22)   Cernicharo, J.; Kisiel, Z.; Tercero, B.; Kolesnikova, L.; Medvedev, I. R.; Lopez, A.; Fortman, S.; Winnewisser, M.; de Lucia, F. C.; Alonso, J. L.; Guillemin, J. C. A Rigorous Detection of Interstellar CH_3NCO: An Important Missing Species in Astrochemical Networks. *Astron. Astrophys.* **2016,** *587*, L4.

(23)   Marcelino, N.; Agundez, M.; Cernicharo, J.; Roueff, E.; Tafalla, M. Discovery of the Elusive Radical NCO and Confirmation of H_2NCO^+ in space. *Astron. Astrophys.* **2018,** *612*, L10.

(24)   Belloche, A.; Menten, K. M.; Comito, C.; Müller, H. S. P.; Schilke, P.; Ott, J.; Thorwirth, S.; Hieret, C. Detection of Amino Acetonitrile in Sgr B2(N). *Astron. Astrophys.* **2008,** *482* (1), 179-196.

(25)   Miller, S. L. A Production of Amino Acids under Possible Primitive Earth Conditions. *Science* **1953,** *117*, 528-529.

(26)   Hollis, J. M.; Lovas, F. J.; Jewell, P. R. Interstellar Glycolaldehyde: The First Sugar. *Astrophys. J.* **2000,** *540* (2), L107-L110.

(27)   Altwegg, K.; Balsiger, H.; Bar-Nun, A.; Berthelier, J. J.; Bieler, A.; Bochsler, P.; Briois, C.; Calmonte, U.; Combi, M. R.; Cottin, H.; De Keyser, J.; Dhooghe, F.; Fiethe, B.; Fuselier, S. A.; Gasc, S.; Gombosi, T. I.; Hansen, K. C.; Haessig, M.; Jackel, A.; Kopp, E.; Korth, A.; Le Roy, L.; Mall, U.; Marty, B.; Mousis, O.; Owen, T.; Reme, H.; Rubin, M.; Semon, T.; Tzou, C. Y.; Hunter Waite, J.; Wurz, P.

Prebiotic Chemicals-Amino Acid and Phosphorus-in the Coma of Comet 67P/Churyumov-Gerasimenko. *Sci. Adv.* **2016,** *2* (5), e1600285.

(28)   Cobb, A. K.; Pudritz, R. E. Nature's Starships. I. Observed Abundances and Relative Frequencies of Amino Acids in Meteorites. *Astrophys. J.* **2014,** *783* (2), 140.

(29)   McGuire, B. A. 2018 Census of Interstellar, Circumstellar, Extragalactic, Protoplanetary Disk, and Exoplanetary Molecules. *Astrophys. J. Suppl. Ser.* **2018,** *239* (2), 17.

(30)   Cernicharo, J.; Heras, A. M.; Tielens, A. G. G. M.; Pardo, J. R.; Herpin, F.; Guélin, M.; Waters, L. B. F. M. Infrared Space Observatory's Discovery of C_4H_2, C_6H_2, and Benzene in CRL 618. *Astrophys. J.* **2001,** *546* (2), L123-L126.

(31)   Lee, K. L. K.; McGuire, B. A.; McCarthy, M. C. Gas-Phase Synthetic Pathways to Benzene and Benzonitrile: a Combined Microwave and Thermochemical Investigation. *Phys. Chem. Chem. Phys.* **2019,** *21* (6), 2946-2956.

(32)   Wakelam, V.; Smith, I. W. M.; Herbst, E.; Troe, J.; Geppert, W.; Linnartz, H.; Öberg, K.; Roueff, E.; Agúndez, M.; Pernot, P.; Cuppen, H. M.; Loison, J. C.; Talbi, D. Reaction Networks for Interstellar Chemical Modelling: Improvements and Challenges. *Space Sci. Rev.* **2010,** *156* (1-4), 13-72.

(33)   Broten, N. W.; Oka, T.; Avery, L. W.; MacLeod, J. M.; Kroto, H. W. The Detection of HC_9N in Interstellar Space. *Astrophys. J.* **1978,** *223*, L105-L107.

(34)   Urness, K. N.; Guan, Q.; Golan, A.; Daily, J. W.; Nimlos, M. R.; Stanton, J. F.; Ahmed, M.; Ellison, G. B. Pyrolysis of Furan in a Microreactor. *J. Chem. Phys.* **2013,** *139* (12), 124305.

(35)   Lovas, F. J.; Suenram, R. D.; Ogata, T.; Yamamoto, S. Microwave Spectra and Electric Dipole Moments for Low-*J* Levels of Interstellar Radicals: SO, C_2S, C_3S, *c*-HC_3, CH_2CC, and *c*-C_3H_2. *Astrophys. J.* **1992,** *399*, 325-329.

(36)   Abeysekera, C.; Joalland, B.; Ariyasingha, N.; Zack, L. N.; Sims, I. R.; Field, R. W.; Suits, A. G. Product Branching in the Low Temperature Reaction of CN with Propyne by Chirped-Pulse Microwave Spectroscopy in a Uniform Supersonic Flow. *J. Phys. Chem. Lett.* **2015,** *6* (9), 1599-1604.

(37)   Agundez, M.; Wakelam, V. Chemistry of Dark Clouds: Databases, Networks, and Models. *Chem. Rev.* **2013,** *113* (12), 8710-8737.

(38)   Penzias, A. A.; Solomon, P. M.; Wilson, R. W.; Jefferts, K. B. Interstellar Carbon Monosulfide. *Astrophys. J.* **1971,** *168*, L53-L58.

(39)   Yamamoto, S.; Saito, S.; Kawaguchi, K.; Kaifu, N.; Suzuki, H. Laboratory Detection of a new Carbon-Chain Molecule C_3S and Its Astronomical Identification. *Astrophys. J.* **1987,** *317*, L119-L121.

(40)   Frerking, M. A.; Linke, R. A.; Thaddeus, P. Interstellar Isothiocyanic Acid. *Astrophys. J.* **1979,** *234*, L143-L145.

(41)   Halfen, D. T.; Ziurys, L. M.; Brünken, S.; Gottlieb, C. A.; McCarthy, M. C.; Thaddeus, P. Detection of a New Interstellar Molecule: Thiocyanic Acid HSCN. *Astrophys. J.* **2009,** *702* (2), L124-L127.

(42)   Agúndez, M.; Cernicharo, J.; Guélin, M. New Molecules in IRC +10216: Confirmation of C_5S and Tentative Identification of MgCCH, NCCP, and SiH_3CN. *Astron. Astrophys.* **2014,** *570*, A45.

(43)   Kolesniková, L.; Tercero, B.; Cernicharo, J.; Alonso, J. L.; Daly, A. M.; Gordon, B. P.; Shipman, S. T. Spectroscopic Characterization and Detection of Ethyl Mercaptan in Orion. *Astrophys. J.* **2014,** *784* (1), L7.

(44)   Müller, H. S. P.; Belloche, A.; Xu, L.-H.; Lees, R. M.; Garrod, R. T.; Walters, A.; van Wijngaarden, J.; Lewen, F.; Schlemmer, S.; Menten, K. M. Exploring

Molecular Complexity with ALMA (EMoCA): Alkanethiols and Alkanols in Sagittarius B2(N2). *Astron. Astrophys.* **2016,** *587*, A92.

(45)   Vidal, T. H. G.; Wakelam, V. A New Look at Sulphur Chemistry in Hot Cores and Corinos. *Mon. Notices Royal Astron. Soc.* **2018,** *474* (4), 5575-5587.

(46)   Palumbo, M. E.; Geballe, T. R.; Tielens, A. G. G. M. Solid Carbonyl Sulfide (OCS) in Dense Molecular Clouds. *Astrophys. J.* **1997,** *479* (2), 839-844.

(47)   Sakai, N.; Sakai, T.; Hirota, T.; Watanabe, Y.; Ceccarelli, C.; Kahane, C.; Bottinelli, S.; Caux, E.; Demyk, K.; Vastel, C.; Coutens, A.; Taquet, V.; Ohashi, N.; Takakuwa, S.; Yen, H. W.; Aikawa, Y.; Yamamoto, S. Change in the Chemical Composition of Infalling Gas Forming a Disk around a Protostar. *Nature* **2014,** *507* (7490), 78-80.

(48)   Podio, L.; Codella, C.; Gueth, F.; Cabrit, S.; Bachiller, R.; Gusdorf, A.; Lee, C. F.; Lefloch, B.; Leurini, S.; Nisini, B.; Tafalla, M. The Jet and the Disk of the HH 212 Low-Mass Protostar Imaged by ALMA: SO and SO_2 Emission. *Astron. Astrophys.* **2015,** *581*, A85.

(49)   Viti, S.; Caselli, P.; Hartquist, T. W.; Williams, D. A. Chemical Signatures of Shocks in Hot Cores. *Astron. Astrophys.* **2001,** *370* (3), 1017-1025.

(50)   Li, J.; Wang, J.; Zhu, Q.; Zhang, J. S.; Li, D. Sulfur-Bearing Molecules in Massive Star-Forming Regions: Observations of OCS, CS, H_2S, and SO. *Astrophys. J.* **2015,** *802* (1), 40.

(51)   Wakelam, V.; Caselli, P.; Ceccarelli, C.; Herbst, E.; Castets, A. Resetting Chemical Clocks of Hot Cores Based on S-Bearing Molecules. *Astron. Astrophys.* **2004,** *422* (1), 159-169.

(52)   Jenkins, E. B. A Unified Representation of Gas-Phase Element Depletions in the Interstellar Medium. *Astrophys. J.* **2009,** *700* (2), 1299-1348.

(53)   Tieftrunk, A.; Pineau des Forets, G.; Schilke, P.; Walmsley, C. M. SO and H_2S

in Low Density Molecular Clouds. *Astron. Astrophys.* **1994,** *289*, 579-596.

(54)   Charnley, S. B. Sulfuretted Molecules in Hot Cores. *Astrophys. J.* **1997,** *481*

(1), 396-405.

(55)   Holdship, J.; Viti, S.; Jimenez-Serra, I.; Lefloch, B.; Codella, C.; Podio, L.;

Benedettini, M.; Fontani, F.; Bachiller, R.; Tafalla, M.; Ceccarelli, C. H_2S in the

L1157-B1 Bow Shock. *Mon. Notices Royal Astron. Soc.* **2016,** *463* (1), 802-810.

(56)   Boogert, A. C. A.; Schutte, W. A.; Helmich, F. P.; Tielens, A. G. G. M.;

Wooden, D. H. Infrared Observations and Laboratory Simulations of Interstellar CH_4

and SO_2. *Astron. Astrophys.* **1997,** *317*, 929-941.

(57)   Agundez, M.; Marcelino, N.; Cernicharo, J.; Tafalla, M. Detection of

Interstellar HCS and its Metastable isomer HSC: New Pieces in the Puzzle of Sulfur

Chemistry. *Astron. Astrophys.* **2018,** *611*, L1.

(58)   Laas, J. C.; Caselli, P. Modeling Sulfur Depletion in Interstellar Clouds

(Accepted Manuscript). *Astron. Astrophys.* **2019**.

(59)   McGuire, B. A.; Martin-Drumel, M. A.; Thorwirth, S.; Brunken, S.; Lattanzi,

V.; Neill, J. L.; Spezzano, S.; Yu, Z.; Zaleski, D. P.; Remijan, A. J.; Pate, B. H.;

McCarthy, M. C. Molecular Polymorphism: Microwave Spectra, Equilibrium

Structures, and an Astronomical Investigation of the HNCS Isomeric Family. *Phys.*

Chem. Chem. Phys. **2016,** *18* (32), 22693-22705.

(60)   Beard, C. I.; Dailey, B. P. The Structure and Dipole Moment of Isothiocyanic

Acid. *J. Chem. Phys.* **1950,** *18* (11), 1437-1441.

(61)   Niedenhoff, M.; Yamada, K. M. T.; Winnewisser, G. Pure Rotational Spectra

of HNCS in the Far Infrared Region: The Three Bending Excited States. *J. Mol.*

Spectrosc. **1997,** *183* (1), 176-199.

(62)   Hirota, T.; Yamamoto, S.; Mikami, H.; Ohishi, M. Abundances of HCN and HNC in Dark Cloud Cores. *Astrophys. J.* **1998,** *503* (2), 717-728.

(63)   Brünken, S.; Yu, Z.; Gottlieb, C. A.; McCarthy, M. C.; Thaddeus, P. Laboratory Detection of Thiocyanic Acid HSCN. *Astrophys. J.* **2009,** *706* (2), 1588-1593.

(64)   Adande, G. R.; Halfen, D. T.; Ziurys, L. M.; Quan, D.; Herbst, E. Observations of the [HNCS]/[HSCN] Ratio in Sgr B2 and TMC-1: Evidence for Low-Temperature Gas-Phase Chemistry. *Astrophys. J.* **2010,** *725* (1), 561-570.

(65)   Cernicharo, J.; Guelin, M. Discovery of the C_8H Radical. *Astron. Astrophys.* **1996,** *309*, L27-L30.

(66)   Sinclair, M. W.; Fourikis, N.; Ribes, J. C.; Robinson, B. J.; Brown, R. D.; Godfrey, P. D. Detection of Interstellar Thioformaldehyde. *Aust. J. Chem.* **1973,** *26* (1), 85.

(67)   Saito, S.; Kawaguchi, K.; Yamamoto, S.; Ohishi, M.; Suzuki, H. Laboratory Detection and Astronomical Identification of a new Free Radical, CCS $^3\Sigma^-$. *Astrophys. J.* **1987,** *317*.

(68)   Gordon, V. D.; McCarthy, M. C.; Apponi, A. J.; Thaddeus, P. Rotational Spectra of Sulfur-Carbon Chains. I. The Radicals C_4S, C_5S, C_6S, C_7S, C_8S, and C_9S. *Astrophys. J., Suppl. Ser.* **2001,** *134* (2), 311-317.

(69)   Hirahara, Y.; Ohshima, Y.; Endo, Y. Pulsed-Discharge-Nozzle Fourier-Transform Microwave Spectroscopy of $HC_3S(^2\Pi_r)$ and $HC_4S(^2\Pi_i)$. *J. Chem. Phys.* **1994,** *101* (9), 7342-7349.

(70)   Gordon, V. D.; McCarthy, M. C.; Apponi, A. J.; Thaddeus, P. Rotational Spectra of Sulfur-Carbon Chains. II. HC_5S, HC_6S, HC_7S, and HC_8S, and H_2C_4S, H_2C_5S, H_2C_6S, and H_2C_7S. *Astrophys. J., Suppl. Ser.* **2002,** *138* (2), 297-303.

(71)   Georgiou, K.; Kroto, H. W.; Landsberg, B. M. The Microwave Spectrum, Substitution Structure, and Dipole Moment of Thioketen, $H_2C=C=S$. *J. Mol. Spectrosc.* **1979,** *77*, 365-373.

(72)   Brown, R. D.; Dyall, K. G.; Elmes, P. S.; Godfrey, P. D.; McNaughton, D. The Generation, Microwave Spectrum, and Structure of Propadienethione, $H_2C=C=C=S$. *J. Am. Chem. Soc.* **1988,** *110* (3), 789-792.

(73)   Brown, R. D.; Godfrey, P. D.; Champion, R.; Woodruff, M. The Microwave Spectrum of Propynethial, $HC\equiv C\text{-}CHS$. *Aust. J. Chem.* **1982,** *35* (9), 1747-1753.

(74)   McCarthy, M. C.; Zou, L.; Martin-Drumel, M. A. To Kink or Not: A Search for Long-Chain Cumulenones using Microwave Spectral Taxonomy. *J. Chem. Phys.* **2017,** *146* (15), 154301.

(75)   Lee, K. L. K.; Martin-Drumel, M. A.; Lattanzi, V.; McGuire, B. A.; Caselli, P.; McCarthy, M. C. Gas Phase Detection and Rotational Spectroscopy of Ethynethiol, HCCSH. *Mol. Phys.* **2018**, 1-11.

(76)   Sun, W.; Davis, R. L.; Thorwirth, S.; Harding, M. E.; van Wijngaarden, J. A Highly Flexible Molecule: The Peculiar Case of Ethynyl Isothiocyanate HCCNCS. *J. Chem. Phys.* **2018,** *149* (10), 104304.

(77)   Sun, W.; van Wijngaarden, J. Isothiocyanato-Containing Carbon Chains: The Laboratory Detection of HCCCCNCS and NCCCNCS via Rotational Spectroscopy. *J. Phys. Chem. A* **2018,** *122* (38), 7659-7665.

(78)   Chiar, J. E.; Tielens, A. G. G. M.; Adamson, A. J.; Ricca, A. The Structure, Origin, and Evolution of Interstellar Hydrocarbon Grains. *Astrophys. J.* **2013,** *770*, 78.

(79)   Tielens, A. G. G. M. Interstellar Polycyclic Aromatic Hydrocarbon Molecules. *Annu. Rev. Astron. Astrophys.* **2008,** *46* (1), 289-337.

(80)   Lacy, J. H.; Carr, J. S.; Evans, N. J., II; Baas, F.; Achtermann, J. M.; Arens, J. F. Discovery of Interstellar Methane: Observations of Gaseous and Solid CH_4 Absorption toward Young Stars in Molecular Clouds. *Astrophys. J.* **1991,** *376*, 556-560.

(81)   Hinkle, K. W.; Keady, J. J.; Bernath, P. F. Detection of C_3 in the Circumstellar Shell of IRC+10216. *Science* **1988,** *241* (4871), 1319-1322.

(82)   Bernath, P. F.; Hinkle, K. H.; Keady, J. J. Detection of C_5 in the Circumstellar Shell of IRC+10216. *Science* **1989,** *244* (4904), 562-564.

(83)   Charnley, S. B.; Kuan, Y.-J.; Huang, H.-C.; Botta, O.; Butner, H. M.; Cox, N.; Despois, D.; Ehrenfreund, P.; Kisiel, Z.; Lee, Y.-Y.; Markwick, A. J.; Peeters, Z.; Rodgers, S. D. Astronomical Searches for Nitrogen Heterocycles. *Adv. Space Res.* **2005,** *36* (2), 137-145.

(84)   Kolesniková, L.; Daly, A. M.; Alonso, J. L.; Tercero, B.; Cernicharo, J. The Millimeter Wave Tunneling–Rotational Spectrum of Phenol. *J. Mol. Spectrosc.* **2013,** *289*, 13-20.

(85)   McGuire, B. A.; Burkhardt, A. M.; Kalenskii, S.; Shingledecker, C. N.; Remijan, A. J.; Herbst, E.; McCarthy, M. C. Detection of the Aromatic Molecule Benzonitrile (c-C_6H_5CN) in the Interstellar Medium. *Science* **2018,** *359* (6372), 202-205.

(86)   Cherchneff, I.; Barker, J. R.; Tielens, A. G. G. M. Polycyclic Aromatic Hydrocarbon Formation in Carbon-Rich Stellar Envelopes. *Astrophys. J.* **1992,** *401*, 269-287.

Chapter 2.   Fourier transform microwave spectroscopy

2.1 Introduction

In this thesis, the rotational transitions of the molecular species under investigation were studied through microwave spectroscopy. Two types of custom-built Fourier transform microwave (FTMW) spectrometers were exploited to make the measurements. Preliminarily, a broadband chirped pulse (cp) FTMW spectrometer was used to reveal the transitions in the range of several Gigahertz rapidly. The accurate line positions with higher resolution (or smaller linewidths) were ultimately collected using the narrowband Balle-Flygare type spectrometer. In this chapter, the instrumental designs of the two types of FTMW spectrometers are illustrated along with a theoretical overview of microwave spectroscopy and the spectral analysis strategy.

2.2 Microwave spectroscopy

2.2.1 Introduction

Microwave spectroscopy, which measures rotational transitions of gaseous molecules in the microwave region ($\sim 1 - 200$ μm), is a powerful technique that is used to study fundamental chemical physics. It probes the electronic structure of molecules by allowing measurement of dipole moments from the Stark effect and through resolving the nuclear quadrupole hyperfine splitting patterns, establishes the barriers of hindered internal motions, and reveals the nature of weak inter- and intra-

molecular interactions such as van der Waals and hydrogen bonding interactions. Since a rotational spectrum is a direct reflection of the molecular geometry, it is a robust tool to investigate the conformational distribution of molecules in the gas phase, which makes it a reliable technique to verify *ab initio* results calculated from modern computational methods. By measuring the rotational transitions from isotopically substituted species, it provides an applicable methodology for the determination of the molecular structure. Moreover, given the fact that the radiation received by radio telescopes such as Atacama Large Millimetre Array (ALMA) are from rotational emissions of molecules in the radiofrequency range, it is also a key technique to explore the chemical compositions of astronomical objects when laboratory spectra are available for confirmation.

In the following section, a brief theoretical description of microwave spectroscopy is provided by referring to spectroscopy textbooks.[1-3]

2.2.2 Linear tops

The rotational Hamiltonian operator for a rigid linear molecule can be expressed by

$$\hat{H} = \frac{\hat{J}^2}{2I} \tag{2.1}$$

in which $\hat{J}$ represents the total angular momentum operator (exclusive of nuclear spin) and I is the moment of inertia (equal to $\sum_i m_i r_i^2$, where m_i is the atomic mass and r_i is the distance of atom i from the center of mass).

By solving the Schrödinger equation, the energy eigenvalue $F(J)$ is

$$F(J) = \frac{h^2}{8\pi^2 I} J(J+1) = BJ(J+1) \tag{2.2}$$

where J is the rotational quantum number (0, 1, 2, …) and B is known as the rotational constant (in Joules in the above equation). Conventionally, the rotational constant B in unit of MHz or cm^{-1} is used in spectroscopy,

$$B(\text{MHz}) = \frac{h}{8\pi^2 I} \times 10^{-6} \tag{2.3a}$$

$$B(\text{cm}^{-1}) = \frac{h}{8\pi^2 cI} \times 10^{-2} \tag{2.3b}$$

where h = 6.606 × 10^{-34} J·s, c = 2.998 × 10^{10} cm s^{-1}.

The transition intensity is proportional to the square of the transition moment, which is given by

$$\text{Probability of Transition} = \int \psi'^*_{J'M'} \hat{\mu}\, \psi''_{J''M''}\, d\tau \tag{2.4}$$

where $\psi''_{J''M''}$ and $\psi'^*_{J'M'}$ represent the wave function for the initial and final rotational states, J and M are the corresponding total angular momentum quantum number and its projection on the conventional z-axis that is perpendicular to the molecular axis and through the center of mass, and $\hat{\mu}$ is the transition dipole moment operator.

The rotational selection rules for microwave spectroscopy, which define the allowed transitions, are as follows,

1. The molecule must have a permanent dipole moment ($\mu \neq 0$).

2. $\Delta J = \pm 1$.

3. $\Delta M = 0, \pm 1$.

Rule 1 shows that only those molecules which do not have an inversion center have allowed rotational transitions. Rule 2 restrains the transition with frequency,

$$\tilde{\nu}_{J+1\leftarrow J} = F(J') - F(J'') = 2B\,(J'' + 1) \tag{2.5}$$

in which J' represents the quantum number of the upper state and J'' represents the quantum number of the lower state. Rule 3 leads to the selection rule for molecules

26

that are in an applied electric or magnetic field in which the degeneracy with respect to *J* may be removed.

Referring to equation 2.5, the rotational transitions are equally *2B* spaced for a linear closed-shell molecule, as shown in Figure 2.1. The *B* rotational constant can be derived directly from the experimental spectrum and is related to the molecular geometry through the moment of inertia expressed in equation 2.3a and 2.3b.
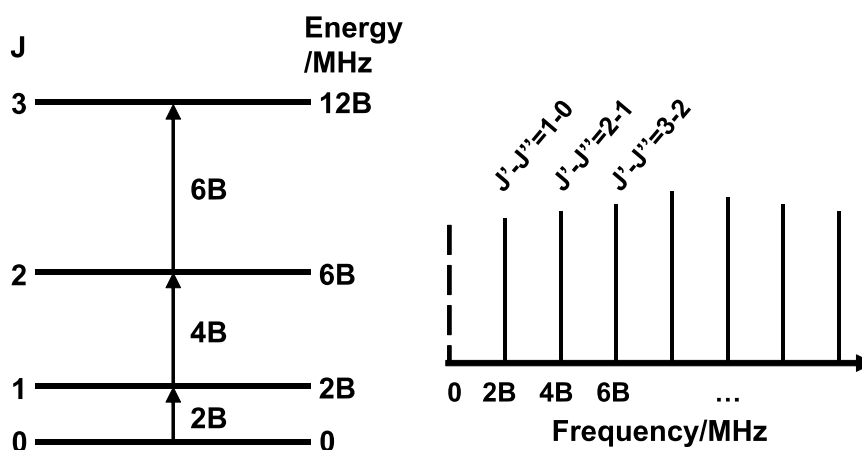
Figure 2.1. Rotational energy diagram (left) of the rigid rotor and the corresponding rotational spectrum associated with the assigned *J'-J''* transitions.

In practice, the molecule is not strictly a rigid rotor. When it rotates, its atoms experience a centrifugal force that distorts the internuclear positions. To treat the molecule as a non-rigid rotor, an additional higher order distortion correction needs to be included in the rotational transition expression, which is given by

$$\tilde{v}_{J+1\leftarrow J} = 2B\,(J+1) - 4D(J+1)^3 \qquad (2.6)$$

where *D* is the centrifugal distortion constant (in MHz or cm^{-1}) and for a diatomic molecule, is related to the vibrational frequency ω in the harmonic approximation,

$$D = \frac{4B^3}{\omega^2} \qquad (2.7)$$

2.2.3 Symmetric tops

Nonlinear molecules with certain symmetry can be classified into three cases based on the values of I_A, I_B, I_C, which are the three moments of inertia for rotation about the a-, b- and c- axes in the principal axis system, respectively,

1. Spherical tops, $I_A = I_B = I_C$, such as CH_4.

2. Prolate tops, $I_A < I_B = I_C$, such as CH_3F.

3. Oblate tops, $I_A = I_B < I_C$, such as NH_3.

For rigid spherical tops, since they have an inversion center, there is no permanent dipole moment and thus no allowed microwave transitions in the ground vibrational state.

For rigid prolate tops ($I_A < I_B = I_C$), the Hamiltonian operator is expressed by

$$\hat{H} = \frac{\hat{J}_a^2}{2I_A} + \frac{\hat{J}_b^2}{2I_B} + \frac{\hat{J}_c^2}{2I_C} = \frac{\hat{J}_a^2}{2I_A} + \frac{1}{2I_B} (\hat{J}_b^2 + \hat{J}_c^2) \tag{2.8}$$

in which $\hat{J}_a^2$, $\hat{J}_b^2$ and $\hat{J}_c^2$ are the rotational angular momentum operators along the a-, b- and c- axes in the principal inertial axis system, respectively.

The rotational constants (in MHz) are expressed to be,

$$A = \frac{h}{8\pi^2 I_A} \times 10^{-6}; \ B = C = \frac{h}{8\pi^2 I_B} \times 10^{-6} \tag{2.9}$$

Likewise, for rigid oblate tops ($I_A = I_B < I_C$), the Hamiltonian operator is

$$\hat{H} = \frac{\hat{J}_a^2}{2I_A} + \frac{\hat{J}_b^2}{2I_B} + \frac{\hat{J}_c^2}{2I_C} = \frac{1}{2I_B} (\hat{J}_a^2 + \hat{J}_b^2) + \frac{\hat{J}_c^2}{2I_C} \tag{2.10}$$

The rotational constants (in MHz) are

$$A = B = \frac{h}{8\pi^2 I_A} \times 10^{-6}; \ C = \frac{h}{8\pi^2 I_C} \times 10^{-6} \tag{2.11}$$

Due to the projection of the rotational angular momentum vector along the axis of symmetry (c-axis), the energy levels for prolate and oblate tops have a

degeneracy of $2J+1$. A second quantum number K is used to label the degeneracy and take values $K = 0, 1, 2, …, J$.

By using the Schrödinger equation and the symmetric top wavefunctions, the energy eigenvalues $F (J, K)$ can be expressed as,

$$F(J,K) = BJ(J + 1) + (A - B)K^2 \text{ (prolate)} \tag{2.12}$$

or

$$F(J,K) = BJ(J + 1) + (C - B)K^2 \text{ (oblate)} \tag{2.13}$$

In this case, the selection rule becomes $\Delta J = \pm 1$, $\Delta M = 0, \pm 1$ and $\Delta K = 0$. The transition frequencies are refined to be,

$$\tilde{v}_{J+1,K \leftarrow J,K} = F(J',K) - F(J'',K) = 2B\ (J'' + 1) \tag{2.14}$$

The spectral pattern is shown as below,
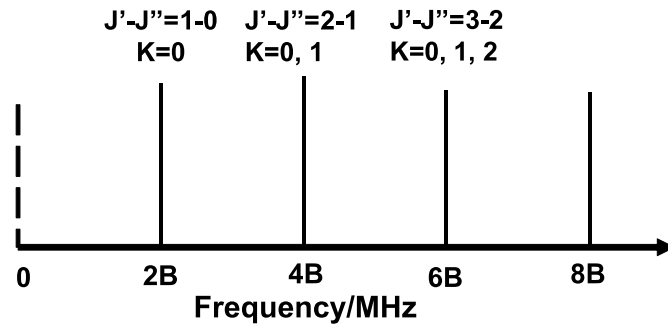
Figure 2.2. Rotational spectral pattern of a symmetric top with assigned J and K quantum numbers.

When the restriction of rigidness is removed, symmetric tops are affected by centrifugal distortion as they rotate. Three distortion constants D_J, D_K, D_{JK} are included to express the effect.

For a prolate top, for example, the expression of the energy levels is altered by,

$$F(J,K) = BJ(J+1) - D_J\big(J(J+1)\big)^2 + (A-B)K^2 - D_K K^4$$

$$- D_{JK}J(J+1)K^2 \qquad (2.15)$$

The frequencies of the transitions are derived as,

$$\tilde{v}_{J+1,K\leftarrow J,K} = F(J',K) - F(J'',K)$$

$$= 2B\,(J''+1) - 4D_J(J''+1)^3 - 2D_{JK}(J+1)K^2 \qquad (2.16)$$

Owing to the D_{JK} term in Equation 2.16, each J'-J'' transition in the simple pure

rotational spectrum (Figure 2.2) now splits out into K frequency components.

2.2.4 Asymmetric tops

With reduced molecular symmetry, the Hamiltonian operator for a rigid

asymmetric rotor ($I_A < I_B < I_C$) is expressed by,

$$\hat{H} = \frac{\hat{J}_a^2}{2I_A} + \frac{\hat{J}_b^2}{2I_B} + \frac{\hat{J}_c^2}{2I_C} \qquad (2.17)$$

Although for rigid rotors, exact solutions can be reached for certain J quantum

numbers, there is no analytic solution of the Schrödinger equation for general

asymmetric tops. The solutions can be obtained only numerically using symmetric

rotor basis functions.

The rotational constants (in MHz) are given by,

$$A = \frac{h}{8\pi^2 I_A} \times 10^{-6}; \; B = \frac{h}{8\pi^2 I_B} \times 10^{-6}; \; C = \frac{h}{8\pi^2 I_C} \times 10^{-6} \qquad (2.18)$$

The energy levels are labelled as J_{KaKc}, where K_a and K_c are convenient labels

to correlate energy levels in the prolate ($K_a = K$) and oblate ($K_c = K$) symmetric top

limits and the sum of them equals to J or $J+1$, as shown in Figure 2.3. Note that, for

prolate and oblate symmetric tops, K_a and K_c are good quantum numbers while they

are not for asymmetric tops.

Prolate top   **Asymmetric top**   **Oblate top**

2 ⎡ 2
2 ⎨ 1
  ⎩ 0

2_{20}
2_{21}
2_{11}
2_{12}
2_{02}

0
1 ⎤ 2
2 ⎦

1 ⎡ 1
  ⎩ 0

1_{10}
1_{11}
1_{01}

0
1 ⎤ 1

0_{00}

0 — 0   0 — 0

J K_a $J_{K_aK_c}$ K_c J
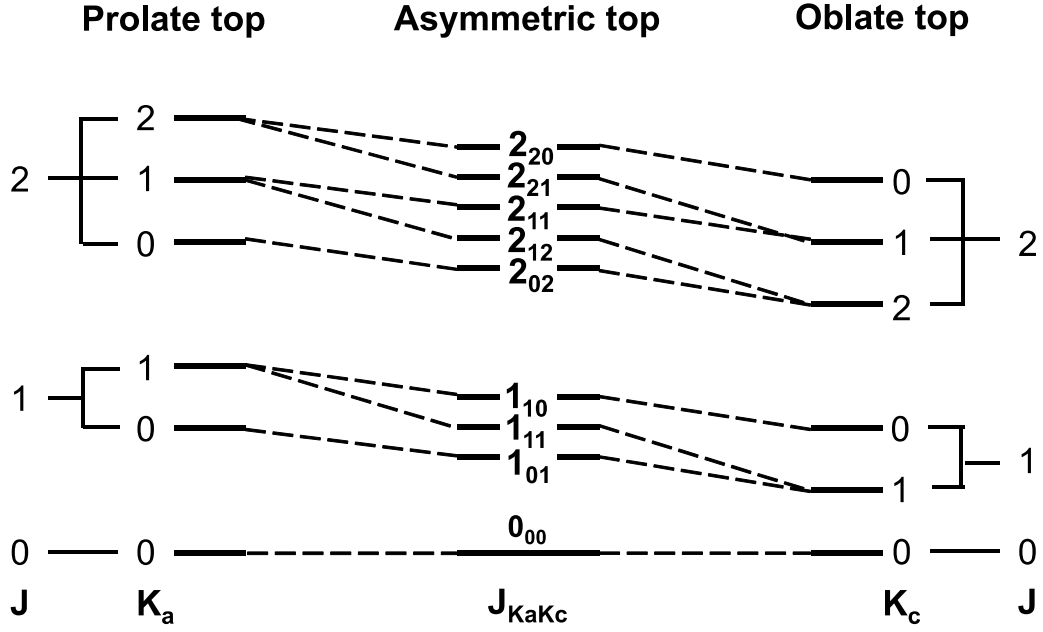
Figure 2.3. Correlation diagram for labelling the energy levels of asymmetric tops. Prolate and oblate tops are their symmetric limits.

In terms of the selection rules, the allowed transitions are classified into three cases owing to the fact that the dipole moment has three components μ_a, μ_b, and μ_c along the a-, b-, and c- axis, respectively. For a given non-zero dipole component, besides $\Delta J = 0, \pm 1$ and $\Delta M = 0, \pm 1$, the transitions also follow

i. a-type transitions. If $\mu_a \neq 0$, transitions with $\Delta K_a = 0$ ($\pm 2, \pm 4, \ldots$) and $\Delta K_c = \pm 1$ ($\pm 3, \pm 5, \ldots$) are allowed.

ii. b-type transitions. If $\mu_b \neq 0$, transitions with $\Delta K_a = \pm 1$ ($\pm 3, \pm 5, \ldots$) and $\Delta K_c = \pm 1$ ($\pm 3, \pm 5, \ldots$) are allowed.

iii. c-type transitions. If $\mu_c \neq 0$, transitions with $\Delta K_a = \pm 1$ ($\pm 3, \pm 5, \ldots$) and $\Delta K_c = 0$ ($\pm 2, \pm 4, \ldots$) are allowed.

For a molecule with low symmetry, all three types could occur together so that some related transitions could form closed loops, as illustrated in Figure 2.4. In this diagram, $v(2_{02}\text{-}1_{10}) + v(1_{10}\text{-}0_{00}) = v(2_{02}\text{-}1_{11}) + v(1_{11}\text{-}0_{00}) = v(2_{02}\text{-}1_{01}) + v(1_{01}\text{-}0_{00})$.

To treat the distortion under the effect of centrifugal forces for non-rigid asymmetric rotors, five centrifugal distortion constants D_J, D_K, D_{JK}, d_J, d_K, are commonly used to express the extent of centrifugal distortion up to the quartic level. If necessary, higher-order distortion corrections can be included in the expression.
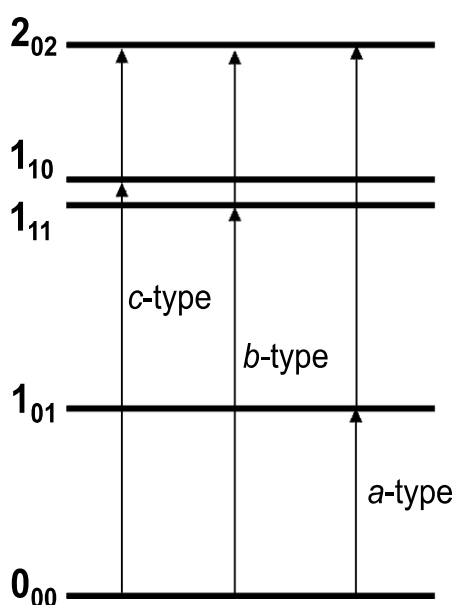
Figure 2.4. *a*-, *b*-, *c*-type rotational transitions.

2.2.5 Nuclear quadrupole interaction

When there is one atom or more with a nuclear spin higher than 1/2 in the molecule, such as ^{14}N isotope ($I = 1$), a signature hyperfine structure can often be observed in the molecular rotational spectrum. This phenomenon arises from the interaction of the non-zero nuclear quadrupole moment with the nonspherical electric field gradient at the nucleus generated by the electrons. Note that, when the isotope

has a spin of 0 or 1/2, the nuclear charge is spherically distributed and hence has no quadrupole moment, which makes the interaction unfeasible.

For the rotating molecule with a single quadrupolar nucleus in an external-field-free environment, the nuclear spin $\vec{I}$ is coupled to the molecular rotational angular momentum $\vec{J}$ (exclusive of nuclear spin) to form a resultant quantum number $\vec{F}$, which is used to represent the total angular momentum instead of $\vec{J}$ in this case. The good quantum number F can then adopt values of $J + I$, $J + I - 1$, $J + I - 2$, …, $| J - I |$. The vector diagram and an example of the energy diagram are illustrated in Figure 2.5. The selection rules for hyperfine transitions are $\Delta F = 0, \pm 1$.
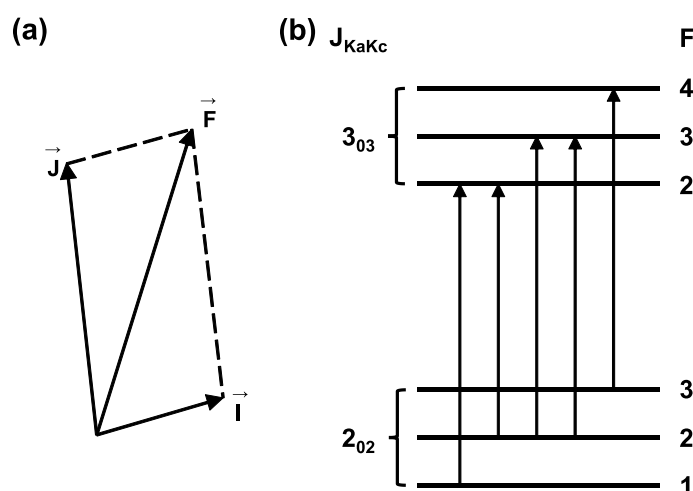
Figure 2.5. (a) Vector diagram of the nuclear quadrupole coupling of one nucleus where $\vec{I}$ is the nuclear spin and $\vec{J}$ is the rotational angular momentum of the molecule. (b) The energy diagram showing the hyperfine splitting arising from nuclear spin $I = 1$ for the 3_{03}-2_{02} rotational transition. The energy levels are not to scale.

For the rotating molecule with more than one coupling nucleus, the hyperfine structure is more complicated. The coupling of each nucleus affects the averaged electric field gradient as well as the interactions of the electric field with all other

coupling nuclei. In the model, $\vec{I_1}$ and $\vec{I_2}$ represent the nuclear spins of the first and second nucleus. While other coupling schemes work, in this thesis, I have used the convention that the quantum number F_1 takes values $J + I_1, J + I_1 - 1, J + I_1 - 2, \ldots, |J - I_1|$ and the final F equals to $F_1 + I_2, F_1 + I_2 - 1, F_1 + I_2 - 2, \ldots, |F_1 - I_2|$. The vector diagram for two coupling nuclei and an example of the energy diagram are given in Figure 2.6. The selection rules for F_1 and F are $\Delta F_1 = 0, \pm 1$ and $\Delta F = 0, \pm 1$, respectively. By resolving the hyperfine structure, high resolution microwave spectroscopy provides a tool to deeply investigate the physical properties of the electronic structure and chemical bonding of molecules.
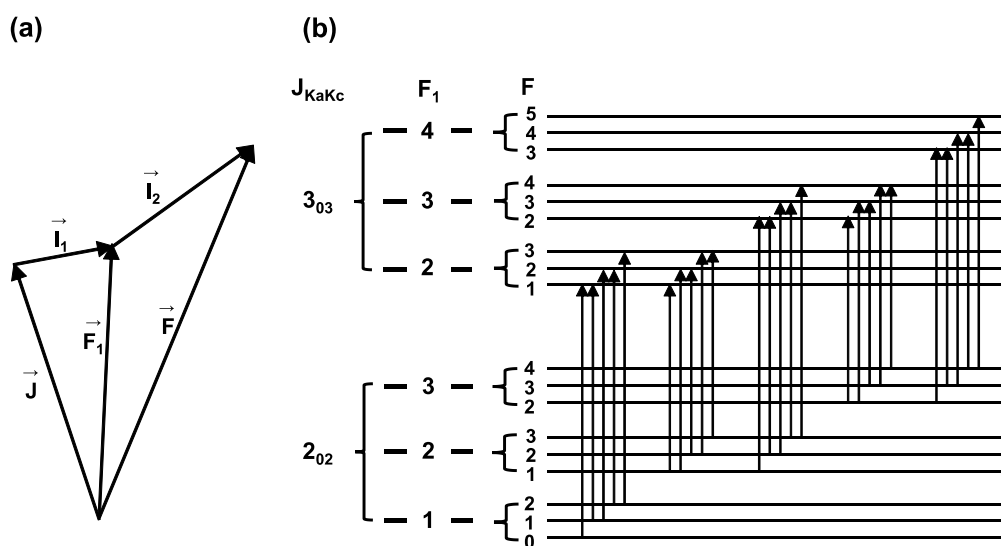
Figure 2.6. (a) Vector diagram of the nuclear quadrupole coupling of two nuclei where $\vec{J}$ is the rotational angular momentum, $\vec{I_1}$ and $\vec{I_2}$ are the spin of the first and second nucleus. (b) The energy diagram of the hyperfine structure arising from two nuclear spin $I = 1$ for the 3_{03}-2_{02} rotational transition. The energy levels are not to scale.

2.2.6 *l*-type doubling

Another topic that will be included in the following thesis is *l*-type doubling. This type of splitting happens to linear polyatomic molecular species and can only be observed for the rotational transitions involving bending vibrational states. When a linear polyatomic molecule bends, it can vibrate in two mutually orthogonal planes. The vibrational transitions corresponding to the bending modes are doubly degenerate. Therefore, the associated rotational transitions in these vibrational states are doubly degenerate as well. As the molecule rotates, the rotational angular momentum and vibrational angular momentum would interact to remove this degeneracy. Ultimately, the pure rotational transition within the bending vibrational states and the rovibrational transitions between the ground state and the vibrational state are split.
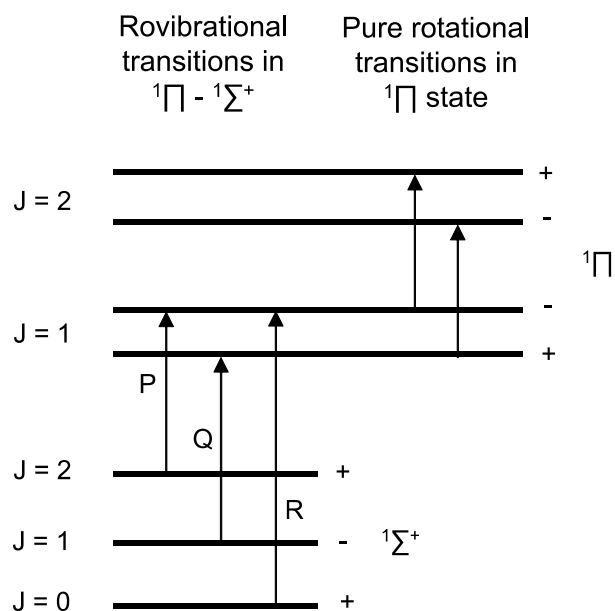
Figure 2.7. Diagram of the energy levels for the rovibrational transitions between the ground state and the bending vibrational state (left) and the pure rotational transitions

within the ground state and the higher vibrational state (right). P, Q, R branches stand for three types of rovibrational transitions. The energy levels are not to scale.

The splitting Δv is given by,

$$\Delta v = qJ(J + 1) \qquad (2.19)$$

where q is called the l-type doubling constant. In this model, $+/-$ labels are used to represent the total parity of the split energy levels for each J and the selection rule is $+ \leftrightarrow -$. The energy-level diagram is shown in Figure 2.7.

2.3 Microwave spectroscopy instrumentation

2.3.1 Introduction

In the current thesis, two types of custom-built FTMW spectrometers, which are the narrowband Balle-Flygare type FTMW spectrometer and the broadband chirped pulse FTMW (cp-FTMW) spectrometer, were employed to record the pure rotational transitions in the microwave region. In the experiments, the studied samples, which are liquidous or gaseous, are introduced into the spectrometers by a neon carrier gas with a stagnation pressure of ~1 atm through a solenoid pulsed nozzle. Non-volatile liquid samples are prepared in glass vials that allow neon gas to bubble through them and carry vapor into the spectrometers while gas samples and the vapors from volatile liquid samples are usually directly diluted by neon gas into gas mixtures. The gas mixtures expand into the vacuum chamber of the spectrometers in a supersonic jet which cools down the rotational temperature of the molecules to a few Kelvin. In the cold jet, which is a nearly collision-free environment, molecules in the low rotational energy states can be excited to higher states by interacting with coherent microwave radiation. After the microwave excitation pulse, the free

induction decay (FID) corresponding to relaxation of the sample can be recorded in the time domain and Fourier transformed to yield a frequency spectrum.

In this section, the working mechanisms of these two types of FTMW spectrometers are briefly demonstrated.

2.3.2 Balle-Flygare FTMW spectrometer

The custom-built Balle-Flygare FTMW spectrometer in the van Wijngaarden lab[4] at the University of Manitoba is a narrowband spectrometer (1 MHz) that follows the Balle-Flygare design.[5] It can be used to study regular stable molecules, which have rotational transitions lying in the range from 4 to 26 GHz, as well as transient species involved in many chemical processes such as thermal decomposition (pyrolysis). The instrument mainly consists of three parts: the Fabry-Pérot cavity, the excitation and detection circuit and is used to measure individual rotational transitions in a step-wise fashion.
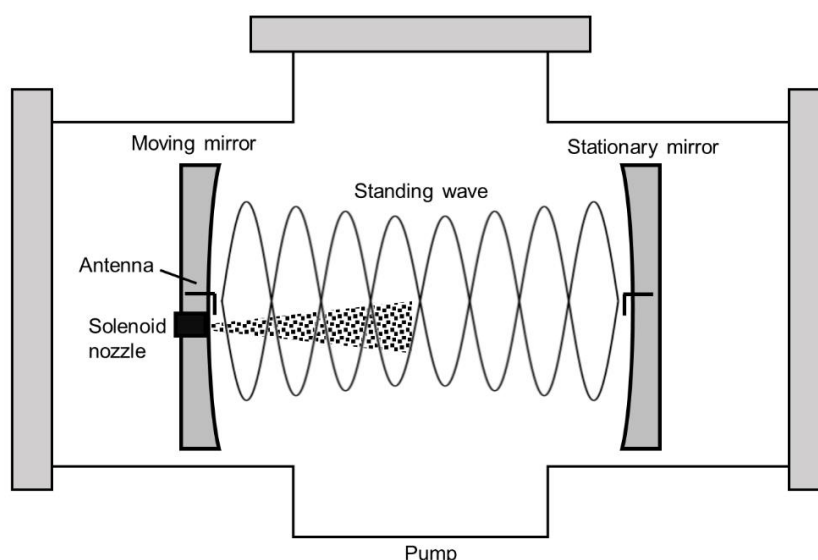
Figure 2.8. The setup inside the vacuum chamber of the Balle-Flygare type FTMW spectrometer.

The Fabry-Pérot cavity is constructed by two spherical aluminum mirrors mounted on four rails inside the large stainless chamber under high vacuum ($\sim 10^{-6}$ Torr). The position of one mirror can be accurately tuned by a motor behind it, while the other one stays still, to form a resonator to trap the microwave signal as shown in Figure 2.8. The cavity resonance is verified using a L-shaped wire hook antenna, which is located at the center of the stationary mirror, connected to a diode detector behind the mirror. At the center of the moving mirror, there is a similar antenna used to broadcast the microwave radiation into the cavity and receive the resulting emission signals from molecules. The pulsed nozzle, which is used to introduce the sample, is located closely below the antenna. In this design, the expansion of the sample is parallel with the cavity axis so that the measured transitions split into doublets due to the Doppler effect, as illustrated in Figure 2.9.
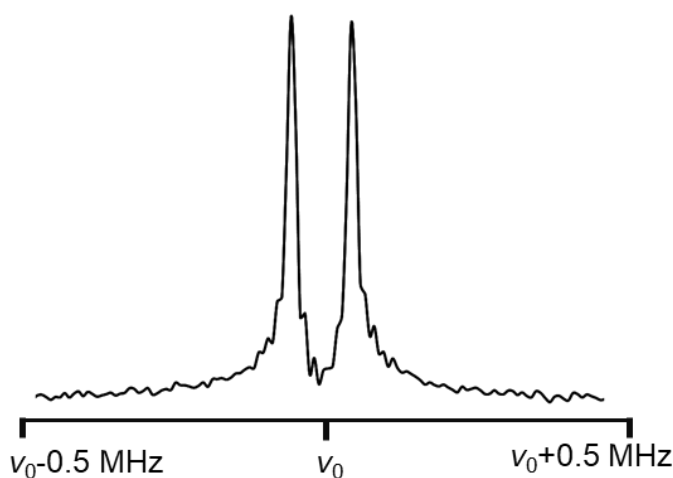
Figure 2.9. A sample spectrum of the split transitions centered at v_0 due to the Doppler effect using the Balle-Flygare FTMW spectrometer.

After the cavity is tuned into resonance with the chosen frequency and the gas sample is seeded into the cavity, the coherent microwave signal that excites the gas sample is created by a microwave synthesizer. Since the number of data points that

need to be sampled and digitized for a typical microwave signal is very large, it is more practical to downconvert the signal from the microwave to the radiofrequency to reduce the demand of the signal processing. Therefore, before that, the excitation microwave source is intentionally set 30 MHz below the required transition frequency. A 30 MHz radiofrequency signal is provided to compensate the offset using the tripled output of the 10 MHz reference signal generated by a radiofrequency synthesizer. The created microwave and radiofrequency signals are mixed together by a single sideband mixer to form the coherent radiation at the chosen transition frequency. In this period, the detection circuit is protected from the powerful microwave input using a single pole double throw (SPDT) switch. A simplified scheme of electrical circuit is given in Figure 2.10.
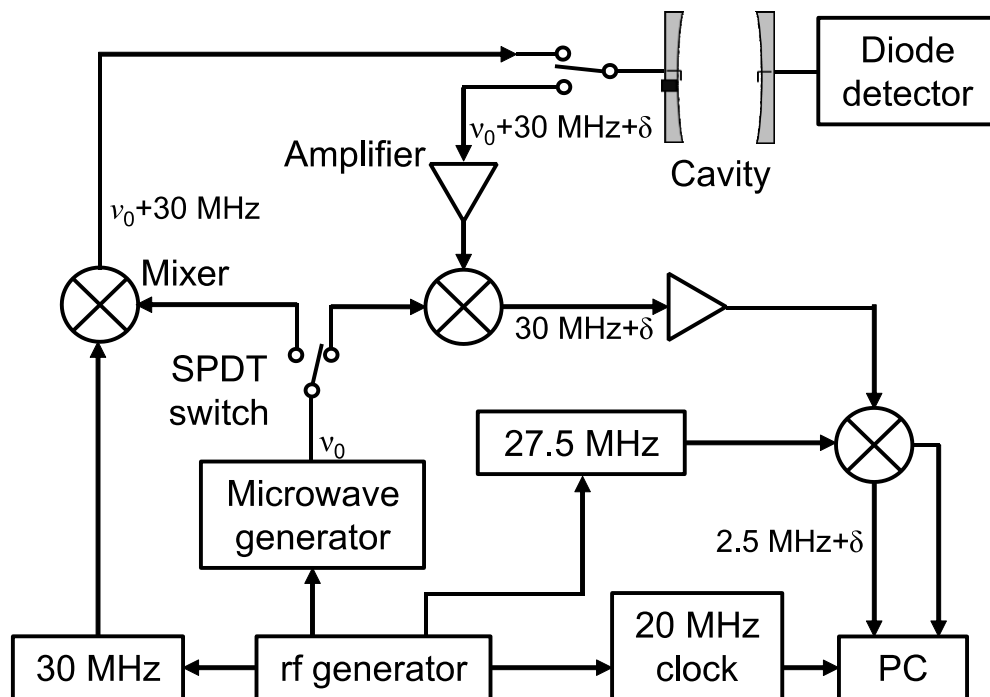
Figure 2.10. A simplified microwave circuit of the Balle-Flygare FTMW spectrometer.

Once generated, the microwave signal pulse with a span of up to 5 µs is introduced into the resonant cavity. In the cavity, the dipole moments of the molecules interact with the polarizing radiation and align to form a macroscopically polarized ensemble. After the microwave pulse, the signal path is switched to the detection circuit to amplify the weak emission signal received by the antenna and record the FID due to the relaxation of the ensemble. The timing of a single data acquisition is illustrated in Figure 2.11.
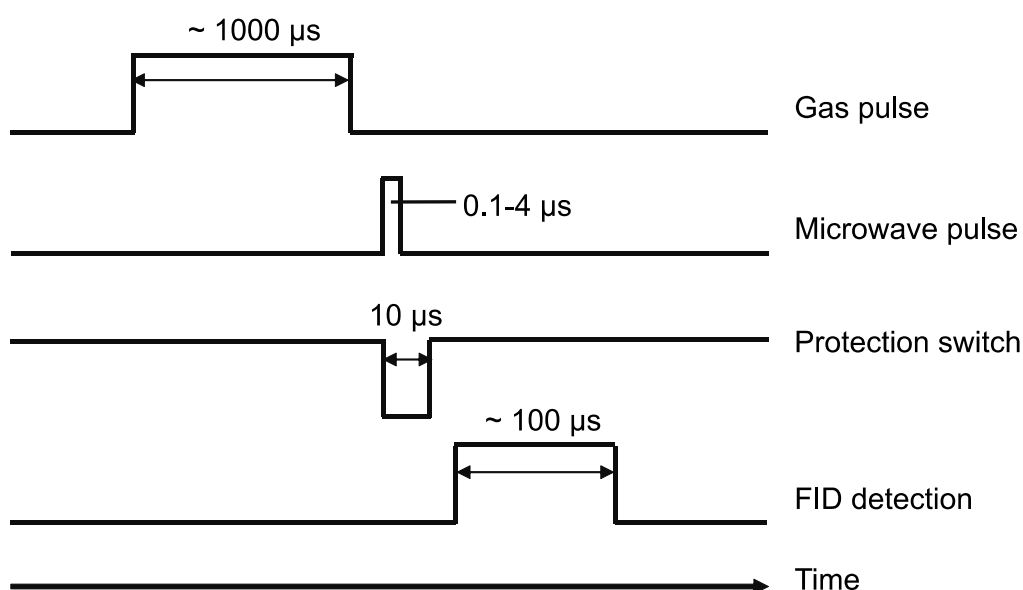
Figure 2.11. A schematic illustration of the timing of a single sample shot carried out by the Balle-Flygare FTMW spectrometer. The time axis is not to scale.

Based on the Nyquist theorem, for a collected FID containing a highest frequency N (in Hertz), the signal must be sampled at least every $1/2\,N$ second to sufficiently characterize the data. In the range of 4 – 26 GHz, directly sampling the data would require an expensive, broadband digitizer. To reduce the technical effort of the signal digitization, the recorded signal in the time domain is downconverted to the radiofrequency range (~30 MHz) by first mixing with the microwave signal from

the microwave generator. It is subsequently downconverted further to ~2.5 MHz by mixing with a 27.5 MHz signal from the radiofrequency synthesizer. Any digitizer with a sampling rate higher than 1.25 MHz is able to process the digitization sufficiently. The collected signal is then digitized by an A/D convertor in the computer and Fourier transformed to a frequency domain spectrum.

As the emission signal is normally weak even below the background noise, it becomes necessary to average a number of phase-synchronized experiment cycles to yield a sufficient signal-to-noise ratio (SNR). In order to guarantee phase synchronization of the repeated FIDs, all frequencies used in the excitation and detection circuit including those used for creating pulses, delays and sampling intervals, are referenced to the same 10 MHz system clock. The typical repetition rate of the experiment is 7 Hz, which is mainly limited by the vacuum throughput. With this design, the instrument achieves a high resolution of ~7 kHz (full width at half max, FWHM) and transitions are typically measured with an accuracy of ~±1 kHz.

2.3.3 Chirped pulse FTMW spectrometer

Different from the narrowband Balle-Flygare type, the cp-FTMW spectrometer, firstly invented by the Pate group at the University of Virginia around 2006,[6] makes it possible to collect a spectrum with a bandwidth of several GHz simultaneously. This scientific innovation improves the speed of the data acquisition ~6000-fold in the van Wijngaarden laboratory by taking advantage of phase-coherent chirped pulses (fast linear frequency sweeps). The custom-built spectrometer that follows the same principle was constructed in 2009[7] and operates in the frequency range of 8 – 18 GHz with a maximum bandwidth of 6 GHz. The instrument design follows the schematic in Figure 2.12.

Pulsed nozzle

Amplifier   Horn antenna

$\nu_0 \pm \nu_w$ SPST
                                                        switch

Mixer ν_0 Microwave
                    synthesizer $\nu_0 \pm \nu_w$

ν_w Microwave ν_0
                                     synthesizer

6 GSa/s ν_w
AWG

PDRO   ←   10 MHz Rb   →   6 GHz
             standard   oscilloscope
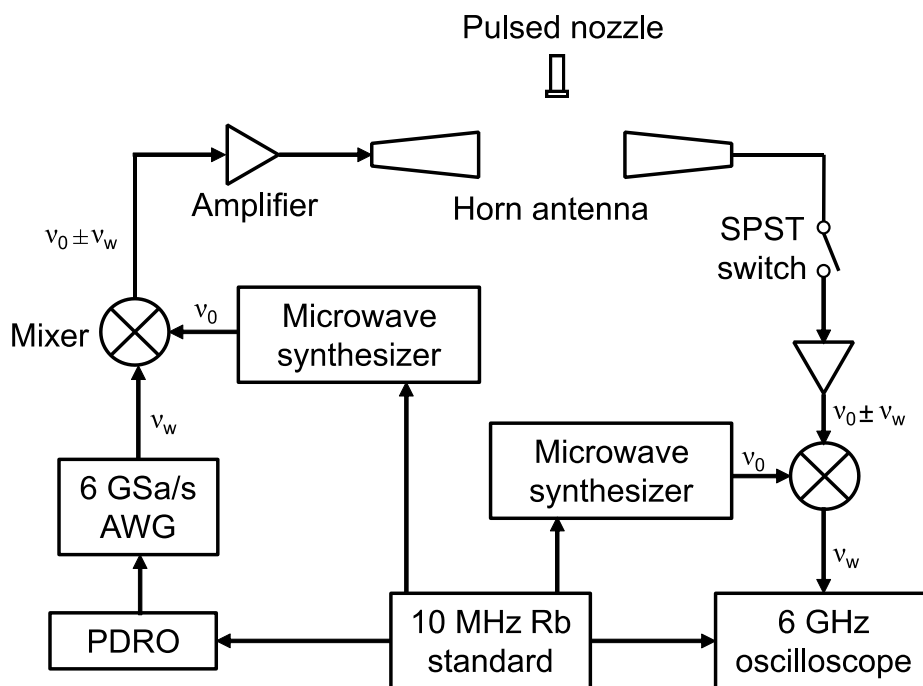
Figure 2.12. A simplified schematic diagram of the chirped pulse FTMW spectrometer design.

In the vacuum chamber, a pair of high gain horn antennae is used to broadcast the chirped microwave pulse and receive the microwave emission as shown in Figure 2.13. The pulsed nozzle is set perpendicular to the radiation axis so that the observed transitions are free of the Doppler effect. The microwave radiation used to excite the molecules is a mixed signal of the center frequency in the range of 8 – 18 GHz output from a microwave signal generator and a chirped pulse signal programmed from an arbitrary waveform generator (AWG). A typical chirped pulse would sweep through 1-3 GHz from the center frequency in the span of 1-5 µs thus creating an excitation pulse sweeping up to 6 GHz. By employing the resulting pulse, the spectrometer is able to excite the sample and ultimately record a broadband spectrum containing rotational transitions across the total bandwidth for each excitation pulse. In contrast, to collect the spectrum with the same span, the cavity of the Balle-Flygare

spectrometer needs to be tuned several thousand times, which is much more time-consuming. Note that, to compensate the loss of the resonator, the microwave input is amplified by a 20 W solid state amplifier before it is sent to the experiment. The amplified signal thus has enough power to sufficiently polarize the sample.
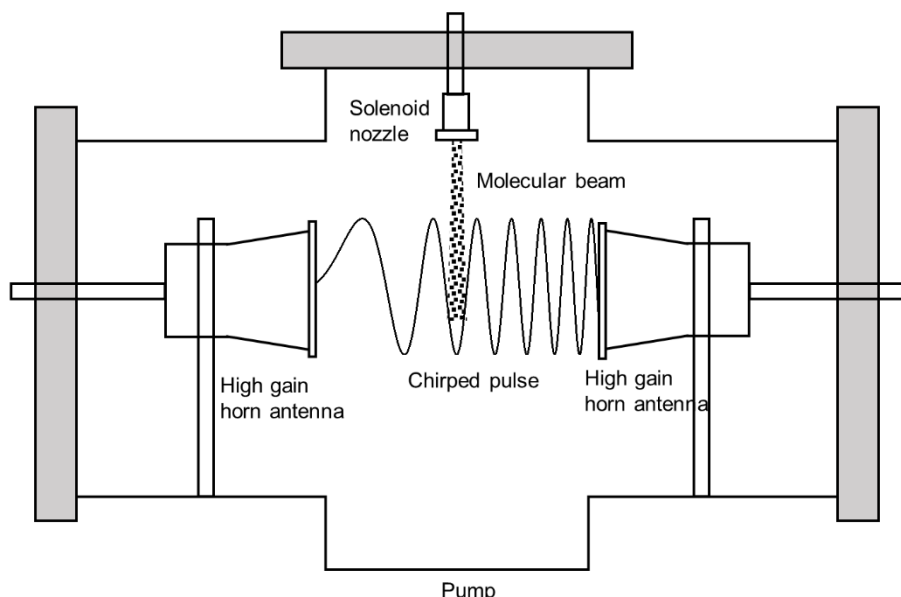
Figure 2.13. The setup inside the vacuum chamber of the chirped pulse FTMW spectrometer.

After the sample is introduced into the vacuum chamber, the high power chirped microwave pulse is broadcast in to excite all transitions simultaneously in the chosen range via the high gain horn antenna. After the chirped pulse, the emission signals are collected by the second horn antenna, amplified and processed by the detection circuit. The application of a powerful broadband oscilloscope with high sampling rate makes the data digitization simpler in contrast with the complicated detection system in Balle-Flygare spectrometer. Instead of mixing down to the radiofrequency range, the amplified emission signal is only downconverted once to shift the center frequency by mixing with the signal generated by a second microwave

synthesizer. The downconverted microwave signal spans the whole bandwidth (up to 6 GHz) of the chirped pulse and is in an appropriate range to be directly digitized by the oscilloscope with a 6 GHz bandwidth and up to 20 GSa/s sampling rate. The processed signal is then Fourier transformed to produce a broadband frequency spectrum, as shown in Figure 2.14.
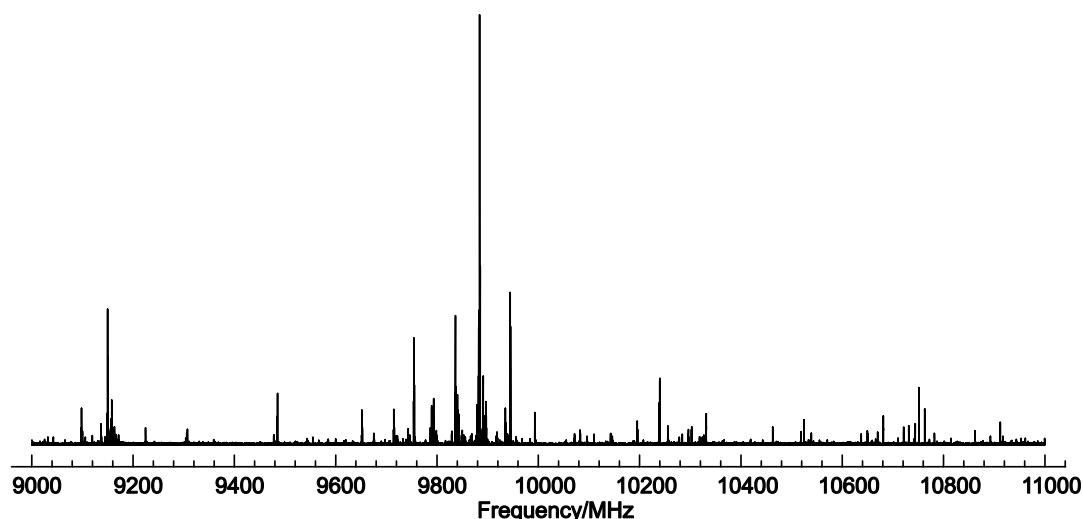
Figure 2.14. A sample broadband spectrum spanning 2 GHz collected using the chirped pulse FTMW spectrometer.

Just like the Balle-Flygare type spectrometer, the recorded molecular emission is very weak, which requires averaging millions of FIDs. The experimental repetition rate is typically 7 Hz and is limited by the data digitization in this spectrometer. To guarantee the phase synchronization of the whole procedure, a 10 MHz rubidium standard is used as a system clock. Besides averaging the signal from multiple experiments, multiple FIDs can be collected and averaged in a single gas pulse by polarizing the same molecular beam multiple times. The timing scheme is given in Figure 2.15.
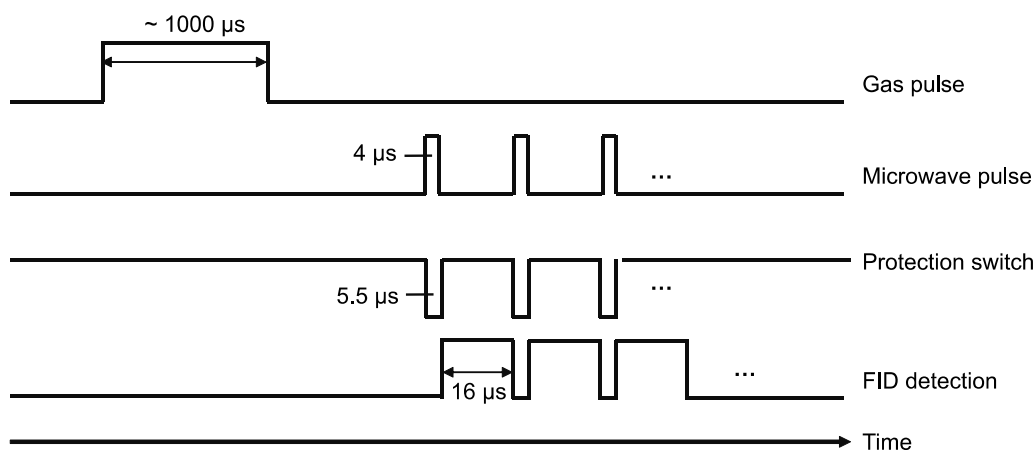
Figure 2.15. The pulse sequence of the multi-FID setup for a single gas shot. The time axis is not to scale.

2.4 Analysis of the spectra

Although the cp-FTMW spectrometer can robustly collect a spectrum spanning several GHz, which is a large improvement in comparison with the <1 MHz window of the Balle-Flygare instrument, it sacrifices sensitivity and resolution to some extent. In the cp-FTMW spectrometer, the perpendicular setup of the pulsed nozzle and the utilization of the high gain horn antennae instead of the coaxial Fabry–Pérot cavity reduce the interacting region and the interaction efficiency, which ultimately affect the sensitivity of the spectrometer. To acquire a spectrum with the same SNR, more FIDs need to be averaged when using the cp-FTMW spectrometer. In practice, a broadband spectrum is usually collected with several million FIDs, while often tens to tens of thousands of FIDs are enough for a narrowband spectrum of a single transition to achieve a comparable SNR using the Balle-Flygare spectrometer.

Moreover, owing to the Doppler broadening, the perpendicular setup of the nozzle in the cp-FTMW spectrometer affects the frequency resolution as well and

typically makes the linewidth ~10 times wider in contrast with the coaxial setup in the Balle-Flygare instrument.[8] Therefore, the cp-FTMW technique does not always have sufficient resolution (FWHM: ~40-100 kHz) to resolve close hyperfine structure arising from the nuclear quadrupole coupling and internal motions. It, thus, is normally used as survey technique to perform preliminary measurements and capture the most intense components. The collected broadband spectra are then used to do the initial fitting to get the rough rotational constants using the PGOPHER spectral simulation and fitting program.[9]

As the starting point, a prediction from *ab initio* rotational constants and dipole moments is often used to understand the observed experimental spectral pattern. If no high theoretical requirements are demanded, geometry optimizations and frequency calculations are carried out typically at the MP2[10] and B3LYP[11] levels of theory with applicable basis sets implemented in the Gaussian 09[12] and Gaussian 16[13] suites of programs. For a polyatomic molecule, multiple conformers may exist. However, in the cold supersonic jet (~5 K), not all stable conformers have sufficient population to be observed. In this case, prior to the geometry optimizations, conformation searches using molecular mechanics (MM) and potential energy surface (PES) scans become crucial to probe possible conformers and give the energy ordering.

Once the spectral pattern of the conformer candidates is recognized, the experimental line positions are manually assigned to the correct transition quantum numbers. The PGOPHER program can then fit the transitions to derive a set of experimental rotational constants with a reasonable error via least squares fitting to a suitable Hamiltonian. The result of such a procedure is illustrated in Figure 2.16 (before fitting) and Figure 2.17 (after fitting). Before fitting, the simulated spectrum

based on *ab initio* rotational constants does not match the experimental spectrum quite so well. By recognizing the pattern of several intense transitions and assigning them to the right peaks which are ~30 MHz shifted in this case, the program is able to fit them into a set of experimental rotational constants. Automatically, the rest of transitions are shifted and match the experimental positions, such as the component beside the 5_{15}-4_{14} rotational transition and the ones on the left side.

After the PGOPHER fitting, transitions in the frequency range of 4 – 26 GHz are predicted using the obtained rotational constants and ultimately measured with high accuracy (~1 kHz) by means of the Balle-Flygare spectrometer. Since the resolution of the Balle-Flygare spectrometer is ~7 kHz, many hyperfine components can be precisely resolved. The final transition frequencies are then fitted using Pickett's SPFIT program to get the refined rotational constants along with other spectroscopic parameters such as the D_J, D_{JK}, D_K, d_J, d_K centrifugal distortion constants.

In terms of isotopically substituted species, since only the number of neutrons varies in the corresponding atomic nuclei, the electronic structure is considered unaffected. However, the change in the atomic mass changes the moments of inertia from that of the normal species which alters the rotational constants and produces a different spectral pattern. If the intensity of the rotational transitions from the normal species is sufficiently high, the same transition from the corresponding singly isotopically substituted species, especially ^{13}C (~1%) and ^{34}S (~4.2%) isotopologues in this work, can be measured in their natural abundances. Thus, the rotational constants for the isotopic species can be obtained and then used to determine the positions of the substituted atoms using the variations in the observed moments of

inertia. As a result, the molecular geometry can be partially derived depending on

how many different isotopes are observed.
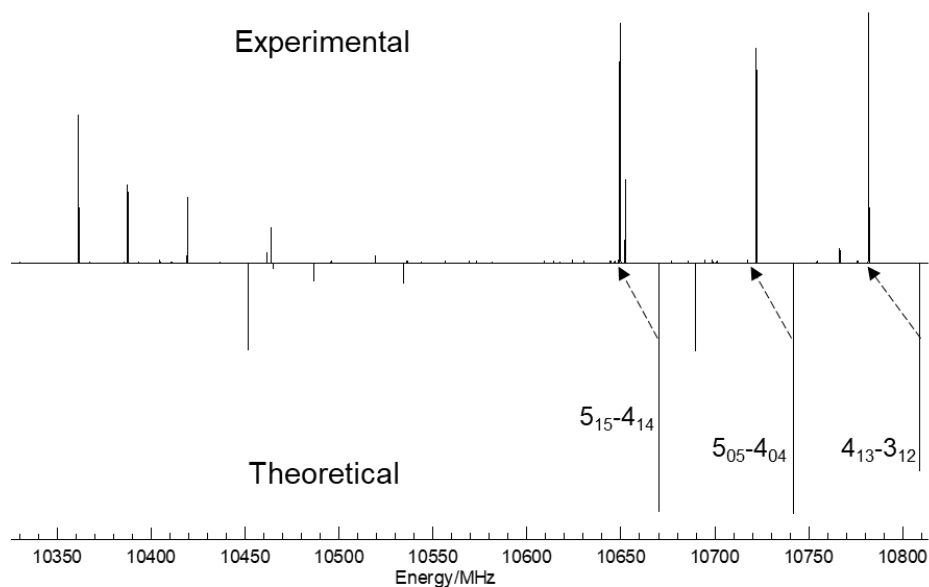
Figure 2.16. A comparison between the experimentally measured spectrum (top) and

the prediction from theoretical rotational constants (bottom).
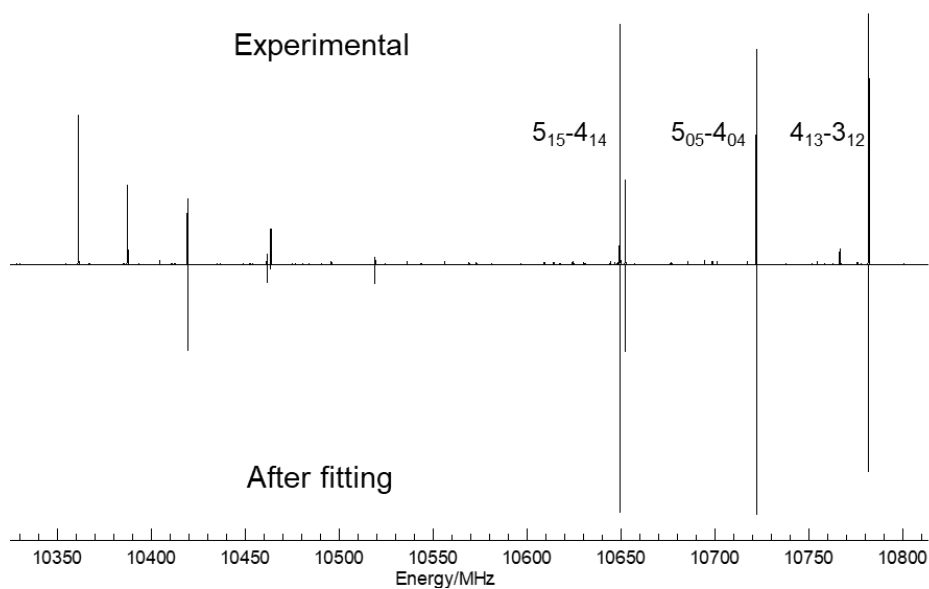
Figure 2.17. The simulation after the spectral fitting (bottom) in comparison with the

original experimental spectrum (top).

To fulfill this purpose, several programs such as STRFIT[14-15] and KRA,[16] can be exploited which are available at the PROSPE website.[17] The KRA program is the one that is used to derive the substitution structures following the aforementioned principles using what are known as Kraitchman's equations.[18] The non-substituted atoms in the molecule are not included in the fit. Moreover, the STRFIT program can be implemented with several other structural treatments, for instance the r_0 fitting which evaluates the effective bond length for the ground vibrational state from the observed ground state rotational constants. In the current thesis work, the ground state effective r_0 structures and the mass dependence r_m structures are normally reported for the studied molecules and are derived using STRFIT. The r_0 geometry is a direct fit from the experimental rotational constants which are measured in the ground vibrational state. For the geometric parameters that involve non-substituted atoms, particularly hydrogen, they are set at the equilibrium r_e values. If a molecule experiences some large-amplitude low-lying vibrational distortions, the r_0 fit may not be able to give a reasonable result. In this case, the mass dependence structure (r_m) is derived instead by accounting for the vibrational contributions.[15]

For each molecule, although the fast broadband survey, which usually takes several hours to record a 2 GHz segment and around one week to cover the whole region from 8 to 18 GHz, dramatically speed up the microwave studies, the subsequent spectral analysis is always the rate-determining step as it may take several months (or years) to fully interpret depending on the complexity. In the following thesis, a detailed spectral analysis will be described for each individual subproject. In Chapter 3, both PhNCO and PhNCS are commercial samples with high purity and only have one conformer. The main effort was required for the assignments of the *b*-type transitions for the parent and the transitions for each heavy atom isotopologue. In

Chapters 4 – 7, with the utilization of the electric discharge to produce some novel species of astrochemical interest from various precursors, the dense spectra contain transitions from both the precursors and many other species created by the discharge. The interpretation of this kind of spectrum is quite tough and will be discussed in detail.

References

(1)   Bernath, P. F. *Spectra of atoms and molecules*. Oxford university press: 2015.

(2)   Gordy, W.; Cook, R. L. *Microwave Molecular Spectra*. Wiley: 1984.

(3)   Hollas, J. M. *Modern spectroscopy*. John Wiley & Sons: 2004.

(4)   Sedo, G.; van Wijngaarden, J. Fourier Transform Microwave Spectra of a "New" Isomer of OCS-CO_2. *J. Chem. Phys.* **2009,** *131* (4), 044303.

(5)   Balle, T. J.; Flygare, W. H. Fabry–Perot Cavity Pulsed Fourier Transform Microwave Spectrometer with a Pulsed Nozzle Particle Source. *Rev. Sci. Instrum.* **1981,** *52* (1), 33-45.

(6)   Brown, G. G.; Dian, B. C.; Douglass, K. O.; Geyer, S. M.; Pate, B. H. The Rotational Spectrum of Epifluorohydrin Measured by Chirped-Pulse Fourier Transform Microwave Spectroscopy. *J. Mol. Spectrosc.* **2006,** *238* (2), 200-212.

(7)   Evangelisti, L.; Sedo, G.; van Wijngaarden, J. Rotational Spectrum of 1,1,1-Trifluoro-2-Butanone Using Chirped-Pulse Fourier Transform Microwave Spectroscopy. *J. Phys. Chem. A* **2011,** *115* (5), 685-90.

(8)   Park, G. B.; Field, R. W. Perspective: The First Ten Years of Broadband Chirped Pulse Fourier Transform Microwave Spectroscopy. *J. Chem. Phys.* **2016,** *144* (20), 200901.

(9)   Pgopher, a Program for Simulating Rotational Structure, C. M. Western, University of Bristol. http://Pgopher.chm.bris.ac.uk.

(10)   Møller, C.; Plesset, M. S. Note on an Approximation Treatment for Many-Electron Systems. *Phys. Rev.* **1934,** *46* (7), 618-622.

(11)   Stephens, P. J.; Devlin, F. J.; Chabalowski, C. F.; Frisch, M. J. *Ab Initio* Calculation of Vibrational Absorption and Circular-Dichroism Spectra Using Density-Functional Force-Fields. *J. Phys. Chem. Lett.* **1994,** *98* (45), 11623-11627.

(12)   Frisch, M. J.; Trucks, G. W.; Schlegel, H. B.; Scuseria, G. E.; Robb, M. A.; Cheeseman, J. R.; Scalmani, G.; Barone, V.; Mennucci, B.; Petersson, G. A.; Nakatsuji, H.; Caricato, M.; Li, X.; Hratchian, H. P.; Izmaylov, A. F.; Bloino, J.; Zheng, G.; Sonnenberg, J. L.; Hada, M.; Ehara, M.; Toyota, K.; Fukuda, R.; Hasegawa, J.; Ishida, M.; Nakajima, T.; Honda, Y.; Kitao, O.; Nakai, H.; Vreven, T.; Montgomery, J. A.; Peralta, J. E.; Ogliaro, F.; Bearpark, M.; Heyd, J. J.; Brothers, E.; Kudin, K. N.; Staroverov, V. N.; Keith, T.; Kobayashi, R.; Normand, J.; Raghavachari, K.; Rendell, A.; Burant, J. C.; Iyengar, S. S.; Tomasi, J.; Cossi, M.; Rega, N.; Millam, J. M.; Klene, M.; Knox, J. E.; Cross, J. B.; Bakken, V.; Adamo, C.; Jaramillo, J.; Gomperts, R.; Stratmann, R. E.; Yazyev, O.; Austin, A. J.; Cammi, R.; Pomelli, C.; Ochterski, J. W.; Martin, R. L.; Morokuma, K.; Zakrzewski, V. G.; Voth, G. A.; Salvador, P.; Dannenberg, J. J.; Dapprich, S.; Daniels, A. D.; Farkas, O.; Foresman, J. B.; Ortiz, J. V.; Cioslowski, J.; Fox, D. J., Gaussian 09, Revision B.01. Wallingford CT, 2010.

(13)   Frisch, M. J.; Trucks, G. W.; Schlegel, H. B.; Scuseria, G. E.; Robb, M. A.; Cheeseman, J. R.; Scalmani, G.; Barone, V.; Petersson, G. A.; Nakatsuji, H.; Li, X.; Caricato, M.; Marenich, A. V.; Bloino, J.; Janesko, B. G.; Gomperts, R.; Mennucci, B.; Hratchian, H. P.; Ortiz, J. V.; Izmaylov, A. F.; Sonnenberg, J. L.; Williams; Ding, F.; Lipparini, F.; Egidi, F.; Goings, J.; Peng, B.; Petrone, A.; Henderson, T.; Ranasinghe, D.; Zakrzewski, V. G.; Gao, J.; Rega, N.; Zheng, G.; Liang, W.; Hada, M.; Ehara, M.; Toyota, K.; Fukuda, R.; Hasegawa, J.; Ishida, M.; Nakajima, T.; Honda, Y.; Kitao, O.; Nakai, H.; Vreven, T.; Throssell, K.; Montgomery Jr., J. A.; Peralta, J. E.; Ogliaro, F.; Bearpark, M. J.; Heyd, J. J.; Brothers, E. N.; Kudin, K. N.; Staroverov, V. N.; Keith, T. A.; Kobayashi, R.; Normand, J.; Raghavachari, K.; Rendell, A. P.; Burant, J. C.; Iyengar, S. S.; Tomasi, J.; Cossi, M.; Millam, J. M.;

Klene, M.; Adamo, C.; Cammi, R.; Ochterski, J. W.; Martin, R. L.; Morokuma, K.; Farkas, O.; Foresman, J. B.; Fox, D. J. *Gaussian 16 Rev. B.01*, Wallingford, CT, 2016.

(14)   Watson, J. K.; Roytburg, A.; Ulrich, W. Least-Squares Mass-Dependence Molecular Structures. *J. Mol. Spectrosc.* **1999,** *196* (1), 102-119.

(15)   Kisiel, Z. Least-Squares Mass-Dependence Molecular Structures for Selected Weakly Bound Intermolecular Clusters. *J. Mol. Spectrosc.* **2003,** *218* (1), 58-67.

(16)   Costain, C. Further Comments on the Accuracy of r_s Substitution Structures. *Trans. Am. Crystallogr. Assoc.* **1966,** *2*, 157-164.

(17)   Kisiel, Z. PROSPE – Programs for ROtational SPEctroscopy. http://www.ifpan.edu.pl/~kisiel/prospe.htm.

(18)   Kraitchman, J. Determination of Molecular Structure from Microwave Spectroscopic Data. *Am. J. Phys.* **1953,** *21* (1), 17-24.

Chapter 3.   Rotational spectra and structures of phenyl isocyanate (PhNCO) and phenyl isothiocyanate (PhNCS)[1]

3.1 Introduction

As briefly overviewed in Chapter 1, several NCO and NCS-containing species have been found in various interstellar molecular clouds. These species include NCO,[1] NCO$^-$,[2] HNCO,[3] HOCN,[4-5] CH$_3$NCO,[6-7] H$_2$NCO$^+$,[1,8] and HNCS,[9-10] HSCN.[10-11] With the presence of the NCO/NCS functional group, they can evolve to a diverse range of biological compounds such as amides and thioamides by reacting with co-existing interstellar species and further provide important information of the chemical evolution and early steps toward life in space.[1] Since these interstellar observations were achieved after their precise spectroscopic characterizations in the laboratory,[4,8,11-14] NCO and NCS-bearing species are of great interest to laboratory astrochemists. Besides the detected species, a number of small sized RNCO and RNCS candidates where R = HCC,[15] C$_2$H$_3$,[16-17] NC,[18-22] C$_2$H$_5$,[23-24] etc. have already been studied using rotational spectroscopy as well.

In this chapter, two commercially available candidates, phenyl isocyanate (PhNCO) and phenyl isothiocyanate (PhNCS), were chosen to be the first topic of the current thesis, which is a good sample to demonstrate the capabilities of the powerful microwave technique. The astrophysical value of these two molecules has been

---

[1] A version of this chapter has been published with the following citation: Sun, W.; Silva, W. G. D. P.; van Wijngaarden, J., Rotational Spectra and Structures of Phenyl Isocyanate and Phenyl Isothiocyanate. J. Phys. Chem. A 2019, 123 (12), 2351-2360. Copyright © 2019 American Chemical Society.

attracting attention from the astronomical community, especially after the recent

detection of the interstellar benzene derivative – benzonitrile (c-C_6H_5CN or PhCN).[25]

Previously, the ground state microwave spectra of the parent PhNCO[26-27] and

PhNCS[26,28] species have been reported including the investigation of their ^{14}N nuclear

quadrupole hyperfine structures.[29] These studies have confirmed that the molecules

are planar with C_s symmetry and overturned the previous assignment in infrared

spectra which were interpreted based on the assumption of C_{2v} symmetry.[30] The

corresponding geometries are shown in Figure 3.1. Later, a low-lying vibrational band

at 100 cm^{-1} was observed for PhNCO, which was first assigned to the in-plane CNC

bending mode[31] but also could be the out-of-plane torsion mode of the NCO group

about the Ph-N bond, which is the key vibration mode that breaks the assumed C_{2v}

symmetry. The vibrational bands for these two modes of PhNCS, both were predicted

at 58 cm^{-1} at the B3LYP/6-311++G(d, p) level, have not been observed to date

experimentally.[32] Apparently, infrared spectroscopy is not an ideal tool to differentiate

between the two symmetries.
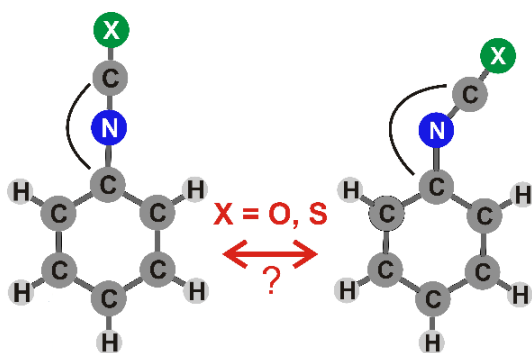
Figure 3.1. The geometry of PhNCX (X = O, S) with C_{2v} (left) and C_s (right)

symmetry.

In the previous microwave studies, only a-type rotational transitions have been

observed, while the signature b-type transitions which are allowed by C_s and

forbidden by C_{2v} symmetry were not observed owing to the small values of the predicted dipole moment along b-axis in the principal axis system. Through re-investigating the microwave spectra of both parent species using the high-sensitivity Fourier transform microwave spectrometers, b-type transitions were assigned for the first time in this work which leaves no doubt to their symmetry properties. Moreover, in order to better understand their geometries, the first microwave spectroscopic study of nine minor isotopologues (seven ^{13}C, one ^{15}N, and one ^{18}O/[34]S) of each species in their natural abundances was carried out. By taking advantage of the high resolution of the cavity-based spectrometer, the rotational constants of each isotopologue were precisely determined. Subsequently, the mass dependence structures ($r_m^{(1)}$) were derived to capture the subtle geometric changes by using the ten sets of rotational constants of each compound for comparsion with computational estimates of the molecular structures. Previous studies on NCO/NCS containing molecules suggest that NCS-bearing species have larger valence bond angles at nitrogen due to the influence of the terminal chalcogen atom, as in the CH_3NCO (140º)[33]/CH_3NCS (151º)[34] and NCNCO (129º)[18]/NCNCS (143º)[20] pairs. As the geometry depends on the electronic structure, to rationalize the subtle differences observed in the experimentally derived geometries, a comprehensive and consistent quantum-chemical investigation including potential energy scans, geometry optimizations and the associated frequency and natural bond orbital (NBO) calculations was performed to understand the observed geometric variations.

3.2 Experimental methods

The PhNCO (98%) and PhNCS ($\geq$ 98.0%) samples were purchased from Sigma Aldrich and used without further purification. Both samples are liquid at room

temperature (mp: -30 ℃ for PhNCO and mp: -21 ℃ for PhNCS) and do not have enough vapor pressure to make a gas mixture owing to the high boiling points (bp: 162-163 ℃ for PhNCO and bp: 218 ℃ for PhNCS). A few milliliters of them were transferred into separate glass vessels that allow the neon gas to bubble through them and deliver their vapors to the pulsed nozzle of the spectrometers. The typical stagnation pressure was set at ~1 atm. Preliminary measurements were performed using the broadband cp-FTMW spectrometer[35] with a bandwidth of 2 GHz in the frequency range of 8 – 18 GHz. This allowed the assignment of rotational transitions for the parent species of PhNCO and PhNCS as well as for their minor isotopologues (^{13}C, ^{15}N, ^{18}O and ^{34}S) in natural abundance. A 140 MHz portion of the broadband spectrum of PhNCO is provided in Figure 3.2 showing the $6_{06}-5_{05}$ rotational transition for the parent species along with that of the six ^{13}C and one ^{15}N minor isotopologues
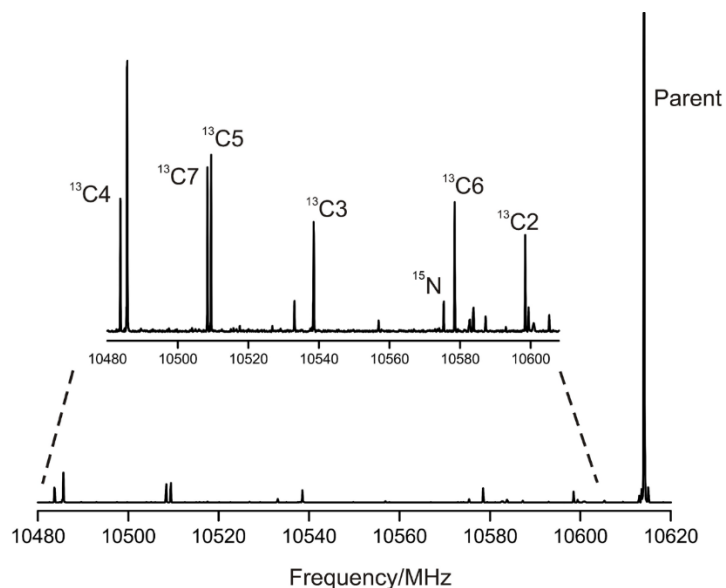
Figure 3.2. 140 MHz portion of the cp-FTMW spectrum collected with 1.5 million FIDs showing the relative intensity of the rotational transition $6_{06}-5_{05}$ for the parent PhNCO species, six ^{13}C and one ^{15}N minor isotopologues.

After the preliminary assignment, individual rotational transitions were collected using the narrowband Balle-Flygare FTMW spectrometer[36] from 4 to 26 GHz. The collected 6_{16}-5_{15} rotational transition is shown in Figure 3.3 with the resolved hyperfine structure arising from the ^{14}N quadrupolar nucleus. Each hyperfine transition appears as doublet in the Balle-Flygare spectrum due to the Doppler effect. The linewidth is typically ~7 kHz and the frequency uncertainty is ~ ±1 kHz.
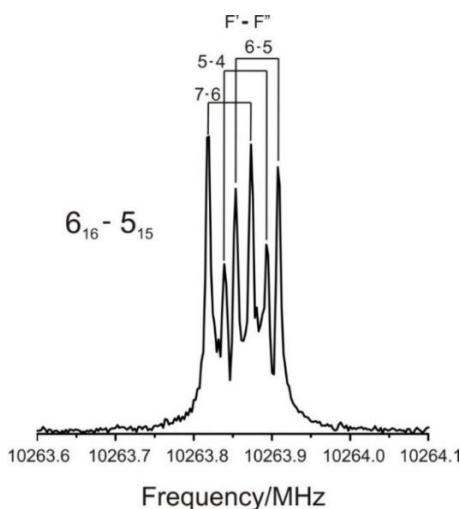
Figure 3.3. Sample of FTMW spectrum (800 cycles) of the 6_{16}-5_{15} rotational transition of PhNCO showing the ^{14}N hyperfine structure.

3.3 Computational details

Quantum chemical calculations were performed to obtain optimized geometries and frequencies using the MP2,[37] B3LYP[38] and B3LYP-D3(BJ)[39] methods with the Dunning's aug-cc-pVTZ basis set[40-42] implemented in the Gaussian 16 program.[43] From the optimized structures, information about the rotational constants, electric dipole components, and the ^{14}N nuclear coupling constants was extracted to assist with the interpretation of the rotational spectra. The resulting equilibrium

structures of PhNCO and PhNCS are shown in their principal axis systems in Figure 3.4.
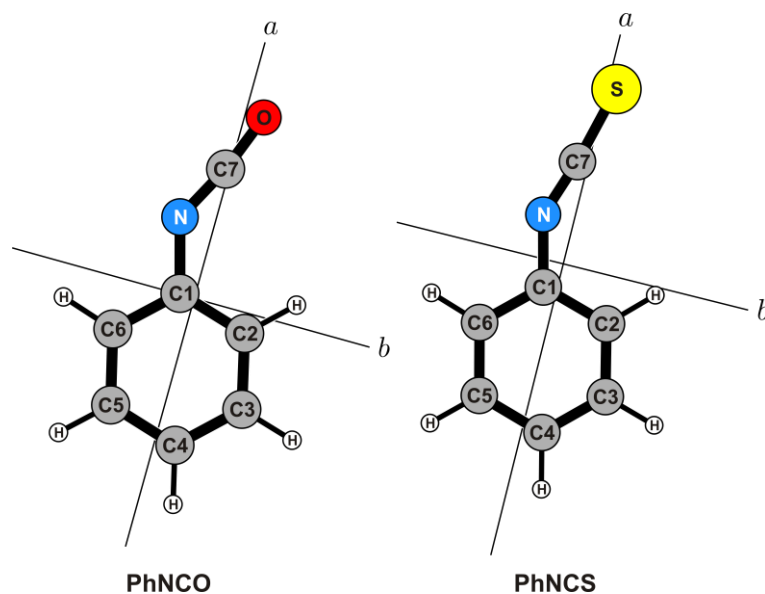
Figure 3.4. Equilibrium geometries of PhNCO and PhNCS in the principal axis system obtained at the MP2/aug-cc-pVTZ level of theory.

To further investigate the energy profiles corresponding to the lowest energy in-plane and out-of-plane vibrational modes, two potential energy scans were carried out about the bending of the ∠C1NC7 angle and torsion about the C1-N bond at each level of theory. In the first scan, ∠C1NC7 was varied from 120º to 180º in steps of 3º within the phenyl plane whereas in the second one, the C2-C1-N-C7 dihedral angle was rotated from 0º to 90º in steps of 10º. During the scan calculations, all other geometrical parameters were relaxed. The potential energy curves are given in Figure 3.5. Note that, when the dihedral angle was set to 90º for PhNCS in the second scan, the relaxed ∠C1NC7 was optimized to be 180º which is the same geometry at 180º in the C1NC7 bending scan.

To better understand the geometries and gain insights into the electronic structure properties of PhNCO and PhNCS, natural bond orbital (NBO) analysis was performed on the equilibrium geometries optimized at the MP2 level. The NBO calculations were carried out using the NBO 6.0 routine[44] at the B3LYP/aug-cc-pVTZ level.
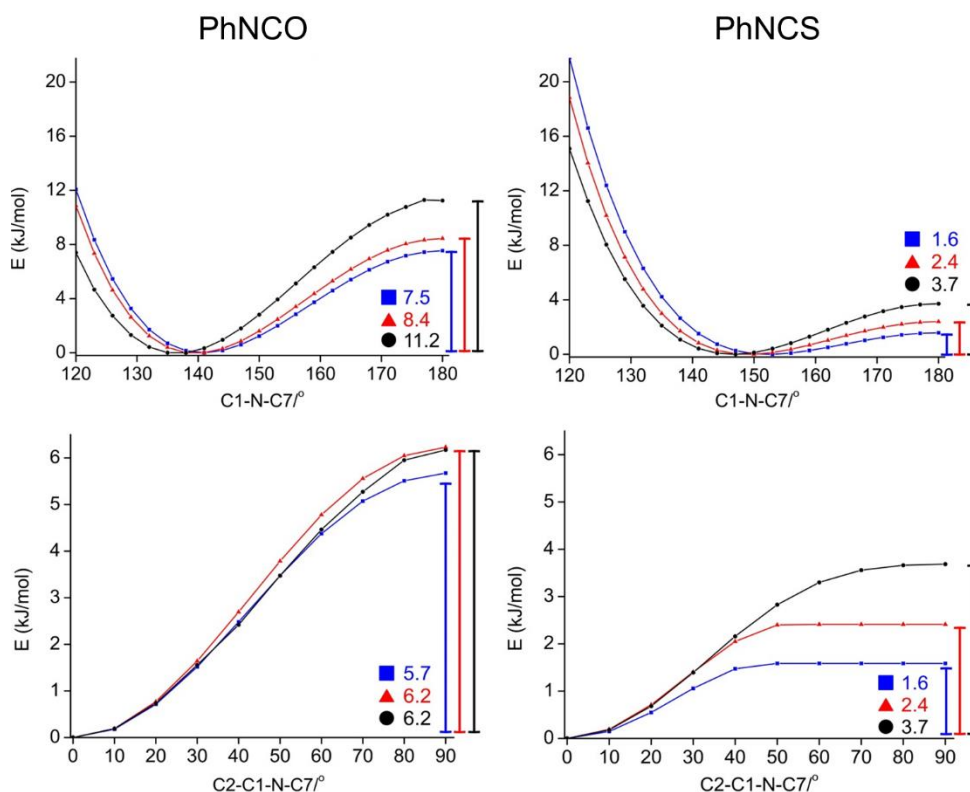
Figure 3.5. Potential energy curves for the ∠C1NC7 angle and the ∠C2C1NC7 dihedral angle for PhNCO and PhNCS.

3.4 Spectral analysis

According to *ab initio* calculations, the absolute values of the dipole moment components of PhNCO were calculated to be 2.77 D and 0.28 D along *a-* and *b-* principal axes, respectively, at the MP2/aug-cc-pVTZ level of theory. The theoretical prediction is comparable with the previous experimental result from Stark

measurements $|\mu_a| = 2.50 \pm 0.02$ D and $|\mu_b| < 0.2$ D.[27] Due to the larger μ_a dipole component, the rotational spectrum is dominated by the a-type rotational transitions. Indeed, 208 a-type transitions with the resolved hyperfine structures were collected for the parent species ranging from $J' = 3 - 11$. Moreover, 36 b-type transitions were measured with relatively low intensity for the first time. Furthermore, the rotational transitions corresponding to each minor isotopologue were assigned. In total, 30 transitions were recorded for the ^{15}N isotopologue along with 41 transitions due to the ^{18}O isotopologue and 60 transitions corresponding to each of the six ^{13}C isotopologues except C1. For the ^{13}C1 isotopologue, as the position of C1 is close to the center of mass, most of the rotational transitions are overshadowed by the analogous transition of the parent species and thus, only 18 lines were measured.

Similarly, PhNCS is predicted to have dipole moment components of $|\mu_a| = 3.15$ D and $|\mu_b| = 0.29$ D (MP2/aug-cc-pVTZ), which indicates that the rotational spectrum of this species is also dominated by a-type rotational transitions. In total, 214 rotational transitions, including 189 a-type and 25 b-type, ranging from $J' = 2 - 15$ were measured for the parent species. The intensities of the observed transitions were sufficient to proceed with the identification of 65 a-type rotational transitions corresponding to the ^{34}S isotopologue, 20 due to the ^{15}N isotopologue, and more than 27 for each of the seven ^{13}C isotopologues.

The rotational, centrifugal distortion, and ^{14}N nuclear quadrupole coupling constants were determined for each compound by fitting the observed rotational transitions using Pickett's SPFIT program[45] set to Watson's A-reduced Hamiltonian.[46] The final results for PhNCO and PhNCS are provided in Tables 3.1 and 3.2, respectively.

Table 3.1. Ground state spectroscopic constants obtained for PHNCO and its isotopologues.

	normal	^{13}C1	^{13}C2	^{13}C3	^{13}C4	^{13}C5	^{13}C6	^{13}C7	^{15}N	^{18}O
Rotational Constants[a] /MHz										
A	5201.7138(3)	5197.76(2)	5142.347(7)	5101.517(9)	5194.081(9)	5154.498(9)	5114.580(8)	5201.243(9)	5178.363(5)	5188.98(2)
B	972.68164(2)	972.714(1)	972.46023(7)	967.23964(8)	959.45580(8)	962.9936(1)	971.06000(9)	961.82997(8)	969.23042(6)	929.1584(1)
C	819.62560(2)	819.5501(4)	817.98219(4)	813.24982(6)	810.03060(6)	811.57503(6)	816.28202(6)	811.89565(6)	816.59922(5)	788.2085(1)
Centrifugal Distortion Constants[b] /kHz										
D_J	0.07264(9)	0.074(2)	0.0726(4)	0.0732(4)	0.0713(4)	0.0692(5)	0.0715(4)	0.0709(4)	0.0710(2)	0.0699(9)
D_{JK}	-0.2403(5)	[-0.2403]	-0.20(1)	-0.26(1)	-0.28(1)	-0.19(1)	-0.22(1)	-0.24(1)	-0.292(3)	-0.27(2)
D_K	3.39(6)	[3.39]	[3.39]	[3.39]	[3.39]	[3.39]	[3.39]	[3.39]	[3.39]	[3.39]
d_J	0.01669(7)	0.018(2)	0.0162(3)	0.0170(3)	0.0166(3)	0.0153(4)	0.0165(3)	0.0158(3)	0.0161(2)	0.0168(9)
d_K	0.451(7)	[0.451]	[0.451]	[0.451]	[0.451]	[0.451]	[0.451]	[0.451]	[0.451]	[0.451]
^{14}N Nuclear Quadrupole Coupling Constants /MHz										
1.5 (χ_{aa})	4.0861(6)	4.2(2)	4.08(1)	4.08(1)	4.10(1)	4.10(1)	4.11(1)	4.10(1)	-	4.07(2)
0.25 (χ_{bb}- χ_{cc})	-0.0427(2)	[-0.0427]	-0.042(5)	-0.034(6)	-0.0042(6)	-0.037(6)	-0.038(6)	-0.035(6)	-	-0.033(7)
rms[c]/kHz	0.7	1.8	0.8	0.9	0.9	1.0	0.9	0.9	0.4	0.9
# lines	244	18	66	63	63	62	63	62	30	41

[a] spectroscopic constants from ref. 29: $A = 5202.103(46)$ MHz, $B = 972.68072(62)$ MHz, $C = 819.62733(61)$ MHz, $D_J = 0.0689(11)$ kHz, $D_{JK} = -0.209(16)$ kHz, $D_K = [0.0]$, $d_J = 0.01210(77)$ kHz, $d_K = [0.0]$, $\chi_{aa} = 2.701(12)$ MHz, $\chi_{bb} = -1.444(15)$ MHz, $\chi_{cc} = -1.258(15)$ MHz.

[b] centrifugal distortion constants in square brackets were fixed to the value from the parent.

[c] microwave rms = $\sqrt{\frac{\sum(obs-calc)^2}{\# \, lines}}$

Table 3.2. Ground state spectroscopic constants obtained for PhNCS and its isotopologues.

	normal	$^{13}C1$	$^{13}C2$	$^{13}C3$	$^{13}C4$	$^{13}C5$	$^{13}C6$	$^{13}C7$	^{15}N	^{34}S
Rotational Constants[a] /MHz										
A	5218.6948(5)	5214.74(5)	5158.17(5)	5115.35(5)	5209.78(7)	5173.07(7)	5131.96(6)	5215.57(6)	5196.16(3)	5214.65(2)
B	634.47256(3)	634.28085(6)	633.86807(8)	630.53423(7)	626.39418(8)	628.17206(8)	632.74748(7)	631.50203(7)	633.97616(4)	616.23303(3)
C	565.63308(3)	565.43467(7)	564.43402(9)	561.27790(8)	559.1056(1)	560.0868(1)	563.22739(9)	563.23546(9)	564.97452(5)	551.04506(4)
Centrifugal Distortion Constants[b] /kHz										
D_J	0.04812(5)	0.0478(7)	0.0494(9)	0.0475(8)	0.046(1)	0.049(1)	0.0483(9)	0.048(1)	0.0478(3)	0.0463(2)
D_{JK}	-0.1303(8)	[-0.1303]	[-0.1303]	[-0.1303]	[-0.1303]	[-0.1303]	[-0.1303]	[-0.1303]	[-0.1303]	[-0.1303]
D_K	7.1(1)	[7.1]	[7.1]	[7.1]	[7.1]	[7.1]	[7.1]	[7.1]	[7.1]	[7.1]
d_J	0.00840(3)	[0.00840]	[0.00840]	[0.00840]	[0.00840]	[0.00840]	[0.00840]	[0.00840]	[0.00840]	[0.00840]
d_K	0.62(1)	[0.62]	[0.62]	[0.62]	[0.62]	[0.62]	[0.62]	[0.62]	[0.62]	[0.62]
^{14}N Nuclear Quadrupole Coupling Constants /MHz										
1.5 (χ_{aa})	2.903(2)	2.91(2)	2.90(2)	2.90(2)	2.92(3)	2.89(2)	2.90(2)	2.91(2)	-	2.92(1)
0.25 (χ_{bb}- χ_{cc})	-0.2423(5)	-0.23(1)	-0.24(1)	-0.23(1)	-0.22(1)	-0.22(1)	-0.23(1)	-0.22(1)	-	-0.26(1)
rms/kHz	0.8	0.7	0.9	0.8	1.0	1.0	0.9	0.9	0.7	1.0
# lines	214	30	27	30	30	29	29	27	20	65

[a] spectroscopic constants from from ref. 29: A = 5219.03(38) MHz, B = 634.4716(16) MHz, C = 565.6340(17) MHz, D_J = 0.0489(52) kHz, D_{JK} = −0.134 (53) kHz, D_K = [0.0], d_J = 0.00918(54) kHz, d_K = [0.0], χ_{aa} = 1.925(14) MHz, χ_{bb} = −1.434(18) MHz, χ_{cc}= −0.491(18) MHz.

[b] centrifugal distortion constants in square brackets were fixed to the value from the parent.

[c] microwave rms = $\sqrt{\frac{\sum (obs-calc)^2}{\# lines}}$

3.5 Structural determination

Based on *ab initio* calculations, both PhNCO and PhNCS have planar equilibrium structures with C_s symmetry. In principle, with ten isotopologues observed for each, the experimental rotational constants can be used to derive substitution structures (r_s) through a Kraitchmann analysis.[47] In practice, as the *a*-axis passes close to C1 and C7 in both molecules, the positions of these atoms are not well-determined by this method and instead, mass dependence structures ($r_m^{(1)}$) as described by Watson[48] were derived as shown for other benzene derivatives.[49-50] The thirty rotational constants from the set of ten isotopologues were used in Kisiel's STRFIT least squares fitting routine[48,51] to estimate key geometric parameters for the heavy atoms while internal parameters involving the H atoms were held fixed at the values obtained from MP2/aug-cc-pVTZ calculations. To preserve the orientation of the H atoms relative to the ring, the difference of the external angles (for example $\angle HC2C1 - \angle HC2C3$) of each H were also held at the *ab initio* values following the example of substituted benzonitriles.[52] The Laurie parameter δ_H was fixed at 0.01Å for each CH bond and $c_a = c_b = c_c$ was assumed as done previously for benzaldehyde.[49] A summary of the results is provided in Table 3.3 under the $r_m^{(1)}$ heading along with the *ab initio* values for the equilibrium structure (r_e) for comparison.

Table 3.3. Mass dependence ($r_m^{(1)}$) and equilibrium (r_e) (MP2/aug-cc-pVTZ) structural parameters (bond Lengths in Å, angles in degrees) determined for PhNCO and PhNCS.

	PhNCO		PhNCS	
	$r_m^{(1)}$	r_e	$r_m^{(1)}$	r_e
r(C1C2)	1.393(4)	1.398	1.398(2)	1.399
r(C2C3)	1.391(5)	1.392	1.401(5)	1.391
r(C3C4)	1.397(2)	1.394	1.399(5)	1.395
r(C4C5)	1.393(3)	1.394	1.397(7)	1.394
r(C5C6)	1.396(2)	1.392	1.398(4)	1.391
r(C1C6)	1.401(5)	1.395	1.399(5)	1.396
r(NC1)	1.393(7)	1.399	1.380(5)	1.385
r(C7N)	1.207(4)	1.214	1.195(7)	1.206
r(C7O/S)	1.173(3)	1.178	1.581(5)	1.576
$\angle$(C3C2C1)	119.9(4)	119.6	119.0(3)	119.3
$\angle$(C4C3C2)	120.4(5)	120.4	120.5(3)	120.4
$\angle$(C5C4C3)	119.6(1)	119.7	119.8(2)	119.8
$\angle$(C6C5C4)	120.5(1)	120.4	120.4(3)	120.4
$\angle$(C1C6C5)	119.7(3)	119.6	119.2(3)	119.4
$\angle$(C2C1C6)	119.9(5)	120.3	121.1(3)	120.7
$\angle$(NC1C2)	122.4(4)	121.7	120.4(1)	120.3
$\angle$(C7NC1)	135.2(4)	136.5	145.1(2)	146.6
$\angle$(NC7O/S)	173.8(6)	172.8	176.6(6)	175.3
c_α ($u^{1/2}$ Å)	0.0168(4)		-0.0123(8)	
σ (u Å^2)	0.0055		0.012	

3.6 Discussion

The spectroscopic parameters for PhNCO and PhNCS were well-determined and compared with the *ab initio* values at each level of theory, as summarized in Table 3.4. In terms of the rotational constants, MP2 calculations provide better agreement with experiment than B3LYP and B3LYP-D3(BJ), while the DFT methods give better overall estimates for ^{14}N quadrupole coupling constants. Note that, as χ_{aa} equals to - ($\chi_{bb} + \chi_{cc}$), in *ab initio* and experimental results, two independent parameters, 3/2 χ_{aa} and 1/4 (χ_{bb} - χ_{cc}), were derived instead of individual χ_{aa}, χ_{bb}, and

χ_{cc}. Therefore, although χ_{bb} and χ_{cc} seem to have larger variations compared to χ_{aa}, the actual fit parameter 1/4 (χ_{bb} - χ_{cc}) is a small number and matches the calculated value quite well. As to centrifugal distortion constants, a previous study on similarly sized ring molecules such as anisole and benzaldehyde showed that harmonic frequency calculations yielded reliable predictions using both MP2 and B3LYP methods with a 6-31G(d, p) basis set.[49] However, calculations at each level of theory employed in this work derived results which are quite different from experimental values, especially for PhNCS. In contrast, frequency calculations with anharmonic corrections significantly improved the estimates of these parameters. This phenomenon is probably attributable to the low-frequency vibrations of the title molecules.

Likewise, the inertial defects ($\Delta_0 = I_c - I_a - I_b$) derived from the experimental rotational constants of the parent species (-0.132 amu·Å^2 for PhNCO and 0.101 amu·Å^2 for PhNCS) are small as expected for planar molecules but non-zero, which also result from the low-frequency vibrations. For PhNCO, the negative value suggests that the out-of-plane vibrational motions make more contributions compared to the in-plane motions. This is consistent with the frequency calculations. The lowest vibrational mode calculated at the MP2/aug-cc-pVTZ level is predicted to correspond to the out-of-plane torsion of the NCO group at 57 cm^{-1}. The second lowest vibration is calculated to be the in-plane C1-N-C7 bending motion which is higher in energy (91 cm^{-1}). This vibration ordering also agrees with the potential energy scans performed on the ∠C1NC7 angle and the C2-C1-N-C7 dihedral angle shown in Figure 3.5. In the scans, the energy barrier of the C1-N-C7 linearization is shown to be 11.8 kJ/mol while the barrier for the out-of-plane torsion of the NCO group is considerably lower at 6.2 kJ/mol. This means that the out-of-plane torsion happens more easily and makes a greater contribution to the negative inertial defect.

Table 3.4. Comparison between experimental and calculated spectroscopic constants for PhNCO and PhNCS at the B3LYP, B3LYP-D3(BJ) and MP2 level of theory. The centrifugal distortion constants are reported for both harmonic (H) and anharmonic (A) frequencies.

PhNCO	Rotational Constants/MHz			^{14}N Quadrupole Coupling Constants /MHz				Centrifugal Distortion Constants /kHz				
	A	B	C	χ_{aa}	χ_{bb}	χ_{cc}		D_J	D_{JK}	D_K	d_J	d_K
This work	5201.7138(3)	972.68164(2)	819.62560(2)	2.7241(4)	-1.4474(4)	-1.2766(4)	H	0.07264(9)	-0.2403(5)	3.39(6)	0.01669(7)	0.451(7)
B3LYP	5348.31	953.95	809.55	2.781	-1.623	-1.157	H	0.0378	2.6191	1.6700	0.0022	1.0739
							A	0.0605	-0.0452	3.0676	0.0135	0.4676
B3LYP-D3(BJ)	5324.92	960.94	813.66	2.768	-1.618	-1.150	H	0.0403	2.5229	1.0960	0.0029	1.0595
							A	0.0630	-0.0993	3.1301	0.0142	0.4568
MP2	5244.99	964.85	814.94	2.730	-1.240	-1.490	H	0.0451	2.3226	0.3723	0.0043	1.0225
PhNCS	A	B	C	χ_{aa}	χ_{bb}	χ_{cc}		D_J	D_{JK}	D_K	d_J	d_K
This work	5218.6948(5)	634.47256(3)	565.63308(3)	1.935(1)	-1.452(1)	-0.483(1)	H	0.04812(5)	-0.1303(8)	7.1(1)	0.00840(3)	0.62(1)
B3LYP	5430.34	617.72	554.63	1.899	-1.479	-0.419	H	0.0181	5.247	47.3640	0.0032	-1.7032
							A	0.0368	0.3776	5.8653	0.0061	0.7200
B3LYP-D3(BJ)	5358.97	625.77	560.34	1.899	-1.524	-0.375	H	0.0188	5.4177	57.3063	0.0040	-1.6672
							A	0.0407	0.1191	6.2556	0.0070	0.6331
MP2	5283.70	627.90	561.21	1.969	-1.144	-0.825	H	0.0181	5.1064	58.0997	0.0041	-1.5284

For PhNCS, in contrast, the two lowest modes are similar in energy (54 cm^{-1} for the NCS out-of-plane torsion and 58 cm^{-1} for C1-N-C7 bending). However, the inertial defect is a small positive value which implies that the in-plane motions must play a larger role in this molecule. The puzzle may be unraveled by the 1D potential energy scans. When scanning the C2-C1-N-C7 dihedral angle from 0º to 90º, the ∠C1NC7 angle was relaxed along with other geometric parameters and became more and more linear at nitrogen. Ultimately, when the dihedral angle was set at 90º, the ∠C1NC7 angle increased to be 180º, which is the same planar C_{2v} geometry from the C1-N-C7 bending scan at 180º. This means that in the calculations, the NCS fragment falls back into the phenyl plane in the middle of the interconversion between the equivalent planar C_s structures. The energy barrier of the two pathways thus appears the same at only 3.7 kJ/mol. This may be a major factor accounting for the positive inertial defect. The differences of the inertial defects and vibrational motions of PhNCO and PhNCS indicate that there are important variations in the electronic environments around nitrogen which must arise from the terminal chalcogen atoms.

As the electronic environment has a direct influence on the molecular structure, valuable information is found in the experimentally derived geometry. In Table 3.3, the well-determined $r_m^{(1)}$ bond lengths and angles for PhNCO and PhNCS match the *ab initio* values with reasonable uncertainties. Closer inspection shows that the parameters of the phenyl ring backbone experience no discernable change when oxygen is replaced by sulfur. This implies that the terminal atom does not change the nature of bonding in the ring itself through electron delocalization for example, which is supported by the similar natural charge distribution in the two phenyl rings calculated by the NBO approach.

Not surprisingly, greater effects are captured by comparsion of the geometries of the NCX groups. However, the role of the terminal chalcogen atoms is not straightforward to extract due to their differences in atomic size, electronegativity, hybridization and so on. The natural charge on oxygen (-0.485) indicates greater electron density at the end of the NCO fragment than in the sulfur (0.029) analog as expected. According to the NBO results, the C7S σ-bond in PhNCS, for example, is characterized by a more even sharing of electrons (48% C7 : 52% S) and the hybrid orbital on sulfur has significantly enhanced p-character (sp^6) in comparison to PhNCO (35% C7 : 65% O, $sp^{2.2}$). There are notable differences in the nature of the π-bonding given in the NBO analysis as well as the lone pair characters of the chalcogen atoms and collectively, these alter the electronic structure of the NCX fragment in PhNCO and PhNCS and lead to the geometric changes at nitrogen.

Therefore, the structural parameters around nitrogen require closer comparison. With recognition that the experimental uncertainties make it difficult to declare that small changes in parameters are meaningful, the trends for both the $r_m^{(1)}$ and r_e structures in Table 3.3 reveal that the largest changes in bond lengths are those involving nitrogen. Both the NC1 and C7N bond lengths are ~0.01 Å shorter in PhNCS compared with PhNCO. This shortening is accompanied by an increase in the ∠C1NC7 by ~10° which suggests that it is the electronic structure at the nitrogen atom that is most affected when replacing oxygen with sulfur. The similar trend in this angle is also observed in other NCO/NCS pairs, such as CH_3NCO (140°)[33]/CH_3NCS (151°).[34]

To better understand these geometric changes, the occupied orbitals for PhNCO and PhNCS were analyzed thoroughly and it is striking to note that there is an orbital identified as a lone pair for nitrogen (n_N, occupancy = 1.646) in PhNCO but

not in PhNCS. Surprisingly, besides the normal π_{N-C7} orbital (occupancy = 1.937, 66%

N and 34% C7), a second π_{N-C7} orbital (occupancy = 1.759) was reported in PhNCS,

which approximates lone pair character as 85% of the electron density of this orbital

is from nitrogen. This orbital is, to a great extent, formed by the overlap of the

original nitrogen lone pair with a barely occupied hybridized orbital from C7. The

shape of this MO is provided in Figure 3.6 together with the MO of the nitrogen lone

pair in PhNCO for comparison. These two MOs show very similar orientation while

the one in PhNCS is more delocalized towards C7. This presumably results from the

lower electronegativity of sulfur and accounts for the contraction of the C7N bond

and the increase in ∠C1NC7 angle. Closer inspection of the hybridization of the

nitrogen atoms reveals that for PhNCS, the electronic structure of that is best

described as a sp hybrid orbital while for PhNCO, it is more like $sp^{1.6}$. Of course, such

sp hybridization of nitrogen does not necessarily lead to a linear geometric

arrangement but does make the angle bigger and the bonds shorter. This subtle

difference in the nature of the orbitals involving nitrogen is in line with the observed

geometry differences in PhNCO and PhNCS and also explains why the latter retains

C_s symmetry rather than adopt C_{2v} symmetry.
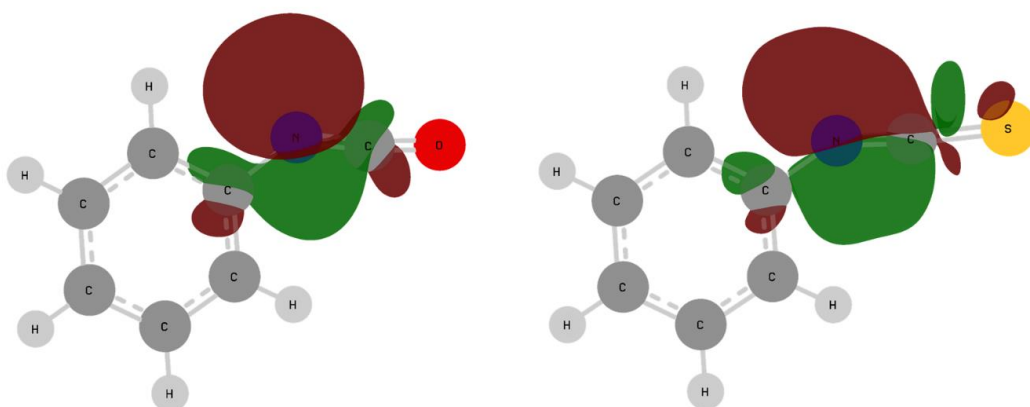
Figure 3.6. The shape and orientation of the n_N MO in PhNCO (left) and the $\pi_{N-C7(2)}$

MO in PhNCS (right).

3.7 Summary

As a demonstration of the use of microwave spectroscopy to derive fundamental properties of molecules, the rotational spectra of both PhNCO and PhNCS were reported for the parent and nine minor isotopologues. For the parent species, b-type transitions arising from the small dipole moment along b-axis in their principal inertial frames were recorded for the first time. By using the rotational constants for all heavy atom isotopologues, the experimental ($r_m^{(1)}$) geometries were obtained and observed to be in good agreement with *ab initio* r_e geometries at the MP2/aug-cc-pVTZ level. The greatest difference in the geometries occurs around nitrogen due to the different hybridizations which are mostly affected by the terminal chalcogen atoms. This difference results in a more linear, sp-like electronic structure of nitrogen in the S-bearing species. Meanwhile, C-N bonds become shorter and ∠CNC angle becomes larger in PhNCS compared with PhNCO. In the following chapters, attention is turned to non-commercial species, which were created from the dc electrical discharge.

References

(1) Marcelino, N.; Agundez, M.; Cernicharo, J.; Roueff, E.; Tafalla, M. Discovery of the Elusive Radical NCO and Confirmation of H_2NCO^+ in space. *Astron. Astrophys.* **2018,** *612*, L10.

(2) Soifer, B. T.; Puetter, R. C.; Russell, R. W.; Willner, S. P.; Harvey, P. M.; Gillett, F. C. The 4-8 Micron Spectrum of the Infrared Source W33 A. *Astrophys. J.* **1979,** *232*.

(3) Snyder, L. E.; Buhl, D. Interstellar Isocyanic Acid. *Astrophys. J.* **1972,** *177*, 619-623.

(4) Brünken, S.; Gottlieb, C. A.; McCarthy, M. C.; Thaddeus, P. Laboratory Detection of HOCN and Tentative Identification in Sgr B2. *Astrophys. J.* **2009,** *697* (1), 880-885.

(5) Brünken, S.; Belloche, A.; Martín, S.; Verheyen, L.; Menten, K. M. Interstellar HOCN in the Galactic Center Region. *Astron. Astrophys.* **2010,** *516*, A109.

(6) Halfen, D. T.; Ilyushin, V. V.; Ziurys, L. M. Interstellar Detection of Methyl Isocyanate CH_3NCO in Sgr B2(N): A Link from Molecular Clouds to Comets. *Astrophys. J.* **2015,** *812* (1), L5.

(7) Cernicharo, J.; Kisiel, Z.; Tercero, B.; Kolesnikova, L.; Medvedev, I. R.; Lopez, A.; Fortman, S.; Winnewisser, M.; de Lucia, F. C.; Alonso, J. L.; Guillemin, J. C. A Rigorous Detection of Interstellar CH_3NCO: An Important Missing Species in Astrochemical Networks. *Astron. Astrophys.* **2016,** *587*, L4.

(8) Gupta, H.; Gottlieb, C. A.; Lattanzi, V.; Pearson, J. C.; McCarthy, M. C. Laboratory Measurements and Tentative Astronomical Identification of H_2NCO^+. *Astrophys. J.* **2013,** *778* (1), L1.

(9)   Frerking, M. A.; Linke, R. A.; Thaddeus, P. Interstellar Isothiocyanic Acid. *Astrophys. J.* **1979,** *234*, L143-L145.

(10)   Adande, G. R.; Halfen, D. T.; Ziurys, L. M.; Quan, D.; Herbst, E. Observations of the [HNCS]/[HSCN] Ratio in Sgr B2 and TMC-1: Evidence for Low-Temperature Gas-Phase Chemistry. *Astrophys. J.* **2010,** *725* (1), 561-570.

(11)   Halfen, D. T.; Ziurys, L. M.; Brünken, S.; Gottlieb, C. A.; McCarthy, M. C.; Thaddeus, P. Detection of a New Interstellar Molecule: Thiocyanic Acid HSCN. *Astrophys. J.* **2009,** *702* (2), L124-L127.

(12)   Beard, C. I.; Dailey, B. P. The Structure and Dipole Moment of Isothiocyanic Acid. *J. Chem. Phys.* **1950,** *18* (11), 1437-1441.

(13)   Jones, L. H.; Shoolery, J. N.; Shulman, R. G.; Yost, D. M. The Molecular Structure of Isocyanic Acid from Microwave and InfraRed Absorption Spectra. *J. Chem. Phys.* **1950,** *18* (7), 990-991.

(14)   Saito, S.; Amano, T. Microwave Spectrum of the NCO Radical. *J. Mol. Spectrosc.* **1970,** *34* (3), 383-389.

(15)   Ross, S. C.; Cooper, T. A.; Firth, S.; Kroto, H. W.; Walton, D. R. M. The Microwave Spectrum and Semirigid Bender Analysis of Isocyanatoethyne, HC≡CNCO. *J. Mol. Spectrosc.* **1992,** *152* (1), 152-167.

(16)   Bouchy, A.; Roussy, G. Geometrical and Electronic Structures of Two Conformers of Vinyl Isocyanate by Microwave Spectroscopy. *J. Mol. Spectrosc.* **1977,** *68* (1), 156-165.

(17)   Caminati, W. The Microwave Spectrum of *s-Trans* Vinyl Isothiocyanate. *J. Mol. Struct.* **1988,** *190*, 227-233.

(18)   Hocking, W. H.; Gerry, M. C. L. The Microwave Spectrum of Cyanogen Isocyanate (NCNCO). *J. Mol. Spectrosc.* **1976,** *59* (3), 338-354.

(19)   King, M. A.; Kroto, H. W.; Landsberg, B. M. Microwave Spectrum of the Quasilinear Molecule, Cyanogen Isothiocyanate (NCNCS). *J. Mol. Spectrosc.* **1985,** *113* (1), 1-20.

(20)   Winnewisser, B. P.; Winnewisser, M.; Medvedev, I. R.; Behnke, M.; De Lucia, F. C.; Ross, S. C.; Koput, J. Experimental Confirmation of Quantum Monodromy: the Millimeter Wave Spectrum of Cyanogen Isothiocyanate NCNCS. *Phys. Rev. Lett.* **2005,** *95* (24), 243002.

(21)   Winnewisser, B. P.; Winnewisser, M.; Medvedev, I. R.; De Lucia, F. C.; Ross, S. C.; Koput, J. Analysis of the FASSST Rotational Spectrum of NCNCS in View of Quantum Monodromy. *Phys. Chem. Chem. Phys.* **2010,** *12* (29), 8158-8189.

(22)   Winnewisser, M.; Winnewisser, B. P.; De Lucia, F. C.; Tokaryk, D. W.; Ross, S. C.; Billinghurst, B. E. Pursuit of Quantum Monodromy in the Far-Infrared and Mid-Infrared Spectra of NCNCS Using Synchrotron Radiation. *Phys. Chem. Chem. Phys.* **2014,** *16* (33), 17373-17407.

(23)   Sakaizumi, T.; Ohashi, O.; Yamaguchi, I. Microwave Spectrum of Ethyl Isothiocyanate. *Bull. Chem. Soc. Jpn.* **1976,** *49* (4), 948-953.

(24)   Sakaizumi, T.; Yamada, O.; Ushida, K.; Ohashi, O.; Yamaguchi, I. The Microwave Spectrum of Ethyl Isocyanate. *Bull. Chem. Soc. Jpn.* **1976,** *49* (11), 2908-2912.

(25)   McGuire, B. A.; Burkhardt, A. M.; Kalenskii, S.; Shingledecker, C. N.; Remijan, A. J.; Herbst, E.; McCarthy, M. C. Detection of the Aromatic Molecule Benzonitrile (*c*-C_6H_5CN) in the Interstellar Medium. *Science* **2018,** *359* (6372), 202-205.

(26)   Higgins, R. J.; Combs, L. L.; Malloy, T. B.; Cook, R. L. Low Resolution Microwave Spectra and INDO Calculations of Phenylisothiocyanate and Phenylisocyanate. *J. Mol. Struct.* **1975,** *25*, 121-127.

(27)   Bouchy, A.; Roussy, G. Microwave Spectrum of Phenyl Isocyanate. *J. Mol. Spectrosc.* **1977,** *65*, 395-404.

(28)   Onda, M.; Kambayashi, S.; Sakaizumi, T.; Yamaguchi, I. Microwave Spectrum of Phenylisothiocyanate. *J. Mol. Struct.* **1976,** *34*, 299-302.

(29)   Kasten, W.; Dreizler, H. Nitrogen Quadrupole Coupling in the Microwave-Spectra of Phenyl Isocyanate and Phenyl Isothiocyanate. *Z. Naturforsch., A: Phys. Sci.* **1987,** *42* (1), 79-82.

(30)   Stephenson, C. V.; Coburn, W. C.; Wilcox, W. S. The Vibrational Spectra and Assignments of Nitrobenzene, Phenyl Isocyanate, Phenyl Isothiocyanate, Thionylaniline and Anisole. *Spectrochim. Acta* **1961,** *17* (9-10), 933-946.

(31)   Forner, W.; Badawi, H. M. Rotational Barriers and Vibrational Spectra of Phenyl Ketene, Azide, and Isocyanate. *J. Theor. Comput. Chem.* **2010,** *2*, 511-529.

(32)   Mani, P.; Umamaheswari, H.; Joshua, B. D.; Sundaraganesan, N. Molecular Structure, Vibrational Spectra and NBO Analysis of Phenylisothiocyanate by Density Functional Method. *J. Mol. Struct.: THEOCHEM* **2008,** *863*, 44-49.

(33)   Koput, J. The Microwave Spectrum of Methyl lsocyanate. *J. Mol. Spectrosc.* **1986,** *115*, 131-146.

(34)   Koput, J. The Microwave Spectrum of Methyl lsothiocyanate. *J. Mol. Spectrosc.* **1986,** *118*, 189-207.

(35)   Evangelisti, L.; Sedo, G.; van Wijngaarden, J. Rotational Spectrum of 1,1,1-Trifluoro-2-Butanone Using Chirped-Pulse Fourier Transform Microwave Spectroscopy. *J. Phys. Chem. A* **2011,** *115* (5), 685-90.

(36)   Sedo, G.; van Wijngaarden, J. Fourier Transform Microwave Spectra of a "New" Isomer of OCS-CO_2. *J. Chem. Phys.* **2009,** *131* (4), 044303.

(37)   Møller, C.; Plesset, M. S. Note on an Approximation Treatment for Many-Electron Systems. *Phys. Rev.* **1934,** *46* (7), 618-622.

(38)   Stephens, P. J.; Devlin, F. J.; Chabalowski, C. F.; Frisch, M. J. *Ab Initio* Calculation of Vibrational Absorption and Circular-Dichroism Spectra Using Density-Functional Force-Fields. *J. Phys. Chem. Lett.* **1994,** *98* (45), 11623-11627.

(39)   Grimme, S.; Ehrlich, S.; Goerigk, L. Effect of the Damping Function in Dispersion Corrected Density Functional Theory. *J. Comput. Chem.* **2011,** *32* (7), 1456-1465.

(40)   Dunning, T. H. Gaussian Basis Sets for Use in Correlated Molecular Calculations. I. The Atoms Boron through Neon and Hydrogen. *J. Chem. Phys.* **1989,** *90* (2), 1007-1023.

(41)   Kendall, R. A.; Dunning, T. H.; Harrison, R. J. Electron Affinities of the First-Row Atoms Revisited. Systematic Basis Sets and Wave Functions. *J. Chem. Phys.* **1992,** *96* (9), 6796-6806.

(42)   Woon, D. E.; Dunning, T. H. Gaussian Basis Sets for Use in Correlated Molecular Calculations. III. The Atoms Aluminum through Argon. *J. Chem. Phys.* **1993,** *98* (2), 1358-1371.

(43)   Frisch, M. J.; Trucks, G. W.; Schlegel, H. B.; Scuseria, G. E.; Robb, M. A.; Cheeseman, J. R.; Scalmani, G.; Barone, V.; Petersson, G. A.; Nakatsuji, H.; Li, X.; Caricato, M.; Marenich, A. V.; Bloino, J.; Janesko, B. G.; Gomperts, R.; Mennucci, B.; Hratchian, H. P.; Ortiz, J. V.; Izmaylov, A. F.; Sonnenberg, J. L.; Williams; Ding, F.; Lipparini, F.; Egidi, F.; Goings, J.; Peng, B.; Petrone, A.; Henderson, T.; Ranasinghe, D.; Zakrzewski, V. G.; Gao, J.; Rega, N.; Zheng, G.; Liang, W.; Hada,

M.; Ehara, M.; Toyota, K.; Fukuda, R.; Hasegawa, J.; Ishida, M.; Nakajima, T.; Honda, Y.; Kitao, O.; Nakai, H.; Vreven, T.; Throssell, K.; Montgomery Jr., J. A.; Peralta, J. E.; Ogliaro, F.; Bearpark, M. J.; Heyd, J. J.; Brothers, E. N.; Kudin, K. N.; Staroverov, V. N.; Keith, T. A.; Kobayashi, R.; Normand, J.; Raghavachari, K.; Rendell, A. P.; Burant, J. C.; Iyengar, S. S.; Tomasi, J.; Cossi, M.; Millam, J. M.; Klene, M.; Adamo, C.; Cammi, R.; Ochterski, J. W.; Martin, R. L.; Morokuma, K.; Farkas, O.; Foresman, J. B.; Fox, D. J. *Gaussian 16 Rev. B.01*, Wallingford, CT, 2016.

(44)   Glendening, E. D.; Landis, C. R.; Weinhold, F. NBO 6.0: Natural Bond Orbital Analysis Program. *J. Comput. Chem.* **2013,** *34* (16), 1429-1437.

(45)   Pickett, H. M. The Fitting and Prediction of Vibration-Rotation Spectra with Spin Interactions. *J. Mol. Spectrosc.* **1991,** *148* (2), 371-377.

(46)   Watson, J. K. G. Centrifugal Corrections for Asymmetric-Top Molecules. *J. Chem. Phys.* **1966,** *45* (4), 1360-1361.

(47)   Kraitchman, J. Determination of Molecular Structure from Microwave Spectroscopic Data. *Am. J. Phys.* **1953,** *21* (1), 17-24.

(48)   Kisiel, Z. Least-Squares Mass-Dependence Molecular Structures for Selected Weakly Bound Intermolecular Clusters. *J. Mol. Spectrosc.* **2003,** *218* (1), 58-67.

(49)   Desyatnyk, O.; Pszczółkowski, L.; Thorwirth, S.; Krygowski, T. M.; Kisiel, Z. The Rotational Spectra, Electric Dipole Moments and Molecular Structures of Anisole and Benzaldehyde. *Phys. Chem. Chem. Phys.* **2005,** *7* (8), 1708-1715.

(50)   Sun, W.; Lozada, I. B.; van Wijngaarden, J. Fourier Transform Microwave Spectroscopic and *Ab Initio* Study of the Rotamers of 2-Fluorobenzaldehyde and 3-Fluorobenzaldehyde. *J. Phys. Chem. A* **2018,** *122* (8), 2060-2068.

(51)   Watson, J. K.; Roytburg, A.; Ulrich, W. Least-Squares Mass-Dependence Molecular Structures. *J. Mol. Spectrosc.* **1999,** *196* (1), 102-119.

(52)   Kamaee, M.; Sun, M.; Luong, H.; van Wijngaarden, J. Investigation of Structural Trends in Mono-, Di-, and Pentafluorobenzonitriles Using Fourier Transform Microwave Spectroscopy. *J. Phys. Chem. A* **2015,** *119* (41), 10279-92.

Chapter 4.   Investigation of the rich chemistry of the dc electrical discharge of 1,2-ethanedithiol

4.1 Introduction

Starting from this chapter, the dc electrical discharge technique is employed to create exotic chemical species that are of great interstellar interest. As the first project, the work in this chapter focuses on sulfur-carbon chains since plenty of them have been characterized in the laboratory after several were detected in interstellar space. By studying well-known species, it allows us to better understand the rich chemistry initiated by electric potential difference on the basis of a considerable number of known molecules identified in the discharge spectrum. With sufficient knowledge of this technique, it is possible to predict the existence of previously unknown species that may be formed in the same discharge plasma.

To date, a number of sulfur-carbon chains starting from small H_mCS species including $C=S$,[1-2] $HS=C$,[3] $HC=S$,[3] and $H_2C=S$,[4] to longer sulfur-containing cumulenes $C=C=S$,[5] $C=C=C=S$,[6-7] and $C=C=C=C=S$,[7-8] have been detected in multiple interstellar and circumstellar molecular clouds such as TMC-1 and IRC +10216. Motivated by these astrophysical observations, laboratory studies on C_nS (n = 1 – 9),[5-6,9-15] HC_nS (n = 2 – 8),[16-19] and H_2C_nS (n = 1 – 7)[19-22] species have been thoroughly carried out using dc electrical discharge sources coupled to microwave spectroscopy. Similarly, with the help of laboratory detection, many related oxygen-carbon chains such as $H_mC=O$ (m = 0 – 2),[1,23-26] $H_mC=C=O$ (m = 0 – 2),[27-29] $C=C=C=O$,[30-31] $HC=C=C=C=C=O$,[32] and $HC=C=C=C=C=C=O$[32-33] have been detected in various

molecular clouds as well. Surprisingly, even though oxygen was found to be ~40 times more abundant than sulfur in the cold cloud TMC-1, C_2S and C_3S[34] are more prevalent than their oxygen counterparts C_2O[28] and C_3O,[30] which makes the astrophysical sulfur chemistry of such regions incredibly interesting. The detection of HC_5O[32] and HC_7O[32-33] in TMC-1 strongly implies that longer sulfur-carbon chains that contain more than five carbons may exist in the same interstellar region and await astronomical detection.

Besides these well-characterized sulfur-containing cumulenes, carbon chain thials ($H(C{\equiv}C)_nCH{=}S$) are the next target for interstellar detection of sulfur-carbon species owing that they are structural isomers of $H_2C_{2n+1}S$. The smallest form $HC{\equiv}CCH{=}S$ has been studied previously by rotational spectroscopy from a waveguide experiment following its production via flash pyrolysis of dipropargyl sulfide.[35] In particular, the astrophysical detection of $HC{\equiv}CCH{=}O$[36] in TMC-1 and recent observation of HCS[3] in space make it a promising sulfur-containing candidate for future line surveys. In the laboratory, the detection of its longer chain forms such as HC_4CHS is of great interest and is a major aim of this work. Apparently, the preparation of these compounds is unfeasible through the traditional benchtop synthesis. Given its excellent performance in producing highly unsaturated carbon chains such as HC_{2n}, $HC_{2n+1}N$, H_mC_nO, and H_mC_nS, the dc electrical discharge technique is exploited to create the desired molecules.

To create species using high voltage electric power, the selection of appropriate precursors is very important as the starting point. A good precursor is supposed to readily provide the target functional group under electric pulse, easy to get from laboratory synthesis or commercial sources, and volatile enough to be introduced into the spectrometer. In the previous discharge experiments reported in

the literature, ethylene (CH_2=CH_2), acetylene (HC≡CH) and diacetylene (HC≡CC≡CH) are normally used to build up the unsaturated carbon chain;[37-38] acetonitrile (CH_3C≡N) and cyanoacetylene (HC≡CC≡N)[39] are used to provide the cyano group; carbon monoxide (C≡O) and carbon dioxide (O=C=O) are precursors to donate the carbonyl group.[40] Even though no previous study was found in the literature, acetaldehyde (CH_3CH=O) is presumably a good precursor to provide the formyl group. When it comes to the thial group, the situation becomes a bit awkward, as no commercially available compound meeting the above criteria provides the thial group. This points out a fact that although a variety of highly unsaturated carbon chain species have been prepared using electrical discharge, the application of this technique was restricted by the availability of precursors in the past which were selected empirically. To explore more possibilities and investigate the intriguing discharge chemistry, the projects in the present thesis were completed using relatively complex molecules as precursors. Large, complex precursors mean that the associated discharge chemistry and resulting products are of great diversity and complications, and the spectrum is more interesting and difficult to interpret. Unfortunately, few previous researches in the literature are available to provide support to study complex precursors. It is a long way to the ultimate destination.

In this chapter, an unconventional precursor, 1,2-ethanedithiol, which is slightly more complex than the aforementioned ones, was chosen as the precursor. Although this compound itself does not contain the HCS functional group, it was hoped to create one from the dc electrical discharge. In addition, a variety of known sulfur-containing species that were created together were simultaneously probed by the microwave spectrometer and identified in the resulting discharge spectrum. The

diversity of the observed species allows us to better understand the chemical environment in this discharge source and gain experience for future studies.

4.2 Experimental and theoretical considerations

The electric discharge assembly is designed to attach to the solenoid pulsed nozzle (General Valve, Series 9) so that it can trigger the discharge reactions immediately after the gas mixture is introduced into the chamber through a small orifice (1 mm diameter), as provided in Figure 4.1. The discharge channel is slightly wider with a diameter of 2 mm and composed of two copper electrodes, two insulating spacers and an Acetal Delrin cap. The copper electrodes (both 5 mm thick) are placed into the Delrin cap with an insulating spacer in between to make the electric arc. Typically, a continuous negative voltage of ~800 V was applied to the second electrode while the first one was grounded. The spacer with a thickness of 7 mm was found to serve better for the discharge reactions while the other one (5 mm thick) is used to isolate the stainless steel nozzle from the high voltage. The discharge can be observed as a flashing glow as it is modulated by the 7 Hz repetition rate of the pulsed nozzle.

Of the transient species created by the dc electrical discharge, some are open-shell radicals and thus paramagnetic. In order to probe their existence in the jet expansion, Earth's magnetic field in the polarization region inside the chamber needs to be eliminated. For this purpose, three pairs of copper wire coils are arranged along three mutually perpendicular axes outside the stainless-steel chamber, which are known as Helmholtz coils. The current applied to the coil pairs can be adjusted to minimize the magnetic field along each direction inside the chamber.
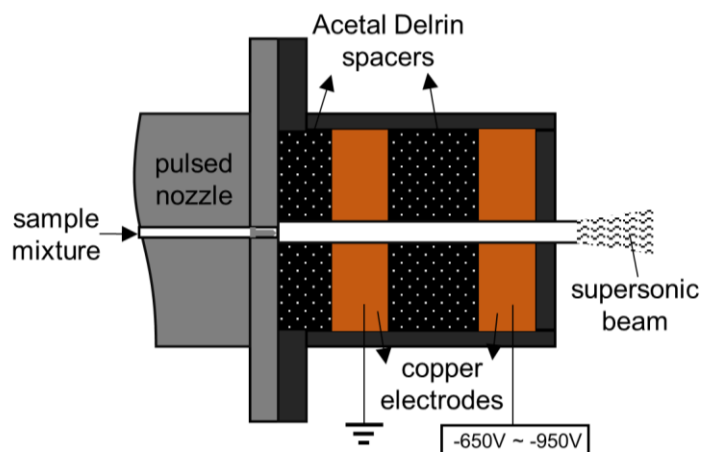
Figure 4.1. Schematic diagram of the electric discharge assembly to generate transient species. The size is not to scale.

After these modifications were set up, the discharge experiments were carried out first with the cp-FTMW spectrometer.[41] To generate the thial compound HC_4CHS, 1,2-ethanedithiol was chosen to be the precursor which was purchased from Sigma Aldrich (≥98.0% chemical purity) and used directly without further purification. Owing to its low vapor pressure (4.8 mmHg at 20 °C) and high boiling point (144 -146 °C), 2 mL of the liquid sample was transferred into a glass bubbler directly without further heating. To carry the organic vapor to the spectrometer, a gas mixture of acetylene (1%) in neon buffer gas was bubbled through the liquid sample with a stagnation pressure of ~1 atm. The mixed gas sample was then seeded into the chamber through the pulsed nozzle. The gas mixture passed through the discharge channel and a percentage of it was broken apart by the high voltage between the copper electrodes. The molecular fragments subsequently collided and recombined to form new species through different types of reactions such as radical-neutral and radical-radical reactions.

83

The spectra were collected in segments of 2 GHz in the frequency range of 8 – 18 GHz which allows for recording transitions due to lots of new species along with the precursors simultaneously. To remove those lines from the precursors, spectra were recorded with the discharge voltage turned off while other experimental conditions were kept the same. Afterwards, the non-discharge lines were picked out by a Python script and formed a non-discharge line list. By removing these lines from the discharge spectrum, a pure discharge dependent spectrum was obtained, which significantly reduced the workload of the following data analysis. The corresponding spectra are provided in Figure 4.2. Once some candidate transitions were identified in the discharge spectrum, the cavity-based Balle Flygare FTMW spectrometer[42] was employed to collect them with a better resolution using the same discharge device and Helmholtz coils.

To assist with the spectral assignment, quantum-chemical calculations were carried out using the Gaussian 16 software.[43] The equilibrium geometry of HC_4CHS along with the rotational constants were obtained at the MP2,[44] B3LYP,[45-47] and B3LYP-D3(BJ)[48] levels of theory with Dunning's cc-pVQZ basis set.[49-50] To allow empirical scaling of the calculated rotational constants, the shorter variant HCCCHS was calculated using the same methods. In addition, to investigate other involved species, analogous MP2 calculations were performed to obtain their structural properties and energies.
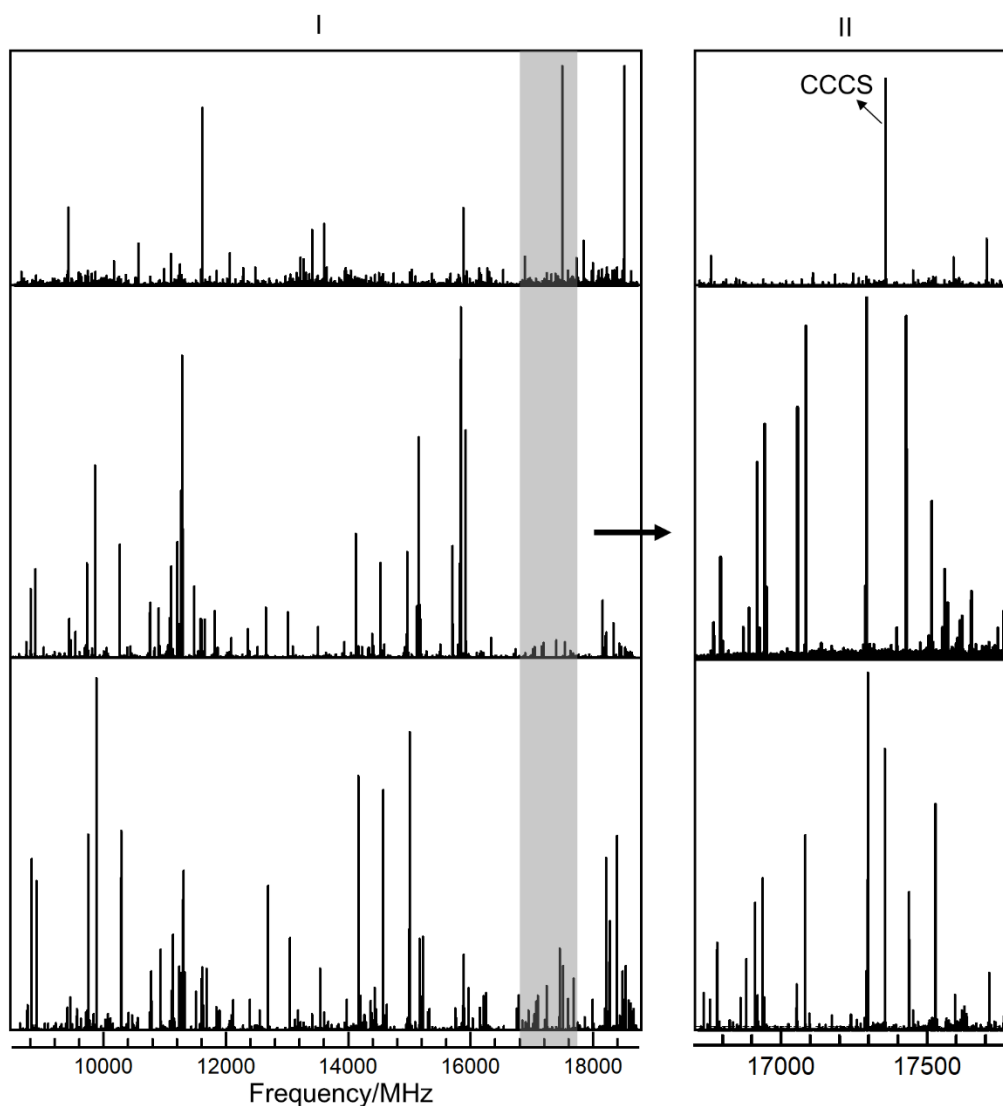
Figure 4.2. (I) Chirped pulse spectrum obtained from a discharge mixture of HSCH$_2$CH$_2$SH + HCCH in the range of 9 – 18 GHz with discharge on (bottom) and off (middle) collected with 1.5 million FIDs for each 2 GHz segment. The top trace is the resulting discharge dependent spectrum by removing the non-discharge transitions from the discharge spectrum. (II) The corresponding zoom-in window between 16.8-17.7 GHz shows a good example of newly formed CCCS species at 17342.26 MHz. The y- axes are arbitrary scale.

4.3 The identified discharge dependent species

As reported previously in the literature, the 1,2-ethanedithiol precursor has ten rotamers and four of them are predominant[51] as shown in Figure 4.3. The most stable rotamer I has no permanent dipole moment and thus, cannot be observed by rotational spectroscopy. The next three rotamers were observed in both non-discharge and discharge spectra in this work. By comparing the intensity of individual transitions observed with and without the electric pulse, ~10% of the precursor molecules are estimated to be involved in the discharge reactions. In total, ~630 discharge dependent transitions out of 1000 total remained in the modified discharge spectrum. Of them, some can be assigned to known species such as sulfur-bearing carbon chains based on their rotational constants or line lists published in the literature. Besides HC_4CHS,[52] 15 sulfur-containing species were identified including several radicals, which are classified into three types based on the functional groups. In the following section, the complex chemistry that generated these discharge products is discussed.

I (0.0 kJ/mol) II (0.2 kJ/mol) III (2.2 kJ/mol) IV (2.3 kJ/mol)
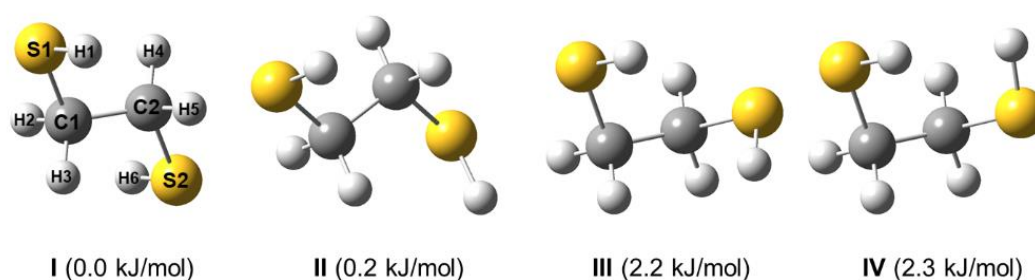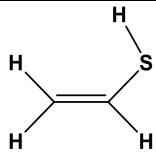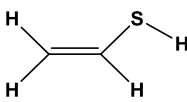
Figure 4.3. The four most stable rotamers of 1,2-ethanedithiol with the relative energies calculated at the B3LYP/6-311++G** level of theory.[51]

4.3.1 Thiols

Although 1,2-ethanedithiol has two thiol groups, vinylthiol (CH_2=CHSH) is the only one which retains the thiol group among the identified discharge species. To form this species, the precursor lost one H on one carbon and one SH group on the other. In the ground vibrational state, two planar rotamers, *syn*[53] and *anti*,[54] arise from the orientation of the S-H bond with respect to the C=C bond of the vinyl group. Both were identified in the discharge spectrum and the observed transitions in the current frequency range are provided in Table 4.1.

Table 4.1. The observed rotational transitions for vinylthiol along with the signal-to-noise ratios (SNR) collected with 1.5 million FIDs.

rotamer		J'_{KaKc}-J''_{KaKc}	type	frequency/MHz	SNR
syn		3_{03}-2_{12}	*b-*	10224.940	7.5
		1_{01}-0_{00}	*a-*	11057.772	15.3
		5_{05}-4_{14}	*b-*	13862.220	13.3
anti		3_{03}-2_{12}	*b-*	9411.050	37.1
		1_{01}-0_{00}	*a-*	11176.630	4.8
		5_{05}-4_{14}	*b-*	14923.940	13.5

However, in the four most stable rotamers of 1,2-ethanedithiol,[51] all the C-C-S-H dihedral angles are less than 90º, which means that all the S-H bonds point inward. These conformational structures favor the formation of *syn*-vinylthiol rather than the *anti* form. The *syn* rotamer was predicted to be ~2 kJ/mol more stable in energy at the MP2/cc-pVQZ level of theory. To investigate the interconversion barrier assuming the *syn* version is preferentially formed, a potential energy scan on the C-C-S-H dihedral angle was carried out at the same computational level and the resulting curve is provided in Figure 4.4. The barrier between the *syn* and *anti* rotamer from the

syn orientation is calculated to be 11.4 kJ/mol. The Boltzmann population of the

rotamers (*syn - anti*) is 100% -0% or 70% - 30% at 5 K and 298 K, respectively.

Given the dipole components of the rotamers (*syn*: $\mu_a = 0.813$ D, $\mu_b = 0.376$ D; *anti*:

$\mu_a = 0.425$ D, $\mu_b = 1.033$ D),[53-54] the estimated relative intensities of the observed

transitions implies that the *anti* rotamer has a population higher than 30% in the jet.

This suggests that the discharge environment is quite hot with a vibrational

temperature[55] above 298 K, which provides sufficient energy to form both rotamers.[56]

After the formation, *anti*-vinylthiol survives in the cold supersonic jet (~ 5 K effective

rotational temperature) due to the high relaxation barrier (9.3 kJ/mol) from *anti* to *syn*

arrangement.
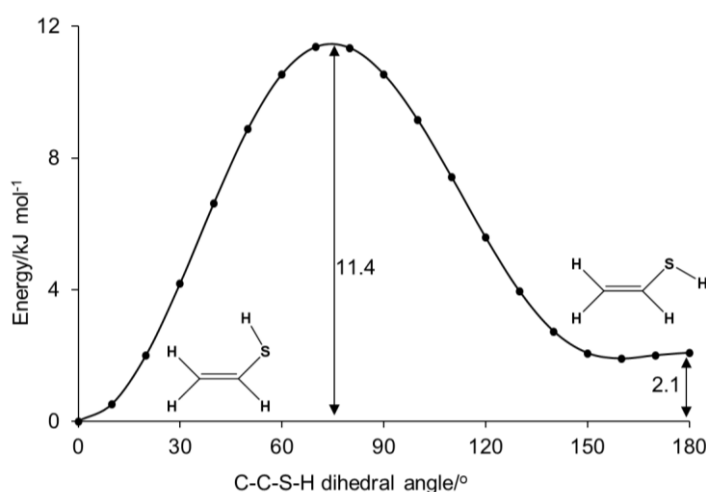
Figure 4.4. Potential energy curve of C-C-S-H dihedral angle between the *syn* and

anti rotamer at the MP2/cc-pVQZ level of theory.

No line was identified in the spectrum for methanethiol CH_3SH[57] or

ethanethiol CH_3CH_2SH.[58] This implies that the hydrogen elimination reaction

(dehydrogenation) which generates unsaturated compounds is more favorable than the

hydrogen addition reaction (hydrogenation) that generates saturated compounds in the

discharge plasma. Moreover, ethynethiol $HC{\equiv}CSH$[59] was not detected in the spectrum

either. This species can be formed by losing two hydrogen atoms from vinylthiol or more likely by combining the ethynyl radical (HC≡C) from the acetylene precursor with the thiol radical (SH) from the 1,2-ethanedithiol precursor. The absence of this species suggests that neither reaction hypotheses are experimentally favorable under the conditions employed. The formation of detectable amounts of vinylthiol is possible because of the high abundance of the 1,2-ethanedithiol precursor and the small (but detectable) quantity the vinylthiol itself limits the subsequent formation of ethynethiol. On the other hand, 1% acetylene was mixed in the gas sample which can provide the HC≡C fragment in the discharge process along with the SH fragment from 1,2-ethanedithiol. The failure to identify HCCSH implies that the recombination of these two fragments is not frequent enough to lead to detectable amounts of ethynethiol.

4.3.2 Thioketene chains

The second type of observed species is the thioketene chains, C_nS (n = 2 - 5),[5-6,9,11-14] HC_nS (n = 2 - 4),[16-18,60] H_2C_nS (n = 2 - 5).[19-22] Of them, C_nS and HC_nS are linear tops and the H_2C_nS are near symmetric tops with C_{2v} molecular symmetry. The observed transitions in the current frequency range are provided in Table 4.2.

Table 4.2. The rotational transitions of identified C_nS, HC_nS, and H_2C_nS species and their SNRs collected with 1.5 million FIDs.

species	$J'-J''$	frequency/MHz	SNR
C=C=S	1-0	11119.440	28.0
C=C=C=S(v=0)	2-1	11561.508	98.3
	3-2	17342.260	140.0
v_4=1	3-2	17371.600	2.6
	3-2	17380.620	2.6

C=C=C=³⁴S	2-1		11281.423	6.7
	3-2		16922.185	6.9
C=C=C=C=S	4-3		12153.65	2.0
C=C=C=C=C=S	6-5		11072.426	2.0

species	J'-J''	F'-F''	frequency	SNR
H-C=C=S	3/2-1/2	1f-0f	17722.400	2.5
		2e-1e	17583.100	4.6
		1e-0e	17591.528	1.8
		2f-1f	17710.230	5.8
H-C=C=C=S	5/2-3/2	3e-2e	13384.040	4.3
		2e-1e	13385.070	1.9
		3f-2f	13394.340	4.0
		2f-1f	13395.890	1.8
H-C=C=C=C=S	9/2-7/2	5-4	12899.333	3.8
		4-3	12899.556	3.3
	11/2-9/2	6-5	15765.880	2.7

species	J'_{KaKc}-J''_{KaKc}	frequency	SNR
H₂C=C=S	101-000	11203.960	10.0
H₂C=C=C=S	212-111	10086.058	4.2
	202-101	10109.915	4.1
	211-110	10133.212	5.4
	313-212	15129.030	3.0
	303-202	15164.840	2.0
	312-211	15199.828	3.0
H₂C=C=C=C=S	414-313	11114.610	4.4
	404-303	11128.800	2.0
	413-312	11142.730	4.0
	515-414	13893.270	6.2
	505-404	13910.990	5.8
	514-413	13928.400	5.7
	616-515	16671.870	7.0
	606-505	16693.200	2.8
	615-514	16714.054	4.8
H₂C=C=C=C=C=S	616-515	10156.510	1.5
	615-514	10172.390	1.5
	717-616	11849.280	2.5
	716-615	11868.820	2.0

Previous studies showed that the ground electronic state of CCS and C_4S are $^3\Sigma^-$ (triplet) while those of C_3S and C_5S are $^1\Sigma^+$ (singlet). With an unpaired electron, the HC_nS species are free radicals that have $^2\Pi$ ground electronic states. Each rotational transition of HC_nS is split twice due to the Λ-type doubling and proton hyperfine structure. Since the assignment of the splitting patterns was well-studied in the literature[16-19,60] and are not the focus of this study, the details are not discussed here.

The existence of most of the listed species was confirmed with several rotational transitions or the unique hyperfine structures from rotational transitions. However, for CCS, H_2CCS, C_4S and C_5S, respectively, only one transition was observed, which is normally not enough to confirm the detection of a molecule, even the simplest linear top. Although C_4S and C_5S have multiple transitions in the current frequency range of the microwave spectrometer, they were not very abundantly produced in the discharge source based on the intensity of the observed spectral lines. On the contrary, the SNR suggests that CCS and H_2CCS are quite abundant in the discharge plasma. Unfortunately, owing to their small molecular size, there is only one rotational transition that falls into the range for each of them. Empirically, given the molecular structure of 1,2-ethanedithiol and the identification of other related sulfur-carbon chains, it is acceptable to use one spectral line that accurately matches the literature frequency to confirm the assignment.

As the H_mCS (m = 0 - 2) species have no rotational transition in the range of 8 – 18 GHz, there is no direct observation of them. However, it is reasonable to predict their existence in the discharge based on other species confirmed to be present. As the 1,2-ethanedithiol precursor only has two carbons, it cannot form a sulfur-carbon chain with three or more carbon atoms through a unimolecular reaction. Therefore, the

detected H_mCCCS (m = 0 - 2) and H_mCCCCS (m = 0, 2) species were formed through secondary reactions. Presumably, on the basis of the formation of H_mCCS, the sulfur-carbon chains were extended to H_mCCCCS by further reacting with acetylene or its radicals. The identified H_mCCCS, especially C_3S with relatively high SNR of the transitions in the ground state, are likely to be produced in the same way which strongly indicates the existence of the H_mCS species. Note that, the SCCS, SCCCS, or SCCCCS species may also be formed by the electric discharge. As they have no permanent dipole moment, they cannot be detected by microwave spectroscopy.

4.3.3 Thials

In this part, the identified species with the thial group (-C(H)=S) are discussed including 2-propenethial ($CH_2=CHC(H)=S$),[61] propynethial ($HC\equiv CC(H)=S$),[35] and its longer chain form ($HC\equiv CC\equiv C(H)=S$).[52] The observed rotational transitions are provided in Table 4.3. These species are likely formed through the combination of the thial group with different hydrocarbyl groups. The thial group is a fragment generated from 1,2-ethanedithiol, which is also an evidence of the formation of H_mCS species above.

Table 4.3. The observed rotational transitions for thials and vinylacetylenes and their SNRs collected with 1.5 million FIDs.

species	J'_{KaKc}-J''_{KaKc}	frequency/MHz	SNR
trans- $CH_2=CHCH=S$	202-101	10861.900	3.0
	303-202	16291.730	3.0
$HC\equiv CCH=S$	212-111	11792.570	7.1
	202-101	12006.400	22.0
	211-110	12222.790	12.0
	313-212	17688.260	30.0
	303-202	18007.301	48.0
	312-211	18333.540	18.0

HC≡CC≡CCH=S	515-414	9527.696	1.5
	616-515	11433.065	1.5
	606-505	11537.388	3.0
	615-514	11644.508	3.0
	717-616	13338.372	2.0
	707-606	13459.710	3.0
	716-615	13585.054	4.0
	909-808	17303.493	2.5
	918-817	17465.947	2.0
CH$_2$=CHC≡CH	101-000	9074.670	1.6
	212-111	17734.540	4.8
	202-101	18146.540	12.5
CH$_2$=CHC≡CC≡CH	404-303	10738.070	3.0
	515-414	13309.350	2.2
	505-404	13422.220	3.3
	514-413	13537.140	6.7

Theoretically, 2-propenethial has two planar rotamers – *cis* and *trans*, although only the latter was detected here and in earlier microwave spectroscopic study.[61] The *cis* conformer was suggested to lie 8.62 kJ/mol higher in energy with a quite high interconversion barrier of 30.33 kJ/mol to the *trans* orientation using *ab initio* SCF method with a basis set of double-zeta (DZ) quality.[62] Besides 2-propenethial, there are another two hydrocarbon molecules observed in this work that contain a vinyl group, which are vinylacetylene (CH$_2$=CHC≡CH)[63] and vinyldiacetylene (CH$_2$=CHC$_4$H).[38] The rotational transitions are also provided in Table 4.3. Apparently, these three vinyl-containing products were formed from the recombination of the vinyl fragment with the C≡C fragment from acetylene or the thial group from 1,2-ethanedithiol. Given the empirical observation that the hydrogenation reaction is not favorable under the conditions employed in the electric discharge, the vinyl group was presumably produced from 1,2-ethanedithiol rather than acetylene. The observation of vinyldiacetylene also implies that longer carbon chains can be formed in the current discharge source.

As acetylene in the precursor mixture is an excellent source to provide the HCC fragment, the more unsaturated variant HCCCHS was observed to be more prevalent in the discharge source once acetylene was added. The formation of *trans*-CH_2CHCHS and HCCCHS implies that 1,2-ethanedithiol is a good precursor to produce the CHS group. With the successful detection of vinylacetylene and its longer chain variant vinyldiacetylene, the formation of HC_4CHS is certainly plausible. However, different functional groups undergo different chemical recombination processes in the discharge plasma, which is no doubt attributed to their unique chemical and physical properties including polarizability, steric hinderance and so on. Based on a pre-test using acetonitrile and acetylene as precursors, the cyano group was found to be attached to up to three $C \equiv C$ triple bonds under the same experimental conditions and formed the long carbon chain $HC \equiv CC \equiv CC \equiv CC \equiv N$.[39] In the present experiment, the HCCCHS thial was detected by multiple rotational transitions with decent SNRs while no transition was observed for the HCCSH thiol. All these results reveal that there was no certain way to assure the formation of the proposed discharge species such as HC_4CHS before the correct spectral assignment.

In the course of this comprehensive study of the discharge plasma of the 1,2-ethanedithiol precursor, the exploration was subsequently reduced due to the successful detection of HC_4CHS in Dr. McCarthy's lab at Harvard Smithsonian Center for Astrophysics.[52] In the work of McCarthy and co-workers, diacetylene ($HC \equiv CC \equiv CH$) was used to provide the carbon chain fragment and CS_2 was to provide the C=S fragment. Both precursors have no permanent dipole moment and thus have no rotational spectrum in the ground vibrational state which makes the spectral analysis much simpler. Using their line list, HC_4CHS was unambiguously identified with eight rotational transitions from the current discharge spectrum which means that

both experiments successfully led to the formation of HC_4CHS. Although the efforts presented in the current study did not lead to the first report of this species, the approach was worthwhile as more complex precursors will be important for laboratory studies to extend astronomical catalogs in the future as more and more complex species are observed.

Thioglyoxal (S=CH-CH=S) is also a candidate for detection in the discharge source. Its *trans* conformer has no permanent dipole and no rotational spectrum. However, the *cis* rotamer lies 18.03 kJ/mol higher in energy with an interconversion barrier of 30.75 kcal/mol from *trans* to *cis*.[62] Of the four most stable conformers of 1,2-ethanedithiol, the two most stable ones have a dihedral angle of the S-C-C-S backbone larger than 90º while those of the other two are smaller than 90º.[51] With the high torsion barrier for the interconversion, if the *cis* rotamer is formed, its spectrum may be captured. Tentative searches yielded no confirmed transitions and this assignment is further complicated by the fact that there are only several *b*-type transitions that fall in the range of the spectrometer.

4.4 Chemical considerations from the dc electrical discharge of 1,2-ethanedithiol

4.4.1 Empirical reaction pathways

There are many techniques that are exploited to explore electrical discharge chemistry such as mass spectrometry,[64] DC slice imaging[65] and infrared spectroscopy.[66] Microwave spectroscopy which is geometry sensitive is also a robust technique to investigate the reactions initiated by the high-voltage electric power. Based on the detected known species, their formation pathways can be empirically

proposed as outlined in Figure 4.5. Through logically connecting the species along the

different branches, the reaction mechanisms can be better understood to a certain

extent which also reflect the reaction environment in the discharge source. Of course,

a comprehensive understanding of this technique and the associated chemistry cannot

be achieved by one or several studies, but every experiment does help us understand

more. With a considerable amount of knowledge accumulated, we will be able to

model the discharge chemistry for chosen precursors and predict the formation of

transient molecular species in this process.
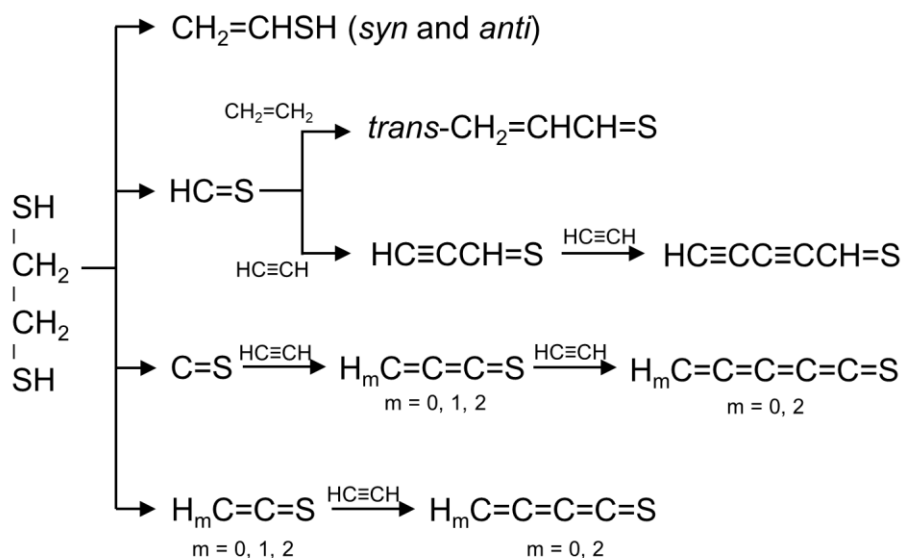
Figure 4.5. A schematic reaction diagram based on the identified transient species in

the discharge spectrum of $HSCH_2CH_2SH + HCCH$.

4.4.2 Prediction of the rotational constants

Besides choosing the right precursors and attempting to produce the target

species with proper discharge conditions, finding the spectral pattern for unknown

species is another major challenge. In the rotational spectrum of the dc electrical

discharge of 1,2-ethanedithiol, over 600 lines were discharge dependent. Of these,

only nine lines with SNR of ~ 3 correspond to HC_4CHS. Therefore, to assist with the spectral assignment, precise predictions of the rotational constants of possible species in the discharge mixture becomes extremely crucial. *Ab initio* and DFT methods are commonly used to calculate the equilibrium structure and the associated rotational constants. However, there is no perfect method in the real world that can predict the rotational constants for all molecules within experimental accuracy, let alone the natural difference between the equilibrium structure and the ground vibrational state structure.

Empirically, the calculated rotational constants can be scaled using the ratio between the experimental and predicted results of some known species with a similar framework.[38] This method is normally used to improve the predicted rotational constants of isotopic species using the results obtained from the parent species as the geometry is considered unchanged with isotopic substitutions. Based on previous studies, it also worked well with several other molecular systems such as vinyl polyacetylenes,[38,67] which implies that the systematic error of the predictions might be close for species with similar frameworks. In this work, the calculated rotational constants of HC_4CHS at the MP2, B3LYP, and B3LYP-D3(BJ) level of theory with cc-pVQZ basis set were also scaled using those from HCCCHS obtained from comparison of experiment (ref. 35) and theory (this work). The results are provided in Table 4.4 with the associated percentage differences. The standard B3LYP method predicts the rotational constants for HCCCHS quite well while the deviations for HC_4CHS are ~3 times larger. Surprisingly, the popular dispersion corrected B3LYP with the Becke-Johnson damping (BJ)[48] makes the results worse. The MP2 method that gives the worst prediction for HCCCHS performed best for HC_4CHS. The deviation of the scaled MP2 rotational constants are consistently reduced. Although

the rotational constants for cyanoacetylenes and vinylacetylenes predicted by the DFT methods can be well scaled,[38] this methodology does not seem to work well for the carbon chain thials. This implies that the scaling method is not a universal way to improve the predictions. A benchmark analysis of quantum-chemical calculations prior to the spectral assignment is always necessary.

Table 4.4. Experimental rotational constants of HCCCHS and HC$_4$HCS compared to the calculated and scaled constants.

	Exp.	MP2	diff.(%)	B3LYP	diff.(%)	B3LYP-D3(BJ)	diff.(%)
	HC≡CCH=S						
A/MHz	42652.0263(40)	41971.35	-1.60	43593.80	2.21	43232.19	1.36
B/MHz	3109.38231(25)	3116.64	0.23	3106.33	-0.10	3116.29	0.22
C/MHz	2894.26571(30)	2901.20	0.24	2899.71	0.19	2906.76	0.43
	HC≡CC≡CCH=S						
A/MHz	26863.6041(7)	25911.62	-3.54	27017.62	0.57	26644.91	-0.81
B/MHz	979.18432(7)	980.96	0.18	983.28	0.42	986.73	0.77
C/MHz	943.93850(6)	945.17	0.13	948.75	0.51	951.50	0.80
	HC≡CC≡CCH=S-scaled constants						
A/MHz		26331.85	-1.98	26433.94	-1.60	26287.34	-2.15
B/MHz		978.67	-0.05	984.25	0.52	984.55	0.55
C/MHz		942.91	-0.11	946.97	0.32	947.41	0.37

*Percentage difference (diff.(%)) in this table is calculated by (theo. - exp.)/exp.

4.4.3 Formation of the thioketene/thiol or thioketene/thial isomer pairs in the electrical discharge source

Moreover, the observation of the carbon chain thioketenes and thials brings out another interesting topic - the formation of isomers in the discharge source. Each thioketene H$_2$C$_n$S (n = 2 – 5) has a possible thiol or thial isomer, which leads to four isomer pairs with n = even giving a thioketene/thiol pair such as H$_2$CCS/HCCSH and H$_2$C$_4$S/HC$_4$SH while n = odd gives rise to thioketene/thial pairs such as

H$_2$CCCS/HCCCHS and H$_2$C$_5$S/HC$_4$CHS. Their relative energies calculated at the MP2/cc-pVQZ level are given in Table 4.5.

Table 4.5. Relative energies between [H$_2$, C$_n$, S] (n = 2 – 5) isomer pairs at the MP2/cc-pVQZ level of theory.

species	H$_2$C=C=S	H$_2$C=C=C=S	H$_2$C=C=C=C=S	H$_2$C=C=C=C=C=S
Energy/Hartree	-474.9432	-512.9362	-550.9515	-588.9498
species	HC≡CSH	HC≡CCHS	HC≡CC≡CSH	HC≡CC≡CCH=S
Energy/Hartree	-474.9199	-512.9352	-550.9378	-588.9537
ΔE/kJ mol^{-1}	61.1	2.6	35.8	-10.4

Of them, the smallest thiol HCCSH was not observed in the present work. Although HC$_4$SH has not been reported in the literature yet, it is also safe to deduce its absence in the current experiment because it is the longer chain form of HCCSH. Interestingly, the successful observation of the HCCSH thiol in a recent study was achieved by using HCCH and H$_2$S as precursors.[59] In that work, HCCSH was produced ~4 times more abundantly than its thioketene isomer H$_2$CCS after taking into account their comparable spectral intensity and quite different dipole moments (μ_a = 0.13 D for HCCSH,[59] μ_a = 1.02 D for H$_2$CCS[21]). The proposed formation pathway of the thiol is a simple radical combination of HCC and HS. Once the species is formed, it needs to overcome a high isomerization barrier of ~80 kJ/mol to produce H$_2$CCS,[68] which is highly unfeasible in the cold jet. Meanwhile, the formation of the co-existing H$_2$CCS was suggested from a different pathway involving atomic sulfur.[59]

In the current work, H$_2$CCS was observed but the HCCSH thiol was not demonstrating the importance of the precursor in directing the chemistry of the source. It is possible that HCCSH has been made in the discharge source via the

combination reaction of HCC and SH, but perhaps not with sufficient quantity for detection. Comparing to the decent SNR of the observed H_2CCS transition, the absence of HCCSH in the discharge spectrum implies that with a neighbouring C-S bond, the SH moiety in 1,2-ethanedithiol is not a good source of the free SH radical like H_2S as one would normally expect. Furthermore, when removing acetylene from the precursor mixture, the transition due to H_2CCS was still detected with similar SNR which implies that this species must be primarily created from 1,2-ethanedithiol by losing several atoms rather than through a pathway that includes the CCH radical.

Rather than being a good provider of the SH fragment, surprisingly, the 1,2-ethanedithiol precursor generated the HCS radical abundantly, which further led to the formation of HCCCHS and HC_4CHS. Based on the MP2 energies, the H_2CCCS thioketene is 2.6 kJ/mol more stable than the isoelectronic HCCCHS thial. As their dipole moments are quite comparable ($\mu_a = 2.06$ D for H_2CCCS,[22] $\mu_a = 1.76$ D for HCCCHS[35]), the more energetic HCCCHS is ~5 times more abundant than H_2CCCS. On the contrary, for the longer chain variants, H_2C_5S is 10.4 kJ/mol less stable than HC_4CHS and both were identified in the discharge spectrum with comparable abundance. These totally agree with the previous suggestions that they were formed from different reaction pathways as shown in Figure 4.5 and did not interconvert through the unimolecular reactions, which also supports the idea that the chemistry in the electrical discharge environment is dominated by kinetics not thermodynamics. Therefore, in such studies, higher energy isomers or conformers should not be excluded simply because they are not thermodynamically favoured.

4.5 Summary

In summary, as the opening chapter describing the electrical discharge work, insights into the reactions were obtained through the product species that were identified in the rotational spectrum from the 1,2-ethanedithiol precursor. Except for vinylthiol which still retains one thiol group, the most common functional group of other sulfur-containing discharge species is carbonothioyl (C=S) which implies that the removal of the hydrogen in SH is very favorable. All of the species with three or more carbon atoms were formed from the recombination of the molecular fragments in the discharge plasma. Isomers produced from different reaction pathways such as the H_2CCCS/HCCCHS isomer pair are maintained in the cold jet expansion when the isomerization barrier is sufficiently high. Although the initial target HC_4CHS was identified by another group in the meantime, the efforts made in analyzing the spectra, proposing reaction pathways, and understanding the isomerization in the discharge environment did provide lots of valuable experience which led to the success of the following projects.

References

(1)   Penzias, A. A.; Solomon, P. M.; Wilson, R. W.; Jefferts, K. B. Interstellar Carbon Monosulfide. *Astrophys. J.* **1971,** *168*, L53-L58.

(2)   Zuckerman, B.; Morris, M.; Palmer, P.; Turner, B. E. Observations of CS, HCN, U89.2, and U90.7 in NGC 2264. *Astrophys. J.* **1972,** *173*, L125-L129.

(3)   Agundez, M.; Marcelino, N.; Cernicharo, J.; Tafalla, M. Detection of Interstellar HCS and its Metastable isomer HSC: New Pieces in the Puzzle of Sulfur Chemistry. *Astron. Astrophys.* **2018,** *611*, L1.

(4)   Sinclair, M. W.; Fourikis, N.; Ribes, J. C.; Robinson, B. J.; Brown, R. D.; Godfrey, P. D. Detection of Interstellar Thioformaldehyde. *Aust. J. Chem.* **1973,** *26* (1), 85.

(5)   Saito, S.; Kawaguchi, K.; Yamamoto, S.; Ohishi, M.; Suzuki, H. Laboratory Detection and Astronomical Identification of a new Free Radical, CCS $^3\Sigma^-$. *Astrophys. J.* **1987,** *317*.

(6)   Yamamoto, S.; Saito, S.; Kawaguchi, K.; Kaifu, N.; Suzuki, H. Laboratory Detection of a new Carbon-Chain Molecule C_3S and Its Astronomical Identification. *Astrophys. J.* **1987,** *317*, L119-L121.

(7)   Bell, M. B.; Avery, L. W.; Feldman, P. A. C_3S and C_5S in IRC +10216. *Astrophys. J.* **1993,** *417*, L37-L40.

(8)   Agúndez, M.; Cernicharo, J.; Guélin, M. New Molecules in IRC +10216: Confirmation of C_5S and Tentative Identification of MgCCH, NCCP, and SiH_3CN. *Astron. Astrophys.* **2014,** *570*, A45.

(9)   Lovas, F. J.; Suenram, R. D.; Ogata, T.; Yamamoto, S. Microwave Spectra and Electric Dipole Moments for Low-*J* Levels of Interstellar Radicals: SO, C_2S, C_3S, *c*-HC_3, CH_2CC, and *c*-C_3H_2. *Astrophys. J.* **1992,** *399*, 325-329.

(10)   Kasai, Y.; Obi, K.; Ohshima, Y.; Hirahara, Y.; Endo, Y.; Kawaguchi, K.; Murakami, A. Laboratory Detection of C_5S by Pulsed-Discharge-Nozzle Fourier Transform Microwave Spectroscopy. *Astrophys. J.* **1993,** *410*, L45-L47.

(11)   Tang, J. A.; Saito, S. Microwave Spectrum of the C_3S Molecule in the Vibrationally Excited States of Bending Modes, v_4 and v_5. *J. Mol. Spectrosc.* **1995,** *169* (1), 92-107.

(12)   Gordon, V. D.; McCarthy, M. C.; Apponi, A. J.; Thaddeus, P. Rotational Spectra of Sulfur–Carbon Chains. I. The Radicals C_4S, C_5S, C_6S, C_7S, C_8S, and C_9S. *Astrophys. J., Suppl. Ser.* **2001,** *134* (2), 311-317.

(13)   Sakai, N.; Takano, S.; Sakai, T.; Shiba, S.; Sumiyoshi, Y.; Endo, Y.; Yamamoto, S. Anomalous ^{13}C Isotope Abundances in C_3S and C_4H Observed toward the Cold Interstellar Cloud, Taurus Molecular Cloud-1. *J. Phys. Chem. A* **2013,** *117* (39), 9831-9839.

(14)   McGuire, B. A.; Martin-Drumel, M. A.; Lee, K. L. K.; Stanton, J. F.; Gottlieb, C. A.; McCarthy, M. C. Vibrational Satellites of C_2S, C_3S, and C_4S: Microwave Spectral Taxonomy as a Stepping Stone to the Millimeter-Wave Band. *Phys. Chem. Chem. Phys.* **2018,** *20* (20), 13870-13889.

(15)   Kewley, R.; Sastry, K. V. L. N.; Winnewisser, M.; Gordy, W. Millimeter Wave Spectroscopy of Unstable Molecular Species. I. Carbon Monosulfide. *J. Chem. Phys.* **1963,** *39* (11), 2856-2860.

(16)   Vrtilek, J. M.; Gottlieb, C. A.; Gottlieb, E. W.; Wang, W.; Thaddeus, P. Laboratory Measurement of the Rotational Spectrum of HCCS. *Astrophys. J.* **1992,** *398*, L73-L76.

(17)   Hirahara, Y.; Ohshima, Y.; Endo, Y. Pulsed‐Discharge‐Nozzle Fourier‐Transform Microwave Spectroscopy of HC_3S($^2\Pi_r$) and HC_4S($^2\Pi_i$). *J. Chem. Phys.* **1994,** *101* (9), 7342-7349.

(18)   McCarthy, M. C.; Vrtilek, J. M.; Gottlieb, E. W.; Tao, F. M.; Gottlieb, C. A.; Thaddeus, P. A Millimeter-Wave Study and Astronomical Search for the HCCCS Radical. *Astrophys. J.* **1994,** *431*, L127-L130.

(19)   Gordon, V. D.; McCarthy, M. C.; Apponi, A. J.; Thaddeus, P. Rotational Spectra of Sulfur‐Carbon Chains. II. HC_5S, HC_6S, HC_7S, and HC_8S, and H_2C_4S, H_2C_5S, H_2C_6S, and H_2C_7S. *Astrophys. J., Suppl. Ser.* **2002,** *138* (2), 297-303.

(20)   Bak, B.; Nielsen, O. J.; Svanholt, H.; Holm, A.; Toubro, N. H.; Krantz, A.; Laureni, J. Microwave Spectra of Thioketene and Four of Its Isotopic Species. *Acta Chem. Scand.* **1979,** *33a*, 161-165.

(21)   Georgiou, K.; Kroto, H. W.; Landsberg, B. M. The Microwave Spectrum, Substitution Structure, and Dipole Moment of Thioketen, $H_2C=C=S$. *J. Mol. Spectrosc.* **1979,** *77*, 365-373.

(22)   Brown, R. D.; Dyall, K. G.; Elmes, P. S.; Godfrey, P. D.; McNaughton, D. The Generation, Microwave Spectrum, and Structure of Propadienethione, $H_2C=C=C=S$. *J. Am. Chem. Soc.* **1988,** *110* (3), 789-792.

(23)   Snyder, L. E.; Hollis, J. M.; Ulich, B. L. Radio Detection of the Interstellar Formyl Radical. *Astrophys. J.* **1976,** *208*, L91-L94.

(24)   Smith, A. M.; Stecher, T. P. Carbon Monoxide in the Interstellar Spectrum of Zeta Ophiuchi. *Astrophys. J.* **1971,** *164*, L43-L47.

(25)   Wilson, R. W.; Jefferts, K. B.; Penzias, A. A. Carbon Monoxide in the Orion Nebula. *Astrophys. J.* **1970,** *161*, L43.

(26)   Snyder, L. E.; Buhl, D.; Zuckerman, B.; Palmer, P. Microwave Detection of Interstellar Formaldehyde. *Phys. Rev. Lett.* **1969,** *22* (13), 679-681.

(27)   Agundez, M.; Cernicharo, J.; Guelin, M. Discovery of Interstellar Ketenyl (HCCO), a Surprisingly Abundant Radical. *Astron. Astrophys.* **2015,** *577*, L5.

(28)   Ohishi, M.; Ishikawa, S.-I.; Yamada, C.; Kanamori, H.; Irvine, W. M.; Brown, R. D.; Godfrey, P. D.; Kaifu, N.; Suzuki, H. Detection of a New Carbon-Chain Molecule, CCO. *Astrophys. J.* **1991,** *380*, L39-L42.

(29)   Turner, B. E. Microwave Detection of Interstellar Ketene. *Astrophys. J.* **1977,** *213*, L75-L79.

(30)   Brown, R. D.; Godfrey, P. D.; Cragg, D. M.; Rice, E. H. N.; Irvine, W. M.; Friberg, P.; Suzuki, H.; Ohishi, M.; Kaifu, N.; Morimoto, M. Tricarbon Monoxide in TMC-1. *Astrophys. J.* **1985,** *297*, 302-308.

(31)   Matthews, H. E.; Irvine, W. M.; Friberg, P.; Brown, R. D.; Godfrey, P. D. A New Interstellar Molecule: Triearbon Monoxide. *Nature* **1984,** *310* (5973), 125-126.

(32)   McGuire, B. A.; Burkhardt, A. M.; Shingledecker, C. N.; Kalenskii, S. V.; Herbst, E.; Remijan, A. J.; McCarthy, M. C. Detection of Interstellar HC_5O in TMC-1 with the Green Bank Telescope. *Astrophys. J.* **2017,** *843* (2), L28.

(33)   Cordiner, M. A.; Charnley, S. B.; Kisiel, Z.; McGuire, B. A.; Kuan, Y. J. Deep K-band Observations of TMC-1 with the Green Bank Telescope: Detection of HC_7O, Nondetection of $HC_{11}N$, and a Search for New Organic Molecules. *Astrophys. J.* **2017,** *850* (2), 187.

(34)   Hirahara, Y.; Suzuki, H.; Yamamoto, S.; Kawaguchi, K.; Kaifu, N.; Ohishi, M.; Takano, S.; Ishikawa, S.-I.; Masuda, A. Mapping Observations of Sulfur-Containing Carbon-Chain Molecules in Taurus Molecular Cloud 1 (TMC-1). *Astrophys. J.* **1992,** *394*, 539-551.

(35)   Brown, R. D.; Godfrey, P. D.; Champion, R.; Woodruff, M. The Microwave Spectrum of Propynethial, HC≡C-CHS. *Aust. J. Chem.* **1982,** *35* (9), 1747-1753.

(36)   Irvine, W. M.; Brown, R. D.; Cragg, D. M.; Friberg, P.; Godfrey, P. D.; Kaifu, N.; Matthews, H. E.; Ohishi, M.; Suzuki, H.; Takeo, H. A New Interstellar Polyatomic Molecule: Detection of Propynal in the Cold Cloud TMC-1. *Astrophys. J.* **1988,** *335*, L89-L93.

(37)   Thorwirth, S.; Harding, M. E.; Dudek, J. B.; McCarthy, M. C. Equilibrium Molecular Structures of Vinyl Carbon Chains: Vinyl Acetylene, Vinyl Diacetylene, and Vinyl Cyanide. *J. Mol. Spectrosc.* **2018,** *350*, 10-17.

(38)   Thorwirth, S.; McCarthy, M. C.; Dudek, J. B.; Thaddeus, P. Fourier Transform Microwave Spectroscopy of Vinyldiacetylene, Vinyltriacetylene, and Vinylcyanodiacetylene. *J. Chem. Phys.* **2005,** *122* (18), 184308.

(39)   McCarthy, M. C.; Levine, E. S.; Apponi, A. J.; Thaddeus, P. Experimental Structures of the Carbon Chains HC_7N, HC_9N, and $HC_{11}N$ by Isotopic Substitution. *J. Mol. Spectrosc.* **2000,** *203* (1), 75-81.

(40)   Mohamed, S.; McCarthy, M. C.; Cooksy, A. L.; Hinton, C.; Thaddeus, P. Rotational Spectra of the Carbon-Chain Radicals HC_5O, HC_6O, and HC_7O. *J. Chem. Phys.* **2005,** *123* (23), 234301.

(41)   Evangelisti, L.; Grabowiecki, A.; van Wijngaarden, J. Chirped Pulse Fourier Transform Microwave Study of 2,2,2-Trifluoroethyl Formate. *J. Phys. Chem. A* **2011,** *115* (30), 8488-92.

(42)   Sedo, G.; van Wijngaarden, J. Fourier Transform Microwave Spectra of a "New" Isomer of $OCS-CO_2$. *J. Chem. Phys.* **2009,** *131* (4), 044303.

(43)   Frisch, M. J.; Trucks, G. W.; Schlegel, H. B.; Scuseria, G. E.; Robb, M. A.; Cheeseman, J. R.; Scalmani, G.; Barone, V.; Petersson, G. A.; Nakatsuji, H.; Li, X.;

Caricato, M.; Marenich, A. V.; Bloino, J.; Janesko, B. G.; Gomperts, R.; Mennucci, B.; Hratchian, H. P.; Ortiz, J. V.; Izmaylov, A. F.; Sonnenberg, J. L.; Williams; Ding, F.; Lipparini, F.; Egidi, F.; Goings, J.; Peng, B.; Petrone, A.; Henderson, T.; Ranasinghe, D.; Zakrzewski, V. G.; Gao, J.; Rega, N.; Zheng, G.; Liang, W.; Hada, M.; Ehara, M.; Toyota, K.; Fukuda, R.; Hasegawa, J.; Ishida, M.; Nakajima, T.; Honda, Y.; Kitao, O.; Nakai, H.; Vreven, T.; Throssell, K.; Montgomery Jr., J. A.; Peralta, J. E.; Ogliaro, F.; Bearpark, M. J.; Heyd, J. J.; Brothers, E. N.; Kudin, K. N.; Staroverov, V. N.; Keith, T. A.; Kobayashi, R.; Normand, J.; Raghavachari, K.; Rendell, A. P.; Burant, J. C.; Iyengar, S. S.; Tomasi, J.; Cossi, M.; Millam, J. M.; Klene, M.; Adamo, C.; Cammi, R.; Ochterski, J. W.; Martin, R. L.; Morokuma, K.; Farkas, O.; Foresman, J. B.; Fox, D. J. *Gaussian 16 Rev. B.01*, Wallingford, CT, 2016.

(44)   Møller, C.; Plesset, M. S. Note on an Approximation Treatment for Many-Electron Systems. *Phys. Rev.* **1934,** *46* (7), 618-622.

(45)   Becke, A. D. Density-Functional Exchange-Energy Approximation with Correct Asymptotic Behavior. *Phys. Rev. A* **1988,** *38* (6), 3098-3100.

(46)   Becke, A. D. Density‑Functional Thermochemistry. III. The Role of Exact Exchange. *J. Chem. Phys.* **1993,** *98* (7), 5648-5652.

(47)   Stephens, P. J.; Devlin, F. J.; Chabalowski, C. F.; Frisch, M. J. *Ab Initio* Calculation of Vibrational Absorption and Circular-Dichroism Spectra Using Density-Functional Force-Fields. *J. Phys. Chem. Lett.* **1994,** *98* (45), 11623-11627.

(48)   Grimme, S.; Ehrlich, S.; Goerigk, L. Effect of the Damping Function in Dispersion Corrected Density Functional Theory. *J. Comput. Chem.* **2011,** *32* (7), 1456-1465.

(49)   Dunning, T. H. Gaussian Basis Sets for Use in Correlated Molecular Calculations. I. The Atoms Boron through Neon and Hydrogen. *J. Chem. Phys.* **1989,** *90* (2), 1007-1023.

(50)   Woon, D. E.; Dunning, T. H. Gaussian Basis Sets for Use in Correlated Molecular Calculations. III. The Atoms Aluminum through Argon. *J. Chem. Phys.* **1993,** *98* (2), 1358-1371.

(51)   Marstokk, K.-M.; Møllendal, H. Structural and Conformational Properties of 1, 2-Ethanedithiol as Studied by Microwave Spectroscopy and *Ab Initio* Calculations. *Acta. Chem. Scand.* **1997,** *51*, 653-663.

(52)   McCarthy, M. C.; Zou, L.; Martin-Drumel, M. A. To Kink or Not: A Search for Long-Chain Cumulenones using Microwave Spectral Taxonomy. *J. Chem. Phys.* **2017,** *146* (15), 154301.

(53)   Tanimoto, M.; Almond, V.; Charles, S. W.; Macdonald, J. N.; Owen, N. L. Microwave Spectrum and Conformation of Vinyl Mercaptan: The *syn* Rotamer. *J. Mol. Spectrosc.* **1979,** *78* (1), 95-105.

(54)   Tanimoto, M.; Macdonald, J. N. Microwave Spectrum and Conformation of Vinyl Mercaptan: The *anti* Rotamer. *J. Mol. Spectrosc.* **1979,** *78* (1), 106-119.

(55)   Sanz, M. E.; McCarthy, M. C.; Thaddeus, P. Vibrational Excitation and Relaxation of Five Polyatomic Molecules in an Electrical Discharge. *J. Chem. Phys.* **2005,** *122* (19).

(56)   Karunatilaka, C.; Shirar, A. J.; Storck, G. L.; Hotopp, K. M.; Biddle, E. B.; Crawley, R.; Dian, B. C. Dissociation Pathways of 2,3-Dihydrofuran Measured by Chirped-Pulse Fourier Transform Microwave Spectroscopy. *J. Phys. Chem. Lett.* **2010,** *1* (10), 1547-1551.

(57)   Kojima, T. Microwave Spectrum of Methyl Mercaptan. *J. Phys. Soc. Jpn.* **1960,** *15* (7), 1284-1291.

(58)   Hayashi, M.; Imaishi, H.; Kuwada, K. Microwave Spectrum, Structure and Dipole Moment of Ethanethiol. I. *Trans* Isomer. *Bull. Chem. Soc. Jpn.* **1974,** *47* (10), 2382-2388.

(59)   Lee, K. L. K.; Martin-Drumel, M. A.; Lattanzi, V.; McGuire, B. A.; Caselli, P.; McCarthy, M. C. Gas Phase Detection and Rotational Spectroscopy of Ethynethiol, HCCSH. *Mol. Phys.* **2018**, 1-11.

(60)   Kim, E.; Habara, H.; Yamamoto, S. Hyperfine Interaction Constants of the HCCS and DCCS Radicals Studied by Fourier Transform Millimeter-Wave Spectroscopy. *J. Mol. Spectrosc.* **2002,** *212* (1), 83-88.

(61)   Georgiou, K.; Kroto, H. W. Microwave Spectrum, Structure, and Dipole Moment of *trans*-2-Propenethial, $CH_2=CHCH=S$. *J. Mol. Spectrosc.* **1980,** *83* (1), 94-104.

(62)   Ha, T.-K.; Nguyen, M. T.; Vanquickenborne, L. Ab Initio Calculations of the Molecular Structures and the Electronic Properties of Sulfur-containing Compounds: III. Thioacrolein ($CH_2=CH–CH=S$) and Thioglyoxal ($S=CH–CH=S$). *Z. Naturforsch., A: Phys. Sci.* **1982,** *37* (2), 125-128.

(63)   Hirose, C. Mirowave Spectra of Vinylacetylene and Monodeutero Vinylacetylene in Ground and Excited Vibrational States. *Bull. Chem. Soc. Jpn.* **1970,** *43*, 3695-3698.

(64)   Hoffmann, V.; Kasik, M.; Robinson, P. K.; Venzago, C. Glow Discharge Mass Spectrometry. *Anal. Bioanal. Chem.* **2005,** *381* (1), 173-188.

(65)   Shi, Y.; Kamasah, A.; Suits, A. G. H Abstraction Channels in the Crossed-Beam Reaction of F + 1-Propanol, 1-Butene and 1-Hexene by DC Slice Imaging. *J. Phys. Chem. A* **2016,** *120* (45), 8933-8940.

(66)   Wagner, J. P.; McDonald, D. C., II; Duncan, M. A. Mid-Infrared Spectroscopy of $C_7H_7^+$ Isomers in the Gas Phase: Benzylium and Tropylium. *J. Phys. Chem. Lett.* **2018,** *9* (16), 4591-4595.

(67)   Martinez, O., Jr.; Lattanzi, V.; Thorwirth, S.; McCarthy, M. C. Detection of Protonated Vinyl Cyanide, CH_2CHCNH^+, a Prototypical Branched Nitrile Cation. *J. Chem. Phys.* **2013,** *138* (9), 094316.

(68)   Gosavi, R. K.; Strausz, O. P. *Ab Initio* Molecular Orbital Studies on Thiirene and its Isomeric Structures. *Can. J. Chem.* **1983,** *61* (11), 2596-2610.

Chapter 5. Rotational spectra of ethynyl isothiocyanate (HCCNCS) and cyanogen isothiocyanate (NCNCS)[1]

5.1 Introduction

Due to their great interest for astrochemistry and astrobiology as reviewed in Chapters 1 and 3, NCO and NCS-bearing species are attracting attention from astronomers and laboratory astrochemists. Besides playing a role as potential interstellar prebiotic molecules in the ISM, they are also well known for the special isomeric arrangement of the NCO/NCS functional group within molecules. For example, the four atoms H, C, N, O can form four existing isomers which are HNCO, HOCN, HCNO, HONC with relative energies of 0, 103.3, 298.8, and 351.9 kJ/mol, respectively calculated using coupled cluster methods.[1] Despite the large energy difference, the three lowest energy forms have been detected in several interstellar sources[1-5] and it was suggested that they were formed from different reaction pathways that are dynamically driven. Their abundance ratios thus are regarded as sensitive probes of the chemical environment such as the density and temperature of the molecular clouds they reside.

Similarly, their sulfur counterparts follow the same energy ordering with a narrower energy range which are HNCS (0.0 kJ/mol), HSCN (27.6 kJ/mol), HCNS (146.9 kJ/mol), HSNC (153.1 kJ/mol) calculated at the ae-CCSD(T)/cc-pwCVQZ

---

level of theory.[6] The lowest energy form (HNCS) was first studied using microwave spectroscopy from a waveguide experiment in 1950[7] and identified in the Sgr B2 molecular cloud in 1979.[8] The second most stable isomer (HSCN) was detected in the laboratory 40 years later by electric discharge coupled to Fourier transform microwave spectroscopy[9] followed by its astrophysical identification in Sgr B2.[10] Both of them were confirmed to be abundant in the cold molecular cloud TMC-1 soon after.[11] Chemical models were proposed to rationalize their abundance ratios in these two sources and suggested their formation through a common precursor $HNCSH^+$. To complete the investigation of the [H, N, C, S] isomeric family, in 2016, the other two higher-energy isomers (HCNS and HSNC) were first characterized in the laboratory using microwave spectroscopy but still await astronomical detection.[6]

In the laboratory, a considerable number of commercial NCO and NCS compounds have been studied such as PhNCO and PhNCS as described in Chapter 3. With the application of the electrical discharge, novel NCO and NCS-containing species may be tailor-made. Motivated by the prevalence of interstellar carbon chain species, this chapter aims to look closer at carbon chain NCO/NCS species. The microwave spectrum of HCCNCO has already been studied in the ground and excited CNC bending states following its formation via pyrolysis of a large precursor $HC \equiv CC(O)N(OSiMe_3)SiMe_3$.[12] Similarly, its isoelectronic form NCNCO[13] and isovalent analog NCNCS[14-15] have been experimentally characterized as well. The equilibrium geometry of these three species is bent at the central nitrogen with a ∠CNC angle of 129°, 140°, and 143° in NCNCO, HCCNCO, and NCNCS, respectively.[16] Their CNC bending motion is governed by a two-dimensional anharmonic potential well function with a barrier in the middle that resembles the bottom of a champagne bottle, which is a potential that can give rise to the phemenon

of quantum monodromy. The top of the barrier in the middle is called the monodromy point and if low enough (below the ground vibrational state), it reflects quasi-linearity of the molecule. Based on microwave spectroscopic studies using a generalized semi-rigid bender (GSRB) Hamiltonian, the barrier to linearity is nearly halved when HCC (537.2 cm^{-1}) replaces NC (1014.8 cm^{-1}) in NCNCO. With S-substitution to form NCNCS, the monodromy point (270 cm^{-1}) is reduced to around one quarter of that of NCNCO, giving rise to complex bending-rotation energy level patterns which have been extensively studied in the microwave through infrared regions.[14-15,17-18] These earlier studies makes their isoelectronic or isovalent analog HCCNCS an excellent target to investigate by rotational spectroscopy. There are no prior experimental or theoretical studies of this molecule in the literature.

5.2 Experimental methods

The title compound HCCNCS was produced from a high voltage dc discharge (~700 V) of a gas mixture containing CH_3NCS (Sigma Aldrich Canada, 97%) and acetylene. The construction of the discharge assembly was described in Chapter 4. As CH_3NCS is solid at room temperature (mp: 30-34°C), a small volume was heated in a glass bubbler seated in a temperature-controlled water bath maintained at 37 °C. A gas mixture of acetylene (0.5%) in neon (1.5 atm) was bubbled through 1-2 mL of the liquid CH_3NCS before passing through the pulsed nozzle to the discharge channel. HCCNCS was formed in the hot dc discharge plasma and cooled to a rotational temperature of several Kelvin in the supersonic expansion.

The rotational spectrum was initially recorded in segments of 2 GHz using the cp-FTMW spectrometer between 8 and 19 GHz.[19] Following tentative assignment of spectral lines to the parent HCCNCS molecule, these same features were later re-

investigated with the higher resolution using the Balle-Flygare FTMW spectrometer[20] to resolve the ^{14}N nuclear quadrupole hyperfine splitting. As the cavity-based instrument offers greater sensitivity, the spectra of the ^{34}S and ^{13}C minor isotopologues were then recorded in their natural abundance by step-scanning small frequency regions. To separate discharge dependent species from background transitions due to the precursor CH_3NCS, background spectra were recorded with the discharge voltage turned off. The non-discharge dependent transitions were removed from the discharge spectra afterwards. Moreover, the experiment was repeated with no acetylene in the precursor mixture to investigate the acetylene dependent species.

5.3 Computational details

In this chapter, all theoretical calculations were carried out with the Gaussian 09 software.[21] To obtain the equilibrium structure of HCCNCS, the geometry was optimized at the MP2,[22] B3LYP,[23-25] and the dispersion corrected B3LYP-D3(BJ)[26] levels of theory using Dunning's aug-cc-pVXZ (X= T, Q)[27-29] and cc-pVQZ basis sets.[27,29] Surprisingly, the employed methods with aug-cc-pVTZ basis set produced a nonlinear equilibrium structure which is bent at nitrogen while the others output a linear geometry. To investigate the potential quasilinearity, the potential energy scan was performed about the ∠CNC angle with a step of 2º between 160º and 180º. Meanwhile, other geometric parameters were relaxed. Moreover, natural bond orbital (NBO) calculation were employed to analyze the orbital configuration at the B3LYP/cc-pVQZ level with the NBO 3.1 code.[30] To make the comparison with its isovalent and isoelectronic counterparts, the same calculation was carried out for HCCNCO, NCNCO, NCNCS, respectively.

5.4 Results and discussion

5.4.1 Electric discharge reactions

As the first electric discharge experiment was performed using the broadband cp-FTMW instrument, hundreds of discharge dependent transitions were observed despite the fact that only four rotational transitions due to the parent HCCNCS fall within the frequency range of 8 – 19 GHz used. Fifteen discharge species were readily identified based on their previously reported microwave spectra. These known species include, for example, NCNCS,[15] HNCS,[7,31] HSCN,[9] HC_3N,[32-33] HC_5N,[34] and CH_3CN[35] and the observed transitions are provided in Table 5.1. Possible reaction pathways are proposed here based on the identified species as presented in Figure 5.1.

Table 5.1. Collection of the discharge species identified from the CH_3NCS precursor mixed with and without HCCH, and the corresponding transition frequencies (MHz) and SNRs.

species	transition	frequency /MHz	CH_3NCS	CH_3NCS+HCCH
			SNR	SNR
CCS	1-0	11119.45	NO	4.4
CCCS	2-1	11561.52	NO	34.6
	3-2	17342.25		13.3
H_2C_2S	$1_{01}-0_{00}$	11203.98	2.5	10.9
H_2C_3S	$3_{13}-2_{12}$	15129.06	NO	9.8
	$3_{03}-2_{02}$	15164.86		9.3
	$3_{12}-2_{11}$	15199.84		9.9
H_2C_4S	$4_{14}-3_{13}$	11114.58	NO	1.7
	$4_{04}-3_{03}$	11128.84		2.0
	$4_{13}-3_{12}$	11142.73		2.2
	$6_{16}-5_{15}$	16671.89		5.0
	$6_{15}-5_{14}$	16714.07		4.9
HCCCHS	$2_{12}-1_{11}$	11792.49	NO	2.4
	$2_{02}-1_{01}$	12006.40		1.9
	$2_{11}-1_{10}$	12222.79		2.2

		3_{03}-2_{02}	18007.34		3.0
HCCCN	1-0	1-1	9097.04	\	41.9
		2-1	9098.34	\	65.9
		0-1	9100.27	\	23.2
	2-1	2-2	18194.87	4.0	22.5
		1-0	18195.10	4.7	29.4
		3-2	18196.24	24.0	115.4
		1-1	18198.30	3.7	17.1
HC$_5$N	4-3	4-4	10649.23	NO	3.2
		5-4	10650.65		52.2
		3-3	10625.50		3.2
	5-4	6-5	13313.36		9.4
	6-5	7-6	15975.95		3.0
	7-6	8-7	18638.60		4.6
CH$_3$CN	1-0	2-2	18396.70	200.0	40.6
		3-2	18397.97	350.0	62.1
		1-2	18399.85	54.0	13.7
CH$_3$CCH	1-0		17091.74	NO	5.2
c-C$_3$H$_2$	1_{10}-1_{01}		18343.14	NO	25.2
NCS	3/2-1/2	5/2 e-3/2 e	18192.90	13.3	6.3
		3/2 e-1/2 e	18200.08	6.3	1.6
		3/2 e-3/2 e	18207.40	6.3	1.8
		1/2 e-1/2 e	18211.25	4.6	1.8
		3/2 f-3/2 f	18439.25	9.0	2.0
		5/2 f-3/2 f	18477.00	28.0	9.0
		1/2 f-1/2 f	18490.10	9.1	2.8
		3/2 f-1/2 f	18510.42	8.0	3.3
HSCN	1_{01}-0_{00}	1-1	11468.64	7.5	2.0
		2-1	11469.85	14.0	4.3
		0-1	11471.70	3.0	\
HNCS	1_{01}-0_{00}	0-1	11728.50	8.5	4.5
		2-1	11729.00	60.0	27.2
		1-1	11729.35	27.5	14.3
NCNCS	4_{14}-3_{13}		12859.95	3.8	\
	4_{04}-3_{03}		12909.51	37.8	9.8
	4_{13}-3_{12}		12975.08	3.6	\
	5_{05}-4_{04}		16136.77	10.5	6.0
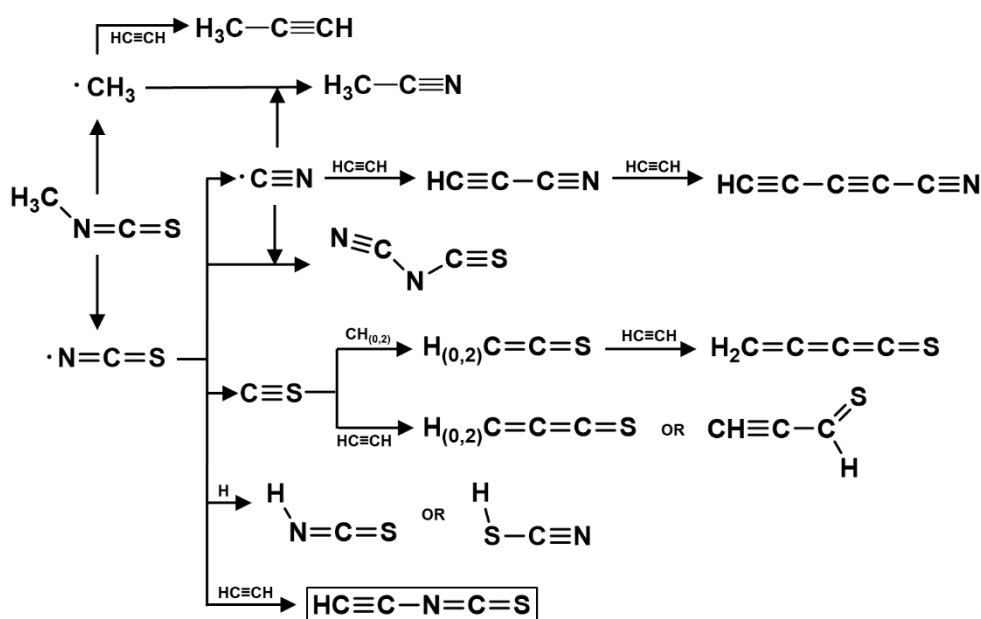
Figure 5.1. Schematic summary of the reaction pathways that are proposed based on the identified discharge species. Among them, HCCNCS in the black box was predicted to be formed.

5.4.2 Rotational spectrum of HCCNCS

Based on the *ab initio* (MP2) and density functional (B3LYP and B3LYP-D3(BJ)) calculations with Dunning-type basis sets (aug-cc-pVXZ (X = T, Q) and cc-pVQZ), the equilibrium geometry of HCCNCS was predicted to be linear or quasilinear with a rotational constant B_e of approximately 1507 MHz and dipole moment of ~1.7 D. Interestingly, all three methods with aug-cc-pVTZ basis set consistently yielded a slightly bent equilibrium structure at nitrogen (∠CNC = 172.5 or ~178). Later, potential energy scans were carried out about the ∠CNC angle and the resulting curves are provided in Figure 5.2. The barrier to linearity is very small (~ 0.02 kJ/mol) which brings up the concern about the symmetry that the molecule may adopt. If HCCNCS is nonlinear, rotational transitions involving K_a =1 levels would

arise due to the lower symmetry. These $K_a = 1$ energy levels will not be highly populated and the resulting transitions will not be experimentally observable in the cold jet based on the predicted rotational constants but this may mislead the relevant laboratory and astrophysical researches in the future if the structure is not well-characterized.
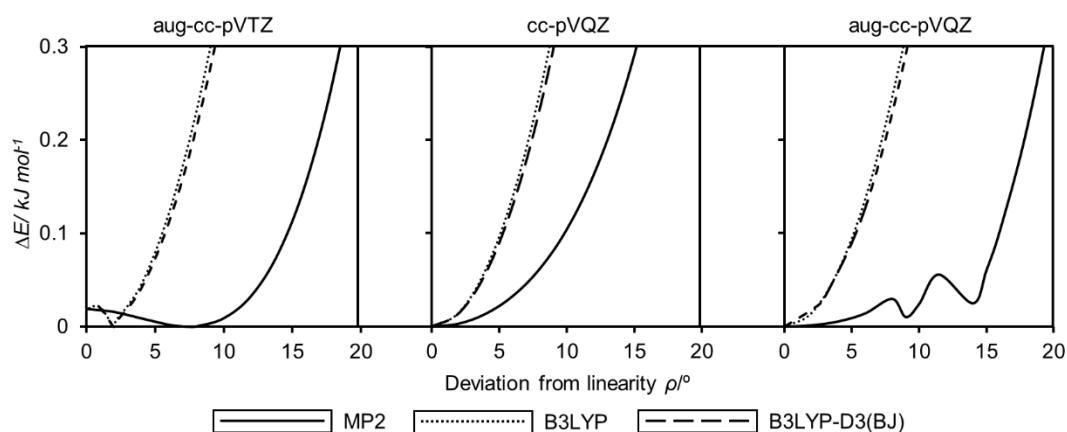
Figure 5.2. The CNC bending (ρ is the deviation from linearity at nitrogen) potential of HCCNCS at the MP2, B3LYP, and B3LYP-D3(BJ) levels of theory with Dunning's basis sets (aug-cc-pVTZ, cc-pVQZ, aug-cc-pVQZ). Note that the fluctuation at the MP2/aug-cc-pVQZ level of theory results from the intramolecular basis set superposition error (BSSE) and is not likely to be real.

To resolve this issue, high level CCSD(T) calculations were performed with a variety of basis sets using the CFOUR program[36] by collaborating with Dr. Michael E. Harding at the Karlsruhe Institut für Technologie (KIT). The results of this work reveal that the optimized geometries show a striking variation with the employed basis set.[37] Nonlinear equilibrium geometries are obtained from valence-only CCSD(T) computations employing ANO0, ANO1, ANO2, cc-pV(T+d)Z, cc-pCVTZ, and cc-pwCVTZ.[38-41] All electron CCSD(T) geometry optimizations yield linear

structures if cc-pCVXZ or cc-pwCVXZ (X = T, Q, and 5) basis sets are used,

however, a nonlinear equilibrium structure is found if diffuse functions are added

(CCSD(T)/aug-cc-pwCVTZ). It thus appears that CCSD(T) computations employing

the aforementioned rather sizeable basis sets are not accurate enough to resolve the

problem. This may be due to intramolecular basis set superposition errors as seen

previously, for example, in the case of the monosubstituted benzenes,[42] or problems

arising from the concepts of the equilibrium structure itself.[43] Given the subtle energy

difference (of just a few cm^{-1}) between linear and nonlinear structural configuration, it

seems that higher level correlation effects beyond CCSD(T), relativistic effects, and

Born-Oppenheimer corrections together with large basis set expansions could be

considered in the future, which is beyond the scope of this study.

The linearity of HCCNCS is irregular in contrast with its isoelectronic

(NCNCS)[14-15,17-18] and isovalent (HCCNCO[12] and NCNCO[13]) counterparts which are

prototypical examples of quantum monodronomy. To precisely probe the potential

energy along the CNC bending coordinate, potential energy scans were carried out for

the four species at the fc-CCSD(T)/cc-pV(T+d)Z level of theory as shown in Figure

5.3. The equilibrium geometry of the molecules tends to be less bent and the barrier to

linearity becomes lower in energy as the cyano group (C≡N) is replaced by the

ethynyl group (HC≡C) and oxygen is substituted with sulfur which agrees with the

previous experimental or theoretical study on these related species.[16] When it comes

to HCCNCS which contains both the ethynyl group and sulfur, the bending potential

becomes so flat (barrier height of ~10 cm^{-1} or 0.12 kJ/mol) that the energy barely

changes with a deviation of over 10º from linearity at nitrogen. The floppiness places

HCCNCS into a fundamentally difficult situation to characterize both experimentally

and theoretically just like the dispute on the linearity of the ground state C_3 species since 1959.[44]
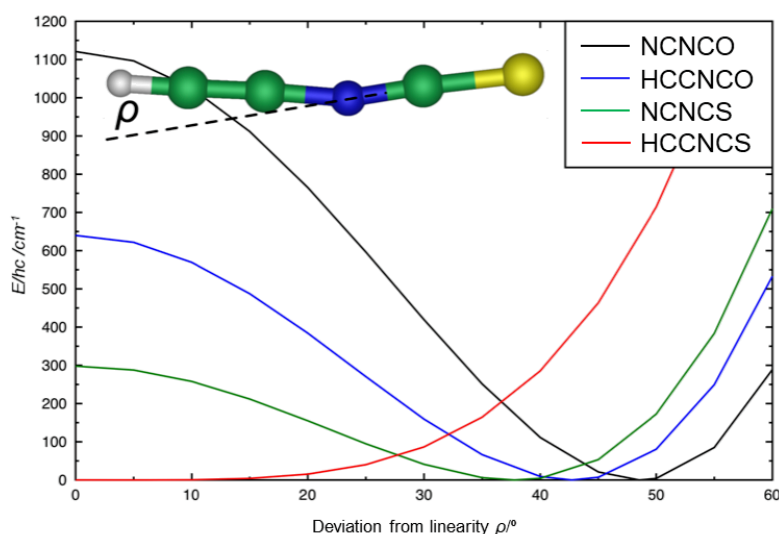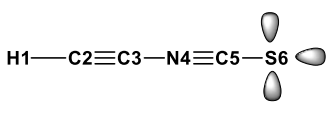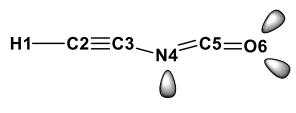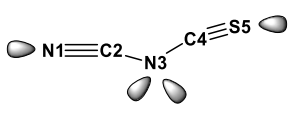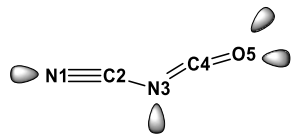
Figure 5.3. Potential energies as a function of the CNC bending angle (ρ) for HCCNCS, NCNCS, HCCNCO, and NCNCO at the fc-CCSD(T)/cc-pV(T+d) Z level of theory. (This image is modified from the published version, 1000 cm^{-1} = 11.96 kJ/mol).

NBO analysis provides information concerning the electronic structure based on the optimized geometry of the four isovalent species NCNCO, HCCNCO, NCNCS and HCCNCS at the B3LYP/cc-pVQZ level of theory. A summary of the occupied NBOs and valence lone pairs for the leading Lewis structures is provided in Table 5.2. The major difference in electronic structure in this set is found at the central nitrogen and the terminal chalcogen atoms. For the two NCO compounds, a lone pair is localized on nitrogen and the sp^2-like hybridization of nitrogen leads to a bent equilibrium geometry. However, the central nitrogen (N3) of NCNCS is more like sp^3-hybridized with two lone pairs. Meanwhile, C4 and S5 form a triple bond in NCNCS. In contrast, the C-S bond in the isoelectronic HCCNCS compound is a

120

single bond and three valence lone pairs are localized on the sulfur end. The valence

orbitals of nitrogen (N4) are sp-like hybridized and form a N≡C triple bond with the

neighbouring C5 which results in the linear or quasilinear ∠CNC angle. It is these

distinct electronic structures that govern the different equilibrium geometries and the

corresponding CNC bending potentials shown above. It is interesting to find such

diversity in the geometries and energetics of these seemingly similar molecules in

contrast to say the PhNCO/PhNCS pair in Chapter 3.

Table 5.2. Summary of electronic properties of the Lewis-like bonding and valence

lone pair NBOs for HCCNCS, HCCNCO, NCNCS, NCNCO computed at the

B3LYP/cc-pVQZ level of theory.

BD(X-Y)	occupancy	X(%)	Y(%)	BD(X-Y)	occupancy	X(%)	Y(%)
σ(H1-C2)	1.988	62.04	37.96	σ(H1-C2)	1.988	38.03	61.97
σ(C2-C3)	1.983	48.63	51.37	σ(C2-C3)	1.985	48.95	51.05
π(C2-C3)	1.938	49.32	50.68	π(C2-C3)	1.965	49.74	50.26
π(C2-C3)	1.938	49.32	50.68	π(C2-C3)	1.958	49.82	50.18
σ(C3-N4)	1.981	37.70	62.30	**σ(C3-N4)**	1.983	38.05	61.95
σ(N4-C5)	1.987	62.87	37.13	**LP(N4)**	1.541	0.00	0.00
π(N4-C5)	1.925	68.26	31.74	**σ(N4-C5)**	1.987	61.23	38.77
π(N4-C5)	1.925	68.26	31.74	**π(N4-C5)**	1.919	72.76	27.24
σ(C5-S6)	1.990	59.05	40.95	σ(C5-O6)	1.995	35.92	64.08
LP(S6)	1.977			π(C5-O6)	1.993	25.78	74.22
LP(S6)	1.572			LP(O6)	1.973		
LP(S6)	1.572			LP(O6)	1.620		

BD(X-Y)	occupancy	X(%)	Y(%)	BD(X-Y)	occupancy	X(%)	Y(%)
LP(N1)	1.963			LP(N1)	1.608		
σ(N1-C2)	1.993	55.85	44.15	σ(N1-C2)	1.995	56.16	43.84

121

π(N1-C2)	1.962	53.90	46.10	π(N1-C2)	1.980	54.00	46.00
π(N1-C2)	1.958	53.83	46.17	π(N1-C2)	1.972	54.21	45.79
σ(C2-N3)	1.983	37.87	62.13	**σ(C2-N3)**	1.978	38.80	61.20
LP(N3)	1.489			**LP(N3)**	1.961		
LP(N3)	1.468			**σ(N3-C4)**	1.986	60.23	39.77
σ(N3-C4)	1.988	62.53	37.47	**π(N3-C4)**	1.913	73.69	26.31
σ(C4-S5)	1.988	58.39	41.61	σ(C4-O5)	1.997	35.75	64.25
π(C4-S5)	1.986	29.31	70.69	πC4-O5)	1.993	26.67	73.33
π(C4-S5)	1.980	31.16	68.84	LP(O5)	1.972		
LP(S5)	1.976			LP(O5)	1.604		

Experimentally, regularly spaced transitions consistent with HCCNCS were identified in the dense broadband discharge spectrum, a subset of which are shown in Figure 5.4 along with some other observed discharge dependent species. The tentative assignment was confirmed using the more sensitive Balle-Flygare spectrometer in the range of 4 – 26 GHz. Altogether, seven rotational transitions ($J'' = 1 - 7$) were collected with the resolved hyperfine structure arising from the ^{14}N nuclear quadrupole moment. Despite the difficulties of establishing its equilibrium structure, the subsequent detection of transitions from the ^{34}S and all three ^{13}C isotopologues in natural abundance leaves little doubt to the assignment of HCCNCS. The measured lines are given in Table S1, Appendix A and sample spectra are shown in Figure 5.5. Effectively, HCCNCS appears to be linear in the ground vibrational state. The rotational spectra of the five isotopologues were fit individually to a linear molecule Hamiltonian in the SPFIT program[45] and the resulting parameters are provided in Table 5.3 along with the predicted parameters at the CCSD(T)/cc-pwCVTZ level (yielding a linear equilibrium geometry).
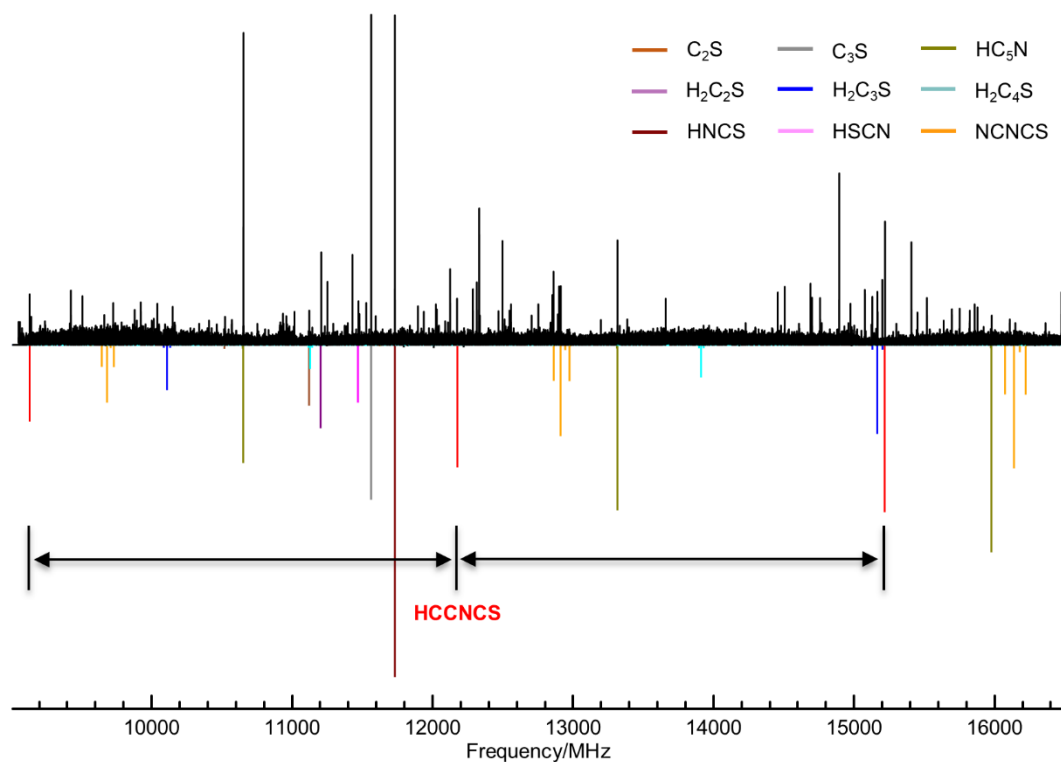
Figure 5.4. Top: discharge dependent lines in the cp-FTMW (obtained with 1.6 million FIDs); bottom: the simulated spectra at 5K for HCCNCS and other species identified as discharge products. The simulated intensities are based on dipole moments but do not account for the abundance of all discharge products.
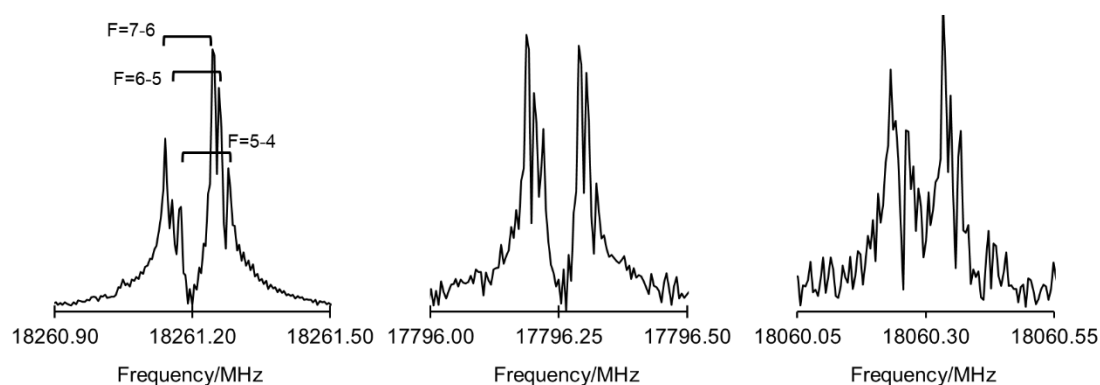
Figure 5.5. ^{14}N hyperfine structure of the J'-J'' = 6-5 transition from the parent (left), ^{34}S species (middle), and one ^{13}C species (right) of HCCNCS, collected with 200, 2000, and 32 000 cycles, respectively. The line intensities are in arbitrary scale.

Table 5.3. Ground state spectroscopic constants of the parent species of HCCNCS and its ^{13}C and ^{34}S isotopologues.

	parent	CCSD(T)/cc-pwCVTZ (calc.)		
B/MHz	1521.77406(4)	1525.0		
D/kHz	0.09630(5)	0.039		
eQq/MHz	2.360(8)	2.39		
rms/kHz	1.95	\		
μ/D		1.79		
# lines	30	\		
	$H^{13}CCNCS$	$HC^{13}CNCS$	$HCCN^{13}CS$	$HCCNC^{34}S$
B/MHz	1478.35699(23)	1505.0314(5)	1520.44966(18)	1483.02745(10)
D/kHz	0.0922(24)	0.096(24)	0.0957(18)	0.0899(12)
eQq/MHz	2.59(22)	2.53(26)	2.27(9)	2.36(3)
rms/kHz	2.01	1.63	1.74	1.66
# lines	7	5	8	16

The calculated rotational constant B and nuclear quadrupole coupling constant eQq are in good agreement with experiment whereas the experimental centrifugal distortion constant D is 2.47 times greater than the theoretical value. It is known that the experimentally determined D_0 is affected by zero point vibrational motions while the equilibrium D_e is independent of the flexibility of the molecule.[46] Based on a series of studies on similar species, such as $C_{2n+1}O$, $C_{2n+1}N^-$, $C_{2n}H^-$, and $NC_{2n-1}H$, by Botschwina and co-workers,[47-48] the ratio of D_0 (exp.)/D_e (theo.) is linked to the degree of floppiness or the flatness of the bending potential of the chain. The flatter the potential, the higher the ratio and the floppier the molecule. Upon comparison with known species, the ratio of D_0 (exp.)/D_e (theo.) of HCCNCS (2.39) derived in the present study is intermediate to that of highly flexible C_3 (7.26) and l-C_3H^+ (1.80).[46]

Assuming linearity, the bond lengths of HCCNCS were estimated via least squares fitting of the semi-experimental equilibrium rotational constants (A_e^{SE}, B_e^{SE}, C_e^{SE}) of the five isotopologues using Kisiel's STRFIT program.[49] These constants were determined by correcting the experimental rotational constants of each

isotopologue with the zero point vibrational effects computed at the VPT2 CCSD(T)/cc-pwCVTZ level of theory by collaborator M. E. Harding. The results are presented in Table 5.4 and show great agreement with the equilibrium structure computed at the CCSD(T) level.

Table 5.4. Equilibrium bond lengths (r_e) at the CCSD(T) level of theory and semi-experimental bond length (r_e^{SE}) from least squares fitting in Å.

	r_e^{SE}	r_e(cc-pwCVTZ)	r_e(cc-pwCVQZ)	r_e(cc-pwCV5Z)
R(H1C2)	1.06211*	1.0621	1.0612	1.061
R(C2C3)	1.207(1)	1.2093	1.207	1.2063
R(C3N4)	1.304(3)	1.3009	1.2991	1.2988
R(N4C5)	1.192(5)	1.1888	1.187	1.1866
R(C5S6)	1.573(3)	1.5726	1.5698	1.569

* For the fit, the H-C bond length was fixed to r_e = 1.0621 Å as the deuterated species was not studied.

In addition, spectral lines attributed to rotational transitions in an excited vibrational state of the parent HCCNCS were subsequently found via step-scanning using the Balle-Flygare instrument. These transitions are split due to l-type doubling as shown in Figure 5.6. The relative intensity of the $J'- J'' = 6 - 5$ transition was ~5% that of the ground state. The measured transitions are provided in Table S2, Appendix A and the excited state constants obtained from fitting the transitions are summarized in Table 5.5. However, this doubly degenerate bending mode cannot be assigned to a particular vibrational state with confidence. Given the fact that the low-lying vibrational modes are cooled in the supersonic jet expansion as reported for other polyatomic species such as HC_3N,[50] the observed vibrational satellites are not necessarily from the lowest-lying CNC-bending mode.

Table 5.5. Spectroscopic constants for the observed excited state of the parent HCCNCS species.

	$v=1$
B /MHz	1522.79930(8)
D /kHz	0.0858(9)
eQq /MHz	2.34(4)
q_v /kHz	314.21(16)
q_vJ /kHz	0.0034(17)
rms/kHz	1.58
# lines	26
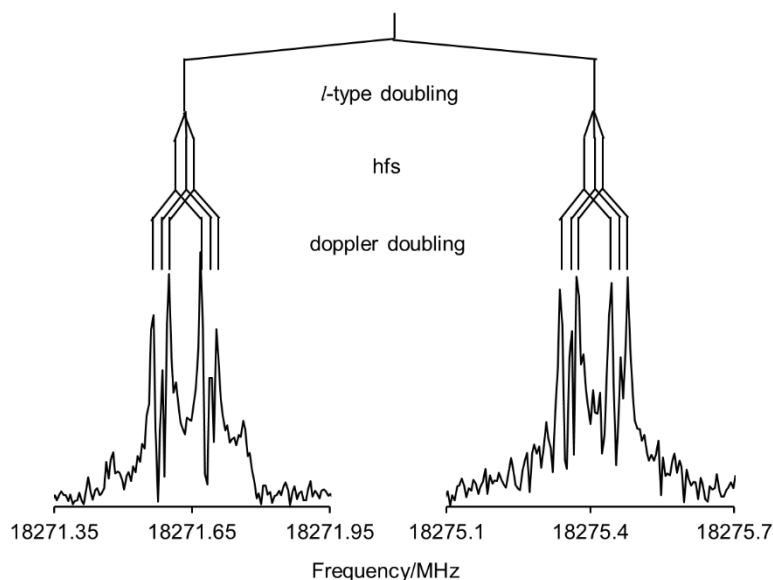
Figure 5.6. The assignment of l-type doubling and ^{14}N hyperfine structure of the *J'-J''* = 6-5 transition in an excited vibrational state of HCCNCS.

5.4.3 Rotational spectrum of NCNCS

In the course of this work to characterize HCCNCS for the first time, additional experiments were performed on NCNCS, the isoelectronic analog of HCCNCS. NCNCS has been extensively studied in the microwave through infrared regions[14-15,17-18] as a prototypical case of quantum monodromy. In these studies, the sample was conventionally prepared through the thermal isomerization of $S(CN)_2$. The rotational

constants and high order distortion constants were well determined for the ground state structure.[14] However, the hyperfine structure arising from the two ^{14}N nuclei in this molecule has not been characterized yet as it is a challenge to assign these features without access to a cavity-based FTMW spectrometer.

As shown in Table 5.1 and the pathways in Figure 5.1, NCNCS was identified as a discharge dependent species which was likely formed through the combination of NC and NCS radicals. Later on, the high-resolution microwave spectrum was re-visited with the resolved ^{14}N nuclear quadrupole hyperfine structures via the Balle-Flygare FTMW spectroscopy. As a better precursor for the CN fragment, acetonitrile (CH$_3$CN) was used instead of acetylene in the gas mixture. In total, 18 rotational transitions with 130 hyperfine components were recorded. The collected hyperfine structure of the 2_{02}-1_{01} transition is provided in Figure 5.7 as an example. The hyperfine structure is assigned following the coupling scheme:

$$\vec{F}_1 = \vec{J} + \vec{I}_{N(C)}; \ \vec{F} = \vec{F}_1 + \vec{I}_{N(CS)}$$

The measured transitions were then fit to Watson's A-reduced Hamiltonian using SPFIT program[45] and the resulting experimental parameters are summarized in Table 5.6.

Table 5.6. Ground state spectroscopic constants of the parent species of NCNCS.

Parameters	parent
A/MHz	97008.1(18)
B/MHz	1628.09798(13)
C/MHz	1599.32113(12)
D_J/kHz	0.39678(50)
D_{JK}/kHz	-991.525(35)
d_J/kHz	0.05724(81)
$1.5\chi_{aa, N1}$/MHz	-4.3655(17)
$0.25(\chi_{bb, N1}$-$\chi_{cc, N1})$/MHz	-0.172(10)

$1.5\chi_{aa, N3}$/MHz	4.0721(17)
$0.25(\chi_{bb, N3}-\chi_{cc, N3})$/MHz	-0.0740(78)
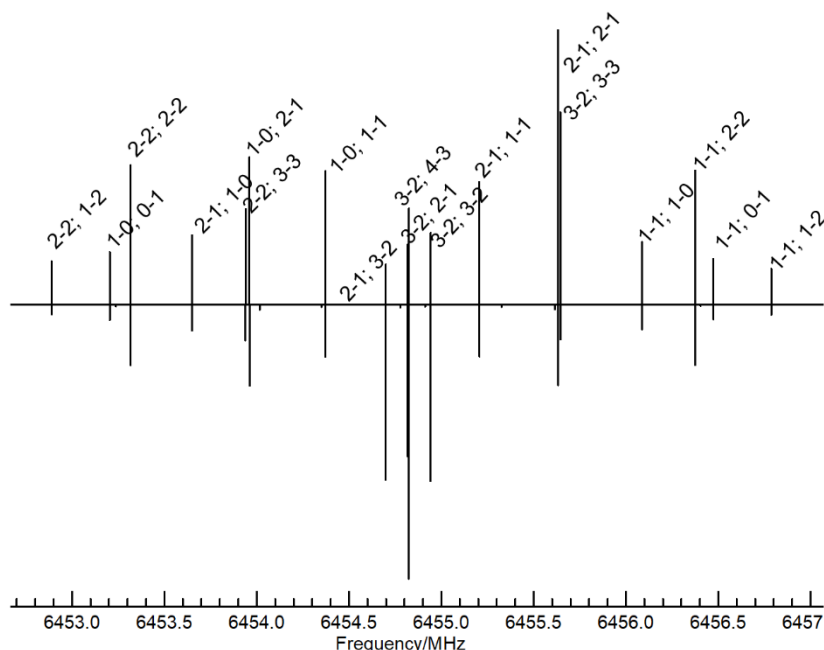
Figure 5.7. The assignment of the hyperfine components (F_1'-F_1''; F'-F'') of the 2_{02}-1_{01} rotational transition arising from two ^{14}N nuclear quadrupole moments in NCNCS (top) and the simulated spectrum (bottom) based on the experimental constants.

5.5 Summary

To sum up, the application of the electric discharge successfully produced HCCNCS by using CH_3NCS and HCCH as precursors. The rotational spectrum of this highly flexible molecular species in its ground and an excited bending vibrational state has been investigated with the resolved ^{14}N hyperfine structure for the first time. The assignment is confirmed by the observation of the ^{34}S and ^{13}C minor isotopic species. The bond lengths derived for the semi-experimental structure are in excellent agreement with calculations at the CCSD(T) level; however, it is surprisingly difficult

to establish the equilibrium geometry due to its extremely flat CNC bending potential. Future theoretical studies including the derivation of a highly accurate potential energy surface would be helpful to model the vibrational-rotational behavior of HCCNCS. In the meantime, the isoelectronic species NCNCS was abundantly generated by replacing HCCH in the gas mixture with CH_3CN. The spectroscopic analysis of the complex hyperfine structure due to two ^{14}N nuclei was performed and precisely determined the nuclear quadrupole coupling constants. The success of creating and characterizing these two species motivated the work presented in the next chapter which describes the study of longer chain variants of these molecules.

References

(1)   Brünken, S.; Gottlieb, C. A.; McCarthy, M. C.; Thaddeus, P. Laboratory Detection of HOCN and Tentative Identification in Sgr B2. *Astrophys. J.* **2009,** *697* (1), 880-885.

(2)   Snyder, L. E.; Buhl, D. Interstellar Isocyanic Acid. *Astrophys. J.* **1972,** *177*, 619-623.

(3)   Buhl, D.; Snyder, L. E.; Edrich, J. An Interstellar Emission Line from Isocyanic Acid at 1.4 Centimeters. *Astrophys. J.* **1972,** *177*, 625-628.

(4)   Brünken, S.; Belloche, A.; Martín, S.; Verheyen, L.; Menten, K. M. Interstellar HOCN in the Galactic Center Region. *Astron. Astrophys.* **2010,** *516*, A109.

(5)   Marcelino, N.; Cernicharo, J.; Tercero, B.; Roueff, E. Discovery of Fulminic Acid, HCNO, in Dark Clouds. *Astrophys. J.* **2009,** *690*, L27-L30.

(6)   McGuire, B. A.; Martin-Drumel, M. A.; Thorwirth, S.; Brunken, S.; Lattanzi, V.; Neill, J. L.; Spezzano, S.; Yu, Z.; Zaleski, D. P.; Remijan, A. J.; Pate, B. H.; McCarthy, M. C. Molecular Polymorphism: Microwave Spectra, Equilibrium Structures, and an Astronomical Investigation of the HNCS Isomeric Family. *Phys. Chem. Chem. Phys.* **2016,** *18* (32), 22693-22705.

(7)   Beard, C. I.; Dailey, B. P. The Structure and Dipole Moment of Isothiocyanic Acid. *J. Chem. Phys.* **1950,** *18* (11), 1437-1441.

(8)   Frerking, M. A.; Linke, R. A.; Thaddeus, P. Interstellar Isothiocyanic Acid. *Astrophys. J.* **1979,** *234*, L143-L145.

(9)   Brünken, S.; Yu, Z.; Gottlieb, C. A.; McCarthy, M. C.; Thaddeus, P. Laboratory Detection of Thiocyanic Acid HSCN. *Astrophys. J.* **2009,** *706* (2), 1588-1593.

(10) Halfen, D. T.; Ziurys, L. M.; Brünken, S.; Gottlieb, C. A.; McCarthy, M. C.; Thaddeus, P. Detection of a New Interstellar Molecule: Thiocyanic Acid HSCN. *Astrophys. J.* **2009,** *702* (2), L124-L127.

(11) Adande, G. R.; Halfen, D. T.; Ziurys, L. M.; Quan, D.; Herbst, E. Observations of the [HNCS]/[HSCN] Ratio in Sgr B2 and TMC-1: Evidence for Low-Temperature Gas-Phase Chemistry. *Astrophys. J.* **2010,** *725* (1), 561-570.

(12) Ross, S. C.; Cooper, T. A.; Firth, S.; Kroto, H. W.; Walton, D. R. M. The Microwave Spectrum and Semirigid Bender Analysis of Isocyanatoethyne, HC≡CNCO. *J. Mol. Spectrosc.* **1992,** *152* (1), 152-167.

(13) Hocking, W. H.; Gerry, M. C. L. The Microwave Spectrum of Cyanogen Isocyanate (NCNCO). *J. Mol. Spectrosc.* **1976,** *59* (3), 338-354.

(14) Winnewisser, B. P.; Winnewisser, M.; Medvedev, I. R.; De Lucia, F. C.; Ross, S. C.; Koput, J. Analysis of the FASSST Rotational Spectrum of NCNCS in View of Quantum Monodromy. *Phys. Chem. Chem. Phys.* **2010,** *12* (29), 8158-8189.

(15) King, M. A.; Kroto, H. W.; Landsberg, B. M. Microwave Spectrum of the Quasilinear Molecule, Cyanogen Isothiocyanate (NCNCS). *J. Mol. Spectrosc.* **1985,** *113* (1), 1-20.

(16) Winnewisser, M.; Winnewisser, B. P.; Medvedev, I. R.; De Lucia, F. C.; Ross, S. C.; Bates, L. M. The Hidden Kernel of Molecular Quasi-Linearity: Quantum Monodromy. *J. Mol. Spectrosc.* **2006,** *798* (1-3), 1-26.

(17) Winnewisser, M.; Winnewisser, B. P.; De Lucia, F. C.; Tokaryk, D. W.; Ross, S. C.; Billinghurst, B. E. Pursuit of Quantum Monodromy in the Far-Infrared and Mid-Infrared Spectra of NCNCS Using Synchrotron Radiation. *Phys. Chem. Chem. Phys.* **2014,** *16* (33), 17373-17407.

(18) Winnewisser, B. P.; Winnewisser, M.; Medvedev, I. R.; Behnke, M.; De Lucia, F. C.; Ross, S. C.; Koput, J. Experimental Confirmation of Quantum Monodromy: the Millimeter Wave Spectrum of Cyanogen Isothiocyanate NCNCS. *Phys. Rev. Lett.* **2005,** *95* (24), 243002.

(19) Evangelisti, L.; Grabowiecki, A.; van Wijngaarden, J. Chirped Pulse Fourier Transform Microwave Study of 2,2,2-Trifluoroethyl Formate. *J. Phys. Chem. A* **2011,** *115* (30), 8488-92.

(20) Sedo, G.; van Wijngaarden, J. Fourier Transform Microwave Spectra of a "New" Isomer of OCS-CO_2. *J. Chem. Phys.* **2009,** *131* (4), 044303.

(21) Frisch, M. J.; Trucks, G. W.; Schlegel, H. B.; Scuseria, G. E.; Robb, M. A.; Cheeseman, J. R.; Scalmani, G.; Barone, V.; Mennucci, B.; Petersson, G. A.; Nakatsuji, H.; Caricato, M.; Li, X.; Hratchian, H. P.; Izmaylov, A. F.; Bloino, J.; Zheng, G.; Sonnenberg, J. L.; Hada, M.; Ehara, M.; Toyota, K.; Fukuda, R.; Hasegawa, J.; Ishida, M.; Nakajima, T.; Honda, Y.; Kitao, O.; Nakai, H.; Vreven, T.; Montgomery, J. A.; Peralta, J. E.; Ogliaro, F.; Bearpark, M.; Heyd, J. J.; Brothers, E.; Kudin, K. N.; Staroverov, V. N.; Keith, T.; Kobayashi, R.; Normand, J.; Raghavachari, K.; Rendell, A.; Burant, J. C.; Iyengar, S. S.; Tomasi, J.; Cossi, M.; Rega, N.; Millam, J. M.; Klene, M.; Knox, J. E.; Cross, J. B.; Bakken, V.; Adamo, C.; Jaramillo, J.; Gomperts, R.; Stratmann, R. E.; Yazyev, O.; Austin, A. J.; Cammi, R.; Pomelli, C.; Ochterski, J. W.; Martin, R. L.; Morokuma, K.; Zakrzewski, V. G.; Voth, G. A.; Salvador, P.; Dannenberg, J. J.; Dapprich, S.; Daniels, A. D.; Farkas, O.; Foresman, J. B.; Ortiz, J. V.; Cioslowski, J.; Fox, D. J., Gaussian 09, Revision B.01. Wallingford CT, 2010.

(22) Møller, C.; Plesset, M. S. Note on an Approximation Treatment for Many-Electron Systems. *Phys. Rev.* **1934,** *46* (7), 618-622.

(23)   Becke, A. D. Density-Functional Exchange-Energy Approximation with Correct Asymptotic Behavior. *Phys. Rev. A* **1988,** *38* (6), 3098-3100.

(24)   Becke, A. D. Density‐Functional Thermochemistry. III. The Role of Exact Exchange. *J. Chem. Phys.* **1993,** *98* (7), 5648-5652.

(25)   Stephens, P. J.; Devlin, F. J.; Chabalowski, C. F.; Frisch, M. J. *Ab Initio* Calculation of Vibrational Absorption and Circular-Dichroism Spectra Using Density-Functional Force-Fields. *J. Phys. Chem. Lett.* **1994,** *98* (45), 11623-11627.

(26)   Grimme, S.; Ehrlich, S.; Goerigk, L. Effect of the Damping Function in Dispersion Corrected Density Functional Theory. *J. Comput. Chem.* **2011,** *32* (7), 1456-1465.

(27)   Dunning, T. H. Gaussian Basis Sets for Use in Correlated Molecular Calculations. I. The Atoms Boron through Neon and Hydrogen. *J. Chem. Phys.* **1989,** *90* (2), 1007-1023.

(28)   Kendall, R. A.; Dunning, T. H.; Harrison, R. J. Electron Affinities of the First-Row Atoms Revisited. Systematic Basis Sets and Wave Functions. *J. Chem. Phys.* **1992,** *96* (9), 6796-6806.

(29)   Woon, D. E.; Dunning, T. H. Gaussian Basis Sets for Use in Correlated Molecular Calculations. III. The Atoms Aluminum through Argon. *J. Chem. Phys.* **1993,** *98* (2), 1358-1371.

(30)   Glendening, E. D.; Reed, A. E.; Carpenter, J. E.; Weinhold, F., NBO Version 3.1.

(31)   Niedenhoff, M.; Winnewisser, G.; Yamada, K. M. T.; Belov, S. P. Pure Rotational Spectra of HNCS in the Far Infrared: Ground State Analysis. *J. Mol. Spectrosc.* **1995,** *169* (1), 224-242.

(32)   Creswell, R. A.; Winnewisser, G.; Gerry, M. C. L. Rotational Spectra of the
^{13}C and ^{15}N Isotopic Species of Cyanoacetylene. *J. Mol. Spectrosc.* **1977,** *65* (3), 420-429.

(33)   Thorwirth, S.; Muller, H. S.; Winnewisser, G. The Millimeter- and Submillimeter-Wave Spectrum of HC_3N in the Ground and Vibrationally Excited States. *J. Mol. Spectrosc.* **2000,** *204* (1), 133-144.

(34)   Bizzocchi, L.; Degli Esposti, C.; Botschwina, P. Millimeter-Wave Spectroscopy of Rare Isotopomers of HC_5N and DC_5N: Determination of a Mixed Experimental–Theoretical Equilibrium Structure for Cyanobutadiyne. *J. Mol. Spectrosc.* **2004,** *225* (2), 145-151.

(35)   Müller, H. S. P.; Drouin, B. J.; Pearson, J. C. Rotational Spectra of Isotopic Species of Methyl Cyanide, CH_3CN, in Their Ground Vibrational States up to Terahertz Frequencies. *Astron. Astrophys.* **2009,** *506* (3), 1487-1499.

(36)   Sun, W.; van Wijngaarden, J. Isothiocyanato-Containing Carbon Chains: The Laboratory Detection of HCCCCNCS and NCCCNCS via Rotational Spectroscopy. *J. Phys. Chem. A* **2018,** *122* (38), 7659-7665.

(37)   Sun, W.; Davis, R. L.; Thorwirth, S.; Harding, M. E.; van Wijngaarden, J. A Highly Flexible Molecule: The Peculiar Case of Ethynyl Isothiocyanate HCCNCS. *J. Chem. Phys.* **2018,** *149* (10), 104304.

(38)   Almlöf, J.; Taylor, P. R. General Contraction of Gaussian Basis Sets. I. Atomic Natural Orbitals for First- and Second-Row Atoms. *J. Chem. Phys.* **1987,** *86* (7), 4070-4077.

(39)   Woon, D. E.; Dunning, T. H. Gaussian Basis Sets for Use in Correlated Molecular Calculations. V. Core-Valence Basis Sets for Boron through Neon. *J. Chem. Phys.* **1995,** *103* (11), 4572-4585.

(40)   Dunning, T. H.; Peterson, K. A.; Wilson, A. K. Gaussian Basis Sets for Use in Correlated Molecular Calculations. X. The Atoms Aluminum through Argon Revisited. *J. Chem. Phys.* **2001,** *114* (21), 9244-9253.

(41)   Peterson, K. A.; Dunning, J. T. H. Accurate Correlation Consistent Basis Sets for Molecular Core–Valence Correlation Effects: The Second Row Atoms Al–Ar, and the First Row Atoms B–Ne Revisited. *J. Chem. Phys.* **2002,** *117* (23), 10548-10560.

(42)   Hrenar, T.; Rauhut, G.; Werner, H.-J. Impact of Local and Density Fitting Approximations on Harmonic Vibrational Frequencies. *J. Phys. Chem. A* **2006,** *110* (5), 2060-2064.

(43)   Stanton, J. F. Note: Is It Symmetric or Not? *J. Chem. Phys.* **2013,** *139* (4), 046102.

(44)   Varandas, A. J. C.; Rocha, C. M. R. C_n (n=2-4): Current Status. *Phil. Trans. R. Soc. A* **2018,** *376* (2115), 20170145.

(45)   Pickett, H. M. The Fitting and Prediction of Vibration-Rotation Spectra with Spin Interactions. *J. Mol. Spectrosc.* **1991,** *148* (2), 371-377.

(46)   Botschwina, P.; Stein, C.; Sebald, P.; Schröder, B.; Oswald, R. Strong Theoretical Support for the Assignment of B11244 to *l*-C_3H^+. *Astrophys. J.* **2014,** *787* (1).

(47)   Botschwina, P.; Oswald, R. Carbon Chains of Type $C_{2n+1}N^-$ (n=2-6): A Theoretical Study of Potential Interstellar Anions. *J. Chem. Phys.* **2008,** *129* (4), 044305.

(48)   Botschwina, P.; Oswald, R. Calculated Spectroscopic Properties for $C_{12}H^-$ and $HC_{11}N$, Molecules of Astrochemical Interest. *J. Mol. Spectrosc.* **2009,** *254* (1), 47-52.

(49)   Kisiel, Z. Least-Squares Mass-Dependence Molecular Structures for Selected Weakly Bound Intermolecular Clusters. *J. Mol. Spectrosc.* **2003,** *218* (1), 58-67.

(50)   Sanz, M. E.; McCarthy, M. C.; Thaddeus, P. Vibrational Excitation and

Eelaxation of Five Polyatomic Molecules in an Electrical Discharge. *J. Chem. Phys.*

2005, *122* (19).

Chapter 6.   Rotational spectra of HC≡CC≡CN=C=S and N≡CC≡CN=C=S[1]

6.1 Introduction

Following the successful detection of HCCNCS and NCNCS, the work in this chapter is an extension of Chapter 5. As mentioned previously, HNCS and HSCN have been detected in two interstellar molecular clouds, Sgr B2[1-2] and TMC-1.[3] Along with their existence, cyanopolyynes (H(C≡C)$_n$C≡N, n = 0 – 4)[4-6] have been found to be abundant in TMC-1 as well as their radicals C$_n$N.[7-8] Of these, HC$_3$N[9] and HC$_5$N,[10] have also been observed in Sgr B2. Moreover, another class of linear carbon chain radicals HC$_n$ (n = 3 – 8),[11-13] a perfect source of carbon for the formation of longer chain species, have been observed in TMC-1. The co-existence of HNCS and HSCN with C$_n$N and C$_n$H radicals provide an excellent environment for the formation of HCCNCS and NCNCS as well as their longer chain variants. This motivated the laboratory detection of HC≡CC≡CN=C=S and N≡CC≡CN=C=S using rotational spectroscopy as described in this chapter.

6.2 Experimental methods

Given the successful generation of HCCNCS and NCNCS in Chapter 5, the search for their longer chain analogs was subsequently carried out. However, the

---

[1] A version of this chapter has been published with the following citation: Sun, W.; van Wijngaarden, J., Isothiocyanato-Containing Carbon Chains: The Laboratory Detection of HCCCCNCS and NCCCNCS via Rotational Spectroscopy. J. Phys. Chem. A 2018, 122 (38), 7659-7665. Copyright © 2019 American Chemical Society

rotational transitions identified for HCCNCS in the broadband discharge spectrum had quite low signal-to-noise ratio (SNR) making it unlikely that more complex versions will be detected by this instrument. In contrast, the line intensities observed with the cavity-based FTMW spectrometer were sufficiently high to allow the collection of transitions of the parent species as well as the ^{13}C and ^{34}S isotopic species in their natural abundance with the ^{14}N hyperfine signature resolved. Therefore, the spectral survey for the longer chain species was directly performed with the narrowband Balle-Flygare spectrometer using a step scan method in which the spectrum was collected using many individual steps over several months.[14]

The same experimental setup was used to produce the title species HC$_4$NCS and NC$_3$NCS as described earlier. The construction of the discharge assembly was described in Chapter 4 and the preparation of the main precursor – methyl isothiocyanate (CH$_3$NCS) was demonstrated in Chapter 5. Initially, to generate HC$_4$NCS, the amount of acetylene was doubled (1%) in the gas mixture. The precursor mixture was then delivered to the spectrometer through the glass bubbler containing CH$_3$NCS with a stagnation pressure of ~1 atm and pulsed into the cavity through the discharge nozzle with a repetition rate of 7 Hz. The spectrometer scanned the spectrum with a step size of 0.25 MHz which is very time consuming in comparison with the fast collection of a 2 GHz window using the cp-FTMW spectrometer. For each step, the cavity must be manually tuned to be in resonance before the spectrum is collected at that frequency and this is repeated each time the incident frequency is changed. After candidate transitions were found for HC$_4$NCS, the acetylene precursor in the gas mixture was replaced by diacetylene HC≡CC≡CH (0.5%). The gas sample of diacetylene was synthesized by a collaborator J. Dourado through a one-step reaction[15] and stored in a small stainless steel cylinder. The

molecular source conditions were optimized for the new gas mixture and the rotational transitions were collected in the range of 4 – 26 GHz. With the utilization of the longer carbon chain precursor, the spectrum was enhanced about 10-fold, which suggested that the observed transitions were due to HC_4NCS. The improved signals allowed for the detection of its ^{34}S isotopologue in natural abundance. Next, in order to produce the isoelectronic analog, NC_3NCS, a precursor mixture of 0.5% acetonitrile (CH_3CN, 99.8%, purchased from Sigma-Aldrich) and 0.5% acetylene (HCCH) in Ne was seeded with the CH_3NCS using the same setup and the spectrum was obtained in the same stepwise manner as described above.

The spectral linewidths with this instrument are typically ~7 kHz (FWHM) which makes it possible to routinely resolve hyperfine components from the ^{14}N nuclear quadrupole moment. The identification of the two linear species was confirmed by the experimental B_0 rotational constants and the characteristic ^{14}N nuclear hyperfine structures which were consistent with theoretical estimates. The accuracy of the frequencies is typically measured to within ±2 kHz. The rotational spectrum of the ^{34}S substituted HC_4NCS species was observed in natural abundance to further confirm the assignment but the signal intensity of NC_3NCS was insufficient to observe transitions of its minor isotopologues.

6.3 Computational details

The equilibrium structures of HC_4NCS and NC_3NCS were found by first optimizing the geometries at the MP2[16] and B3LYP[17-19] levels of theory with Dunning's cc-pVQZ basis set[20-21] implemented in the Gaussian 09 software.[22] To investigate the CNC bending potential energy curves about these minima, both methods were then used to complete a series of single point calculations by varying

the CNC angle from 175º to 180º with a step size of one degree. For each point, the chosen value for the CNC angle was kept constant while all other structural parameters were optimized. The potential energy curves confirmed that both species are linear rather than quasilinear as observed under similar levels of theory for HCCNCS owing to its very flat potential.[23] The results are shown in Figure 6.1. Coupled-cluster calculations with the CCSD(T) method[24-25] were then carried out with the cc-pVTZ basis set[20-21,26] using the ORCA program[27] and provided further confirmation of the linear configuration of both chains. A summary of the calculated rotational constants, ^{14}N nuclear quadrupole coupling constants and permanent electric dipole moment of HC_4NCS and NC_3NCS at all three levels of theory is shown in Table 6.1.
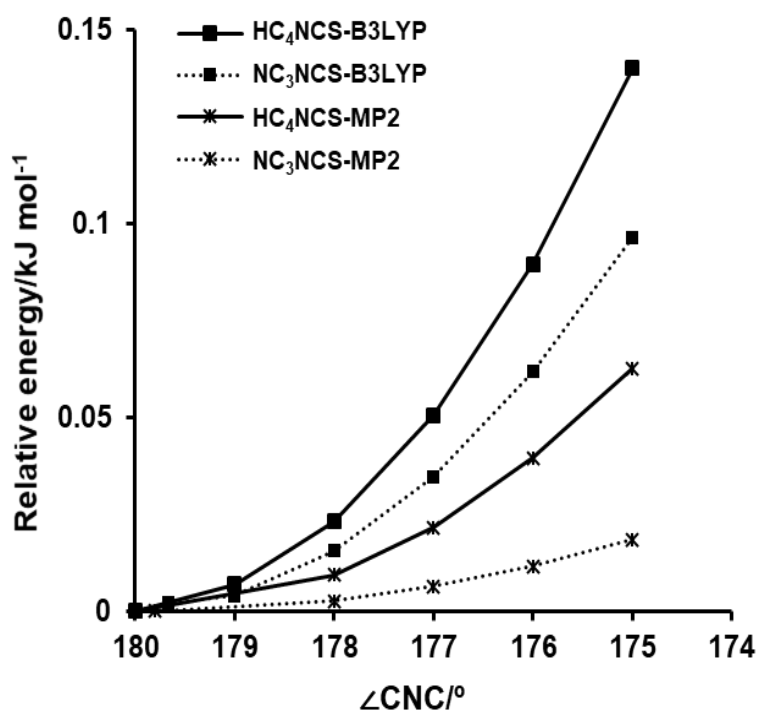
Figure 6.1. Plot of the CNC bending potentials of HC_4NCS and NC_3NCS from single point calculations with the B3LYP/cc-pVQZ and MP2/cc-pVQZ methods.

Table 6.1. Computed rotational constants B_e, ^{14}N nuclear quadrupole coupling

constants and dipole moment of HC$_4$NCS and NC$_3$NCS at various levels of theory.

Parameters	HC$_4$NCS			NC$_3$NCS		
	MP2[a]	B3LYP[a]	CCSD(T)[b]	MP2[a]	B3LYP[a]	CCSD(T)[b]
B_e/MHz	588.4	596.3	586.5	589.1	595.0	585.2
eQq(NCS)/MHz	2.30	2.24	2.26	2.42	2.37	2.39
eQq(NC)/MHz	\	\	\	-3.90	-4.89	-4.01
μ/D	1.26	1.12	1.65	4.24	4.11	3.75

[a]cc-pVQZ basis set.
[b]cc-pVTZ basis set.

6.4 Spectroscopic characterization of HCCCCNCS and

NCCCNCS

As expected based on the computational results, the rotational spectra

observed for both HC$_4$NCS and NC$_3$NCS were those of a linear molecule with

regularly spaced transitions. A total of 17 rotational transitions ($J'' = 3 - 19$) were

recorded for the HC$_4$NCS parent and the observed frequencies are listed in Table S3,

Appendix B. The Balle-Flygare FTMW spectrometer was able to resolve [14]N

hyperfine structure for those with J'' values less than 9. A sample spectrum of the

resolved hyperfine structure (hfs) of the $J' - J'' = 6 - 5$ transition is provided in

Figure 6.2. The full set of observed transitions was fit to a linear top Hamiltonian

using Pickett's SPFIT program.[28-29] The resulting spectroscopic constants are reported

in Table 6.2. The constants, including the ^{14}N nuclear quadrupole coupling constant

eQq, 2.30(5) MHz, are in favorable agreement with the *ab initio* values in Table 6.1.

Rotational transitions of the [34]S substituted species were well-predicted by scaling the

experimental B_0 constant of the parent species. In total, eight rotational transitions

were collected for the [34]S species and fit in the same way as the parent. The rms error

of each fit falls below 2 kHz.

Figure 6.2. Example FTMW spectrum of the $J'–J'' = 6 – 5$ rotational transition of the HC$_4$NCS parent showing the assigned ^{14}N hyperfine structure after averaging 3000 cycles.

Table 6.2. Spectroscopic constants of the parent and ^{34}S singly substituted species of HC$_4$NCS, and the parent of NC$_3$NCS.

Parameters	HC$_4$NCS-parent	HC$_4$NCS-^{34}S	NC$_3$NCS
B_0/MHz	595.09307(2)	580.67632(1)	596.26344(2)
D_0/Hz	7.50(6)	7.1(1)	19.71(4)
$eQq(NCS)$/MHz	2.27(6)	2.3(1)	2.39(3)
$eQq(NC)$/MHz	\	\	4.2(1)
#lines	27	13	28
rms/kHz	1.82	1.87	1.29

As NC$_3$NCS needs molecular fragments from three precursors CH$_3$NCS, CH$_3$CN and HCCH for formation in the jet, the intensity of its rotational transitions was very low and only about 1/10 that of HC$_4$NCS despite the larger predicted dipole moment at all levels of theory (Table 6.1). Due to the presence of two ^{14}N nuclear quadrupole moments, there are more hyperfine components for each rotational

transition which provides a convenient means to confirm the observation of this long chain analog of HC_4NCS. In total, 15 rotational transitions ($J'' = 3 - 19$) were recorded and the hyperfine structure was resolved and assigned for the two ^{14}N nuclei. The $J' - J'' = 5 - 4$ and $8 - 7$ rotational transitions were not observed as they were overshadowed by intense spectral lines of the precursors. The assignment was made using quantum numbers corresponding to the coupling scheme:

$$\vec{F_1} = \vec{J} + \vec{I}_{N(C)}; \vec{F} = \vec{F_1} + \vec{I}_{N(CS)}$$

The observed frequencies are summarized in Table S4, Appendix B. The rms error of the global fit is 1.3 kHz using the SPFIT program set to a linear top Hamiltonian. The experimentally determined parameters including the two ^{14}N nuclear quadrupole coupling constants are provided in Table 6.2. The two quadrupole hyperfine constants, eQq(NC) and eQq(NCS), are in good agreement with the *ab initio* results in Table 6.1 given the difficulty in assigning the complex splitting pattern. A sample spectrum of the $J' - J'' = 7 - 6$ hyperfine transitions along with a simulated spectrum from the fit spectroscopic constants is shown in Figure 6.3.

6.5 Discussion

The rotational constants of HC_4NCS and NC_3NCS are well-predicted by the theoretical calculations. The differences in the B rotational constants between the experimental and the theoretical values at the B3LYP and MP2 levels of theory with cc-pVQZ basis set and at the CCSD(T) level of theory with cc-pVTZ basis set are 0.20%, -1.13%, -1.44% for HC_4NCS and -0.20%, -1.20%, -1.86% for NC_3NCS, respectively. Hyperfine structure from the nitrogen nucleus ($I_N = 1$) was resolved for both molecules for some of the low J rotational transitions, as illustrated in Figure 6.2 and Figure 6.3, and the distinct hyperfine splitting patterns are consistent with those

143

predicted for HC$_4$NCS and NC$_3$NCS. Furthermore, ^{34}S singly substituted HC$_4$NCS

was observed in natural abundance and confirmed the identification of the parent

species. For NC$_3$NCS, the signal intensity was too low to observe minor

isotopologues in natural abundance, however, the identification was substantiated by

testing the parent signal response to turning the discharge off, and to removing

CH$_3$NCS and CH$_3$CN from the precursor mixture. A survey of an extra 200 MHz on

each side from the most intense parent transitions ($J'-J'' = 10-9$ for HC$_4$NCS, $J'-$

$J'' = 15-14$ for NC$_3$NCS) was carried out to search for transitions involving excited

levels of the bending modes as was reported for HCCNCS in Chapter 5 but no

additional transitions were found. This is likely due to the low intensity of even the

ground state transitions which required averaging thousands (and tens of thousands)
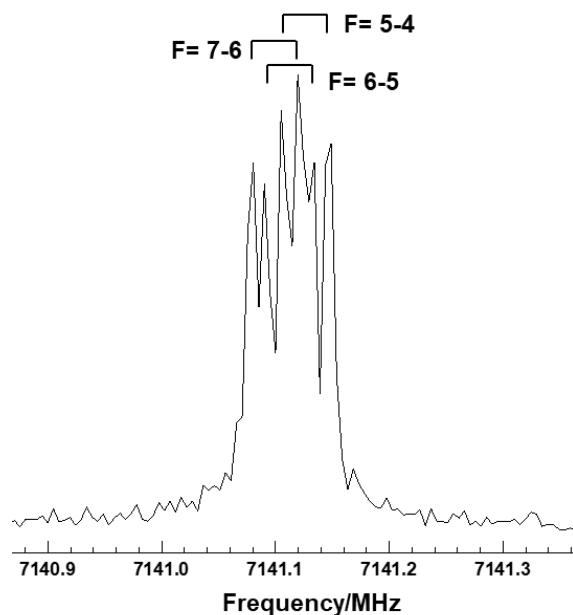
of FIDs.
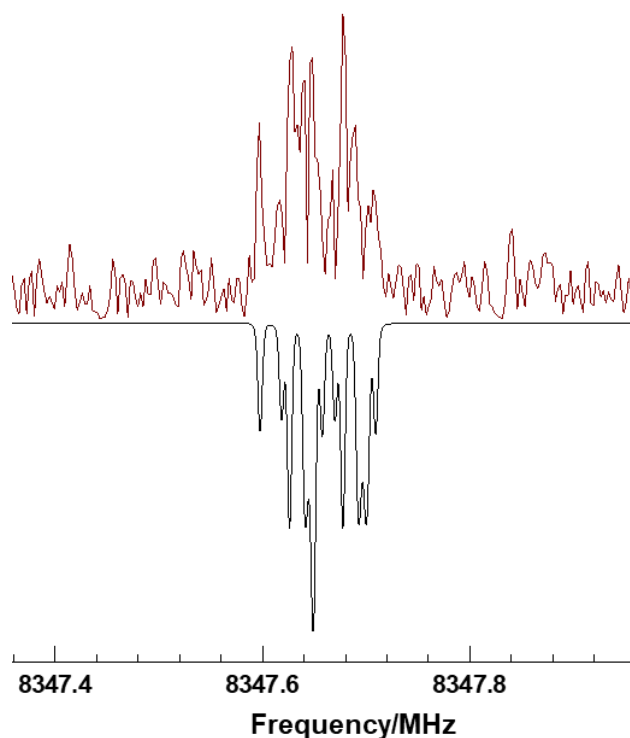
Figure 6.3. Sample FTMW spectrum (top) of the $J'-J'' = 7-6$ rotational transition of

the NC$_3$NCS parent showing the assigned ^{14}N hyperfine structure after averaging

144

32500 cycles and the simulated spectrum (bottom) based on the experimental

constants.

As reported previously, HCCNCS is effectively a linear molecule despite the

fact that its isoelectronic analog NCNCS is bent ($\angle$ NCN = 183.5°, $\angle$ CNC = 143.0°

and $\angle$ NCS = 185.4°) in the ground vibrational state.[30] With the elongation of the

carbon chain by one C≡C triple bond, both HC_4NCS and NC_3NCS are predicted to be

linear at the B3LYP/cc-pVQZ and MP2/cc-pVQZ levels. To confirm that the

geometries are linear (rather than quasilinear), the CNC bending potential energy

curves were computed. The curves are presented in Figure 6.1 and neither reveal a

barrier at $\angle$ CNC =180°. This trend towards linearity at nitrogen with increasing

carbon chain length is consistent with the reported geometries of related species. For

example, the angle at the nitrogen atom increases from HNCO ($\angle$ HNC = 128.0°)[31] to

HCCNCO ($\angle$ CNC = 140.67°)[32] and also from HNCS ($\angle$ HNC = 131.0°)[33] to

HCCNCS ($\angle$ CNC = 180°).[23] This change in geometry is compatible with increased

sp-character on the nitrogen atom of the isothiocyanato- moiety presumably due to

increased stabilization from conjugation with the added alkyne subunits. The same

trend is observed for the cyano-terminated chains with NC_3NCS being linear and

NCNCS having $\angle$ CNC = 143.0°.[30]

For closed-shell linear molecules, the mathematical relationship between B_0

and D_0 as a function of carbon chain length L has been explored by Thaddeus *et al.*[34]

In this work, they invoked a simple semi-classical theory to treat multiple series of

carbon chain molecules as elastic rods with cross-sectional area σ, density per unit

length ρ and a common Young's modulus E to derive an expression for the energy

levels of a rigid rotor as a function of L with a correction term for non-rigidity due to elastic deformation of the rod. In this model, the ratio of the centrifugal distortion constant to the rotational constant (D_0/B_0) has a L^{-4} dependence such that a plot of $\log(D_0/B_0)$ versus $\log(L)$ should yield a straight line with a slope of -4. As proof of concept, they plotted the experimental spectroscopic constants from more than 20 different carbon chain species, such as $HC_{2n+1}N$[34-35] and $CH_3C_{2n}CH$,[36] and found strong agreement with this model. In Figure 6.4, the $\log(D_0/B_0)$ of HC_4NCS and NC_3NCS versus $\log(L)$ are plotted together with those of $HC_{2n+1}N$ (n = 1 – 5) for comparison where L is estimated from the CCSD(T) geometry (HC_4NCS and NC_3NCS) or from the experimental structure ($HC_{2n+1}N$, n = 1 – 5)[37] and the slope shown is the theoretical value of -4. It is seen that HC_4NCS falls on the linear trend while the data for NC_3NCS gives rise to a positive deviation which is a result of the experimental D_0 constant that is 2.6 times larger than that of its isoelectronic counterpart HC_4NCS. This unusually large D_0 constant is likely a consequence of the flatter potential for NC_3NCS along the CNC bending coordinate as reported in Figure 6.1 which should give rise to a lower frequency bending vibration and a more fluxional rod.
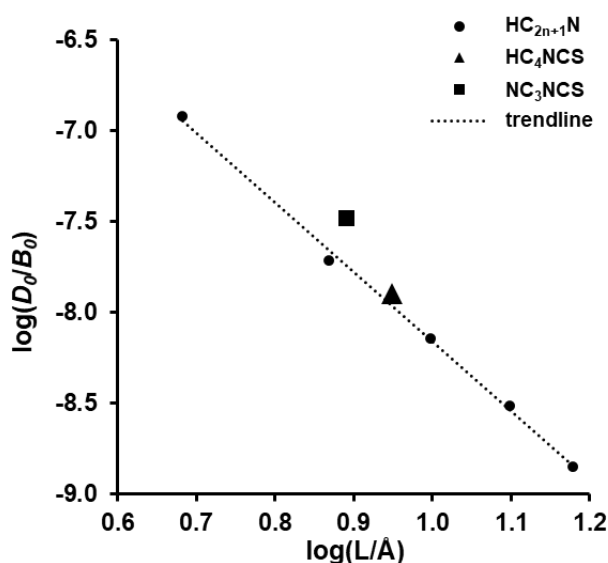
Figure 6.4. Log-log plot of the D_0/B_0 ratio as a function of chain length L (in Å) for the cyanopolyynes $HC_{2n+1}N$ (solid circles) and the title molecules HC_4NCS (solid triangle), NC_3NCS (solid square).

6.6 Conclusion

In closing, the present study reports the successful production of two new C chain species, HC_4NCS and NC_3NCS, using electric discharge and their pure rotational spectra in the ground state through microwave spectroscopy. Even though these two molecules have the same number of electrons and have very similar moments of inertia, the hyperfine splitting patterns due to the ^{14}N quadrupole nuclei are unique because of the different number of nitrogen atoms. Combined with theoretical calculations, the rotational spectra with the resolved hyperfine structures confirm the linear geometries for these species. As cyano-substituted polyynes and HNCS are known astrophysical molecules, the present carbon chain species serve as potential future targets for observation in the centimeter wave range.

References

(1)   Halfen, D. T.; Ziurys, L. M.; Brünken, S.; Gottlieb, C. A.; McCarthy, M. C.; Thaddeus, P. Detection of a New Interstellar Molecule: Thiocyanic Acid HSCN. *Astrophys. J.* **2009,** *702* (2), L124-L127.

(2)   Frerking, M. A.; Linke, R. A.; Thaddeus, P. Interstellar Isothiocyanic Acid. *Astrophys. J.* **1979,** *234*, L143-L145.

(3)   Adande, G. R.; Halfen, D. T.; Ziurys, L. M.; Quan, D.; Herbst, E. Observations of the [HNCS]/[HSCN] Ratio in Sgr B2 and TMC-1: Evidence for Low-Temperature Gas-Phase Chemistry. *Astrophys. J.* **2010,** *725* (1), 561-570.

(4)   Hirota, T.; Yamamoto, S.; Mikami, H.; Ohishi, M. Abundances of HCN and HNC in Dark Cloud Cores. *Astrophys. J.* **1998,** *503* (2), 717-728.

(5)   Bell, M. B.; Watson, J. K. G.; Feldman, P. A.; Travers, M. J. The Excitation Temperatures of HC_9N and Other Long Cyanopolyynes in TMC‐1. *Astrophys. J.* **1998,** *508* (1), 286-290.

(6)   Snell, R. L.; Schloerb, F. P.; Young, J. S.; Hjalmarson, A.; Friberg, P. Observations of HC_3N, HC_5N, and HC_7N in Molecular Clouds. *Astrophys. J.* **1981,** *244*, 45-53.

(7)   Guelin, M.; Neininger, N.; Cernicharo, J. Astronomical Detection of the Cyanobutadiynyl Radical C_5N. *Astron. Astrophys.* **1998,** *335*, L1-L4.

(8)   Friberg, P.; Hjalmarson, A.; Guelin, M.; Irvine, W. M. Interstellar C_3N: Detection in Taurus Dark Clouds. *Astrophys. J.* **1980,** *241*, L99-L103.

(9)   Turner, B. E. Detection of Interstellar Cyanoacetylene. *Astrophys. J.* **1971,** *163*, L35-L39.

(10)   Avery, L. W.; Broten, N. W.; MacLeod, J. M.; Oka, T.; Kroto, H. W. Detection of the Heavy Interstellar Molecule Cyanodiacetylene. *Astrophys. J.* **1976,** *205*, L173-L175.

(11)   Bell, M. B.; Feldman, P. A.; Watson, J. K. G.; McCarthy, M. C.; Travers, M. J.; Gottlieb, C. A.; Thaddeus, P. Observations of Long C_nH Molecules in the Dust Cloud TMC‑1. *Astrophys. J.* **1999,** *518* (2), 740-747.

(12)   Olano, C. A.; Walmsley, C. M.; Wilson, T. L. The Relative Distribution of NH_3, HC_7N and C_4H in the Taurus Molecular Cloud 1 (TMC 1). *Astron. Astrophys.* **1988,** *196*, 194-200.

(13)   Thaddeus, P.; Gottlieb, C. A.; Hjalmarson, A.; Johansson, L. E. B.; Irvine, W. M.; Friberg, P.; Linke, R. A. Astronomical Identification of the C_3H Radical. *Astrophys. J.* **1985,** *294*, L49-L53.

(14)   Sedo, G.; van Wijngaarden, J. Fourier Transform Microwave Spectra of a "New" Isomer of OCS-CO_2. *J. Chem. Phys.* **2009,** *131* (4), 044303.

(15)   Johnson, A. W. 218. 2-Butyne-1 : 4-Diol. Part I. Reactions of the Hydroxyl Groups. *J. Chem. Soc.* **1946,** *0*, 1009-1014.

(16)   Møller, C.; Plesset, M. S. Note on an Approximation Treatment for Many-Electron Systems. *Phys. Rev.* **1934,** *46* (7), 618-622.

(17)   Becke, A. D. Density-Functional Exchange-Energy Approximation with Correct Asymptotic Behavior. *Phys. Rev. A* **1988,** *38* (6), 3098-3100.

(18)   Becke, A. D. Density‑Functional Thermochemistry. III. The Role of Exact Exchange. *J. Chem. Phys.* **1993,** *98* (7), 5648-5652.

(19)   Stephens, P. J.; Devlin, F. J.; Chabalowski, C. F.; Frisch, M. J. *Ab Initio* Calculation of Vibrational Absorption and Circular-Dichroism Spectra Using Density-Functional Force-Fields. *J. Phys. Chem. Lett.* **1994,** *98* (45), 11623-11627.

(20)   Dunning, T. H. Gaussian Basis Sets for Use in Correlated Molecular Calculations. I. The Atoms Boron through Neon and Hydrogen. *J. Chem. Phys.* **1989,** *90* (2), 1007-1023.

(21)   Woon, D. E.; Dunning, T. H. Gaussian Basis Sets for Use in Correlated Molecular Calculations. III. The Atoms Aluminum through Argon. *J. Chem. Phys.* **1993,** *98* (2), 1358-1371.

(22)   Frisch, M. J.; Trucks, G. W.; Schlegel, H. B.; Scuseria, G. E.; Robb, M. A.; Cheeseman, J. R.; Scalmani, G.; Barone, V.; Mennucci, B.; Petersson, G. A.; Nakatsuji, H.; Caricato, M.; Li, X.; Hratchian, H. P.; Izmaylov, A. F.; Bloino, J.; Zheng, G.; Sonnenberg, J. L.; Hada, M.; Ehara, M.; Toyota, K.; Fukuda, R.; Hasegawa, J.; Ishida, M.; Nakajima, T.; Honda, Y.; Kitao, O.; Nakai, H.; Vreven, T.; Montgomery, J. A.; Peralta, J. E.; Ogliaro, F.; Bearpark, M.; Heyd, J. J.; Brothers, E.; Kudin, K. N.; Staroverov, V. N.; Keith, T.; Kobayashi, R.; Normand, J.; Raghavachari, K.; Rendell, A.; Burant, J. C.; Iyengar, S. S.; Tomasi, J.; Cossi, M.; Rega, N.; Millam, J. M.; Klene, M.; Knox, J. E.; Cross, J. B.; Bakken, V.; Adamo, C.; Jaramillo, J.; Gomperts, R.; Stratmann, R. E.; Yazyev, O.; Austin, A. J.; Cammi, R.; Pomelli, C.; Ochterski, J. W.; Martin, R. L.; Morokuma, K.; Zakrzewski, V. G.; Voth, G. A.; Salvador, P.; Dannenberg, J. J.; Dapprich, S.; Daniels, A. D.; Farkas, O.; Foresman, J. B.; Ortiz, J. V.; Cioslowski, J.; Fox, D. J., Gaussian 09, Revision B.01. Wallingford CT, 2010.

(23)   Sun, W.; Davis, R. L.; Thorwirth, S.; Harding, M. E.; van Wijngaarden, J. A Highly Flexible Molecule: The Peculiar Case of Ethynyl Isothiocyanate HCCNCS. *J. Chem. Phys.* **2018,** *149* (10), 104304.

(24)   Gauss, J.; Stanton, J. F. Analytic CCSD(T) Second Derivatives. *Chem. Phys. Lett.* **1997,** *276* (1-2), 70-77.

(25) Stanton, J. F.; Lopreore, C. L.; Gauss, J. The Equilibrium Structure and Fundamental Vibrational Frequencies of Dioxirane. *J. Chem. Phys.* **1998,** *108* (17), 7190-7196.

(26) Kendall, R. A.; Dunning, T. H.; Harrison, R. J. Electron Affinities of the First-Row Atoms Revisited. Systematic Basis Sets and Wave Functions. *J. Chem. Phys.* **1992,** *96* (9), 6796-6806.

(27) Hočevar, T.; Demčar, J. Computation of Graphlet Orbits for Nodes and Edges in Sparse Graphs. *J. Stat. Softw.* **2016,** *71* (10).

(28) Kisiel, Z. PROSPE – Programs for ROtational SPEctroscopy. http://www.ifpan.edu.pl/~kisiel/prospe.htm.

(29) Pickett, H. M. The Fitting and Prediction of Vibration-Rotation Spectra with Spin Interactions. *J. Mol. Spectrosc.* **1991,** *148* (2), 371-377.

(30) Winnewisser, B. P.; Winnewisser, M.; Medvedev, I. R.; Behnke, M.; De Lucia, F. C.; Ross, S. C.; Koput, J. Experimental Confirmation of Quantum Monodromy: the Millimeter Wave Spectrum of Cyanogen Isothiocyanate NCNCS. *Phys. Rev. Lett.* **2005,** *95* (24), 243002.

(31) Hocking, W. H.; Gerry, M. C. L.; Winnewisser, G. The Microwave and Millimetre Wave Spectrum, Molecular Constants, Dipole Moment, and Structure of Isocyanic Acid, HNCO. *Can. J. Phys.* **1975,** *53* (19), 1869-1901.

(32) Ross, S. C.; Cooper, T. A.; Firth, S.; Kroto, H. W.; Walton, D. R. M. The Microwave Spectrum and Semirigid Bender Analysis of Isocyanatoethyne, HC≡CNCO. *J. Mol. Spectrosc.* **1992,** *152* (1), 152-167.

(33) McGuire, B. A.; Martin-Drumel, M. A.; Thorwirth, S.; Brunken, S.; Lattanzi, V.; Neill, J. L.; Spezzano, S.; Yu, Z.; Zaleski, D. P.; Remijan, A. J.; Pate, B. H.; McCarthy, M. C. Molecular Polymorphism: Microwave Spectra, Equilibrium

Structures, and an Astronomical Investigation of the HNCS Isomeric Family. *Phys. Chem. Chem. Phys.* **2016,** *18* (32), 22693-22705.

(34) Thaddeus, P.; McCarthy, M. C.; Travers, M. J.; Gottlieb, C. A.; Chen, W. New Carbon Chains in the Laboratory and in Interstellar Space. *Faraday Discuss.* **1998,** *109*, 121-135.

(35) Travers, M. J.; McCarthy, M. C.; Kalmus, P.; Gottlieb, C. A.; Thaddeus, P. Laboratory Detection of the Linear Cyanopolyyne $HC_{11}N$. *Astrophys. J.* **1996,** *469* (1), L65-L68.

(36) Chen, W.; McCarthy, M. C.; Novick, S. E.; Thaddeus, P. Microwave Spectra of the Methylpolyynes $CH_3(C \equiv C)_6H$ and $CH_3(C \equiv C)_7H$. *J. Mol. Spectrosc.* **1999,** *196* (2), 335-337.

(37) Thaddeus, P.; McCarthy, M. C. Carbon Chains and Rings in the Laboratory and in Space. *Spectrochim. Acta A, Mol. Biomol. Spectrosc.* **2001,** *57* (4), 757-774.

Chapter 7.   Predicting key reactions in the thiazole electric discharge: microwave spectroscopy and theoretical modeling

7.1 Introduction

Although dc electrical discharge has shown its power for generating exotic molecules of astrophysical interest, as a technique that is at a relatively early stage of development, it is still like a black box and has lots of questions to be answered. By processing appropriate precursors, it can readily generate target products as expected and as described in earlier chapters. However, without knowing the thermodynamic and kinetic processes in the discharge source, it is always hard to predict whether the chosen precursor will work or not. For instance, using CH_3NCS + HCCH as precursors, HNCS, HSCN and HCCNCS were abundantly formed under empirically optimized discharge conditions as described in Chapter 5. When methyl thiocyanate (CH_3SCN) was used to replace CH_3NCS in the precursor mixture, HNCS was detected under the same conditions while HSCN and HCCNCS were not. Afterwards, the electric voltage was varied from -500 to -1500 V and still yielded no HSCN or HCCNCS. A similar experiment with a gas mixture of CH_3CH_2NCO + HCCH also failed to produce HCCNCO in the discharge source. These successful and unsuccessful experiences drive one to understand the electrical discharge chemistry that governs molecule formation. In this chapter, the discharge of a heterocyclic compound thiazole (C_3H_3NS) was studied to shed some light on this mysterious technique.

Thiazole, an aromatic five-membered ring, contains one nitrogen and one sulfur atom , is a very fundamental moiety in terrestrial natural products such as vitamin B_1 and drugs like antibiotic bacitracin[1] and anticancer epothilones.[2] It also commonly appears in many biomolecules, for instance, peptides.[3] Although it has not been detected in space yet, its ring analog thiophene and several associated derivatives were found in 3-billion-year-old mudstones on Mars.[4] The non-terrestrial existence of thiophene indicates that the formation of heterocycles in space may be possible. Especially in the Sgr B2 molecular cloud, many small species that are potential precursors of thiazole have been observed such as CH_2CNH[5]/ HCS+,[6] CH_2CN[7]/HCS+,[6] CCS[8]/HCN,[9] $HNCS$[10]/HCCH pairs. With their existence, the ring-closure reaction is likely to happen and create interstellar thiazole under certain conditions.

Thiazole is chosen to be the precursor in this study because of its signature heterocyclic ring that can form CS, CN and NCS-containing species via decomposition which are the major focus of the studies in this thesis. The purpose of this work is threefold. First, it aims to rationalize the formation of the detected discharge products. Under high voltage, the thiazole ring is opened and rapidly decomposes to small species including closed-shell compounds and open-shell radicals, which are recorded simultaneously by rotational spectroscopy and are unambiguously identified in the discharge spectrum. The backbone of thiazole is one carbon bigger than CH_3NCS. By comparing with the results from the CH_3NCS only and the CH_3NCS + HCCH discharge experiments in Chapter 5, the conclusions and speculations will be more convincing.

Second, by recognizing the products from unimolecular decomposition, the possible decomposition pathways can be investigated with the help of extensive

quantum-chemical computations. Although the dc electrical discharge is well known for creating highly unsaturated carbon chains, studies that monitor or model the relevant gas-phase reaction processes are not prevalent. Unlike conventional thermal pyrolysis[11-14] that has fewer variables to control in the experiments and is more straightforward to model in theory, the electric discharge is a much more harsh process and the transient reactions are hard to predict owing to the excessive energy released between the copper electrodes. In the discharge source, radicals are a dominant type of species which are highly reactive to form products through recombination reactions[15] and contain sufficient internal energy to achieve further dissociations and isomerizations.[16] This unimolecular decomposition of the fragments subsequent to the primary ring-opening step is a good chemical process to model. On the basis of the detected species in the thiazole discharge and theoretically proposed reaction pathways, the precursor fragments leading to them can be deduced which is the key to understand the discharge environment. In the future, with more and more compounds studied in this way, the database will be greatly expanded and be used to predict discharge products for any given molecule via machine learning for example. At that time, when one wants to study a specific species of interest, it would be easier for them to choose the correct precursors.

Third, many decomposed products, including several that are directly detected in the discharge spectrum and several that are not detected but proposed in the theoretical models, are known interstellar species. These species are small in size and most of them cannot be stably maintained in the laboratory. The gas-phase synthesis of the thiazole compound seems highly unfeasible. However, if we think about this in another way, the opposite of a synthesis reaction is a decomposition reaction. By

investigating its gas-phase decomposition process and analyzing the resulting products, some valuable information can be obtained.

7.2   Experimental methods

A commercial sample of thiazole was purchased from Sigma Aldrich with a purity of ≥ 99% and used without further purification. The vapor from the liquid sample was prepared with the buffer gas (Ne) to make a ~ 0.5% gas mixture. The precursor sample was seeded into the spectrometer in a supersonic jet through the aforementioned pulsed nozzle at a backing pressure of ~ 1 bar. The static discharge voltage across the copper electrode pair in the discharge assembly was maintained at ~750 V. The high electric potential difference between the electrodes initiated the heterocyclic ring dissociation and produced new molecular species from the fragments simultaneously in a hot plasma environment. Fragment rearrangement and recombination reactions were likely to happen at this stage and subsequently, the rotational temperature of the hot products was rapidly (on the scale of ms) lowered to several Kelvin via collisions with the Ne carrier gas in the supersonic jet.[15,17] Helmholtz coils were employed to counter the Earth's magnetic field in the vacuum chamber so that open-shell radicals could be detected as well.

The rotational spectrum of the resulting products was recorded using the broadband cp-FTMW spectrometer in the frequency range of 8 – 19 GHz with a 2 GHz segmentation and each segment involved averaging of 1.5 million FIDs. To reduce the complexity of the spectral analysis, the experiment was repeated with the dc electric discharge turned off and the non-discharge dependent lines were removed from the discharge spectra.

7.3 Computational details

A previous study on the mechanism of the thermal pyrolysis of thiophene, a five-membered ring analog of thiazole, suggested that the CBS-QB3[18]//B3LYP[19-21] scheme could accurately describe molecular geometries and reaction energies for such a system with a low computational cost.[17] Therefore, in this study, the geometries corresponding to all stationary points including local minima and transition states were first optimized at the B3LYP/CBSB7 level of theory. Transition states were confirmed to have only one imaginary frequency and further validated by the intrinsic reaction coordinate (IRC) approach while local minima yielded only real frequencies. Afterwards, the composite *ab initio* method, CBS-QB3, was performed to refine the energies using the B3LYP/CBSB7 optimized geometries. In the following sections, the relative energies being discussed are the electronic energies (0 K) at the CBS-QB3 level. For convenience, the compounds are denoted by the decomposition pathway they reside (P1 – P6) and the species type where TS and IM stand for transition state and intermediate, respectively. All of these quantum-chemical calculations were carried out with the Gaussian 16 suite of programs.[22]

7.4 Detected discharge dependent species

In total, 19 known species were identified in the spectrum as being produced in the thiazole discharge. They are grouped in four classes based on their distinct functional groups as shown in Table 7.1 and the line list is provided in Table 7.2. Of these products, six species which are HC_5N,[23] C_3S,[24] H_2C_3S,[25] H_2C_4S,[26] c-C_3H_2,[27] HCCCHS[28] have a carbon chain of three or more carbons which indicates that these could not be formed from simple rearrangements and thus, are considered as products of fragment recombination in the discharge plasma. This implies that not only

unimolecular decomposition happens in the hot plasma, but also two-body collision

reactions as suggested for the formation mechanism of HCCNCS in Chapter 5 and

HC$_4$NCS in Chapter 6. Moreover, the previous generation of NC$_3$NCS involved the

combination of the three fragments of NC, CC, and NCS. Prior to proposing the

unimolecular decomposition channels, the formation of the detected products should

be rationalized and the possibility of the radical-radical or radical-neutral reactions in

their formation processes should be clarified to the greatest extent.

In Chapter 5, the methyl isothiocyanate (CH$_3$NCS) discharge was investigated

with and without acetylene (HCCH). The backbone of this precursor alone is one

carbon smaller than that of the five-membered ring of thiazole. Some discharge

dependent species that were identified in both experiments can provide crucial

information to infer thiazole dissociation pathways. Furthermore, acetylene was

believed to be a key product of the thiazole discharge. Although with no permanent

dipole moment, it cannot be directly observed via the pure rotational spectrum, the

formation of HC$_5$N, H$_2$C$_4$S, HCCCHS, and c-C$_3$H$_2$ showed evidence of its existence.

The previous results from the CH$_3$NCS + HCCH discharge also helped to distinguish

the role of HCCH in the thiazole plasma.

Table 7.1. Summary of the 19 species detected from the thiazole discharge.

NCS species	NC species	CS species	Hydrocarbons
·N=C=S	H$_3$C—C≡N	C=C=S	HC=CH (c̈)
H\N=C=S	H$_2$C=CH (N≋C)	HĊ=C=S	
H\S—C≡N	H$_2$C=CH (C≋N)	H$_2$C=C=S	
H$_3$C\N=C=S	HC≡C—C≡N	C=C=C=S	
H$_2$C=C(H)\N=C=S	HC≡—C≡C—C≡N	H$_2$C=C=C=S	
HC≡C—N=C=S		H$_2$C=C=C=C=S	
		HC≡C—CH(S)	

158

Table 7.2. The observed transition frequencies (MHz) due to the 19 discharge dependent species and their SNRs collected with 1.5 million FIDs

species	transitions			frequency/MHz	SNR
NCS	3/2-1/2		5/2 e-3/2 e	18192.90	14.7
			3/2 e-1/2 e	18200.08	3.7
			3/2 e-3/2 e	18207.40	4.0
			1/2 e-1/2 e	18211.25	3.5
			3/2 f-3/2 f	18439.25	5.3
			5/2 f-3/2 f	18477.00	18.3
			1/2 f-1/2 f	18490.10	4.0
			3/2 f-1/2 f	18510.42	5.5
HNCS	1_{01}-0_{00}		0-1	11728.50	11.0
			2-1	11729.00	90.0
			1-1	11729.35	40.0
HSCN	1_{01}-0_{00}		1-1	11468.64	
			2-1	11469.85	11.5
			0-1	11471.70	
CH$_3$NCS	2_{02}-1_{01}		A2-A2	10052.13	2.0
	3_{03}-2_{02}		A1-A1	15078.25	5.0
trans- CH$_2$CHNCS	5_{15}-4_{14}			14940.31	6.5
	5_{05}-4_{04}			15028.44	12.5
	5_{14}-4_{13}			15116.76	4.5
	6_{16}-5_{15}			17928.21	2.0
	6_{06}-5_{05}			18033.87	2.0
	6_{15}-5_{14}			18140.47	1.5
HCCNCS	3-2			9130.61	2.7
	4-3			12174.14	10.0
	5-4			15217.68	8.0
	6-5			18261.18	10.0
CH$_3$CN	1-0		1-1	18396.73	17.8
			2-1	18398.01	27.8
			0-1	18399.89	5.6
CH$_2$CHNC	1_{01}-0_{00}			10255.58	8.5
CH$_2$CHCN	1_{01}-0_{00}		1-1	9484.08	13.9
			2-1	9485.22	24.4
	2_{12}-1_{11}		2-1	18512.15	38.8
			3-2	18513.30	68.8
	2_{02}-1_{01}		2-2	18965.39	9.4
			1-0	18965.60	15.6
			3-2	18966.60	46.7
			1-1	18968.43	7.2

HCCCN	1-0	1-1	9097.03	8.3
		2-1	9098.33	17.8
		0-1	9100.27	6.7
	2-1	2-2	18194.90	64.0
		1-0	18195.11	62.0
		3-2	18196.26	160.0
		1-1	18198.36	40.0
HC$_5$N	4-3		10650.65	\
	5-4		13313.35	\
	6-5		15975.96	2.1
	7-6		18638.65	1.8
CCS	1-0		11119.95	28.3
HCCS	3/2-1/2	2e-1e	17583.08	20.0
		1e-1e	17583.60	3.4
		1e-0e	17591.53	7.1
		1f-1f	17695.79	3.6
		2f-1f	17710.20	19.3
		1f-0f	17722.40	8.6
H$_2$CCS	1_{01}-0_{00}		11203.98	61.1
H$_2$CCCS	2_{12}-1_{11}		10086.03	1.7
	2_{02}-1_{01}		10109.91	6.2
	2_{11}-1_{10}		10133.23	2.3
	3_{13}-2_{12}		15129.06	5.0
	3_{03}-2_{02}		15164.85	5.3
	3_{12}-2_{11}		15199.84	4.2
CCCS	2-1		11561.52	13.6
	3-2		17342.25	12.0
H$_2$CCCCS	4_{14}-3_{13}		11114.61	2.5
	4_{13}-3_{12}		11142.71	2.0
	5_{05}-4_{04}		13911.00	1.7
	5_{14}-4_{13}		13928.49	4.5
HCCCHS	2_{12}-1_{11}		11792.57	4.3
	2_{02}-1_{01}		12006.24	17.5
	2_{11}-1_{10}		12222.85	10.0
	3_{13}-2_{12}		17688.23	6.5
	3_{03}-2_{02}		18007.32	22.5
	3_{12}-2_{11}		18333.54	8.3
c-C$_3$H$_2$	1_{10}-1_{01}		18343.14	18.3

7.4.1 Evidence for the existence of elemental carbon: Formation of cyclopropenylidene (c-C_3H_2)

One signature rotational transition was measured for c-C_3H_2 in the thiazole discharge, which is the first carbene ring detected in space,[27] whereas c-C_3H radical[24] and c-C_3H_4[29] were not observed under the same conditions. In an earlier discharge study of 2,3-dihydrofuran, the cyclic carbene was detected as well and two formation mechanisms were proposed.[16] They suggested that this molecule could be formed from an intermediate product propyne (CH_3CCH) or via the stable cyclopropenyl cation (c-$C_3H_3^+$) formed from acetylene and ethane. However, with a heavy carrier gas such as Ne and Ar, the ion-molecule reactions were greatly reduced[15] so that $C_3H_3^+$ was safely excluded as a primary intermediate. In the present study, c-C_3H_2 was detected whereas CH_3CCH was not, which negates the first mechanism as well. Owing that the carbon atoms in the thiazole ring are separated by the sulfur and nitrogen atoms, there is no direct rearrangement or dissociation pathway that could lead to this product involving three adjacent carbon atoms. The formation of c-C_3H_2 in the thiazole discharge plasma may occur, for example, through a reaction of elemental C and HCCH. If so, this implies that the fragments created by the electric pulse were not only molecular species but also elements, which is also evidenced by the formation of soot on the nozzle assembly over time. The existence of elemental C along with many identified molecular species (closed and open-shell) strongly suggests that the ring-opening of thiazole via the dc electric discharge is not like the regular thermal decomposition which dissociate chemical bonds gradually following the bond energy ordering.[17,30-33] Therefore, instead of focusing on the primary ring-opening pathways, the computational efforts described in this chapter are mainly

made to demonstrate the formation of the identified species by proposing possible initial fragments.

7.4.2 Secondary reactions: Formation of sulfur- or nitrogen- bearing carbon chain (n >3) species

As mentioned before, besides c-C_3H_2, there are five species, N-bearing HC_5N and S-bearing C_3S, H_2C_3S, H_2C_4S and HCCCHS, which were formed through secondary recombination reactions. Presumably, beyond the 19 identified species, some small ones such as CS, HCS, HCCH, HCN were produced by the electric discharge and were the primary sources of the secondary reactions. Due to the small molecular size of the polar fragments, for example CS, HCS, and HCN, or non-polar species such as HCCH, there are no rotational transitions that fall in the frequency range of 8 – 18 GHz and they cannot be detected directly in this experiment. However, the detection of longer chain species (three or more carbons) suggests the presence of these small organic species. The formation reactions involved are proposed as follows:

$$HC\equiv CC\equiv N + HC\equiv CH \rightarrow HC\equiv CC\equiv CC\equiv N + 2H\bullet \qquad (7.1)$$

$$C\equiv S + HC\equiv CH \rightarrow C=C=C=S + 2H\bullet \qquad (7.2)$$

$$C\equiv S + HC\equiv CH \rightarrow H_2C=C=C=S \qquad (7.3)$$

$$C\equiv S + HC\equiv CH \rightarrow HC\equiv CC(H)=S \qquad (7.4)$$

$$C=C=S + HC\equiv CH \rightarrow H_2C=C=C=C=S \qquad (7.5)$$
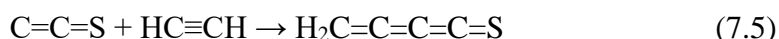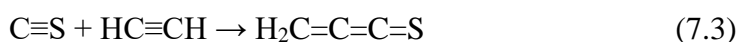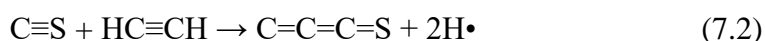
These reactions, especially the isomerization of H_2CCCS and HCCCHS, have been previously discussed in Chapters 4 and 5. As H loss is a ubiquitous phenomenon under discharge conditions, the direct dissociation of the C-H bond of the sulfur bearing species, for example the thermochemical connection between reaction 7.2 and 7.3, are not discussed here. In Chapter 4, with the $HSCH_2CH_2SH$ precursor, products

in reactions 7.2 – 7.5 have been observed in the discharge spectrum as well. However, it is difficult to distinguish whether they could be formed by HCCH reacting with closed-shell C_nS species or not since open-shell HC_nS radicals were readily produced in the discharge source and are expected to be more reactive. In Chapter 5, using the CH_3NCS + HCCH precursor mixture which generated CS species, both H_2CCCS and HCCCHS were detected. This supports the proposed reactions 7.3 and 7.4 in the thiazole discharge. Likewise, HCS radical, if being created, could also react with HCCH and its radicals to produce these molecules by a radical-neutral reaction mechanism.

7.4.3 Unimolecular decompositions: Formation of vinyl (CH_2=CH-) and methyl (CH_3-) species

Other than the aforementioned species which were generated through appropriate secondary reactions, there are several detected species that could be readily produced directly from unimolecular decomposition which are NCS,[34] HNCS,[35] HSCN,[36] CCS,[24] HCCS,[37] and H_2CCS.[38] Interestingly, beyond these, two NCS and three NC species bearing a terminal vinyl or methyl group were identified in the discharge spectrum. There are two possible mechanisms that could lead to their formation. Since c-C_3H_2 was proposed to be created by the combination of HCCH and C, the vinyl and methyl groups might be formed by reactions of HCCH and C/CH with H atoms, respectively. The resulting functional groups produced the observed vinyl and methyl species by further collisions with NC or NCS fragments. However, with similar discharge conditions, no vinyl species were observed from the CH_3NCS + HCCH discharge. Furthermore, neither CH_2CHCHS,[39] CH_2CHCCH[40-41] nor CH_3CHS,[42] CH_3CCH[43] were detected from the thiazole discharge, Therefore, it is

unlikely that this mechanism is favoured under the experimental conditions. Another hypothesis is that they were formed via unimolecular decomposition reactions. The processes must involve isomerization reactions such as H migrations and backbone rearrangements which need energy to overcome the activation barriers. As suggested by previous studies,[15-16] other than barrierless radical-radical/neutral reactions, subsequent isomerization reactions could occur following molecular dissociation in the hot discharge source. In the following section, unimolecular decomposition pathways leading to these species will be modeled using quantum-chemical calculations.

7.5 Unimolecular reactions and theoretical modelling

7.5.1 Formation of *trans*-vinyl isothiocyanate (*trans*-CH$_2$CHNCS) and ethynyl isothiocyanate (HCCNCS)

Trans-CH$_2$CHNCS[44] is a linear isomer of thiazole (**Tz**). Its formation from thiazole requires two steps: ring-opening and H migration. The proposed reaction pathways and the corresponding relative energies are provided in Figures 7.1 and 7.2, respectively. The ring-opening process was initiated by the electric pulse and produced a biradical **Tz-1** by opening the C5-S1 bond. **P1-IM1** is a resonant form of **Tz-1** with a C2-N3 single bond. In general, the two unpaired electrons occupying two molecular orbitals in **Tz-1** could have parallel (open-shell triplet) or antiparallel (open-shell singlet) spins and thus have different electronic energies. **Tz-1** and **P1-IM1** differ in energy as well due to different electron configurations. Multireference approaches such as the complete active space SCF (CASSCF) method are well known to characterize the electronic energies with different electron occupancies by defining active electrons and active orbitals.[31,45] Owing that it is not the key discussion point of

this project, **Tz-1/P1-IM1** was treated as an unrestricted triplet state using the CBS-QB3 method which lies 409.53 kJ/mol above thiazole.
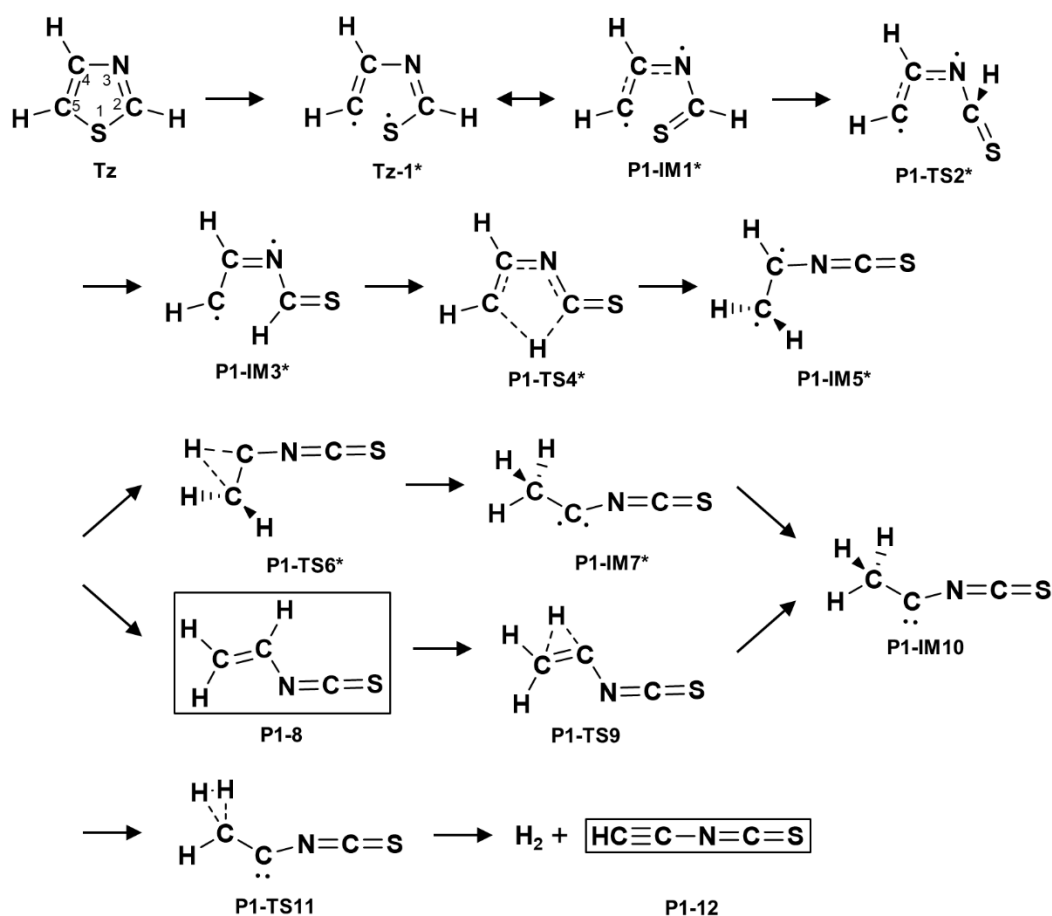
Figure 7.1. Proposed unimolecular decomposition pathway of thiazole (P1) for the formations of *trans*-CH$_2$CHNCS and HCCNCS. The molecular species in the black boxes are detected species from the thiazole discharge and the geometries labelled with an asterisk (*) are in their triplet states.
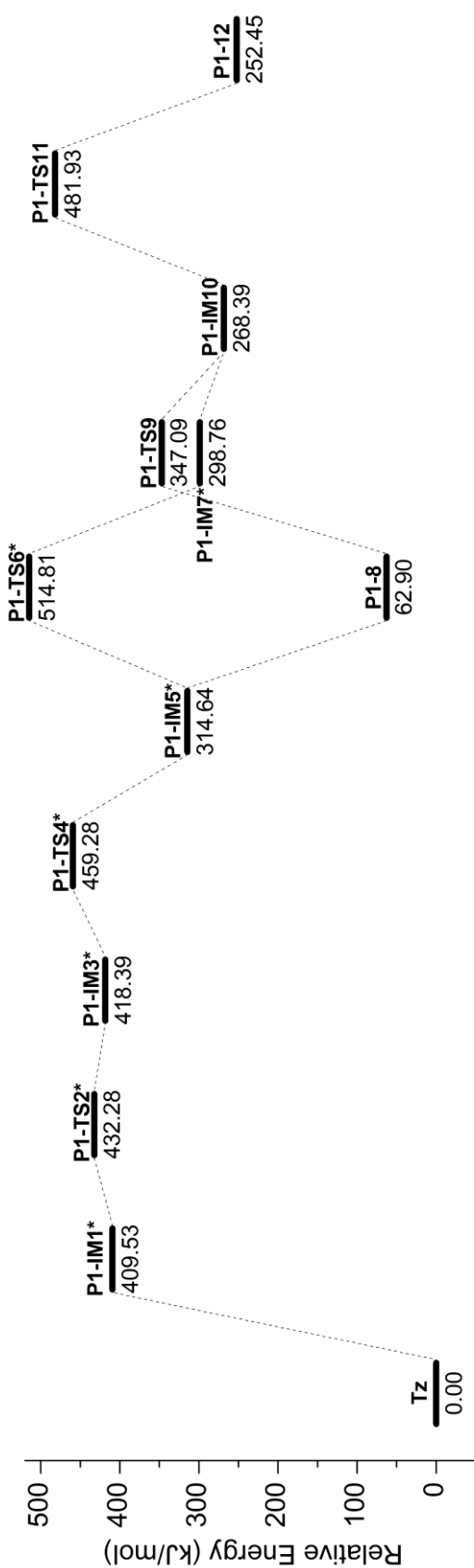
Figure 7.2. The relative energies of the stationary points on the potential energy surface along the unimolecular decomposition coordinate of thiazole (P1), which yields *trans*-CH$_2$CHNCS and HCCNCS. All energies are calculated using the CBS-QB3 method at 0 K and the energy of thiazole is set at 0 kJ/mol. The reaction coordinates with an asterisk (*) correspond to triplet states.

To transfer the hydrogen on C2 to C5, the HCS group of **P1-IM1** is rotated to the **P1-IM3** configuration via transition state **P1-TS2** with a barrier of 22.75 kJ/mol and a single imaginary frequency of 102i cm^{-1}. The nature of the imaginary frequency was carefully checked and corresponds to the right chemical process. The 1,4-H-transfer from C2 to C5 could subsequently occur through a five-membered transition state **P1-TS4**, which is 40.89 kJ/mol higher than intermediate **P1-IM3** with an imaginary frequency of 1524i cm^{-1}. Vinyl isothiocyanate in a triplet state (**P1-IM5**) was formed and converted to its singlet ground state (**P1-8**). The reaction (**P1-IM1 →** **P1-8**) was found to be -346.63 kJ/mol exothermic with a barrier of 49.76 kJ/mol, which should be easy to overcome once this pathway was triggered.

Moreover, a further product HCCNCS[46] was identified in the discharge spectrum as well. Given the existence of HCCH and NCS radical in the hot source, HCCNCS could be formed through radical-neutral reactions as reactions 7.1 – 7.5. However, given the detection of HC$_3$N and HC$_5$N, the CN fragment is also believed to be created in the source but NCNCS was not detected. In the earlier studies presented in Chapter 5, CH$_3$NCS is one carbon smaller than thiazole and its dc discharge created both NCS and CN fragments and a very strong signal was detected for NCNCS. Later, by adding an excess amount of HCCH, both species (HCCNCS and NCNCS) were observed. In the present study, HCCNCS was detected whereas NCNCS was not which implies that the radical-neutral mechanism is not the primary channel yielding HCCNCS. Thus, it may be formed as a hydrogen elimination product of vinyl isothiocyanate. The simpler way is direct H cleavage, which requires vey high energy for each C-H bond (approximately 700 kJ/mol) to rupture. In this study, a hydrogen elimination mechanism that requires less thermochemical effort is investigated.

A previous theoretical study on a H-elimination mechanism of ethene suggested two easy pathways that involve ethylidene (CH_3CH) or vinylidene (H_2CC) as intermediates and one indirect 1,2-H-elimination pathway with two imaginary frequencies.[47] Based on extensive computational searches, an ethylidene-type intermediate **P1-IM10** is found to be the only one connecting CH_2CHNCS and HCCNCS. **P1-IM10** can be formed through two possible paths, triplet **P1-TS6** and **P1-IM7** or singlet **P1-8** and **P1-TS9**, the reaction barrier of which is 200.17 and 284.19 kJ/mol, respectively. In the triplet state channel, an intermediate CH_3CNCS (**P1-IM7**) was formed with an open-shell electron configuration at C4. Its closed-shell singlet state (**P1-IM10**) is a carbene intermediate which is 30.37 kJ/mol more stable in energy. Thus, **P1-IM7** converts to its singlet state and subsequently follows the singlet state channel (**P1-8 → P1-TS9**) to the reaction coordinate corresponding to **P1-IM10**. Afterwards, HCCNCS (**P1-12**) may be formed through transition state **P1-TS11** which lies 213.54 kJ/mol above **P1-IM10** with a single imaginary frequency of 1475i cm^{-1}. The reaction **P1-8 → P1-12** is 189.55 kJ/mol endothermic with a barrier of 419.03 kJ/mol while **P1-IM5 → P1-12** via **P1-TS6** is -62.20 kJ/mol exothermic with a barrier of 200.17 kJ/mol.

7.5.2 Formation of vinyl isocyanide (CH_2CHNC), vinyl cyanide (CH_2CHNC), and cyanoacetylene (HC_3N)

Another two observed molecular species bearing a vinyl group are isomers CH_2CHNC[48] and CH_2CHCN[49] which are only one sulfur smaller than thiazole. Thus, the first step of their formations should be the removal of sulfur by cleavage of two C-S bonds which requires ~ 500 kJ/mol in total. The rearrangement of the resulting fragments (**P2-IM1**) may yield singlet CH_2CHNC (**P2-6**) via a similar formation

pathway as proposed above for CH$_2$CHNCS and is shown in Figures 7.3 and 7.4. The transition state (**P2-TS2**) of the 1,4-H-transfer was found to be 55.86 kJ/mol higher than **P2-IM1** with an imaginary frequency of 944i cm^{-1}. The reaction energy (**P2-IM1** → **P2-6**) is -351.50 kJ/mol exothermic.

Figure 7.3. Proposed unimolecular decomposition pathway of thiazole (P2) for the formation of CH$_2$CHNC, CH$_2$CHCN and HC$_3$N. The molecular species in the black boxes are detected species from the thiazole discharge and the geometries labelled with an asterisk (*) are in their triplet states.
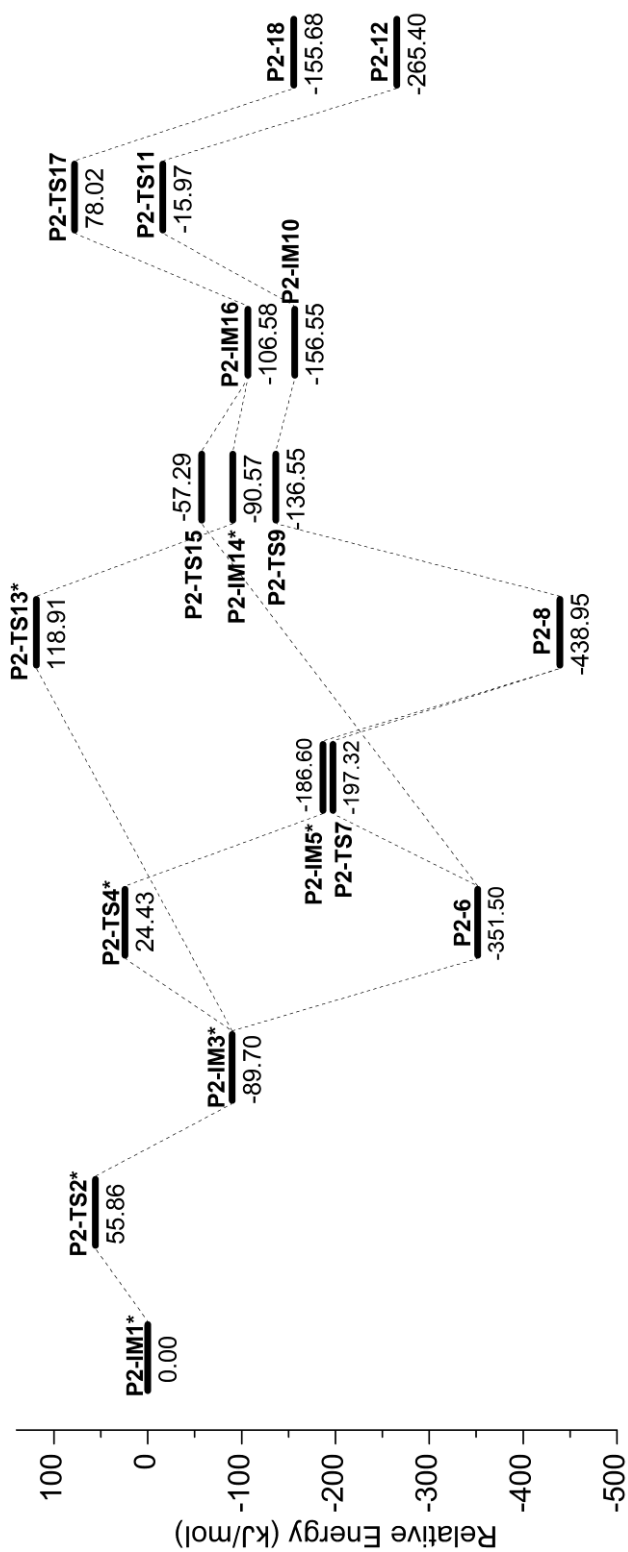
Figure 7.4. The relative energies of the stationary points on the potential energy surface along the unimolecular decomposition coordinate of thiazole (P2), which leads to the formation of CH_2CHCNC, CH_2CHCN, HC_3N, and $HCCNC$. All energies are calculated using the CBS-QB3 method at 0 K and the energy of **P2-IM1** is set at 0 kJ/mol. The reaction coordinates with an asterisk (*) correspond to triplet states.

In the hot discharge source, CH_2CHNC (**P2-6**) can easily isomerize to CH_2CHCN (**P2-8**), which is 87.45 kJ/mol more stable in energy at 0 K, through a common three-centered isocyanide-cyanide rearrangement.[50] The transition state is found to be **P2-TS7** lying 154.17 kJ/mol above **P2-6**. Both species were detected in the spectrum as local minima. The formation of CH_2CHCN (**P2-8**) via a triplet reaction channel (**P2-IM3 → P2-8**) was also investigated requiring the cyano group to turn over in the triplet state which has a barrier of 114.13 kJ/mol and a reaction energy of -349.25 kJ/mol. Finally, **P2-8** loses two H atoms and produces HC_3N (**P2-12**) like the process of the HCCNCS (**P1-12**) formation.

Interestingly, while both CH_2CHCN (**P2-8**) and HC_3N (**P2-12**) were detected, HCCNC[51] was not observed together with CH_2CHNC (**P2-6**). To rationalize the proposed mechanism, the pathway leading to HCCNC (**P2-18**) was explored and is shown in Figure 7.5. The energy pathway was combined into Figure 7.4. Like the formations of HCCNCS (**P1-12**) and HC_3N (**P2-12**), HCCNC (**P2-18**) is predicted to be formed via a similar carbene intermediate (**P2-IM16**). The transition state of the 1,1-H-elimination (**P2-TS17**) lies 184.60 kJ/mol above **P2-IM16** with an imaginary frequency of 1415i cm^{-1}. The carbene intermediate could be created via a triplet (**P2-TS3 → P2-IM14**) or singlet (**P2-6 → P2-TS15**) channel. However, the transition states of both channels are higher than those of the two CH_2CHNC (**P2-6**) isomerization channels, respectively. This suggests that before **P2-IM3** or **P2-6** obtain enough energy to form **P2-IM6**, the rearrangement from isocyanide to cyanide may occur instead which explains the absence of HCCNC (**P2-18**) in the discharge spectrum. Note that with enough precursor concentration and sufficient secondary reactions, HCCNC could potentially be created via radical recombination.
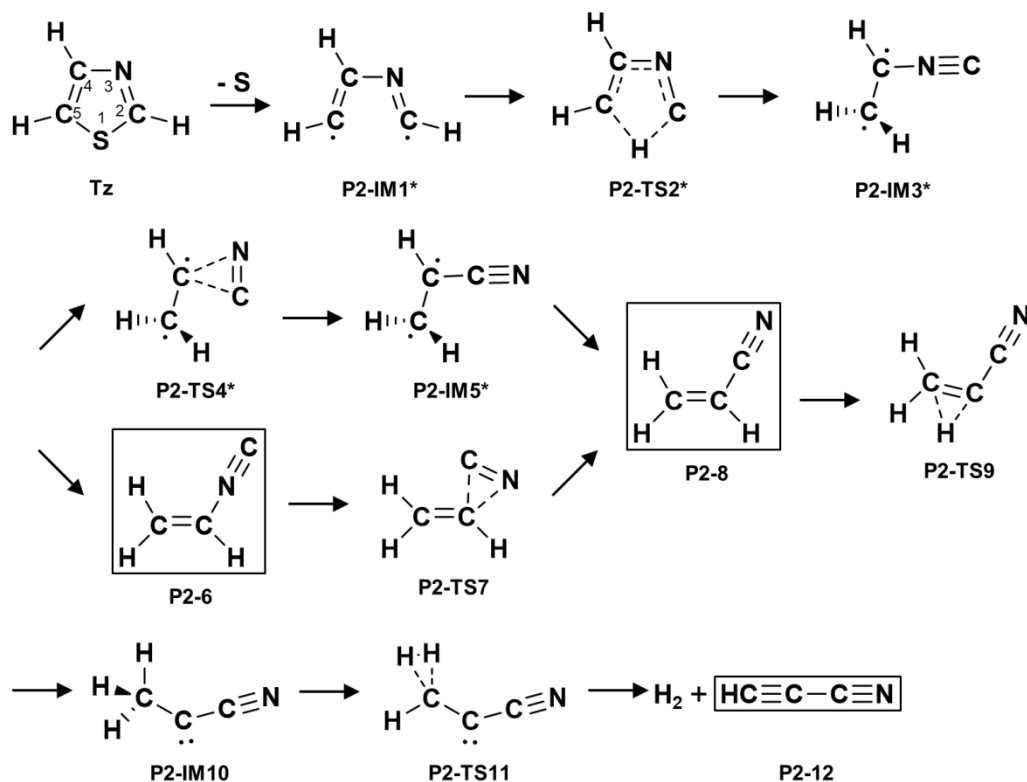
Figure 7.5. Unimolecular decomposition pathway of thiazole for the formation of HCCNC. The molecular species in the black box is a detected species from thiazole discharge and the geometries labelled with an asterisk (*) are in their triplet states.

7.5.3 Formation of methyl thiocyanate (CH₃NCS) and methyl cyanide (CH₃CN)

In terms of the formation of CH_3NCS, there is only one unimolecular mechanism that yields this compound (**P3-4**) as illustrated in Figure 7.6. To preserve all the hydrogen atoms and dissociate a single carbon, the H on C5 must migrate to C4 via the transition state **Tz-2-TS** which is located 275.63 kJ/mol higher in energy than thiazole and has an imaginary frequency of 981i cm⁻¹. In the discharge environment, bare C5 can be cut from the ring backbone by cleavages of the C-C and C-S bond which takes ~700 kJ/mol to happen. The triplet residual **P3-IM1** can produce a more stable singlet state **P3-IM2** (-172.60 kJ/mol lower). The singlet fragment can eventually convert to **P3-4** through a four-membered transition state to facilitate 1,3-H-transfer (**P3-TS3**) that lies 258.55 kJ/mol above **P3-IM2** and the one and only imaginary frequency is found to be 1064i cm⁻¹. This reaction (**P3-IM1 →P3-4**) requires overcoming a barrier of 85.94 kJ/mol and would yield a reaction energy of -265.03 kJ/mol.

172

Figure 7.6. Proposed unimolecular decomposition pathway of thiazole (P3) for the formation of CH₃NCS. The molecular species in the black box is detected in the thiazole discharge and the intermediate **P3-IM1*** is in the triplet state.

Given the existence of CH₃CN (**P4-6**), a second decomposition channel starting from **Tz-2** was explored and is shown in Figures 7.7 and 7.8. Instead of removing a single C, the CS species is removed from the ring in this path. A transition state (**P4-TS1**) was found to correspond to this decomposition reaction. It is located 179.89 kJ/mol above **Tz-2** and would be produced via a carbene intermediate **P4-IM2**. As discussed before, even though CS is too small to be detected in the spectrometer frequency range, the detection of CCCS, H₂CCCS and HCCCHS indirectly supports its existence in the discharge plasma. After the removal of CS, **P4-IM2** can produce methyl isocyanide CH₃NC (**P4-4**) via (**P4-TS3**), a similar four-membered transition state as **P3-TS3**, and **P4-4** can isomerize to CH₃CN (**P4-6**) via the isocyanide-cyanide rearrangement. If CH₃NC (**P4-4**) could be detected in the spectrum, that would offer a great support for this mechanism. Unfortunately, its rotational transitions are located outside the frequency range of the spectrometer and cannot be observed in the present study.
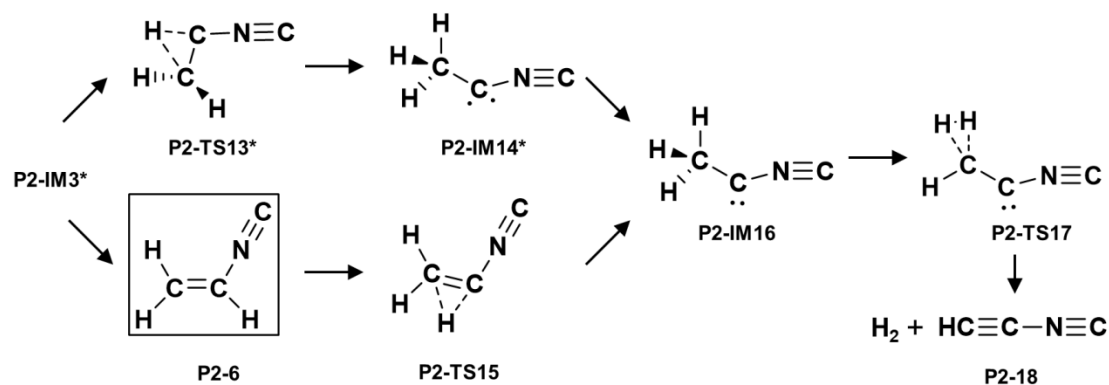
Figure 7.7. One plausible unimolecular decomposition pathway of thiazole (P4) for the formation of CH_3CN. The molecular species in the black box is a detected species in the thiazole discharge.

Another possible mechanism that yields CH_3CN (**P4-6**) can be initiated with a different H-migration channel as illustrated in Figure 7.9. The energy pathway is combined in Figure 7.8 to make a comparison with the first proposal above. To lose a CS fragment and keep all hydrogen atoms, the C2 hydrogen is first shifted to N3 via **Tz-3-TS** and the C4 hydrogen migrated to C5 via **P4-TS7** which forms an intermediate (**P4-IM8**) with two carbene sites. Surprisingly, if the C4 hydrogen shifted first, the subsequent migration of the C2 hydrogen to N3 prefers to open the ring backbone and does not lead to **P4-IM8**. After **P4-IM8** is formed, it can decompose to two closed-shell species, CS and CH_2CNH (**P4-10**). **P4-10** can overcome the 266.56 kJ/mol barrier of the T-shaped transition state **P4-TS11** which is higher than the reaction barrier of the first mechanism (134.00 kJ/mol), and eventually can isomerize to CH_3CN (**P4-6**). This reaction energy (**P4-10 → P4-6**) is -113.12 kJ/mol.
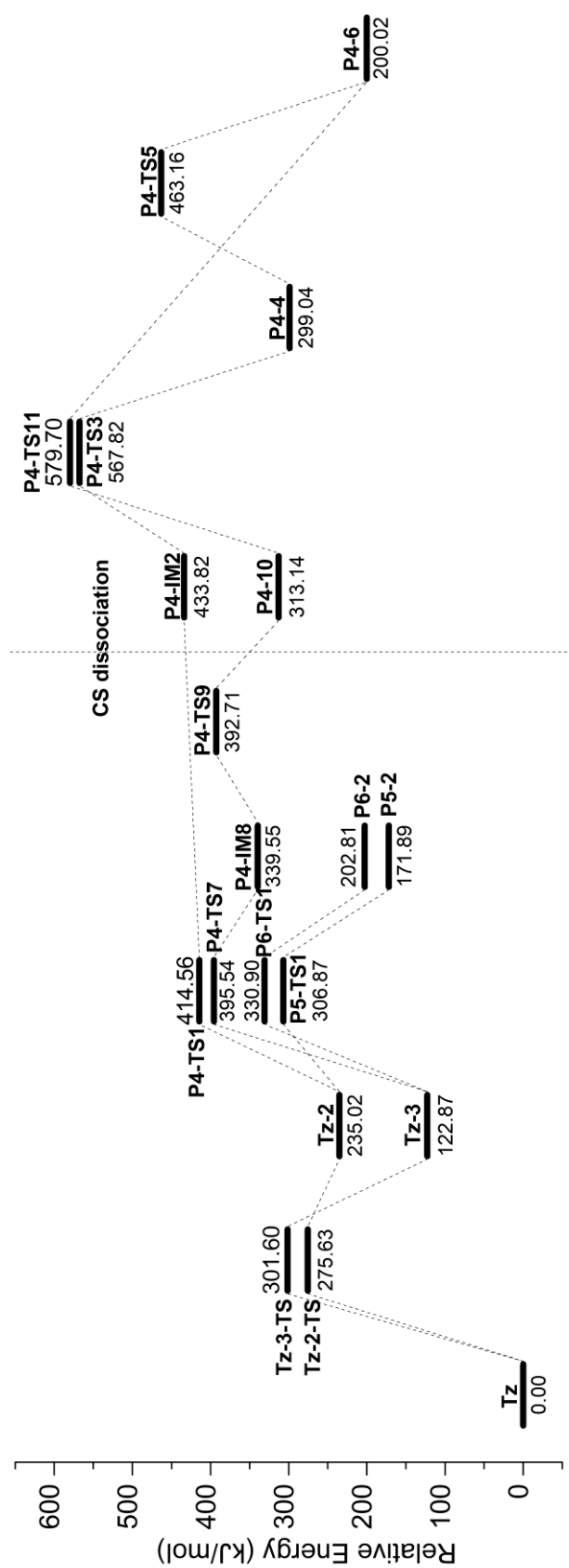
Figure 7.8. The relative energies of the stationary points on the potential energy surface along the unimolecular decomposition coordinate of thiazole (P4 – P6) which yields CH_3CN and H_2CCS. All energies are calculated using the CBS-QB3 method at 0 K and the energy of thiazole is set at 0 kJ/mol.
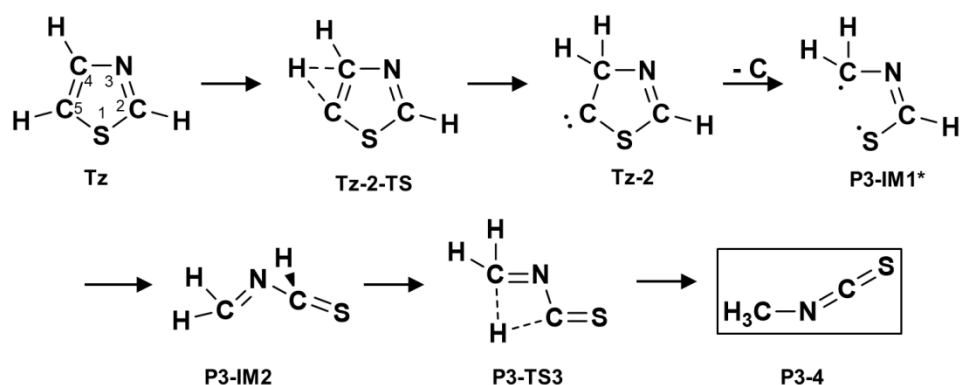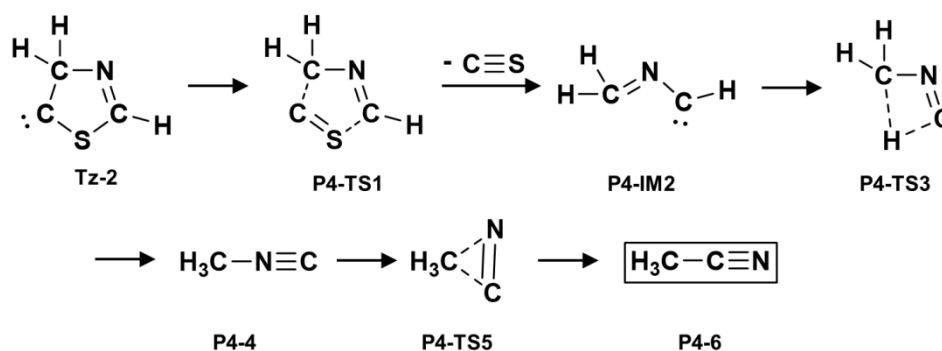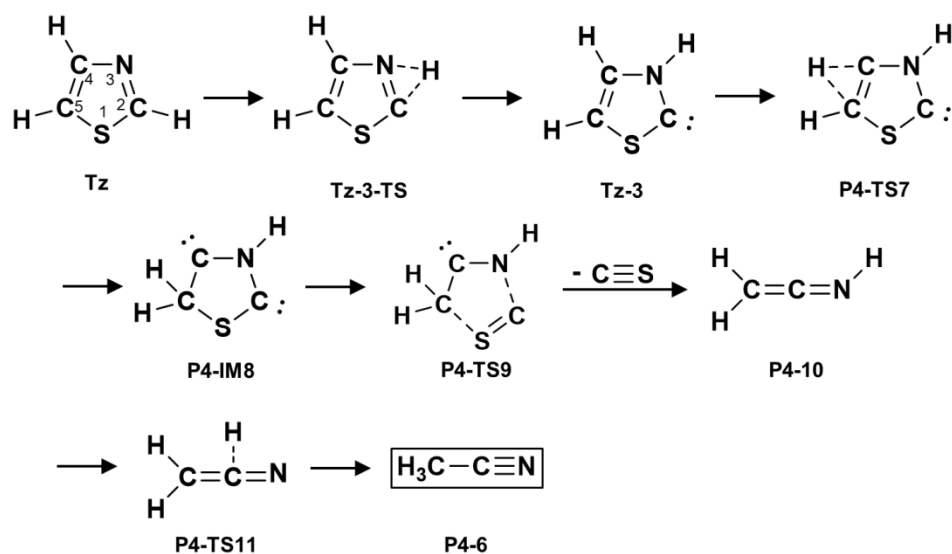
Figure 7.9. A second possible unimolecular decomposition pathway of thiazole (P4) for the formation of CH_3CN. The molecular species in the black box is a detected species in the thiazole discharge.

Unfortunately, like CH_3NC (**P4-4**), CH_2CNH (**P4-10**) does not have any rotational transition that fall in frequency range lower than 19 GHz and thus, there is no evidence to validate this hypothesis. However, this pathway suggests a good theoretical model for the formation of thiazole in interstellar molecular clouds. CH_2CNH (**P4-10**) is a known isomer of CH_3CN (**P4-6**), both of which have been observed in Sgr B2.[5,52] Although currently there is no direct observation of CS in the same molecular cloud, its protonated variant HCS^+[6] and thioformaldehyde H_2CS[53] along with another four CS-containing species, CCS,[8] OCS,[54] HNCS,[10] and HSCN,[55] have already been detected there. The neutral-neutral reaction of CH_2CNH (**P4-10**) with CS to form thiazole, which is the reverse direction of the proposed thiazole decomposition to **P4-10**, is a highly exothermic reaction which yields 313.14 kJ/mol at 0 K and has a low barrier of 82.40 kJ/mol. If both CS and CH_2CNH appear in the same region, given sufficient evolution time and activation energy, thiazole could be

synthesized in this way. Likewise, another pair of radicals , CH$_2$CN and HCS that were found in Sgr B2[56], could react and yield thiazole as well as shown in Figure 7.10. This is a barrierless radical recombination reaction with an exothermic energy of -387.10 kJ/mol at 0 K.
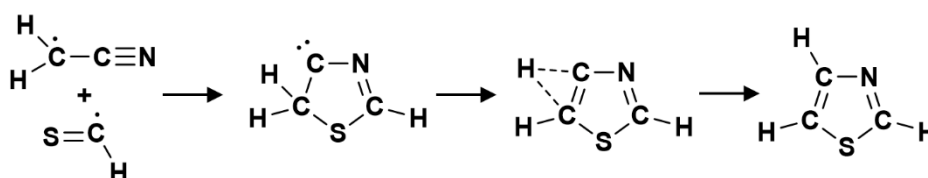
Figure 7.10. Reaction pathway of CH$_2$CN and HCS radicals that yields thiazole.

7.5.4 Decomposition to other small products

Other than CH$_3$NCS (**P3-4**) and CH$_3$CN (**P4-6**), **Tz-2** could directly decompose to H$_2$CCS and HCN. The full decomposition pathway is given in Figure 7.11 and the relative energies are shown in Figure 7.8 in contrast with the CH$_3$CN (**P4-6**) formation pathways. The transition state **P5-TS1** is 71.85 kJ higher than **Tz-2** with an imaginary frequency of 470i cm^{-1}. Even though the whole reaction pathway (**Tz** → **P5-2** + HCN) is endothermic, 171.89 kJ/mol, the decomposition starting from intermediate **Tz-2** is exothermic, -63.13 kJ/mol. When using HSCH$_2$CH$_2$SH (chapter 4) and CH$_3$NCS + HCCH (chapter 5) as precursors, under the same experimental conditions, the signal-to-noise ratios (SNR) of H$_2$CCS are 10 and 9, respectively. In this study, the corresponding SNR is ~60, which implies that this is a highly favourable decomposition pathway yielding H$_2$CCS (**P5-2**). As it is a potential interstellar species, the reverse reaction of **P5-2** + HCN could synthesize thiazole with an activation energy of 134.98 kJ/mol and a reaction energy (0 K) of -171.89 kJ/mol.
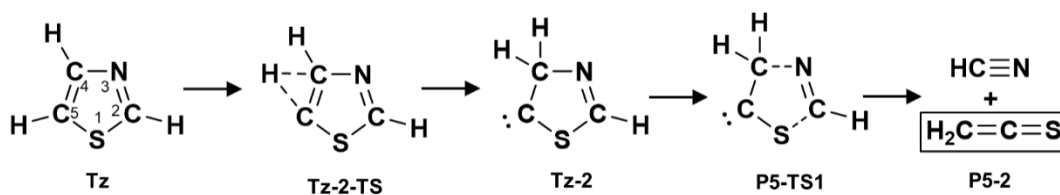
Figure 7.11. Unimolecular decomposition pathway of thiazole to HCN + H$_2$CCS (P5). The molecular species in the black box is a detected species in the thiazole discharge.

Likewise, H-migration isomer **Tz-3** could also decompose to two stable compounds, HNCS + HCCH, as shown Figure 7.12, and their relative energies are given in Figure 7.8. Even though **Tz-3** is more stable than **Tz-2**, it needs more energy (208.04 kJ/mol) to overcome the barrier (**P6-TS1**). The electronic energy of HCCH + HNCS is located 30.95 kJ/mol above that of HCN + H$_2$CCS. Since HNCS is also an interstellar species confirmed in Sgr B2,[10] it might be a possible precursor of the interstellar formation of thiazole. The reaction (**P6-2** + HCCH → **Tz**) is exothermic by -202.81 kJ/mol and the activation barrier at 0 K is 128.09 kJ/mol. Another mechanism to form HNCS is the radical reaction of NCS with a H atom. In the CH$_3$NCS discharge, the source produced more NCS radical and HSCN but less HNCS based on their SNRs compared to the thiazole discharge. The SNR ratio of HNCS in both discharge experiments suggests that this dissociation channel at least leads to one third of the HNCS formation. Additionally, the H-migration from C2 to S1 was also investigated. The H-shift resulted in a cleavage of C2-S1 single bond and did not decompose to HSCN.
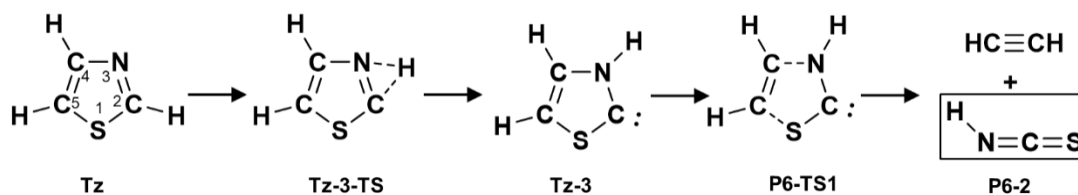
Figure 7.12. Unimolecular decomposition pathway of thiazole to HCCH + HNCS (P6). The molecular species in the black box is a detected species in the thiazole discharge.

7.6 Summary

In this work, 19 known discharge species were detected in the thiazole discharge using microwave spectroscopy. Their formation has been investigated by comparing with the previous work in Chapters 4 and 5 and have been modeled with quantum chemistry calculations. Six of them must be formed via secondary recombination reactions and 13 could potentially be formed as unimolecular dissociation products. Other than some directly decomposed compounds such as H_2CCS, HNCS and HSCN, the dc electric discharge also created small fragments that are not as predictable as in a strictly thermal equilibrium process. Further rearrangements of these fragments can yield detectable molecules as well. On the basis of this, the reaction pathways of the detected vinyl and methyl-bearing species were explored using CBS-QB3//B3LYP calculations. Meanwhile, four pathways based on the detected species in Sgr B2 molecular cloud: CH_2CNH + CS, CH_2CN + HCS, H_2CCS + HCN, HNCS + HCCH, which could possibly lead to interstellar formation of thiazole were investigated in this work as well.

References

(1) Ratti, E.; Lauinger, C.; Ressler, C. Configuration of the Asparaginyl and Aspartyl residues of Bacitracin. *J. Org. Chem.* **1968,** *33* (3), 1309-1310.

(2) Bollag, D. M.; McQueney, P. A.; Zhu, J.; Hensens, O.; Koupal, L.; Leisch, J.; Goetz, M.; Lazarides, E.; Woods, C. M. Epothilones, a New Class of Microtubule-stabilizing Agents with a Taxol-like Mechanism of Action. *Cancer Res.* **1995,** *55*, 2325-2333.

(3) Roy, R. S.; Gehring, A. M.; Milne, J. C.; Belshaw, P. J.; Walsh, C. T. Thiazole and Oxazole Peptides: Biosynthesis and Molecular Machinery. *Nat. Prod. Rep.* **1999,** *16* (2), 249-263.

(4) Eigenbrode, J. L.; Summons, R. E.; Steele, A.; Freissinet, C.; Millan, M.; Navarro-Gonzalez, R.; Sutter, B.; McAdam, A. C.; Franz, H. B.; Glavin, D. P.; Archer, P. D., Jr.; Mahaffy, P. R.; Conrad, P. G.; Hurowitz, J. A.; Grotzinger, J. P.; Gupta, S.; Ming, D. W.; Sumner, D. Y.; Szopa, C.; Malespin, C.; Buch, A.; Coll, P. Organic Matter Preserved in 3-Billion-Year-Old Mudstones at Gale Crater, Mars. *Science* **2018,** *360* (6393), 1096-1101.

(5) Lovas, F. J.; Hollis, J. M.; Remijan, A. J.; Jewell, P. R. Detection of Ketenimine (CH_2CNH) in Sagittarius B2(N) Hot Cores. *Astrophys. J.* **2006,** *645* (2), L137-L140.

(6) Thaddeus, P.; Guelin, M.; Linke, R. A. Three New 'Nonterrestrial' Molecules. *Astrophys. J.* **1981,** *246*, L41-L45.

(7) Ozeki, H.; Hirao, T.; Saito, S.; Yamamoto, S. Laboratory Microwave Spectroscopy of the Cyanomethyl Radical, CH_2CN. *Astrophys. J.* **2004,** *617* (1), 680-684.

(8) Saito, S.; Kawaguchi, K.; Yamamoto, S.; Ohishi, M.; Suzuki, H. Laboratory Detection and Astronomical Identification of a new Free Radical, CCS $^3\Sigma^-$. *Astrophys. J.* **1987,** *317*.

(9) Linke, R. A.; Goldsmith, P. F.; Wannier, P. G.; Wilson, R. W.; Penzias, A. A. Isotopic Abundance Variations in Interstellar HCN. *Astrophys. J.* **1977,** *214*, 50-59.

(10) Frerking, M. A.; Linke, R. A.; Thaddeus, P. Interstellar Isothiocyanic Acid. *Astrophys. J.* **1979,** *234*, L143-L145.

(11) Prozument, K.; Barratt Park, G.; Shaver, R. G.; Vasiliou, A. K.; Oldham, J. M.; David, D. E.; Muenter, J. S.; Stanton, J. F.; Suits, A. G.; Barney Ellison, G.; Field, R. W. Chirped-Pulse Millimeter-Wave Spectroscopy for Dynamics and Kinetics Studies of Pyrolysis Reactions. *Phys. Chem. Chem. Phys.* **2014,** *16* (30), 15739-15751.

(12) Kidwell, N. M.; Vaquero-Vara, V.; Ormond, T. K.; Buckingham, G. T.; Zhang, D.; Mehta-Hurt, D. N.; McCaslin, L.; Nimlos, M. R.; Daily, J. W.; Dian, B. C.; Stanton, J. F.; Ellison, G. B.; Zwier, T. S. Chirped-Pulse Fourier Transform Microwave Spectroscopy Coupled with a Flash Pyrolysis Microreactor: Structural Determination of the Reactive Intermediate Cyclopentadienone. *J. Phys. Chem. Lett.* **2014,** *5* (13), 2201-2207.

(13) Guan, Q.; Urness, K. N.; Ormond, T. K.; David, D. E.; Ellison, G. B.; Daily, J. W. The Properties of a Micro-Reactor for the Study of the Unimolecular Decomposition of Large Molecules. *Int. Rev. Phys. Chem.* **2014,** *33* (4), 447-487.

(14) Urness, K. N.; Guan, Q.; Golan, A.; Daily, J. W.; Nimlos, M. R.; Stanton, J. F.; Ahmed, M.; Ellison, G. B. Pyrolysis of Furan in a Microreactor. *J. Chem. Phys.* **2013,** *139* (12), 124305.

(15)   Lee, K. L. K.; McGuire, B. A.; McCarthy, M. C. Gas-Phase Synthetic Pathways to Benzene and Benzonitrile: a Combined Microwave and Thermochemical Investigation. *Phys. Chem. Chem. Phys.* **2019,** *21* (6), 2946-2956.

(16)   Karunatilaka, C.; Shirar, A. J.; Storck, G. L.; Hotopp, K. M.; Biddle, E. B.; Crawley, R.; Dian, B. C. Dissociation Pathways of 2,3-Dihydrofuran Measured by Chirped-Pulse Fourier Transform Microwave Spectroscopy. *J. Phys. Chem. Lett.* **2010,** *1* (10), 1547-1551.

(17)   Song, X.; Parish, C. A. Pyrolysis Mechanisms of Thiophene and Methylthiophene in Asphaltenes. *J. Phys. Chem. A* **2011,** *115* (13), 2882-91.

(18)   Montgomery Jr., J. A.; Frisch, M. J.; Ochterski, J. W.; Peterson, G. A. A Complete Basis Set Model Chemistry. VI. Use of Density Functional Geometries and Frequencies. *J. Chem. Phys.* **1999,** *110*, 2822.

(19)   Stephens, P. J.; Devlin, F. J.; Chabalowski, C. F.; Frisch, M. J. *Ab Initio* Calculation of Vibrational Absorption and Circular-Dichroism Spectra Using Density-Functional Force-Fields. *J. Phys. Chem. Lett.* **1994,** *98* (45), 11623-11627.

(20)   Becke, A. D. Density‐Functional Thermochemistry. III. The Role of Exact Exchange. *J. Chem. Phys.* **1993,** *98* (7), 5648-5652.

(21)   Becke, A. D. Density-Functional Exchange-Energy Approximation with Correct Asymptotic Behavior. *Phys. Rev. A* **1988,** *38* (6), 3098-3100.

(22)   Frisch, M. J.; Trucks, G. W.; Schlegel, H. B.; Scuseria, G. E.; Robb, M. A.; Cheeseman, J. R.; Scalmani, G.; Barone, V.; Petersson, G. A.; Nakatsuji, H.; Li, X.; Caricato, M.; Marenich, A. V.; Bloino, J.; Janesko, B. G.; Gomperts, R.; Mennucci, B.; Hratchian, H. P.; Ortiz, J. V.; Izmaylov, A. F.; Sonnenberg, J. L.; Williams; Ding, F.; Lipparini, F.; Egidi, F.; Goings, J.; Peng, B.; Petrone, A.; Henderson, T.; Ranasinghe, D.; Zakrzewski, V. G.; Gao, J.; Rega, N.; Zheng, G.; Liang, W.; Hada,

M.; Ehara, M.; Toyota, K.; Fukuda, R.; Hasegawa, J.; Ishida, M.; Nakajima, T.; Honda, Y.; Kitao, O.; Nakai, H.; Vreven, T.; Throssell, K.; Montgomery Jr., J. A.; Peralta, J. E.; Ogliaro, F.; Bearpark, M. J.; Heyd, J. J.; Brothers, E. N.; Kudin, K. N.; Staroverov, V. N.; Keith, T. A.; Kobayashi, R.; Normand, J.; Raghavachari, K.; Rendell, A. P.; Burant, J. C.; Iyengar, S. S.; Tomasi, J.; Cossi, M.; Millam, J. M.; Klene, M.; Adamo, C.; Cammi, R.; Ochterski, J. W.; Martin, R. L.; Morokuma, K.; Farkas, O.; Foresman, J. B.; Fox, D. J. *Gaussian 16 Rev. B.01*, Wallingford, CT, 2016.

(23)   Bizzocchi, L.; Degli Esposti, C.; Botschwina, P. Millimeter-Wave Spectroscopy of Rare Isotopomers of HC_5N and DC_5N: Determination of a Mixed Experimental–Theoretical Equilibrium Structure for Cyanobutadiyne. *J. Mol. Spectrosc.* **2004,** *225* (2), 145-151.

(24)   Lovas, F. J.; Suenram, R. D.; Ogata, T.; Yamamoto, S. Microwave Spectra and Electric Dipole Moments for Low-*J* Levels of Interstellar Radicals: SO, C_2S, C_3S, *c*-HC_3, CH_2CC, and *c*-C_3H_2. *Astrophys. J.* **1992,** *399*, 325-329.

(25)   Brown, R. D.; Dyall, K. G.; Elmes, P. S.; Godfrey, P. D.; McNaughton, D. The Generation, Microwave Spectrum, and Structure of Propadienethione, $H_2C=C=C=S$. *J. Am. Chem. Soc.* **1988,** *110* (3), 789-792.

(26)   Gordon, V. D.; McCarthy, M. C.; Apponi, A. J.; Thaddeus, P. Rotational Spectra of Sulfur-Carbon Chains. II. HC_5S, HC_6S, HC_7S, and HC_8S, and H_2C_4S, H_2C_5S, H_2C_6S, and H_2C_7S. *Astrophys. J., Suppl. Ser.* **2002,** *138* (2), 297-303.

(27)   Thaddeus, P.; Vrtilek, J. M.; Gottlieb, C. A. Laboratory and Astronomical Identification of Cyclopropenylidene, C_3H_2. *Astrophys. J.* **1985,** *299*, l63-l66.

(28)   Brown, R. D.; Godfrey, P. D.; Champion, R.; Woodruff, M. The Microwave Spectrum of Propynethial, $HC \equiv C\text{-}CHS$. *Aust. J. Chem.* **1982,** *35* (9), 1747-1753.

(29)   Benson, R. C.; Flygare, W. H. Molecular g Values, Magnetic Susceptibilities, Molecular Quadrupole Moments, and Sign of the Electric Dipole Moment in Cyclopropene. *J. Chem. Phys.* **1969,** *51* (7), 3087-3096.

(30)   Liu, R.; Zhou, X.; Zhai, L. Theoretical Investigation of Unimolecular Decomposition Channels of Furan4. *J. Comput. Chem.* **1998,** *19* (2), 240-249.

(31)   Sendt, K.; Bacskay, G. B.; Mackie, J. C. Pyrolysis of Furan: *Ab Initio* Quantum Chemical and Kinetic Modeling Studies. *J. Phys. Chem. A* **2000,** *104* (9), 1861-1875.

(32)   Ur Rahman Memon, H.; Williams, A.; Williams, P. T. Shock Tube Pyrolysis of Thiophene. *Int. J. Energy Res.* **2003,** *27* (3), 225-239.

(33)   Abeysekera, C.; Hernandez-Castillo, A. O.; Stanton, J. F.; Zwier, T. S. Broadband Microwave Spectroscopy of 2-Furanyloxy Radical: Primary Pyrolysis Product of the Second-Generation Biofuel 2-Methoxyfuran. *J. Phys. Chem. A* **2018,** *122* (34), 6879-6885.

(34)   McCarthy, M. C.; Cooksy, A. L.; Mohamed, S.; Gordon, V. D.; Thaddeus, P. Rotational Spectra of the Nitrogen‐Sulfur Carbon Chains NC_nS,n= 1–7. *Astrophys. J., Suppl. Ser.* **2003,** *144* (2), 287-297.

(35)   Beard, C. I.; Dailey, B. P. The Structure and Dipole Moment of Isothiocyanic Acid. *J. Chem. Phys.* **1950,** *18* (11), 1437-1441.

(36)   Brünken, S.; Yu, Z.; Gottlieb, C. A.; McCarthy, M. C.; Thaddeus, P. Laboratory Detection of Thiocyanic Acid HSCN. *Astrophys. J.* **2009,** *706* (2), 1588-1593.

(37)   Kim, E.; Habara, H.; Yamamoto, S. Hyperfine Interaction Constants of the HCCS and DCCS Radicals Studied by Fourier Transform Millimeter-Wave Spectroscopy. *J. Mol. Spectrosc.* **2002,** *212* (1), 83-88.

(38)   Georgiou, K.; Kroto, H. W.; Landsberg, B. M. The Microwave Spectrum, Substitution Structure, and Dipole Moment of Thioketen, $H_2C=C=S$. *J. Mol. Spectrosc.* **1979,** *77*, 365-373.

(39)   Georgiou, K.; Kroto, H. W. Microwave Spectrum, Structure, and Dipole Moment of *trans*-2-Propenethial, $CH_2=CHCH=S$. *J. Mol. Spectrosc.* **1980,** *83* (1), 94-104.

(40)   Hirose, C. Mirowave Spectra of Vinylacetylene and Monodeutero Vinylacetylene in Ground and Excited Vibrational States. *Bull. Chem. Soc. Jpn.* **1970,** *43*, 3695-3698.

(41)   Thorwirth, S.; Harding, M. E.; Dudek, J. B.; McCarthy, M. C. Equilibrium Molecular Structures of Vinyl Carbon Chains: Vinyl Acetylene, Vinyl Diacetylene, and Vinyl Cyanide. *J. Mol. Spectrosc.* **2018,** *350*, 10-17.

(42)   Kroto, H. W.; Landsberg, B. M.; Suffolk, R. J.; Vodden, A. The Photoelectron and Microwave Spectra of the Unstable Species Thioacetaldehyde, CH_3CHS, and Thioacetone, $(CH_3)_2CS$. *Chem. Phys. Lett.* **1974,** *29* (2), 265-269.

(43)   R., T.; Gordy, W. The Microwave Spectrum and Structure of Methyl Acetylene. *J. Chem. Phys.* **1950,** *18* (12), 1613.

(44)   Caminati, W. The Microwave Spectrum of s-Trans Vinyl Isothiocyanate. *J. Mol. Struct.* **1988,** *190*, 227-233.

(45)   Roos, B. O.; Taylor, P. R.; Siegbahn, P. E. M. A Complete Active Space SCF Method (CASSCF) using a Density Matrix Formulated Super-CI Approach. *Chem. Phys.* **1980,** *48* (2), 157-173.

(46)   Sun, W.; Davis, R. L.; Thorwirth, S.; Harding, M. E.; van Wijngaarden, J. A Highly Flexible Molecule: The Peculiar Case of Ethynyl Isothiocyanate HCCNCS. *J. Chem. Phys.* **2018,** *149* (10), 104304.

(47)   Jensen, J. H.; Morokuma, K.; Gordon, M. S. Pathways for H_2 Elimination from Ethylene: A Theoretical Study. *J. Chem. Phys.* **1994,** *141* (21), 214203.

(48)   Yamada, K.; Winnewisser, M. Ground State Centrifugal Distortion Constants of Vinyl Isocyanide, CH_2-CH-NC, from the Microwave and Millimeter Wave Rotational Spectra. *Z. Naturforsch., A: Phys. Sci.* **1975,** *301* (5), 672-689.

(49)   Agúndez, M.; Fonfría, J. P.; Cernicharo, J.; Pardo, J. R.; Guélin, M. Detection of Circumstellar CH_2CHCN, CH_2CN, CH_3CCH, and H_2CS. *Astron. Astrophys.* **2008,** *479* (2), 493-501.

(50)   Van Dine, G. W.; Hoffmann, R. Isocyanide-Cyanide and Isoelectronic Rearrangements. *J. Am. Chem. Soc.* **1968,** *90* (12), 3227-3232.

(51)   Guarnieri, A.; Hinze, R.; Krüger, M.; Zerbe-Foese, H.; Lentz, D.; Preugschat, D. The Millimeter-Wave Spectrum of Ethynylisocyanide ($H-C \equiv C-N=C$). *J. Mol. Spectrosc.* **1992,** *156* (1), 39-47.

(52)   Solomon, P. M.; Jefferts, K. B.; Penzias, A. A.; Wilson, R. W. Detection of Millimeter Emission Lines from Interstellar Methyl Cyanide. *Astrophys. J.* **1971,** *168*.

(53)   Sinclair, M. W.; Fourikis, N.; Ribes, J. C.; Robinson, B. J.; Brown, R. D.; Godfrey, P. D. Detection of Interstellar Thioformaldehyde. *Aust. J. Chem.* **1973,** *26* (1), 85-91.

(54)   Jefferts, K. B.; Penzias, A. A.; Wilson, R. W.; Solomon, P. M. Detection of Interstellar Carbonyl Sulfide. *Astrophys. J.* **1971,** *168*.

(55)   Halfen, D. T.; Ziurys, L. M.; Brünken, S.; Gottlieb, C. A.; McCarthy, M. C.; Thaddeus, P. Detection of a New Interstellar Molecule: Thiocyanic Acid HSCN. *Astrophys. J.* **2009,** *702* (2), L124-L127.

(56)   Irvine, W. M.; Friberg, P.; Hjalmarson, A.; Ishikawa, S.; Kaifu, N.; Kawaguchi, K.; Madden, S. C.; Matthews, H. E.; Ohishi, M.; Saito, S.; Suzuki, H.;

Thaddeus, P.; Turner, B. E.; Yamamoto, S.; Ziurys, L. M. Identification of the Interstellar Cyanomethyl Radical (CH$_2$CN) in the Molecular Clouds TMC-1 and Sagittarius B2. *Astrophys. J.* **1988,** *334*, L107-L111.

Chapter 8.   Summary and future outlook

8.1 Summary

This thesis has presented a selection of microwave spectroscopic studies that mainly focused on sulfur-bearing molecules of particular astrophysical interest and aimed to provide unique fingerprints for future astronomical detection. In these studies, the rotational spectra were collected using the custom-built broadband chirped pulse type[1] and narrowband Balle-Flygare type[2] FTMW spectrometers in the van Wijngaarden group at the University of Manitoba. Besides the commercially available compounds (PhNCO and PhNCS), exotic molecular species created by the dc electrical discharge were the major targets.

The dc electrical discharge technique is well known for producing highly unsaturated long carbon chain species,[3-6] many of which, such as $HC_{2n+1}N$ with up to nine carbons,[7-11] are found in various interstellar and circumstellar molecular clouds. In earlier experiments reported in the literature, the precursors are rather small and simple which largely limited the application of this technique and the diversity of discharge products. To explore more possibilities, the work in this thesis involved the use of more complex precursors in comparison with the previously tested precursors such as CO, CS_2, and so on. However, as a custom-built assembly, the experimental conditions required for making novel species were difficult to predict at the beginning. Therefore, the first discharge experiment reported herein aimed to empirically explore the discharge conditions by investigating a well known class of species – sulfur-carbon chains.[3-4] Afterwards, with a certain understanding of the electrical discharge source, three molecules including HCCNCS,[12] HCCCCNCS,[13]

and NCCCNCS[13] were successfully formed under the optimized conditions and their microwave spectra were recorded by rotational spectroscopy for the first time.

In the course of these studies, some problems were revealed from the experiments as well. Besides the difficulties of analyzing the complicated discharge spectra where many newly created species were probed together with the remaining precursors, the selection of the precursors proved critical in these experiments. Once benchmarked, it was shown that some precursors worked well to create the desired compounds whereas some others with very similar structural geometries did not. Without knowing more about the detailed thermodynamic and kinetic processes in the discharge plasma, it was difficult to predict the products for given precursors. This created significant uncertainty in each project. As a technique, comprehensive studies that investigate its 'harsh' reaction environment in detail are rather scarce.

Following a number of successful and unsuccessful experiences, it was clear that it was important to shed some light on this black box technique by studying the chemical behaviours of the thiazole compound in the discharge plasma more completely. As many new species were created in the discharge source with sufficient abundance to record the microwave spectrum simultaneously, their formation was rationalized empirically by comparing with the results from the CH_3NCS discharge. Subsequently, the formation of the observed molecules was modeled using quantum-chemical methods with a focus on unimolecular decomposition reactions. Although the proposed dissociation or isomerization pathways are highly speculative and hard to prove experimentally, this study does help us know more about the high reactive discharge environment to a certain extent.

In addition to these technical considerations, the molecules being studied in this thesis are of great interest for their fundamental astrophysical and chemical

values. For instance, the chemical bonding nature of the heteroatomic functional groups NCO and NCS is one of the biggest concerns, especially the valence bond angle of the R-NC part which reflects the electronic environment at the nitrogen site. For PhNCO and PhNCS, with the observation of the pure rotational spectra due to the parent species and nine minor isotopologues including seven ^{13}C, one ^{15}N, and one ^{18}O/^{34}S in natural abundance, their experimental $r_m^{(1)}$ geometries were precisely derived from the well-determined rotational constants.[14] The ∠CNC angle was fit to be 135.2(4)° for PhNCO and 145.1(2)° for PhNCS, respectively which follows the trend ∠R-NC(S) > ∠R-NC(O). Further, NBO analysis at the MP2/aug-cc-pVTZ level of theory revealed the subtle differences in the nature of the electronic structure of nitrogen which revealed that the hybridization is sp-like for PhNCS while more like sp$^{1.6}$ for PhNCO.

Surprisingly, when it comes to HCCNCS, it is effectively a linear molecule, where the ∠CNC angle is 180°.[12] The linear CNC geometric arrangement of HCCNCS is very different from that of PhNCS (145°) as well as its isovalent analogs HCCNCO (140°),[15] NCNCS (143°),[16] NCNCO (129°).[17] This study thus proposed that both the HCC fragment and the S atom tend to make such species more linear than their NC fragment and O substituted counterparts based on extensive theoretical investigations. Afterwards, HCCNCS and NCNCS were elongated with addition of one more alkyne subunit and formed HCCCCNCS and NCCCNCS in the discharge source.[14] As HCCNCS is effectively linear, its longer chain form is linear with little surprise whereas NCNCS, as a typical V-shaped molecule, becomes a linear top when elongated to NCCCNCS. Ultimately, these fundamental studies provide important reference data for astronomers, further development of accurate computational methods and assist with organic compound designs.

8.2 Future outlook

In the future, the work presented in this dissertation can be extended in several ways:

First, the spectroscopic study can be extended to shorter wavelength (higher frequency) regions and higher energy levels, as the current work was performed only in the microwave region and probed the very lowest energy levels of these species. Many ground-based radio telescopes, such as ALMA, operate at sub-millimeter (THz in frequency) and millimeter wavelengths, where rotational transitions have higher quantum numbers and molecules experience greater centrifugal distortion effects. Given the highly flexible nature of these species, especially HCCNCS, the determined spectroscopic constants will not necessarily lead to the precise prediction of the spectral pattern in the higher frequency regions. In this case, extensive studies will be significantly helpful for future astronomical detection. Moreover, a precise characterization of the energy levels in the excited vibrational states of these species, particularly in the submillimeter and far infrared regions is also desired. The corresponding rovibrational spectra will help people to fundamentally understand the molecular energy levels and potentials which governs the chemistry and properties of these molecules. There are many ground-, aircraft-, and spacecraft-based high-resolution infrared telescopes like ISO that are used to receive molecular signals due to these rovibrational transitions.

Second, the dc electrical discharge decomposition study can be extended to explore more compounds, such as $CH_3C{\equiv}CNCS$, $P{\equiv}CNCS$. With more and more studies in the database, the chemical processes in the hot discharge environment can be modeled better theoretically which could be further used to accurately predict the discharge products for given precursors. If successful, the dc electric discharge

technique will be a much more efficient approach to create desired novel chemical species which cannot be synthesized on the laboratory benchtop.

Third, more NCO and NCS-containing compounds can be studied to investigate the interesting nature of the NCO/NCS moiety. So far, only several R-NCOs and R-NCSs have been experimentally characterized by rotational spectroscopy, where R = H,[18-19] CH_3,[20-21] CH_3CH_2,[22-23] $CH_2=CH$,[24-25] c-C_6H_5 (Ph),[14] $HC\equiv C$,[12,15] $N\equiv C$.[16-17] Of them, only HNCO/S, PhNCO/S, HCCNCO/S have been studied with minor isotopologues allowing the corresponding geometries to be experimentally determined. These studies are fundamental and important. For instance, in the earlier study, the CNC angle in *trans*-CH_2CH-NCS was reported to be 137.6º calculated using an unclear *ab initio* method[24] while in the calculation reported in this work at the B3LYP/cc-pVQZ level of theory, this angle is 150º. The basis set and level of theory are clearly critical for accurate modelling as demonstrated in this work for HCCNCS in particular. Besides an in-depth study of the aforementioned compounds, more unknown NCO and NCS derivatives await precise spectroscopic characterization as well. For instance, the allyl ($CH_2=CHCH_2$) variants are predicted to adopt multiple conformers in the gas phase by various computational methods whereas different theoretical models probe different energy profiles and local minima. As a solvent-free and shape-sensitive technique, microwave spectroscopy is absolutely a perfect tool to examine the accuracy of these computational functionals by unambiguously investigating the low energy forms. With sufficient information collected for a range of compounds, their physical and chemical properties such as the molecular quasi-linearity of the NCO/S group and the intramolecular interaction between the NCO/S and R groups can be systemically explored. It is such

fundamental studies that establish a solid ground for scientific research and facilitate

more advanced projects.

References

(1)   Evangelisti, L.; Sedo, G.; van Wijngaarden, J. Rotational Spectrum of 1,1,1-Trifluoro-2-Butanone Using Chirped-Pulse Fourier Transform Microwave Spectroscopy. *J. Phys. Chem. A* **2011,** *115* (5), 685-90.

(2)   Sedo, G.; van Wijngaarden, J. Fourier Transform Microwave Spectra of a "New" Isomer of OCS-CO_2. *J. Chem. Phys.* **2009,** *131* (4), 044303.

(3)   Gordon, V. D.; McCarthy, M. C.; Apponi, A. J.; Thaddeus, P. Rotational Spectra of Sulfur-Carbon Chains. II. HC_5S, HC_6S, HC_7S, and HC_8S, and H_2C_4S, H_2C_5S, H_2C_6S, and H_2C_7S. *Astrophys. J., Suppl. Ser.* **2002,** *138* (2), 297-303.

(4)   Gordon, V. D.; McCarthy, M. C.; Apponi, A. J.; Thaddeus, P. Rotational Spectra of Sulfur-Carbon Chains. I. The Radicals C_4S, C_5S, C_6S, C_7S, C_8S, and C_9S. *Astrophys. J., Suppl. Ser.* **2001,** *134* (2), 311-317.

(5)   McCarthy, M. C.; Chen, W.; Travers, M. J.; Thaddeus, P. Microwave Spectra of 11 Polyyne Carbon Chains. *Astrophys. J., Suppl. Ser.* **2000,** *129* (2), 611-623.

(6)   McCarthy, M. C.; Travers, M. J.; Kovacs, A.; Gottlieb, C. A.; Thaddeus, P. Eight New Carbon Chain Molecules. *Astrophys. J., Suppl. Ser.* **1997,** *113* (1), 105-120.

(7)   Hirota, T.; Yamamoto, S.; Mikami, H.; Ohishi, M. Abundances of HCN and HNC in Dark Cloud Cores. *Astrophys. J.* **1998,** *503* (2), 717-728.

(8)   Bell, M. B.; Watson, J. K. G.; Feldman, P. A.; Travers, M. J. The Excitation Temperatures of HC_9N and Other Long Cyanopolyynes in TMC-1. *Astrophys. J.* **1998,** *508* (1), 286-290.

(9)   Olano, C. A.; Walmsley, C. M.; Wilson, T. L. The Relative Distribution of NH_3, HC_7N and C_4H in the Taurus Molecular Cloud 1 (TMC 1). *Astron. Astrophys.* **1988,** *196*, 194-200.

(10)   Snell, R. L.; Schloerb, F. P.; Young, J. S.; Hjalmarson, A.; Friberg, P. Observations of HC_3N, HC_5N, and HC_7N in Molecular Clouds. *Astrophys. J.* **1981,** *244*, 45-53.

(11)   Turner, B. E. Detection of Interstellar Cyanoacetylene. *Astrophys. J.* **1971,** *163*, L35-L39.

(12)   Sun, W.; Davis, R. L.; Thorwirth, S.; Harding, M. E.; van Wijngaarden, J. A Highly Flexible Molecule: The Peculiar Case of Ethynyl Isothiocyanate HCCNCS. *J. Chem. Phys.* **2018,** *149* (10), 104304.

(13)   Sun, W.; van Wijngaarden, J. Isothiocyanato-Containing Carbon Chains: The Laboratory Detection of HCCCCNCS and NCCCNCS via Rotational Spectroscopy. *J. Phys. Chem. A* **2018,** *122* (38), 7659-7665.

(14)   Sun, W.; Silva, W. G. D. P.; van Wijngaarden, J. Rotational Spectra and Structures of Phenyl Isocyanate and Phenyl Isothiocyanate. *J. Phys. Chem. A* **2019,** *123* (12), 2351-2360.

(15)   Ross, S. C.; Cooper, T. A.; Firth, S.; Kroto, H. W.; Walton, D. R. M. The Microwave Spectrum and Semirigid Bender Analysis of Isocyanatoethyne, $HC \equiv CNCO$. *J. Mol. Spectrosc.* **1992,** *152* (1), 152-167.

(16)   Winnewisser, B. P.; Winnewisser, M.; Medvedev, I. R.; Behnke, M.; De Lucia, F. C.; Ross, S. C.; Koput, J. Experimental Confirmation of Quantum Monodromy: the Millimeter Wave Spectrum of Cyanogen Isothiocyanate NCNCS. *Phys. Rev. Lett.* **2005,** *95* (24), 243002.

(17)   Bak, B.; Svanholt, H.; Holm, A. On the Molecular Structure of Gaseous Cyanogen Isocyanate N≡C-N=C=O. *Acta. Chem. Scand. A* **1979,** *33*.

(18)   Jones, L. H.; Shoolery, J. N.; Shulman, R. G.; Yost, D. M. The Molecular Structure of Isocyanic Acid from Microwave and InfraRed Absorption Spectra. *J. Chem. Phys.* **1950,** *18* (7), 990-991.

(19)   Beard, C. I.; Dailey, B. P. The Structure and Dipole Moment of Isothiocyanic Acid. *J. Chem. Phys.* **1950,** *18* (11), 1437-1441.

(20)   Koput, J. The Microwave Spectrum of Methyl Isothiocyanate. *J. Mol. Spectrosc.* **1986,** *118* (1), 189-207.

(21)   Koput, J. The Microwave Spectrum of Methyl lsocyanate. *J. Mol. Spectrosc.* **1986,** *115*, 131-146.

(22)   Sakaizumi, T.; Yamada, O.; Ushida, K.; Ohashi, O.; Yamaguchi, I. The Microwave Spectrum of Ethyl Isocyanate. *Bull. Chem. Soc. Jpn.* **1976,** *49* (11), 2908-2912.

(23)   Sakaizumi, T.; Ohashi, O.; Yamaguchi, I. Microwave Spectrum of Ethyl Isothiocyanate. *Bull. Chem. Soc. Jpn.* **1976,** *49* (4), 948-953.

(24)   Caminati, W. The Microwave Spectrum of *s-Trans* Vinyl Isothiocyanate. *J. Mol. Struct.* **1988,** *190*, 227-233.

(25)   Bouchy, A.; Roussy, G. Geometrical and Electronic Structures of Two Conformers of Vinyl Isocyanate by Microwave Spectroscopy. *J. Mol. Spectrosc.* **1977,** *68* (1), 156-165.

Appendix A: Measured rotational transitions of HCCNCS

Table S1. The measured transition frequencies for HCCNCS and its ^{13}C and ^{34}S isotopologues.

$J'-J''$	$F'-F''$	v_{obs}/MHz	$o\text{-}c$/kHz
		parent	
2-1	1-1	6085.9132	0.0
	3-2	6087.0431	0.4
	2-1	6087.0936	0.4
	1-0	6087.6833	0.0
	2-2	6087.8010	-0.2
3-2	2-2	9129.5720	0.0
	4-3	9130.6064	0.5
	3-2	9130.6343	0.3
	2-1	9130.7520	0.1
	3-3	9131.3924	-0.2
4-3	3-3	12173.1559	-0.5
	5-4	12174.1505	0.5
	4-3	12174.1676	-0.2
	3-2	12174.2185	0.1
	4-4	12174.9539	-0.6
5-4	4-4	15216.7091	0.0
	6-5	15217.6801	0.0
	5-4	15217.6938	1.3
	4-3	15217.7199	-0.6
	5-5	15218.4963	-0.7
6-5	5-5	18260.2384	-1.7
	7-6	18261.1955	-0.9
	6-5	18261.2060	0.4
	5-4	18261.2257	2.2
	6-6	18262.0214	-1.0
7-8	8-7	21304.6963	-1.5
	7-6	21304.7043	-0.4
	6-5	21304.7202	3.0
8-7	9-8	24348.1813	-1.0
	7-6	24348.1976	0.7

		HCCNC³⁴S	
3-2	4-3	8898.1278	0.8
	3-2	8898.1554	0.3
	2-1	8898.2726	-0.3
4-3	5-4	11864.1797	0.9
	4-3	11864.1951	-1.5
	3-2	11864.2466	-0.5
5-4	6-5	14830.2146	-2.6
	5-4	14830.2314	1.8
	4-3	14830.2564	-1.2
6-5	7-6	17796.2397	-2.9
	6-5	17796.2537	1.9
	5-4	17796.2720	2.4
7-6	8-7	20762.2547	0.6
	6-5	20762.2750	1.6
8-7	9-8	23728.2473	-2.4
	7-6	23728.2651	0.9
		H¹³CCNCS	
4-3	5-4	11826.8148	2.1
	4-3	11826.8292	-3.1
6-5	7-6	17740.1919	0.9
	6-5	17740.2058	-1.2
	5-4	17740.2256	-2.3
8-7	6-5	23653.5180	1.6
	9-8	23653.5317	1.8
		HC¹³CNCS	
4-3	5-4	12040.2099	2.1
	4-3	12040.2247	-2.1
6-5	7-6	18060.2835	-1.2
	6-5	18060.2942	-0.2
	5-4	18060.3151	1.5
		HCCN¹³CS	
4-3	5-4	12163.5573	1.7
	4-3	12163.5716	-1.1
	3-2	12163.6202	-1.2
6-5	7-6	18245.3020	-2.5
	6-5	18245.3132	0.0
	5-4	18245.3337	3.2
8-7	6-5	24326.9923	-0.9
	9-8	24327.0081	0.7

Table S2. Assigned transitions for HCCNCS in a bending vibrational state.

J'-J''	F'-F''	e/f	v_{obs}/MHz	o-c/kHz
4-3	5-4	(-1)-(1)	12181.0831	1.1
	3-2	(-1)-(1)	12181.1087	-3.6
	4-3	(-1)-(1)	12181.1766	1.5
	5-4	(1)-(-1)	12183.5974	0.8
	3-2	(1)-(-1)	12183.6255	-1.4
	4-3	(1)-(-1)	12183.6886	-1.0
5-4	6-5	(1)-(-1)	15226.3589	0.6
	4-3	(1)-(-1)	15226.3832	-0.8
	5-4	(1)-(-1)	15226.4093	0.1
	6-5	(-1)-(1)	15229.5022	0.1
	4-3	(-1)-(1)	15229.5284	0.4
	5-4	(-1)-(1)	15229.5526	-0.4
6-5	7-6	(-1)-(1)	18271.6181	0.0
	5-4	(-1)-(1)	18271.6358	-2.3
	6-5	(-1)-(1)	18271.6498	0.2
	7-6	(1)-(-1)	18275.3933	1.7
	5-4	(1)-(-1)	18275.4104	-1.1
	6-5	(1)-(-1)	18275.4251	2.0
7-6	8-7	(1)-(-1)	21316.8626	0.1
	7-6	(1)-(-1)	21316.8883	4.6
	8-7	(-1)-(1)	21321.2659	-0.1
	7-6	(-1)-(1)	21321.2858	-1.3
8-7	9-8	(-1)-(1)	24362.0888	-2.0
	8-7	(-1)-(1)	24362.1050	-0.8
	9-8	(1)-(-1)	24367.1249	0.0
	8-7	(1)-(-1)	24367.1403	0.3

Appendix B: Measured rotational transitions of HC≡CC≡CN=C=S and N≡CC≡CN=C=S

Table S3. Observed rotational transition frequencies of the parent and ^{34}S singly substituted analog of HC$_4$NCS.

	HCCCCNCS-parent		
J'-J''	*F'-F''*	v_{obs}/MHz	*o-c* /kHz
4-3	5-4	4760.7243	-0.4
	4-3	4760.7419	-0.1
	3-2	4760.7900	-0.9
5-4	6-5	5950.9134	-0.9
	5-4	5950.9297	3.5
	4-3	5950.9503	-3.0
6-5	7-6	7141.1000	-0.7
	6-5	7141.1114	1.9
	5-4	7141.1264	-0.3
7-6	8-7	8331.2826	-2.4
	7-6	8331.2948	3.1
	6-5	8331.3064	2.8
8-7	9-8	9521.4677	0.4
	8-7		-4.9
	7-6	9521.4825	1.1
9-8	10-9	10711.6481	0.3
	9-8		-4.0
	8-7	10711.6615	2.7
10-9	11-10	11901.8259	-0.5
	10-9		-4.0
	9-8	11901.8389	3.6
11-10	12-11	13092.0042	1.2
	11-10		-1.8
	10-9		-6.1
12-11	13-12	14282.1801	2.5
	12-11		0.0
	11-10		-3.6
13-12	14-13	15472.3514	1.6
	13-12		-0.6
	12-11		-3.5
14-13	15-14	16662.5212	1.5
	14-13		-0.4
	13-12		-3.0
15-14	16-15	17852.6886	1.6
	15-14		0.0
	14-13		-2.2
16-15	17-16	19042.8533	1.8
	16-15		0.3
	15-14		-1.6
17-16	18-17	20233.0147	1.5
	17-16		0.2
	16-15		-1.4

J'-J''	F'-F''	v_{obs}/MHz	o-c /kHz
18-17	19-18	21423.1736	1.8
	18-17		0.6
	17-16		-0.8
19-18	20-19	22613.3287	1.6
	19-18		0.5
	18-17		-0.8
20-19	21-20	23803.4797	0.8
	20-19		-0.2
	19-18		-1.4

HCCCCNC^{34}S			
J'-J''	F'-F''	v_{obs}/MHz	o-c /kHz
5-4	6-5	5806.7471	-1.0
	5-4	5806.7623	2.6
6-5	7-6	6968.0994	-1.9
	6-5	6968.1131	3.4
	5-4	6968.1261	-0.3
7-6	8-7	8129.4505	-1.8
	6-5	8129.4661	-5.1
8-7	9-8	9290.7995	-2.0
	7-6	9290.8133	-1.8
10-9	11-10	11613.4946	0.0
	10-9		-3.4
J'-J''	F'-F''	υobs/MHz	o-c /kHz
10-9	9-8	11613.5064	3.3
11-10	12-11	12774.8404	2.1
	11-10		-0.8
	10-9		-4.9
14-13	15-14	16258.8597	2.8
	14-13		0.9
	13-12		-1.5
15-14	16-15	17420.1940	2.2
	15-14		0.6
	14-13		-1.5

* The unresolved hyperfine components were fit to the same frequency as the one above.

Table S4. Observed rotational transition frequencies of the parent species of NC_3NCS.

J'-J''	F1'-F1''	F'-F''	v_{obs}/MHz	o-c /kHz
4-3	5-4	6-5	4770.1159	-0.1
6-5	5-4	4-3	7155.1326	1.9
		6-5	7155.1570	-0.8
	6-5	5-4	7155.1204	-0.4
		6-5	7155.1765	-1.7
	7-6	6-5	7155.0887	-1.2
		7-6	7155.1326	1.4
		8-7	7155.1497	-1.4
7-6	6-5	5-4	8347.6519	0.2
		7-6	8347.6702	-2.6
	7-6	6-5	8347.6433	-0.6
		7-6	8347.6824	-0.8
		8-7	8347.6775	1.7
	8-7	7-6	8347.6213	-1.8
		8-7	8347.6519	0.3
		9-8	8347.6653	-1.1
9-8	8-7	8-7	10732.6875	-1.8
		9-8	10732.6948	1.8
	9-8	9-8	10732.6948	-0.4
		10-9	10732.6948	1.3
	10-9	9-8	10732.6655	2.5
		11-10	10732.6875	-0.2
10-9	9-8	9-8	11925.1968	2.9
		10-9		-0.5
	10-9	10-9		-1.0
		11-10		-0.4
11-10	10-9	11-10	13117.6983	1.2
	11-10	11-10		1.7
		12-11		1.5
12-11	11-10	12-11	14310.1932	1.3
	12-11	12-11		2.3
		13-12		1.8
13-12	12-11	13-12	15502.6820	0.8
	13-12	13-12		2.2
		14-13		1.4
14-13	13-12	13-12	16695.1629	0.9
		14-13		-1.4
	14-13	14-13		0.1
		15-14		-0.8
	15-14	16-15		1.6
15-14	14-13	14-13	17887.6395	0.6
		15-14		-1.5
	15-14	15-14		0.1
		16-15		-0.8
	16-15	17-16		1.2
16-15	15-14	15-14	19080.1084	-0.2
		16-15		-2.2
	16-15	16-15		-0.6
		17-16		-1.5
	17-16	18-17		0.3
17-16	16-15	16-15	20272.5695	-1.4

		17-16		-3.2
	17-16	17-16		-1.6
		18-17		-2.5
	18-17	19-18		-1.0
18-17	17-16	17-16	21465.0258	0.6
		18-17		-1.0
	18-17	18-17		0.6
		19-18		-0.4
	19-18	20-19		1.0
19-18	18-17	18-17	22657.4713	0.3
		19-18		-1.2
	19-18	19-18		0.3
		19-18		-0.6
	20-19	21-20		0.7
20-19	19-18	19-18	23849.9087	0.9
		20-19		-0.5
	20-19	20-19		0.9
		21-20		0.1
	21-20	22-21		1.2

* The unresolved hyperfine components were fit to the same frequency as the one above.